NASA TECHNICAL TRANSLATION

NASA TT F-759

NASA TT F-759



# IONOSPHERIC MEASUREMENTS

*by A. I. Galkin, N. M. Yerofeyev,*
*E. S. Kazimirovskiy, and V. D. Kokourov*

*"Nauka" Press, Moscow,* 1971



NATIONAL AERONAUTICS AND SPACE ADMINISTRATION • WASHINGTON, D. C. • JULY 1974

| 1. Report No. NASA TT F-759 | 2. Government Accession No. | 3. Recipient's Catalog No. |
|---|---|---|
| 4. Title and Subtitle<br>IONOSPHERIC MEASUREMENTS | | 5. Report Date<br>July 1974<br>6. Performing Organization Code |
| 7. Author(s)<br>A.I. Galkin, N.M. Yerofeyev, E. S. Kazimirovskiy and V.D. Kokourov | | 8. Performing Organization Report No.<br>10. Work Unit No.<br>11. Contract or Grant No.<br>NASW-2038 |
| 9. Performing Organization Name and Address<br>Translation Consultants, Ltd<br>Arlington, VA | | 13. Type of Report and Period Covered<br>Translation |
| 12. Sponsoring Agency Name and Address<br>National Aeronautics and Space Administration<br>Washington, D.C. 20546 | | 14. Sponsoring Agency Code |

15. Supplementary Notes

Translation of "Ionosfernyye izmereniya," "Nauka" Press, Moscow, 1971, 176 pages

16. Abstract

Procedural questions of radio and physical measurements of ionospheric plasma parameters by space vehicles are discussed. Methods that use pulsed radio sounding of the ionosphere by ground stations and by artificial earth satellites are described. Questions concerned with the use of ionospheric data in radio communication practice are touched upon.

| 17. Key Words (Selected by Author(s)) | 18. Distribution Statement |
|---|---|
| | Unclassified - unlimited<br>STAR Category 13 |

| 19. Security Classif. (of this report) | 20. Security Classif. (of this page) | 21. No. of Pages | 22. Price* |
|---|---|---|---|
| Unclassified | Unclassified | 259 | ~~$6.50~~ 9.00 |

*For sale by the National Technical Information Service, Springfield, Virginia 22151

FOREWORD

Theoretical and experimental research on circumterrestrial space, and in particular, that region of it that has come to be called the ionosphere, has undergone rapid development in recent years. The ionosphere is a weakly ionized, low-temperature plasma, the state of which is determined primarily by the structure of the neutral atmosphere and by solar radiation. The physical processes in the ionosphere can be studied by using experimental data obtained by equipment installed in artificial earth satellites and geophysical rockets, as well as in ground complexes. Without disparaging the value of direct experiments using space vehicles, it should be pointed out that the tremendous volume of information on space-time variations in ionospheric parameters needed to build physically correct models of the ionosphere can be obtained today primarily by ground radio and physical methods of taking ionospheric measurements. Some of these methods, such as variable frequency pulse radio sounding for example, have been known for a comparatively long time (40 to 50 years). Others, such as the incoherent scattering of radio waves method, have come about only in the last decade. But it is quite obvious that all measurement methods must be developed and improved in order to ensure their calibration with respect to each other as well as the completeness of experimental research in order to solve scientific and applied problems of physics of the ionosphere.

The need to train specialists in the field of space physics has resulted in the inclusion of special courses on "Physics of the Ionosphere" in the curricula of many universities in the Soviet Union. But there are no textbooks explaining the fundamentals of ionospheric measurements. The monographs that have been published in the last 10 to 15 years, and which discuss problems of physics of the ionosphere [3, 73, 91, 112, 115, 117], are concerned primarily with information on measurement results and the physical interpretation of those results, but the information on techniques and procedures for taking ionospheric measurements in existing textbooks used in the course "Propagation of Radio Waves" [59, 67] are completely inadequate. Much of the information, particularly with respect to new measurement methods, or on existing modifications to known methods, has been scattering through numerous articles in foreign, as well as domestic, scientific periodicals.

This book is an attempt to set forth in as small a volume as possible the

principal procedural and instrumentation questions involved in radio and physical methods of obtaining ionospheric measurements based on radar observations of ionospheric plasma and the study of the characteristics of radio waves propagating in the ionosphere. Elucidated at the same time are methods of evaluating the influence of the ionosphere on conditions for the propagation of radio waves in the ionosphere, in addition to methods for measuring individual parameters of the ionosphere (electron concentration, temperature, inhomogeneous structure, and the like).

This task made it necessary to divide the basic content of the book into two parts. The first part concerns itself with existing methods of determining ionospheric parameters by radio sounding of the ionosphere by ionospheric stations on the ground and by artificial earth satellites, incoherent scattering installations, diversity reception, radar observations of meteor tracks, and F-scattering in the ionosphere. The second part deals with questions of measuring ionospheric absorption of radio waves, oblique and back oblique sounding, and the use of ionospheric data in radio communication practice.[1] Most of the attention is given to studying the E and F regions.

Wherever necessary, reference has been made to the source containing more detailed information on the procedure or instrumentation discussed.

Sections 1.1.1, 1.1.2, 1.2, and 2.6 were written by A. I. Galkin; sections 2.1 through 2.5 by N. M. Yerofeyev; the introduction and sections 1.3 and 2.7 by E. S. Kazimirovskiy; and sections 1.1.3, and 1.4 through 1.6 by V. D. Kokourov.

The authors hope the book will be useful to scientists and engineers working in the field of the physics of the ionosphere, as well as to graduate students and students taking advanced courses in the corresponding specialties. Comments by readers concerning shortcomings in the book will be appreciated.

---

1. It was not until the manuscript for this book had been delivered to the publishers that news of the launching by the Soviet Union of Kosmos 381, carrying a small ionopsheric probe for vertical pulse sounding of the ionosphere, became known. The article by M. Fedorov, R. Rabinovich, and V. Matazov, "Predicting Electrical Weather," was published in Aviatsiya i Kosmonavtika (1971, No. 3).

TABLE OF CONTENTS

## INTRODUCTION

Before embarking on a discussion of the different methods that can be used /5* to measure the parameters of ionospheric plasma it was thought best to provide a brief review of certain of the information about the ionosphere known at this time, as well as of conclusions from the theory of the propagation of radio waves in the ionosphere that are important to an understanding of the physical bases of ionospheric measurement procedures.

1. The name ionosphere has been accepted for the partially ionized region of the terrestrial atmosphere resulting from shortwave and corpuscular radiation from the sun. The degree of ionization in the ionosphere is sufficient to have an effect on the propagation of radio waves. From this point of view, the lower boundary of the ionosphere is at a height of approximately 50 kilometers, and sometimes lower than that [117]. The upper boundary of the ionosphere is not quite as definite but evidently is at a height of ~ 2,000 km [27]. The individual physical parameters of the gas change by more than five orders of magnitude within the limits of the ionosphere.

The degree of ionization of the ionosphere, that is, the electron concentration N, depends on the energy of the ionizing radiation from the sun, the coefficient of absorption of this energy by the gas, and the original density of the atmospheric gas. Since atmospheric density decreased with height, and since solar radiation entering the atmosphere from above and ionizing it decreases with decrease in height, there is some height at which the degree of ionization should be maximum. This process should lead to the appearance of a maximum for N on an electron concentration-height curve, N(h). But the composition of the atmosphere is complex, its different components are ionized in different ways by different sections of the solar spectrum [78], so several maxima are formed on the N(h) curve, and these are particularly sharp in the daytime. These maxima usually are identified with the positions of individual "layers," or "regions," of the ionosphere. These layers are called the D, E, F1, and F2 layers in order of increasing height. The height, thickness, and degree of ionization of the ionospheric layers have a significant dependence on time of day (local), season of the year, and level of solar activity, as well as on the coordinates, naturally. Figure 0.1 shows typical day and night N(h) distributions. Data are for the middle

---

* Numbers in the margin indicate pagination in the foreign text.

latitudes and have been reduced individually for solar activity maximum and minimum. Above the maximum for the F2 layer the electron concentration decreases slowly and monotonously to a distance of several earth radii where it becomes comparable to the concentration of electrons in the interplanetary medium.

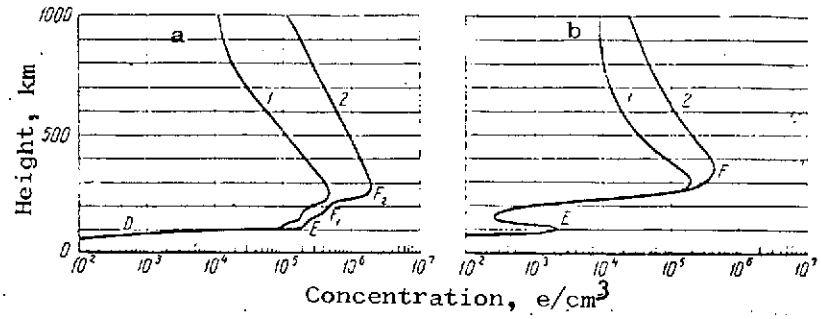


Figure 0.1. Distribution of electrons at time of solar activity extrema. a - day; b - night; 1 - minimum; 2 - maximum.

The ionosphere as an entity is a quasi-neutral medium, that is, the sum of the electron concentration and the concentration of negative ions is equal to the concentration of positive ions. The fundamental processes determining the state of the ionosphere are ionization of neutral gas, recombination of charged particles, diffusion of electron-ionized gas in the gravity field, and drift of charted particles. The general form of the ionization balance equation is

$$\frac{dN}{dt} = q - L - \operatorname{div}(N\overline{V}) = q - L - N \operatorname{div}\overline{V} - \overline{V} \operatorname{grad} N, \quad (0.1)$$

where

q is the ion production and electron liberation rate; /6

L is the charged particle disappearance rate;

$\overline{V}$ is the mean rate of charged particle motion.

If it is taken that $\overline{V}$ and N change much more rapidly vertically than horizontally

$$\operatorname{div}\overline{V} \approx \frac{dV_z}{dh} \quad (0.2)$$

$$\operatorname{grad} N \approx \frac{dN}{dh} \quad (0.3)$$

where

$V_z$ is the vertical, upward directed, component of the motion,

so that Eq. (0.1) becomes

$$\frac{dN}{dt} = q - L - \frac{d(NV)}{dh} = q - L - \frac{NdV_z}{dh} - \frac{V_z dN}{dh}. \qquad (0.4)$$

All of the magnitudes included in Eq. (0.4) are complex functions of coordinates and time. Special monographs [78, 115, 63] are devoted to analysis of photochemical reactions, ionization-recombination processes. What is of importance to us is that ionospheric measurements of N(t, h), taken by different methods, are the experimental basis for calculating these magnitudes and for checking the theoretical hypotheses with respect to the coefficients of rates of these reactions, of the influence of temperature, diffusion, and electromagnetic forces on the dynamics of charged particles, and the like.

The motion of charged particles in the ionosphere under the influence of hydrodynamic and electromagnetic forces is the motion of a conductor in a geomagnetic field, with the result that a current is induced. The current is created in that part of the ionosphere that has come to be called the "dynamo region" (up to 140 km). The dynamo current is accompanied by an electrostatic field which, evidently, can reach the higher regions of the ionosphere, causing currents to flow there as well. Their interactions with the geomagnetic field can cause electron-ion gas to move into these distant regions of the ionosphere. The currents in the ionosphere are the source of the observed geomagnetic variations. It is possible, by assigning equations of motion, to calculate the ionospheric currents, but, on the other hand, we can, proceeding from the magnitude of the currents in the E region, calculated with respect to geomagnetic variations, determine the nature of the motions these currents could cause, as well as movements in the F region. Here the ionosphere is considered to be an anisotropic conductor with conductivity tensor T = $\overline{j}/E$, where $\overline{j}$ is current density and E is the electric field. If E and the intensity of the magnetic field, H, are mutually perpendicular, the conductivity tensor is

$$T = \begin{vmatrix} \sigma_1 & -\sigma_2 & 0 \\ \sigma_2 & \sigma_1 & 0 \\ 0 & 0 & \sigma_0 \end{vmatrix}, \qquad (0.5)$$

where

$$\sigma_0 = \left(\frac{n_e}{m_e \nu_e} + \frac{n_i}{m_i \nu_i}\right) e^2, \qquad (0.6)$$

$$\sigma_1 = \left[\frac{n_e}{m_e \nu_e}\left(\frac{\nu_e^2}{\nu_e^2 + \omega_e^2}\right) + \frac{n_i}{m_i \nu_i}\left(\frac{\nu_i^2}{\nu_i^2 + \omega_i^2}\right)\right] e^2, \qquad (0.7)$$

$$\sigma_2 = \left[\frac{n_e}{m_e \nu_e}\left(\frac{\omega_e \nu_e}{\nu_e^2 + \omega_e^2}\right) + \frac{n_i}{m_i \nu_i}\left(\frac{\omega_i \nu_i}{\nu_i^2 + \omega_i^2}\right)\right] e^2. \qquad (0.8)$$

In Eqs. (0.6)-(0.8) n, m, and v are the concentration, mass, and frequency of collision of charged particles; $\omega = (eH)/(mc)$ is the gyrofrequency. The subscripts e and i refer to the electrons and heavy ions, respectively. $\sigma_0$ is the conductivity along the geomagnetic field, $\overline{H}$, that is, the so-called longitudinal conductivity. $\sigma_1$ is the conductivity along the electric field, E, the transverse conductivity. $\sigma_2$ is the so-called Hall conductivity, associated with the current component perpendicular to the electric field, E (the Hall effect).

Experimental measurement of the motion of a neutral gas, and of charged particles, in the lower ionosphere containing the dynamo region, as well as in the F region, should be the primary means for obtaining information concerning ionospheric currents and conductivity, and for verifying the basic assumptions of the "dynamo theory."

The D region (50-85 km) is the lowest, and least studied, region of the ionosphere. Investigation of this region by radio and physical methods is made much more difficult by the relatively low electron concentration, requiring the use of low frequencies for the investigations (see section 1.1), and by the high frequency of collisions, leading to great attenuation of electromagnetic waves. This is why rocket measurements provide the principal data on aeronomic processes in the D region, as well as on the ion and electron structure. Radio and physical methods, such as the measurement of the absorption of radio waves passing through the D region, measurement of the polarization of these waves, study of cross modulation phenomena, the use of weak, partially reflected, low radio frequencies from the region during pulse sounding, phase and amplitude measurements during the propagation of radio waves at frequencies below 150 kHz over main radio lines, study of the propagation of very-low oscillations of the atmospherics type ($\sim$ 10 kHz) in the "earth-ionosphere" waveguide, provide indirect, supplemental, albeit undoubtedly extremely valuable, information.

The electron concentration maximum in the D layer is near 80 km and is of the order of $10^3$ e/cm$^3$. The D layer virtually disappears at night, the result of recombination of electrons with positive ions and the attachment of electrons to neutral atoms to form negative ions. Negative ions play a bigger part in the physical processes taking place in the D region than they do in other regions of the ionosphere.

The properties of the D region, and the degree to which they act on radio

waves, is unusually closely associated with solar activity. Experimental research has shown that the magnitude $\int$ Nvdh for the D region has a 27-day periodicity, characteristic of the variation in solar activity, and this correlates well with variations in the number of sun spots, R. This correlation is greater in the summertime in the middle latitudes. Sudden ionospheric disturbances, the result of solar flares, and causing virtually total curtailment of long-range shortwave radio communication over the whole of the illuminated hemisphere (radio /8 blackouts), also are the result of an increase in ionization in the D region. Changes in the D region of the polar ionosphere determine absorption of radio waves at the polar cap and in the auroral zone (see section 2.2).

The E region of the ionosphere (85-140 km) is formed by the effect of soft X-ray solar radiation, with the principal ions in this region molecular oxygen, $O_2^+$, and nitric oxide, $NO^+$. The electron concentration in the E region at noon is of the order of $10^5$ e/cm$^3$ in a period of minimum solar activity, and approximately 50% greater in a period of maximum. N changes with time of day, season, and latitude, and for a specified level of solar activity, the concentration at the layer maximum, $N_{max}$, is approximately a unique function of the sun's zenith distance, $\chi$, where $\chi$ changes with respect to time for a given point, or with geographic position for a given moment in time. This relationship can be found from

$$N_{max} = \left[\frac{q_0}{\alpha}\cos\chi\right]^{1/2}, \qquad (0.9)$$

where

$q_0$ is the ion formation rate when $\chi = 0$;

$\alpha$ is the so-called effective recombination coefficient, with $\alpha \approx 10^{-8}$ cm$^3 \cdot$sec$^{-1}$.

The electron concentration in the E layer has a maximum at about midday and fades almost symmetrically on either side of that maximum. Globally, the maximum N is observed at the equator, with gradual fading toward the poles. The E layer usually exists in the daytime, but residual ionization often can be observed at heights in the region, and this is the night E layer in which electron concentration experiences rapid, irregular, oscillations.

Often observed inside the E region is an increased electron concentration in a thin layer (a few kilometers) at a height of about 100 km as compared to higher and lower regions. This phenomenon is called the sporadic E layer ($E_s$).

The $E_s$ layer usually forms at night in the high latitudes, and during the day near the magnetic equator. Seasonal variations in the frequency of appearance of the $E_s$ layer, and in its intensity in these latitudes, are small. The $E_s$ layer is less intense in the middle latitudes and the diurnal variation is ill-defined. At the same time, the seasonal variation is extremely well-defined. The maximum for frequency of appearance of the $E_s$ layer in the middle latitudes is found in the summer, during the day. The $E_s$ layer, particularly in the high latitudes, is closely associated with the intrusion into the terrestrial atmosphere of streams of high-energy particles, with the aurorae, and with geomagnetic disturbances. The $E_s$ layer characteristics in the middle latitudes correlate well with the quantity of meteoric matter burning in the atmosphere at heights close to the $E_s$ layer height. There are experimental data pointing to a close connection between the $E_s$ layer and the wind regime in the E region of the ionosphere, and with turbulence [42]. Certain properties of the $E_s$ layer, such as its often observed semitransparency to radio waves, for example, can evidently be explained by the fact that the distribution of the electron concentration in the horizontal direction is nonuniform, while the $\Delta N/N$ ratio in the nonuniformities is quite large (N is the concentration of electrons in the medium surrounding the nonuniformity, $\Delta N$ is the difference between the electron concentrations within and outside the nonuniformity).

The F1 region of the ionosphere, intermediate between the E and F2 regions, is found at heights of 160-200 km. The electron concentration maximum is at heights of 170-180 km. The F1 layer appears most frequently during the summer, in the daytime, and during periods of solar activity minima. The F1 layer does not appear at all at night, during solar activity maxima, or at any time during the winter. The electron concentration at the layer maximum, $N_{max}$, changes with season and geographic position approximately in accordance with Eq. (0.9), where $\alpha \approx 5 \cdot 10^{-9}$ $cm^3 \cdot sec^{-1}$. It is true that the exponent differs somewhat in the case of $(\cos \chi)^n$; $n < 0.5$ for solar activity minimum. Seasonal variations /9 in this magnitude can be observed as well. The nonsteady-state nature of the processes taking place in the ionosphere, and associated with dynamic processes in the neutral medium, influence the conditions under which the F1 layer appears. The observed asymmetry in the diurnal behavior of the frequency of appearance of the F1 layer is indicative of this fact, and the nature of the asymmetry is

clearly latitudinal. Conditions for the development of the F1 layer are more favorable during the forenoon hours in latitudes above 50°, but the reverse is true in the zone of latitudes below 35 to 40°. Systematic asymmetry does not occur in the intermediate zone. Observation of the F1 layer, and measurement of its characteristics, can yield valuable information on the structure of the neutral atmosphere under ionospheric conditions, and on the ion structure of the ionized component [115].

The F2 region of the ionosphere is the broadest and most complex region above 200 km. The principal ions in this region are atmospheric nitrogen and oxygen ($N^+$ and $O^+$), with heavy predominance of $O^+$ [115, 65]. The electron concentration at the F2 maximum changes in a complex manner, while the effective recombination coefficient, $\alpha$, changes with height from $10^{-9}$ $cm^3 \cdot sec^{-1}$ at the base to $10^{-12}$ $cm^3 \cdot sec^{-1}$ in the upper part of the region. The behavior of the F2 layer can be characterized by significant deviations from the conclusions of elementary theory, with which, let us say, the behavior of the lower-lying layers agrees. These deviations have come to be called the "F2 layer anomalies." Well known is the diurnal anomaly, when the concentration of electrons at the layer maximum at noon does not have a maximum, as should be the case in accordance with simple theory, but a clear-cut minimum. The diurnal variation in $M_{max}$ usually either has one maximum, greatly displaced relative to noon, or two maxima. The geographic anomaly appears because there is, near the magnetic equator, a minimum in the noon $N_{max}$ in its latitudinal progress when, because of the verticality in the drop in solar radiation, a maximum should have been observed. The seasonal anomaly appears because $N_{max}$ at noon is particularly large during the local winter everywhere, and especially so near the latitute of 50°. There is, in addition, a so-called December anomaly between 50° N and 35° S latitudes during which $N_{max}$ at noon is abnormally large in November, December, and January. The December anomaly intensifies seasonally in the northern hemisphere. The F2 layer winter anomaly is sharpest in the period of maximum solar activity.

The characteristics of the F2 layer, their variations, correlate closely with the overall level of solar activity, as well as with the more detailed phenomena on the sun, such as flares, flocculi, and the like.

The oxygen ion content decreases rapidly above the F2 layer maximum, and hydrogen ions predominate in the outermost region of the ionosphere, with these

latter evidently the result of direct photoionization of hydrogen atoms by solar radiation, as well as that of charge exchanges of the type

$$O^+ + H \rightleftarrows H^+ + O. \qquad (0.10)$$

Helium ions too play an important part in the outer ionosphere.

The theory of the formation of regular ionospheric layers explicitly or implicitly stems from the premise of a so-called smooth, or homogeneous, ionosphere. This ionosphere should be a plasma in which there is, at each given moment in time, a rapid, monotonous, change in electron density N with height, and a slow change in N in the horizontal plane. The real ionosphere, however, has what is substantially an inhomogeneous structure. There is, in the ionosphere, the whole spectrum of irregularities in the electron density, from tens of meters to hundreds of kilometers, and this is in addition to those large-scale irregularities already mentioned in the discussion of $E_s$ layer properties.

Ionospheric irregularities occur as a result of many mechanisms [115], including turbulence in the lower ionosphere, convective type instability, winds /10
in the upper ionosphere, vertical transfer of inhomogeneous electric fields from the dynamo region to the F region of the ionosphere, the intrusion into the ionosphere of streams of charged particles from the radiation belts and of particles of solar origin, propagation within the ionosphere of magnetohydrodynamic oscillations from the boundary of the earth's magnetosphere, and the like. Even this simple listing will indicate the complexity of the inhomogeneous structure and the unavoidably broad spectrum of its parameters.

Ionospheric irregularities participate in the complex motion under the effects of hydrodynamic and electromagnetic forces. It is comparatively simple to detect these irregularities by radio and physical methods (see sections 1.1, 1.4, 1.6), so they serve as unique datum points when studying the dynamics of the ionosphere, the general circulation of the atmosphere at ionospheric levels [83], and plasma drift. At the same time, investigation of the inhomogeneous structure, measurement of dimensions, shape, intensity ($\Delta N/N$) and rate of movement of irregularities in the electron concentration in the ionosphere, is of applied importance because the scattering of radio waves by the irregularities in the ionosphere plays an important role in ground and space radio communication.

2. The peculiarities in the propagation of electromagnetic oscillations in the partially ionized inhomogeneous plasma found in a magnetic field are used in

radio and physical methods of measuring ionospheric characteristics. A huge amount of special effort [53] has been devoted to the theoretical elucidation of this problem, so our task simply is one of citing those fundamental principles and expressions that can be used in echo sounding the ionosphere and in measuring the absorption of radio waves.

An ionized gas with electron density N, disregarding collisions, is, for radio waves, a dispersing dielectric, the relative dielectric constant for which depends on radio wave frequency and electron density, and can be determined from

$$\varepsilon = n^2 = 1 - \frac{N_e^2}{m\omega^2} = 1 - 80.8\,\frac{N\ e/cm^3}{f^2_{kHz}}\ . \qquad (0.11)$$

The presence of large ions need not be considered in this case because $m_i \gg m_e$, and their presence has no significant effect on the index of refraction, n, because we still have not taken collisions into consideration.

Consideration of collisions of electrons with other particles leads us to the fact that the ionized gas becomes dispersing, as well as semiconducting, the relative dielectric constant and conductivity ($ohm^{-1}\cdot m^{-1}$) of which become functions of the effective number of collisions. These latter can be determined from

$$\varepsilon = 1 - 3190\,\frac{N}{\omega^2 + \nu^2}, \qquad (0.12)$$

$$\sigma = 2{,}82\cdot 10^{-8}\,\frac{N\nu}{\omega^2 + \nu^2}. \qquad (0.13)$$

If $\omega^2 \gg \nu^2$ ( a frequent occurrence in the ionosphere)

$$\left.\begin{aligned} \varepsilon &\approx 1 - 80{,}8\,\frac{N}{f^2}, \\ \sigma &\approx 2{,}82\cdot 10^{-8}\,\frac{N\nu}{\omega^2}. \end{aligned}\right\} \qquad (0.14)$$

And if $\omega^2 \ll \nu^2$ (for low-frequency oscillations)

$$\left.\begin{aligned} \varepsilon &\approx 1 - 3190\,\frac{N}{\nu^2}, \\ \sigma &\approx 2{,}82\cdot 10^{-8}\,\frac{N}{\nu}. \end{aligned}\right\} \qquad (0.15)$$

The presence of a geomagnetic field, and the influence of the Lorentz forces /11 on the electrons moving as a result of the effect created by radio waves (gyromagnetic resonance) associated with that field, make the ionosphere a magnetoactive

plasma, an anisotropic medium. The dielectric constant and the coefficient of refraction associated with it become functions of the magnetic field intensity. The ionosphere becomes a double-refracting medium, splitting the radio wave into two rays, the ordinary ray and the extraordinary ray, differing in polarization. In the general case, a linearly polarized ray will be split into two elliptically polarized rays. These rays will be propagated at different velocities because the index of refraction for each will be different, the major axes of their ellipses of polarization are orthogonal, and the directions of rotation of the electric vectors of the waves are opposite.

The index of refraction of an ionized gas, with the geomagnetic field but not collisions, taken into consideration is equal to [67]

$$n_{1,2}^2 = 1 - \frac{\omega_0^2}{\omega^2 - \frac{\omega^2\omega_t^2}{2(\omega^2-\omega_0^2)} \mp \sqrt{\left[\frac{\omega^2\omega_t^2}{2(\omega^2-\omega_0^2)}\right]^2 - \omega_l^2\,\omega^2}}. \qquad (0.16)$$

where

$\omega$ is the radio wave working frequency;

$\omega_0 = Ne^2/m$ is the ionosphere's plasma frequency;

$\omega_t = (eH_t)/(mc)$, $\omega_l = (eH_l)/(mc)$ are transverse and longitudinal (with respect to the direction of wave propagation) gyrofrequencies;

$H_t$ and $H_l$ are the respective geomagnetic field components.

The upper symbol and the subscript 1 refer to the extraordinary ray, the lower and the subscript 2 to the ordinary ray. State of polarization is determined by the ratio of the amplitudes of the transverse components of the wave's electric field. If a plane wave is propagated along the x axis, and if its electric field can be determined from

$$\left.\begin{aligned} E_y &= E_{my}e^{-i\frac{\omega}{c}nx}, \\ E_z &= E_{mz}e^{-i\frac{\omega}{c}nx}, \end{aligned}\right\} \qquad (0.17)$$

under the conditions considered

$$\left(\frac{E_{my}}{E_{mz}}\right)_{1,2} = i\left\{\frac{\omega_t^2\,\omega}{2(\omega^2-\omega_0^2)\omega_l} \pm \sqrt{\left[\frac{\omega_t^2\,\omega}{2\omega_l(\omega^2-\omega_0^2)}\right]^2 + 1}\right\}. \qquad (0.18)$$

Important special cases are the longitudinal ($H_l = 0$) and transverse ($H_t = 0$) propagation of radio waves. Vertical echo sounding of the ionosphere at the geomagnetic pole, and at the geomagnetic equator, corresponds to these cases. Eqs. (0.17) and (0.18) will take the following forms in the case of purely longitudinal propagation

$$n_{1,2}^2 = 1 - \frac{\omega_0^2}{\omega(\omega \mp \omega_1)}, \tag{0.19}$$

$$\left(\frac{E_{my}}{E_{mx}}\right)_{1,2} = \mp i. \tag{0.20}$$

Thus, the polarization of the magnetoionic components is circular, with the upper symbol corresponding to clockwise rotation, and the lower to counterclockwise (when considered along the direction of propagation of the wave). In the case of transverse propagation /12

$$n_1^2 = 1 - \frac{\omega_0^2}{\omega^2 - \frac{\omega^2\omega_t^2}{\omega^2 - \omega_0^2}}, \tag{0.21}$$

$$n_2^2 = 1 - \frac{\omega_0^2}{\omega^2}, \tag{0.22}$$

$$\left|\left(\frac{E_{my}}{E_{mx}}\right)_1\right| = \infty, \qquad \left|\left(\frac{E_{my}}{E_{mx}}\right)_2\right| = 0. \tag{0.23}$$

It is obvious that the expression for $n_2^2$ is in complete coincidence with Eq. (0.11); that is, the transverse magnetic field has no influence on the propagation of an ordinary ray. Polarization of both rays is linear.

Consideration of collisions when a magnetic field is present leads to serious complication of the mathematical expressions for the index of refraction, and the physical consequence of collisions is attenuation of the radio wave at the same time that the coefficients of absorption are different for ordinary and nonordinary rays.

The real ionosphere is an inhomogeneous medium, and this inhomogeneity expresses itself primarily by the change in electron concentration with height in a complex manner, at least from the point of view of the propagation of radio waves. If the ionosphere is considered as a unit layer with one maximum, the electron concentration will increase from its base, and the index of refraction for a radio wave will decrease in accordance with Eq. (0.11) because of its penetration into the layer. This corresponds to curvature of a ray trajectory.

A ray entering a flat (for purposes of simplicity) ionosphere at angle $\varphi_0$ can undergo the phenomenon of complete internal reflection. Let the index of refraction at the point of reflection be $n_n$ (and the angle of incidence at this point be $\varphi_n = 90°$). The condition required for reflection is, in accordance with the laws of optics

$$\sin \varphi_0 = \sin \varphi_n n_n = n_n. \tag{0.24}$$

Substituting Eq. (0.11) for $n_n$

$$\sin \varphi_0 = \sqrt{1 - 80{,}8 \frac{N}{f^2}}. \tag{0.25}$$

Assuming the ray to be incident vertically ($\varphi_0 = 0$):

$$\left.\begin{aligned} 0 &= \sqrt{1 - 80{,}8 \frac{N}{f_v^2}}, \\ f &= f_v \sec \varphi_0. \end{aligned}\right\} \tag{0.26}$$

This expression, defining the relationship between the frequency of flat ray f and vertical ray $f_v$, reflected from the same region of the ionosphere, is called the "secant law" and has a fundamental value for the ionospheric propagation of radio waves.

The Eq. (0.24) reflection condition shows that one always can find that value $\varphi_0$ so as to have reflection from the ionosphere for a specified N value. But this relationship is valid only for a "flat" ionosphere and for the terrestrial surface. The sphericity of the earth and of the concentric ionosphere limit the upper value of $\varphi_0$ because the flattest ray is tangent to the earth's surface. This value, $\varphi_{0\,max}$, is determined by the curvature of the earth's surface and by the height of the point of reflection in the ionosphere (Figure 0.2)

$$\sin \varphi_{0max} = \frac{a}{a + h}, \tag{0.27}$$

where

a is the radius of the earth;

h is the height of the ionosphere.

This limitation of $\varphi_0$ means that for a specified N value at the point and a specified angle of elevation, $\beta$, of radiations of radio waves (angle with the horizon), radio waves with a frequency higher than some maximum will not be reflected from this point in the ionosphere, but will be propagated above it. Quite obviously, the maximum reflection frequency under these conditions will be

associated with the maximum value for the electron concentration in the layer, $N_{max}$. This frequency can be found from

$$f_{max} = \left[\frac{80{,}8N_{max}\left(1+\frac{2h}{a}\right)}{\sin^2\beta+\frac{2h}{a}}\right]^{\frac{1}{2}}. \qquad (0.28)$$

When $\beta = 0$ (the flattest ray)

$$f_{max\,0} = \left[\frac{80{,}8N_{max}\ (a+2h)}{2h}\right]^{\frac{1}{2}}. \qquad (0.29)$$

Radio waves with frequency $f > f_{max\,0}$ are not reflected from the given layer of the ionosphere, but pass through the latter.

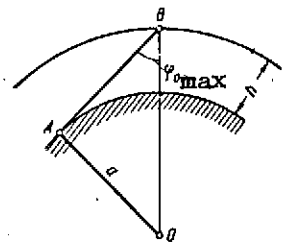


Figure 0.2. Determination of maximum angle of incidence on the ionosphere.

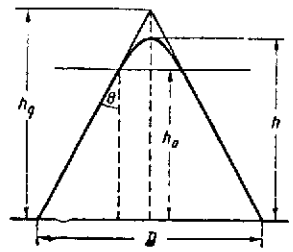


Figure 0.3. Actual and equivalent trajectories for a wave.

When $\beta = \pi/2$, (vertical incidence on the ionosphere)

$$f_{max\,\frac{\pi}{2}} = [80{,}8N_{max}]^{\frac{1}{2}}. \qquad (0.30)$$

This maximum frequency, reflected from a specified ionospheric layer when there is vertical incidence, is called the critical frequency.

We know [53] that electromagnetic waves are propagated in an ionized gas at group velocity, $V_g < c$, whereas they have curved trajectories in the ionosphere. The actual curved trajectory of propagation at velocity $V_g$ often is replaced in practical calculations by the so-called equivalent trajectory with a propagation velocity equal to the velocity of light in free space, c. The equivalent trajectory is composed by constructing an isosceles triangle with base D (Figure 0.3) and altitude $h_a$, where $h_a$ is the actual height of reflection, determined from ionospheric measurements using vertical radio sounding (see

section 1.1). This transition from the actual to the equivalent trajectory simplifies the calculations and makes it possible to determine the angle of incidence of the ray at the lower boundary of the ionosphere.

PART ONE

MEASUREMENT OF IONOSPHERIC PLASMA CHARACTERISTICS

## 1.1. The Pulse Radio Sounding Method

The concentration of free electrons is one of the basic, characteristic parameters of ionospheric plasma with purely scientific, as well as great applied, value. There are different ways in which to determine this parameter. The most widely used one is the pulse radio sounding, first used by Breit and Tuve in 1925, to observe the condition of the ionosphere. /14

The physical basis of the method is one of relationships determining the magnitude of the index of refraction in a magnetically active plasma and of conditions for the reflection of radio waves propagating in such medium. The method is realized as follows in practice.

A pulsed transmitter on the terrestrial surface radiates a series of pulses. Their width is of the order of $10^{-4}$ to $10^{-5}$ second, so quasimonochromatic groups of waves are radiated into the ionosphere. Analysis of the propagation of such quasimonochromatic pulses [53, 54] leads to the belief that the pulse is propagated into the ionosphere as a single whole, without significant distortions. The pulse is propagated along a straight line at speed c from the earth's surface to the beginning of the intrinsically ionized region. Then, as has been pointed out, the pulse trajectory curves. Its propagation rate begins to change at the same time. The rate is lower the higher the concentration of free electrons determining the index of refraction. The pulse rate drops to zero at the point for which satisfaction of Eq. (0.26) is characteristic, and reflection takes place from this region.

The concept of a group path, $L_g$, which can be found because if the pulse traveled its path from the point of radiation to the point of recording after reflection from the layer in a vacuum at speed c

$$L_g = c\Delta t_g, \tag{1.1}$$

is introduced to simplify the solution.

Time $\Delta t_g$, called group delay time, can be found in accordance with [53] as the time interval between recording times at some fixed observation point of

radiated and reflected signals. The magnitude $\Delta t_g$ has a clearly expressed physical meaning and can be measured experimentally. Pulses with sufficiently steep edges must be selected to achieve a high degree of accuracy in its determination (because, as has been pointed out, particularly in [34], accuracy /15 in recording the pulse with respect to time is fixed by the width of its spectrum).

In the simplest (classical) variant of realization of the pulse method, the pulses are radiated vertically upward and the receiver is in the immediate vicinity of the transmitter. In this case the group delay time is determined as the dual passage of the pulse over the distance from the radiation-reception point to the region in which the reflection is formed. Clearly, then, the true height of the point at which pulse reflection took place (segment $O_1A$, Figure 1.1) is hard to establish. Consequently, the apparent height of reflection can be determined directly during the experiment by assuming that the pulse travels its path to the point of reflection and back at constant speed, equal to the speed of light in a vacuum. Then the apparent (actual) height of the point of reflection can be determined from the measured time interval, $\Delta t_g$, by using the simplest of relationships

$$h' = c\Delta t_g/2. \qquad (1.2)$$

### 1.1.1. Variable frequency sounding

The basic task of the pulse method of investigating the ionosphere is to obtain a profile of the distribution of electron concentration in terms of height.

If the transmitter carrier frequency is changed, pulses characterized by different $\omega$ values will be reflected from regions with different electron density as per Eq. (0.26). Since electron density changes with height, these pulses experience group delays that differ in magnitude. The possibility therefore arises of an experimental way to obtain the height profile of the electron concentration in the ionosphere.

It should be recalled that only signals reflected from the ionosphere are recorded in this way. And since reflection can be obtained only if the index of refraction is reduced by virtue of penetration into the layer, we can, by using this method, record only those sections of the height profile of the electron concentration that can be characterized by an electron concentration

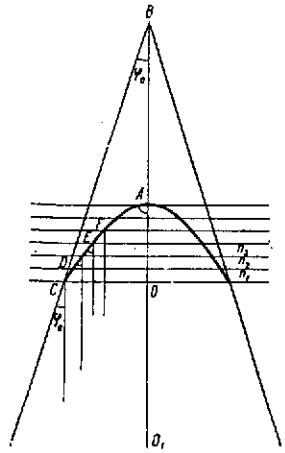

Figure 1.1. Trajectory of a radio wave reflected from a plane-layered ionosphere.

increasing monotonically with height. If the profile is nonmonotonic, those sections of it associated with reduction in $N_e$ with increase in height will not be recorded. Specifically, it is impossible to obtain electron concentration distribution above the main ionization maximum, where the number of free electrons begins to decrease with increase in h, by sounding from the earth's suface. A similar comment should be made with respect to interlayer ionization. The method must be modified by changing the technique used to conduct the experiment, or by advancing additional physical premises, in order to answer the question of how electron concentration changes with height in the intervals between layers and above the main maximum.

We can obtain a so-called height-frequency curve (HFC), the real (apparent) height of reflection of a radio pulse in terms of its carrier frequency, directly from the experiment. Analysis of the h'(f) configuration can be used to determine many ionospheric parameters, particularly the critical frequencies of the layers of the ionosphere, and their height, characteristic knowledge of which is of primary importance for providing stable, and dependable, radio communication.

Analysis of the results obtained by the pulse method of sounding the ionosphere with a variable frequency enables us to estimate a number of other parameters characterizing the condition of the atmosphere, and this is in addition to the data obtained on electron concentration distribution. A direct determination can be made, in particular, of the ionization-recombination constants of many ionospheric processes by analyzing temporal variations in the magnitudes recorded during the experiment. The possibility of making these determinations is all the more significant because this is practically the only method for making direct estimates of these constants on mass scales because rocket experiments,

/16

which also make it possible to obtain these estimates, are single, brief, events.

Clearly, then, pulse sounding of the ionosphere with a variable frequency makes it comparatively simple to obtain a large volume of information on the condition of the ionosphere, and is, therefore, at this time, the most widely used method of obtaining information on basic ionospheric parameters.

## Basic Specifications

Ionosondes (ionospheric sounders) can be used for pulse sounding of the ionosphere. Figure 1.2a is a simplified block diagram of an ionospheric sounder.

The transmitter, which operates in the pulse mode, radiates pulses at radio frequencies the carrier of which changes in limits ensuring reflection from the entire thickness of the ionosphere during the sounding session. A receiver, synchronized with the transmitter, operates such that it always can receive signals radiated by the transmitter and reflected from the ionosphere. A broadband antenna system radiates the signals.

The use of a common master oscillator serves to synchronize the operation of transmitter and receiver. This will be taken up in more detail below when the detailed functional diagram is analyzed.

Incoming signals are displayed on a scope which, in addition to the echoes, is supplied with height and frequency calibration markers from special generators.

The sounder, in addition to the units mentioned, has a control unit, a synchronizer that matches the operation of all units in the ionospheric sounder.

Let us, briefly, formulate the specifications for an ionospheric sounder.

1. The limits of change in the carrier frequency are limited by the range of possible values of electron concentration encountered in the ionosphere. Known is the fact that the upper limit of N is $5 \times 10^6$ e/cm$^3$, corresponding to a critical frequency of 20.0 MHz. The lower the electron concentration, the lower the carrier frequency used to obtain reflections from the layer. Absorption of the sounding signal begins to increase sharply with approach to the lower limit of N values, and this calls for a substantial increase in radiated power. There remains a whole series of technical limitations associated, in particular, with making the antenna systems more complicated. This is why the low frequency limit of the majority of ionospheric sets is selected as 1.0 MHz, corresponding

to a free electron concentration of $1.5 \times 10^4$. This is quite satisfactory for fixing the lower boundary of the E region.

2. Consideration of the physical behavior patterns determining the formation of the ionosphere (see Introduction) shows that the main ionization maximum, distribution of an electron concentration above which it is impossible to radiate using the method under consideration, is no more than 500 km above the terrestrial surface. Bear in mind that the pulse radiated by the sounder transmitter can be reflected from the ionospheric layer, as well as from the terrestrial surface, many times, forming so-called multiple reflections, investigation of which is known to be of interest. Also to be taken into consideration is the fact that a pulse propagated in an ionized medium is greatly delayed, particularly during /18 the approach to critical frequencies.

These considerations are the basis for the selection of the range of heights for the installations, limited by the magnitude of the time interval between two successive main pulses, by the duration of one cycle of operation of the sounder. If the interval between adjacent pulses is too small, the reflections from the layers at great heights (and multiple reflections in particular) will be recorded by the receiver during the next unit cycle, and this can lead to distortion of the real physical picture. The command pulses controlling sounder operation usually are shaped from the alternating current at the industrial frequency supplying the sounder. The interval between two pulses is 3,000 km, based on the calibration used for the height scale. The low limit of the height range will be determined by the receiver channel time constant, that is, by the time interval after which the receiver is restored to normal response. This usually is a few score kilometers.

3. The delay between signal radiation and reflection from the ionosphere should be recorded with a predetermined accuracy, not below that of some specified value. In accordance with the theory of optimum reception, the accuracy with which a pulse signal is recorded on the time axis is determined by the width of the signal frequency spectrum. This imposes a requirement on the shape of the main pulse. Its edges should be steep enough, yet impose limitations on the bandwidth of the sounder's receiving channel.

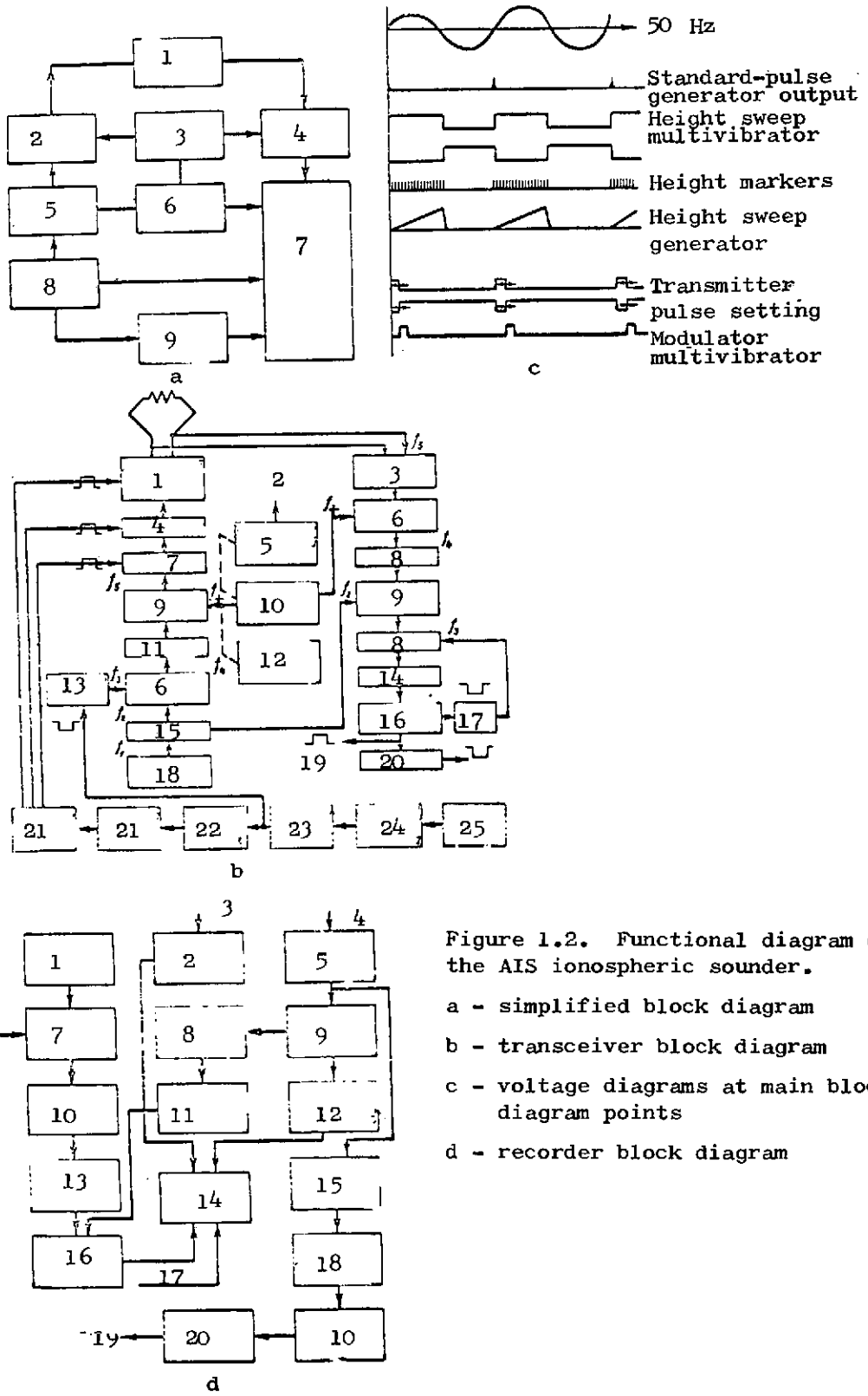


Figure 1.2. Functional diagram of the AIS ionospheric sounder.

a - simplified block diagram

b - transceiver block diagram

c - voltage diagrams at main block diagram points

d - recorder block diagram

LEGEND FOR FIGURE 1.2.

Figure 1.2 a.

1 - antenna system; 2 - transmitter; 3 - master oscillator; 4 - receiver; 5 - modulator; 6 - frequency markers generator; 7 - scope; 8 - synchronizer; 9 - height markers generator.

Figure 1.2 b.

1 - push-pull power amplifier; 2 - to horizontal sweep amplifier; 3 - input stage; 4 - phase inverter; 5 - horizontal sweep potentiometer; 6 - 1st mixer; 7 - broadband amplifier; 8 - IF amplifier; 9 - 2nd mixer; 10 - continuously-functioning local oscillator, 31-48 MHz; 11 - amplifier; 12 - controls for cams and contacts; 13 - 0.9 MHz local oscillator; 14 - detector; 15 - multiplier; 16 - video-amplifier; 17 - automatic gain control; 18 - quartz oscillator; 19 - video signal; 20 - video; 21 - cathode followers; 22 - pulse modulator amplifier; 23 - transmitter trigger multivibrator; 24 - transmitter pulse setting; 25 - synchronizer.

Figure 1.2 d.

1 - 1 MHz quartz oscillator; 2 - horizontal sweep amplifier; 3 - from horizontal sweep potentiometer; 4 - 50 Hz; 5 - synchronizer; 6 - from continuously-functioning local oscillator, 31-48 MHz; 7 - mixer; 8 height markers generator, 3 kHz; 9 - height markers multivibrator; 10 - amplifier; 11 - shaper and amplifier; 12 - sawtooth generator vertical sweep amplifier; 13 - frequency markers multivibrator; 14 - B scope; 15 - transmitter pulse setting; 16 - markers mixer; 17 - video signal; 18 - modulator multivibrator; 19 - to modulator cathode follower; 20 - cathode follower.

The width of the edges of pulses radiated by the transmitter of an ionospheric sounder usually are of an order of magnitude of 10 μsec, imposing the need to use a receiver with at least a 10-15 kHz band. Here the potential accuracy in the determination of the pulse's height coordinate is ±0.45 km for a signal/noise ratio of 6 to 8.

4. The sounder should be able to function under radio reception conditions that change greatly. Set operation should be possible when industrial and other noise levels are high. Moreover, heavy ionospheric absorption, when the signal reflected from the ionosphere will have a very small amplitude, should be anticipated. At the same time, the sounder should generate as little radio noise as possible.

All of this means that the receiving channel in the sounder must be very responsive, and that the transmitter must radiate a pulse with sufficiently high power. The magnitudes of these parameters vary substantially, even within the limits of sounders of the same class. Long years of experience in the operation of sounders have established that the pulse power radiated must be in kilowatts, and that the response of the receiving channel must be 5 to 10 μV at the input, in order to be optimum for performing typical sounding tasks (taking observations in accordance with the standard international program).

5. It is desirable to obtain sounding data in a form that lends itself to effective use, to operational processing at the time the experiment is conducted, and to long-term subsequent storage.

This set of specifications is extremely broad, and often contains contradictions. It imposes a series of rigid conditions on the standard units used to build ionospheric sounders, and these conditions sometimes simply cancel each other out. Since they cannot be met in toto, compromise often is resorted to, ignoring certain of the specifications according to the specifics of the task assigned, and the conditions under which the set will be operating.

## Functional Diagram of a Modern Ionospheric Sounder

Let us consider each of the main units in the sounder shown in Figure 1.2a /19 in more detail, focusing attention on the sounder's functional purpose, and on those principle and design features that caused the unit to be used in the

particular block diagram. The circuitry adopted for the design of the type AIS panoramic ionospheric sounder will be considered the main variant [137].

Master Oscillator

One of the basic requirements imposed on sounders for panoramic vertical sounding is that of generating radio frequencies in the interval permitting the reception of reflections from all the main ionospheric layers. In accordance with what has just been said, the band from 1.0 to 20 MHz is optimum. Coverage of this band is quite a complicated engineering problem. Earlier models divided this band into subbands by using changeable tank circuits, switched mechanically [123]. This breakdown into subbands subsequently was done away with in favor of the dual frequency conversion principle.

What this operation amounts to, in essence, is that the original carrier frequency, $f_1$, is transformed by a device called a frequency converter into another radio frequency, $f_2$. This results in a nonlinear conversion (in the adding of the original oscillations, the source of which is the master oscillator, to the oscillations of a second oscillator, called the local oscillator) into an intermediate frequency differing from the original carrier value [124]. This operation improves the response of the receiving stages, as well as their noise resistance.

A single master oscillator is used in the absolute majority of types of modern ionospheric sounders to obtain the frequencies for the transmitter and receiver operating bands, and to obtain the frequency markers. Use of a common oscillator provides a simpler and more reliable method of synchronous tuning of the circuits in the sounder's receiving and transmitting sections. The oscillator frequency is continuously adjustable from 31 to 50 MHz.

The magnitude of the time period over which the master oscillator should cover the entire frequency spectrum must be estimated. Earlier sounder models took quite a long time to cover the frequency band. A long session ensured a sufficiently high degree of reliability of the data received because a large number of pulses were radiated at approximately the same frequency (the frequency changed continuously, but slowly). However, slow coverage of the frequency band had its own adverse aspects. The chief drawback was the inability to record rapid changes in the ionosphere. It is extremely important, for example, to have a series of ionograms (height-frequency curves) following one after the other when analyzing vertically changing disturbances. The time

spent on a single session began to decrease just as soon as this became possible, and today most sounder designs incorporate an interval the magnitude of which is of the order of 20 to 30 seconds and which is optimum for the majority of the tasks that must be performed by the vertical panoramic sounding method. Continuous change in the generated frequency (the natural frequency of the master oscillator circuit) takes place with rotation of the rotor of a variable condenser.

Known from the practice of ionospheric observations is the fact that the /20
critical frequencies of the main ionization maximum (the limit frequencies at which reflections from the layer still can be observed) change substantially during the day, and from session to session. There are, therefore, quite long time intervals when there is no need to use all the frequencies generated up to the maximum. In such cases it is desirable to change the frequency band, and this is done by switching the fixed condensers in the master oscillator circuit. This is the procedure used in the AIS sounder to switch from the 1-18 MHz band to the 1-10 MHz band.

Use of the narrower band makes it possible to more carefully study the layer structure, because in this case the image of the height-frequency curve is formed at a larger scale. A similar comment can be made concerning change in the height band.

Ionospheric Sounder Transmitter

The dual frequency conversion principle, well known from the literature and widely used in different radio installations, is used to generate the carrier frequency within specified limits.

The application of this principle does away with mechanical switches and covers the frequency band with one tuner, a variable condenser in the master oscillator. Moreover, use of dual frequency conversion improves such characteristics of the sounder's receiving channel as response and noise resistance [124].

The circuitry in the transmitter in the ionospheric sounder is about as follows (Figure 1.2b).

The quartz local oscillator generates oscillations at frequency $f_1$. It is used to improve the stability of the frequencies radiated by the transmitter.

A multiplier is used in the transmitter circuit because there is no way to engineer the direct generation of sufficiently high frequency. The multiplier tube functions to quadruple the frequency, and its plate circuit contains a circuit for this purpose tuned to the fourth harmonic of the frequency generated by the quartz local oscillator.

Oscillations at frequency $f_2 = 4f_1$ are fed into the input of the 1st mixer in the transmitter where they are mixed with oscillations at frequency $f_3$, fed into this same mixer from the output of the corresponding oscillator. This oscillator, as will be seen from the block diagram, functions in the pulse mode.

The 1st mixer load is a circuit tuned to the summed frequency $f_4 = f_3 + f_2$. Radio pulses filled by the carrier frequency, $f_4$, are separated in the circuit.

These pulses are fed into the input of the transmitter's 2nd mixer. Oscillations from the output of the master oscillation, $f_t$, also are fed into the input to this mixer. The frequency changes continuously between 31 and 50 MHz. Since the value of frequencies $f_2$ and $f_3$ were selected such that $f_4 = 30$ MHz, oscillations at the difference frequency, $f_5 = f_t - f_4$, will be separated at the output of the 2nd mixer and will be those in the 1-20 MHz band we require. They are amplified by a wide-band amplifier (Figure 1.2b) and are fed to the antenna through isolating condensers and the antenna relay contacts.

Radiated pulse power will vary from hundreds of watts to as much as 15 to 20 kW, depending on the conditions under which it is proposed to operate the ionospheric sounder. The power of ionospheric transmitters sometimes is raised to several decades of kilowatts for special investigations. The concrete circuity for the transmitter used in the AIS (three stages of wide-band amplification and a final push-pull stage using a GMI-83 tube [38]) provides delivery of a 2.5 kW pulse to the antenna.

Modulator

A special set of modulators is included in the circuitry to provide for /21
transmitter operation in the pulse mode. To this end, those stages that should operate in the pulse mode are under constant negative bias. They function only when a modulating pulse is supplied to their control inputs.

The basis of the modulator unit is a multivibrator generating a rectangular

pulse of the order of a few tenths of a microsecond in width with what are approximately ten-microsecond edges. Conventional multivibrator circuits [28] are reliable for generating a voltage of similar shape.

The multivibrator circuitry used in the modulator unit usually is such that the width of the shaped pulse can be changed within certain limits (in the AIS from 50 to 70 μsec). The pulse, after shaping, is fed from the multivibrator output to the modulating pulse amplifier, then through a series of cathode followers to the grids of the tubes that should function in the pulse mode. It is desirable to use separate transmitter stage control to improve the operating stability of the high-frequency stages in the transmitter circuits. An individual cathode follower can be used to supply the modulating pulse to each stage. This will diminish significantly the interaction between the stages.

Receiver

The receiver in the ionospheric sounder is designed to amplify the high-frequency pulses reflected from the ionosphere and picked up by the antenna and to convert them into direct current pulses (video pulses) which then are fed to the scope. Modern sounders use receivers of the superheterodyne type with dual frequency conversion. The radio signals reflected from the ionosphere, and the oscillations from the output of the master oscillator, are fed into the first mixer input. Since the radiated and received frequency is $f_5 = f_t - f_4$, and since this frequency is constantly mixed with frequency $f_t$, there always will be difference-frequency oscillations at the output of the first mixer of

$$f_t - f_5 = f_t - (f_t - f_4) = f_4.$$

A second mixer, supplied with oscillations at frequencies $f_4$ and $f_2$, is included after amplification of the first intermediate frequency. The difference frequency $f_4 - f_2 = f_3$ (see above) is fed from the output of this mixer to the 3-stage resonant amplifier.

The significant point to be made concerning the resonant stage in the receiver is their bandwidth. The bandwidth should be selected such that signals reflected from the ionosphere will be received without significant distortion. A bandwidth of the order of 15 kHz is sufficient to meet this requirement. Generally speaking, the bandwidth can be narrower, but this will result in distortion in

the shape of the received pulse, to pulling of its edges [53]. At the same time, the potential accuracy in the recording of the temporal position of the pulse, and thus of the height coordinate of the record reflection, will be reduced. The receiver channel bandwidth also should include the fact that the frequency to which the receiver is tuned changes continuously. This means that the carrier frequency of a pulse reflected from different heights will differ to a different degree from the frequency to which the receiver is tuned at the time the signal is received. The receiver channel must have a sufficiently wide bandwidth if the time to cover the sounder's frequency band has been selected as short if dependable reception of reflected signals is to take place over the /22 whole of the range of heights. If, for example, radiation takes place for 5 seconds between 1 and 16 MHz, the carrier frequency will have changed by 30 kHz in one one-hundredth of a second, which, on the time scale, corresponds to a height of 1500 km, and reflections from the limiting heights will not be recorded by a receiver with a standard bandwidth of 15 kHz. Expansion in the receiver channel bandwidth reduces the ionospheric sounder's resistance to noise. This contradiction must be borne in mind when developing and designing sounders.

Pulses amplified to the second intermediate frequency are fed into a diode detector, and the useful video signal then is fed from the detector's ballast resistor to the grid of the first tube in a video amplifier through a filter and an isolating condenser. The filter (this is a parallel circuit tuned to frequency $f_2$ in the AIS) will not pass the voltage at the second intermediate frequency to the supply circuit, but will pass it to the video amplifier input. The video signal, after amplification, is fed to the scope.

Scopes

The most frequently used scopes in ionospheric equipment are cathode ray tubes. They have many advantages, primary among which are good reviewability and visualization of the results of the sounding. The image that appears on the scope can be recorded on motion picture film and kept indefinitely.

Type A scopes, with linear sweep, as well as type B panoramic scopes, can be used.

A conventional height-time sweep is used in the type A scope. A time-

dependent sawtooth voltage is supplied to one pair of plates (usually the horizontal pair). The duration of the linearly changing sweep voltage, or current, is selected equal to the time interval between two successively radiated transmitter pulses. The beam's return trace is extinguished conventionally. The oscillator can be synchronized with a command pulse, so the scope presents a stable image. Receiver output voltage is supplied to the second pair of deflection plates. A blip, repeating the shape of the signal received by the receiver, appears on the scope upon the arrival of the reflected signal. The image of the transmitter pulse always will appear at the sweep origin, if the picture is rigidly synchronized, and the height of the reflecting region can be determined by measuring the distance between the leading edges of the radiated pulse and received reflection.

A type B scope, the second scope variant, is more often used in modern ionospheric sounders because it provides a much better visual picture of the relationship between the magnitude of the delay in the reflected radio pulses and their carrier frequency. Here the voltage from the height sweep sawtooth generator is supplied to one pair of plates (vertical sweep). The scope parameters, and the manner in which this particular scope is synchronized, are similar to those for the type A scope. The frequency sweep is obtained from the second pair of plates, and takes place as follows. A frequency sweep potentiometer is mounted on the same shaft as the rotor of the master oscillator variable condenser. This variable condenser determines the sounder operating frequency, so the magnitude of the voltage across the potentiometer will be proportional to the operating frequency. This voltage is supplied to the second pair of plates, which then perform the horizontal sweep. The result is to cause the vertical line (the height sweep) to move across the scope parallel to itself in the process of removal of the height-frequency curve with change in master oscillator frequency. Its position along the horizontal will be /23 determined uniquely by the carrier frequency at which the sounding is being made at the particular moment in time.

Signals from the receiver output, the pulses for the height and frequency markers, and the pulses for intensifying the outgoing trace of the vertical sweep, are supplied to the cathode and control grid of the scope tube.

The AIS uses a 23LM34 tube. A luminous raster, 150 x 150 mm, is created on the face. A dark calibrated grid, the horizontal lines are height markers every 50 km, the vertical lines frequency markers at 1 MHz intervals, is formed on the raster. The echoes, about which mention was made above, create a darkening, breaks in the sweep, on the bright raster.

These scopes can be used as visual scopes when the requirement is for information on the condition of the ionosphere at the time the experiment is being conducted. Used for this purpose are tubes with steady persistence so the image of the height-frequency curve will remain on the screen for quite a long period of time. The type B scope provides a two-dimensional graphic image of the height-frequency curve (its panorama), so sounders using this type of scope are called panoramic sounders.

The image seen on the screen is photographed on motion picture film to record in documentary form the results of the experiment. This method is quite graphic, informative, and technically comparatively simple to use.

Conventional still photography is used when it is necessary to fix the image on the type B scope. The camera is synchronized with the ionospheric sounder control device and the film is transported in the intervals between sessions. Each photograph taken, in addition to the image of the height-frequency curve, includes the caption and the clocks indicating the location and time the experiment was performed.

## Calibrating Generators

Frequency markers generator. A frequency markers generator is included in the circuitry of the ionospheric sounder to increase accuracy in reading the frequency coordinate. A quartz local oscillator is the basic component. Oscillations from the output of this local oscillator, acting on the mixer tube grid, cause a high grid current to flow, badly distorting the shape of the voltage and creating oscillations in the plate current that are full of harmonics. A voltage from the sounder's master oscillator is supplied to the second input of the mixer. Beats at audio frequency will occur in the mixer plate circuit as soon as the continuously-functioning oscillator frequency passes through values coinciding with the harmonics of the quartz oscillator. These beats, in the form of pulses, then are amplified by the direct current amplifier with a bandwidth

of the order of 10 kHz. They then are fed to the scope after amplification and clipping, in the form of short pulses.

Height markers generator. The height markers generator generates short, sharp-tipped pulses of known repetition frequency that serve as reference pulses when reading the heights at which reflected signals are recorded.

Its basis is a conventional autooscillator with autotransformer coupling. The circuit included in the makeup of this generator is shunted by the low resistance of a control tube which, in its conventional state, is open because its grid voltage is higher than zero. The circuit now is aperiodic, and does not oscillate. When a negative pulse reaches the control tube grid the tube is triggered for the time this pulse is acting and oscillations at the frequency to which the circuit is tuned are generated. These oscillations are amplified, clipped differentiated, and supplied to the cathode follower. Pulses of one /24 polarity only are separated at the cathode follower ballast and are the height markers supplied to the scope.

Synchronizer

All units in the ionospheric sounder should function matched. The primary requirement to be satisfied is to synchronize the time a pulse is radiated from the ionospheric sounder's transmitter and the time the height sweep and height markers generators are triggered. The sounder's circuitry includes a synchronizer that controls the operation of the above-indicated units for purposes of meeting this requirement. The basis of the synchronizer is a command pulse shaper. The pulse repetition frequency determines the duration of a single cycle of operation of the sounder (the interval between two successive transmitter pulses). As has been noted, the simplest design in the formulation of the basic specifications is selection of a pulse repetition frequency of 50 Hz.

A 50 Hz sine voltage is supplied to the amplifier stage input. The stage functions because of the selection of the corresponding negative bias in the mode in which part of the negative half-wave of the voltage supplied to the input is cut off by the grid current. The next stage in the amplifier operates in the saturated mode, resulting in the cutoff of the upper, positive, section of the sine wave. The result is the formation from the sine voltage of a chain of

pulses very nearly rectangular in shape. These pulses are differentiated and the sharp-tipped positive peaks with the frequency of the sine voltage (Figure 1.2c) are used to synchronize the operation of the units in the sounder.

These peaks (command pulses) first trigger the height sweep multivibrator, serving to synchronize the operation of the scope circuits. The multivibrator circuitry is that of a driven multivibrator with cathode coupling. The circuit features great stability in the width of the pulses generated. The pulse width determines the sounder's height range. The multivibrator must be able to generate pulses with different widths in order to provide sounder operation in the different height ranges. This is done by switching condensers $C_7$-$C_9$ in the circuit. The pulse width can, in addition, be regulated within small limits by variable resistance $R_2$, which is connected in the grid circuit of the first tube. A pulse with negative polarity is supplied from the plate of the left tube of the multivibrator to the input of the height markers generator and to the input of the sawtooth generator (height sweep), and from the plate of the right tube to intensify the outgoing beam trace of the vertical sweep. Figure 1.3a is the principal schematic diagram of the height sweep multivibrator used in the AIS.

The same negative pulse from the output of the height sweep multivibrator is used to trigger the sawtooth voltage generator, and the height markers generator, so the first height marker always coincides with the origin of the vertical (height) sweep and provides the first (zero) range marker.

The triggering of the modulator stages controlling the operation of the transmitter also must be synchronized with the command pulse if the times of triggering the height sweep and the radiation of the main pulse are to coincide uniquely. The following circuitry is used to this end.

The synchronizing, or time control (command), pulse triggering the vertical /25
sweep multivibrator also is the trigger pulse for the transmitter pulse-setting multivibrator (Figures 1.2c and 1.3b). The negative pulse from the first plate of this tube ($T_2$ in Figure 1.3b) is differentiated by the $C_6R_{17}$ network and the signal corresponding to the trailing edge of the differentiated pulse is supplied to the next unit, which is the direct generator of the modulating pulse (the pulse that triggers the transmitter modulator). Here too a multivibrator circuit

is used. The first multivibrator pulse width can be changed manually by one of the potentiometers.[2] The time at which the second multivibrator is triggered with respect to the first also is changed and this corresponds to a change in the time of radiation of the main signal relative to the beginning of operation of the height sweep generator.

Use of this circuitry shifts the main pulse with respect to the height sweep, setting it, and exactly superposing the leading edge on one of the height markers. This then reduces the error in the height reading that can occur when the transmitter pulse is not superposed on the calibrated markers.

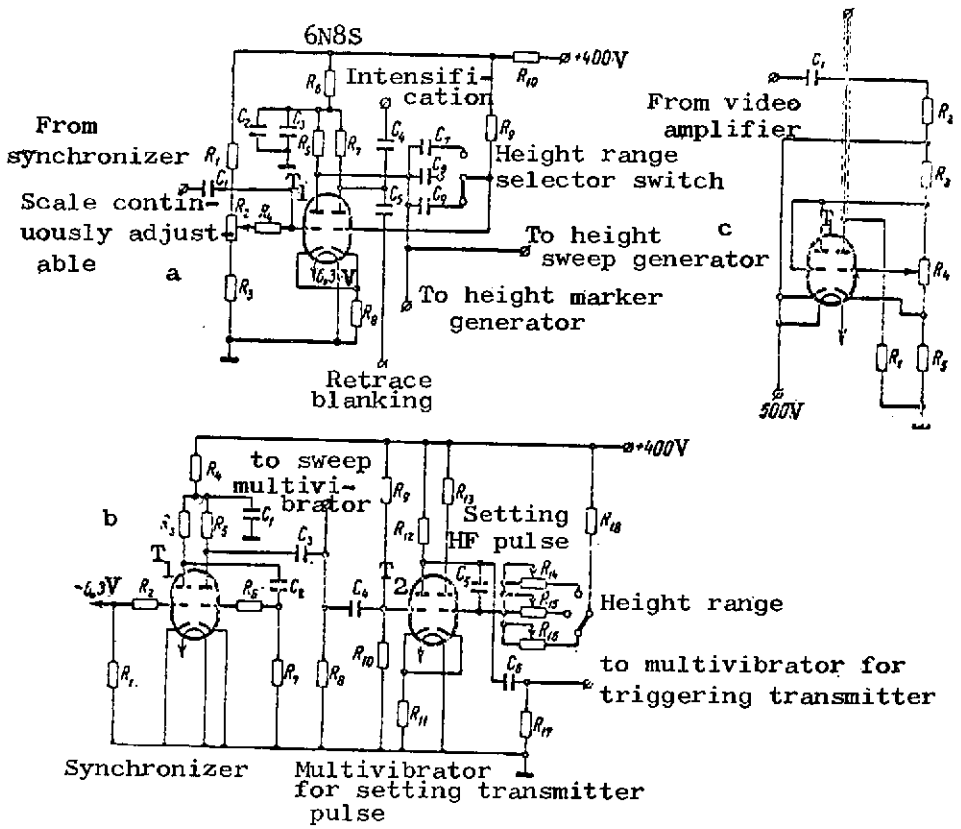


Figure 1.3. Some of the basic circuits in the AIS. a - principal schematic diagram of the height sweep multivibrator; b - principal schematic diagram for triggering the control units; c - diagram of the circuit for protecting the scope against interference.

2. $R_{14}$-$R_{16}$, depending on the height range in which the sounder is operating.

## Technical Features of the Main Units

Now let us review the technical features of the main units used to build specific variants of radio circuits for ionospheric sounders. /26

1. As may be seen from what has been reviewed, the second intermediate frequency for the receiver coincides with the local oscillator frequency of 0.9 MHz used in the transmitter circuitry (Figure 1.2b). The pulse operating mode is envisaged for the $f_3$ generator in the transmitter in order, in this case, to reduce the transmitter-receiver interaction. This is accomplished as follows.

The $f_3$ generator is a conventional three-point circuit with autotransformer coupling to one of the halves of a twin triode. The second half of the generator tube is the control half. The generator circuit proper, tuned to 900 kHz, is connected to the cathode circuit of this tube.

The control tube is open at all times. Its grid is connected to the plate voltage source through a high-valued resistor (1 megohm). The tube's grid current causes a voltage drop across this resistor such that control tube current flows through the tube, and, accordingly, through the generator circuit. At the same time, the resistor connected in the plate circuit of the tube completely shunts the high-frequency generator circuit, through the filter rectifier condenser, thus disrupting the self-excitation mode. There are no oscillations in the circuit.

The control tube will be blocked when a negative pulse is supplied to the grid of the control tube, and will remain blocked for so long as the pulse acts. The generator now shifts to the self-excitation mode. When the pulse dies out the oscillations in the circuit are interrupted until the arrival of the next negative pulse at the control tube grid.

2. The receiver in the ionospheric sounder should be designed to receive pulse signals. The optimum receiver channel passband in this case can be found from the relationship $\Delta f_{opt} = k/\tau_s$, where $\tau_s$ is signal width. The value of k can be taken as very nearly unity in our case. The passband must be selected much broader than the optimum if accurate height measurements are required. Moreover, the time constants for the receiver channel stages must be no higher than certain selected values in order to reproduce the shapes of the incoming pulses with minimum distortion.

Both receiver and transmitter have several wideband stages. Correction must be included to provide for a uniform attenuation ratio over the entire band from 1 to 20 MHz. Specifically, the correcting coils are inductively coupled to the plate circuits of the tubes in the transmitter's wideband amplifier.

3. The receiver and transmitter in the ionospheric sounder are in direct proximity to each other, so the receiver must be reliably protected against the overloads that occur at the instant the set's transmitter radiates a pulse. An input stage consisting of a GU-29 tube, which is a wideband push-pull amplifier with a gain factor of 2 to 4, serves this purpose in the AIS. The stage functions as follows. The first positive half-wave charges the condensers in the tube's grid circuits at the instant the main pulse is radiated by the transmitter. The charging circuit can be closed through the grid-cathode spacing in each half of the tube (because the amplitude of the high-frequency oscillations is very great, the resistance of the grid-cathode section is very low for the positive half-wave of the high-frequency voltage because of the appearance of a grid current). During the negative half-wave of the high-frequency voltage the condensers discharge through the resistors, but because the time constant for the discharge is much greater than the half-period for /27
the high-frequency voltage, the condensers are only slightly discharged and a high negative voltage remains across the resistors, blocking both halves of the tube. Thus, the first tube in the receiver is, for all practical purposes, cut out for the entire time the main pulse is being transmitted. The amplitude of the pulse supplied to the input of the next receiver stage now is of much lesser amplitude than the main pulse and cannot cause undesirable overloads on the first stages.

Once the main pulse has been transmitted the condensers in the GU-29 tube grid circuits discharge completely, and by the time a signal reflected from the ionosphere arrives this tube is open and functions as a Class A voltage amplifier. The condenser discharge time constant is selected such as to fully restore receiver response within 300 μsec after the initiation of radiation, corresponding to a height of 45 km.

4. The types of panoramic scopes most widely used are those that provide

a negative image of the ionospheric curve on the screen. The tubes thus are open at all times when there is no signal at the control grid, and blocked only when the reflected signal is present. This operating mode is provided for by selecting that permanent negative bias for the grid of the tube in the receiver's output stage that will cause the tube to function at the cut off threshold. The tube is open when a positive video pulse is supplied to the tube grid and a negative pulse is formed at the tube's plate ballast, which, upon being supplied to the cathode ray tube, blocks it. The beam is extinguished for so long as the pulse is present and a dark spot forms on the scope.

Reference [37] describes a recording method in which a positive image of the height-frequency curve is used. Here the point forming the raster flares only at the time of arrival of reflected signals, as well as when height and frequency markers pass. Technically, this reduces to changing the kinescope operating mode. The authors of reference [37] are of the opinion that their proposed recording method will reduce the magnitude of subjective errors in readings permitted operators estimating the quantitative values of the ionogram parameters.

5. The electrical circuit for the cathode ray tube is designed to increase the tube's capacity to resist interference. The left half of the tube in the output stage, together with the differentiating circuit (see the main schematic diagram in Figure 1.3c), the time constant for which is selected such that the useful signals pass through the circuit without distortion, are used in the AIS circuitry in particular to protect the tube against the effects of pulse interference, the duration of which is greatly in excess of that of the useful signal. This time constant is 180 μsec in the AIS, and pulses with widths of 50-100 μsec are virtually undistorted. The result of passage of wider pulses through a circuit such as this is the formation of two signals at the circuit output. One, corresponding to the commencement of the differentiated pulse, is position. It, just as does the original pulse, extinguishes the beam on the tube screen, but more quickly. The second signal at the circuit output corresponds to the trailing edge of the differentiated pulse. Its polarity is negative, so upon reaching the scope it will intensify the brightness of the beam, something that is undesirable. The left half of the tube in the output stage, connected to a diode that will not pass noise voltage to the output stage, can be used to eliminate this effect. The result is a "cleaner" image of the ionospheric curve on the scope.

A negative video pulse is supplied from the receiver output directly to the cathode ray tube control grid. A noncapacitive coupling is used to provide undistorted pulse transmission. This then results in the supply to the cathode ray tube of the constant voltage available across the output stage load resistor because of the plate current flowing in the tube. The negative voltage supplied to the cathode ray tube is a maximum of 10 to 15 volts because the receiver output stage operating mode is such that this tube is almost blocked when there is no reflected signal. The resultant reduction in brightness can be compensated for by the corresponding selection of the modes for the other electrodes in the cathode ray tube. However, if powerful continuous noise should enter the receiver, the direct current mode of the output stage changes drastically and this can result in partial, or even complete, disappearance of the sweep. This causes image quality to deteriorate. /28

Antenna Systems

Antenna systems with the radiation pattern main lobe in the vertical plane are used with ionospheric sounders to radiate and receive electromagnetic energy. So-called rhombic antennas (Figure 1.4) are most often used. Two systems of rhombuses, and the corresponding transfer switch at the transmitter output, are used to cover the entire band.

"Delta" type antennas do not work as well [108].

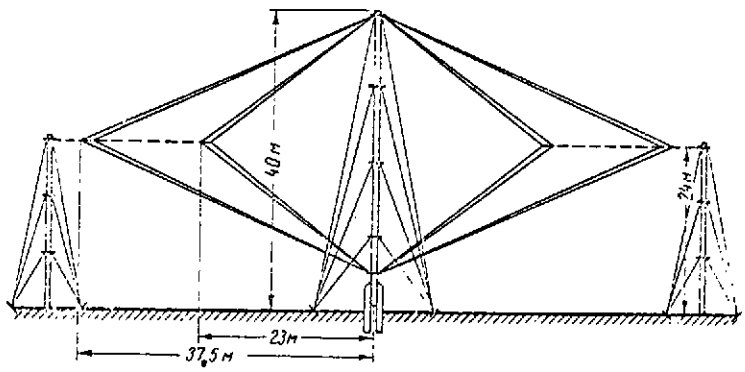


Figure 1.4. An antenna system for a pulse radio sounding installation (vertical split rhombus).

## Principal Modifications to Modern Ionospheric Sounders

Expansion in the range of physical tasks, completion of which required the use of data from panoramic vertical sounding, necessitated modernizations of the basic circuitry in the panoramic ionospheric sounder. Changes in the circuitry were determined by a specific, concrete task, and were quite diverse. For example, field experiments necessitated a reduction in sounder size and power requirements, as well as an increase in mechanical strength. Recording of partial reflections necessitated a considerable increase in radiated power, and particular attention had to be given to noise resistance when the work was to be done under conditions when there were a great many outside noise sources. There were other stipulations as well.

The following basic trends in perfecting the design of panoramic sets can be formulated: improvement in resistance to noise; reduction in size and an increase in economical use of power; expansion in automation of the processes involved in data acquisition and processing.

Let us use some concrete examples to see how these basic trends have been realized.

### Digital Recording of Ionograms

The photographic method of data recording now quite widely used has certain /29
disadvantages, as well as advantages. The information entering the sounder is converted from one form to another several times before becoming available to the consumer. There is, initially, the matter of the time interval between two packages of high-frequency oscillations. These pulses are converted into video pulses in the receiving channel. A sawtooth voltage generator is used to fix the time interval in the recording channel, so the time interval is converted into a three-dimensional image on the scope. This image then is transferred to motion picture film. Each such conversion includes unavoidable additional errors and reduces the authenticity and accuracy of the data acquired. Even the most tentative of calculations made in reference [50] show that the coordinates of reflected signals have a frequency error of ±130 kHz and a height error of ±10 km when copied from a standard image of a height-frequency curve. Moreover, the linear dimensions of cathode ray tubes used in sounder designs do not permit the separate fixing of the coordinates of each of the reflected

succession of pulses. This would increase the authenticity of the observed picture, but there is no way to fix fine details, or to use the equipment to study microspatial and microtemporal variations in recorded parameters.

There is yet another aspect of the obsolescence of the photographic method of data recording, one that developed when electronic computers were brought in to process the original experimental material. The coordinates of the height-frequency curve must be converted into discrete form so the data can be put into the computer. Since the photographic image is used as the fundamental principle, the conversion most often must be done manually, and this drastically reduces the effectiveness of computer use. Special photoreaders, of the type described in [15, 202] have been developed.

Taken here as the material used for conversion into a digital code was the photographic frame of an ionogram. The processor followed the outline of the height-frequency curve with a sensing switch. This resulted in the automatic conversion of the coordinates of the points on the curve into binary numbers which were punch-carded immediately [202], or which went directly to machine storage [15] through a special buffer register. Machine efficiency was improved but the drawbacks associated with the low level of authenticity of the data obtained remained, and even were aggravated because added to all the preceding errors in fixing the coordinates of reflected signals were new errors, the result of the conversion of the photographic image into code.

This then raised the question of obtaining data from panoramic vertical sounding in a form that could be put directly into the computer from the output of an ionospheric sounder. The very first steps in this direction showed just how bright the future was for the approach to the problem.

The time-pulse conversion principle is the most desirable one to apply to the coding of the coordinates of reflected signals. Here the time interval between radiated and reflected signals can be converted directly into code. Reference [185] describes an automatic device for direct conversion of the time interval into a digital form. The device makes use of a constant frequency pulse generator working in synchronism with the ionospheric sounder transmitter. These pulses are fed into an electronic counter in the interval between pulse radiation by the transmitter and arrival of the reflected signal. However, the /30

device built and described by the authors [185] is far from optimum because first of all the device has but one channel and can record only the height coordinate of a single reflected signal. If several parallel channels are used one can obtain in digital form virtually all the information obtained by panoramic vertical sounding; that is, avoid all losses as compared to those involved in the use of conventional recording on a photographic frame, at least in principle. And the number of intermediate conversions would be greatly reduced, thus improving the authenticity and accuracy of the information obtained. Reference [45] describes an installation of this type with four channels operating in parallel. Separate recording of the coordinates of each reflected signal makes the integrating properties of the previously used method useless while making it possible to investigate the fine structure of the height-time relationships. Reference [46] contains the first results of the use of the installation. Oscillations in the apparent heights of ionospheric reflections were recorded with a quasi-period of the order of tenths of a second. This effect must be averaged in the photographic recording case, and this simply leads to some spreading of the trace of the reflected signal along the height axis. Recording of sounding results in a form suitable for direct input into an electronic digital computer has been used as well in connection with the operation of satellite ionospheric sounders [198].

### Continuous Parameter Recording

Direct recording is effective when the need arises to record rapid temporal variations in some particular ionospheric parameter. Naturally enough, standard recorders are not suited to this purpose, so special recorders must be used [39, 205].

Recording of the temporal variations in the following parameters usually is necessary: minimum layer height, $h_{min}$; minimum and maximum (limit) frequencies at which reflections are observed.

The general principle applied to obtain a continuous record of $h_{min}$, $f_{min}$, and $f_{max}$ is that of cutting out one of the panoramic scope sweeps. The height-frequency curve then degenerates into segments of a straight line on the scope. The end points of the segment are the sought for values of the parameters. Let us consider one of the technical variants in the recording of actual minimum

heights of the ionosphere with an AIS type ionospheric sounder [39]. The following changes were made in the scope design. The negative image of the height-frequency curve was replaced by a positive and the frequency sweep and frequency markers generator were cut out. Now when the sounder was energized what was seen on the remaining vertical height sweep were bright fixed points corresponding to the ground pulse, to the signals reflected from the ionosphere, and to the height markers (Figure 1.5a).

Ground pulse and height markers images remain fixed during passage across the frequency band, but the reflection trace moves up the scope vertically as the frequency at which the sounding is taking place approaches the critical frequency for the layer. Naturally, the trace will remain in one place longer, and will, therefore, be brighter, in the section of heights with minimum effect, where the trace is horizontal.

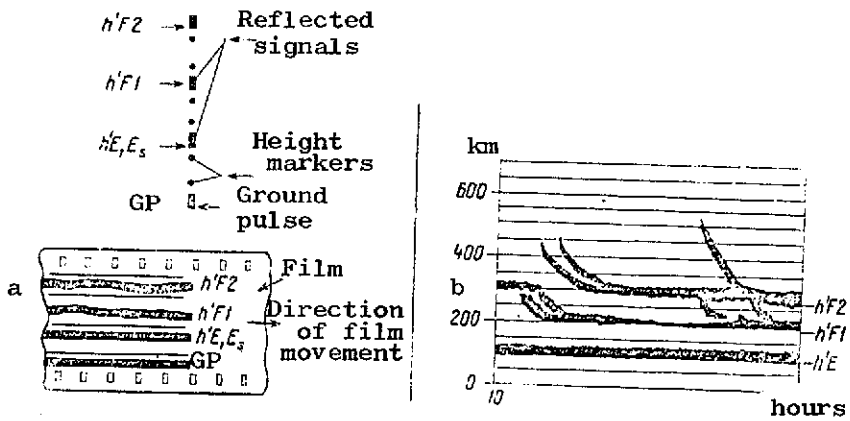


/31

Figure 1.5. Continuous recording of heights with minimum effect. a - installation operation schematic; b - examples of recording of h'(t)-curves.

The image obtained is recorded on motion picture film moving continuously across the scope in a direction perpendicular to the sweep. The film is exposed only where images of bright points strike it. We obtain a horizontal line if the layer height remains temporally constant. The configuration of this line will change when the layer rises, or falls. Figure 1.5b shows examples of a recording of h'(t)-curves.

Discrete Frequency Sounding

The principal feature of the proposed modification simply involves replacement of the continuously functioning oscillator in the principal schematic of the ionospheric sounder with a set of oscillators operating at discrete frequencies.

Known from the general theoretical hypotheses defining radio receiver operating conditions is the fact that a wide-band receiver stage can be characterized as being less resistant to interference than stages containing tunable components. The noise level discernible to the receiver is proportional to the receiving channel passband. There usually are no selective circuits in the sounder receiver input. In this case the passband must be estimated from the magnitude of the sounder's frequency range. If a selective stage with a passband of the order of 100 kHz is used in the receiver input, we obtain a noise level gain of approximately 25 db as compared to a nontunable input. Using these two receiver variants, we must, in the case of the former, increase the radiated power by a factor of 400 in order to ensure identical reception conditions because from [124] we know that the signal/noise ratio, which serves as the criterion of noise resistance in the operation of an ionospheric sounder, is a square-law variation of the radiated power.

Hence, it is clear that the insertion of switched selective high-frequency amplifiers in the input to the receiver in an ionospheric sounder will narrow the passband and drastically reduce the transmitter power required for dependable operation and will, at the same time, increase resistance to noise.

And the use of electronic switching of working frequencies will, when necessary, reduce the time needed to cover the entire frequency band. In this case, the carrier frequency radiated by the transmitter will change in steps and there will be no need for unusual expansion in the receiver channel passband, as is the case in the design of a sounder with continuous coverage of the band if the entire band is covered in a short time interval (see p. 27).

Use of sounders operating on fixed frequencies provides a potential for /32
determining the frequencies at which the sounding is taking place with as great an accuracy as may be desired. This is a highly important quality, for the use of such equipment makes it possible to investigate superfine effects associated

with the difference in the propagation of signals on carrier frequencies that differ by very small magnitudes. Reference [228] describes an ionospheric sounder operating in the USA in which the values of adjacent carrier frequencies differ by 0.1 kHz.

The selection of the net of sounder working frequencies is extremely important in the design of panoramic discrete frequency ionospheric sounders. The number of such frequencies will determine the specifics of the physical task assigned. The USA, for example, developed an ionospheric sounder with six fixed frequencies [209] in order to investigate resonance phenomena in ionospheric plasma above the main ionization maximum, as well as to study the structure of the horizontal gradients of electron concentrations and localized irregularities with a horizontal extent of 100 km and less. The USA also has built a portable ionospheric sounder operating in the 1.8-28.8 MHz band on 128 fixed frequencies to test radio communication lines. We already have mentioned the ionospheric sounder [228] the authors of the development call a dynamic sounder. This equipment operates on 2400 fixed frequencies in the band from 0.5 to 32 MHz. There are fixed frequency ionospheric sounder developments in the USSR as well [35, 113].

The selection of the spacing in the net of working frequencies should incorporate the fact that even though there are many cases when the task assigned calls for continuous change in carrier frequency on which the sounding is made, approximations are in fact made when using the experimental results. The approximation of the height dependency of the electron density on a definite law is postulated on an interval of 0.1 MHz, and sometimes even more, in the N(h)-profile calculation.

### Wide-Band Signal Sounding

Pulse signals, the envelope of which is rectangular (or more precisely, trapezoidal with adequately steep edges), usually are used to sound the ionosphere. Pure amplitude modulation is used. Characteristic of these signals is the following relationship between signal width T and signal spectrum width $\Delta F$: $\Delta F \approx 1/T$. Signal spectrum width is fixed as the magnitude minimally necessary to have undistorted transmission of its shape. Signals of this type are called small-base signals. The base in this case is understood to mean the product of signal width by spectrum width, whereupon the magnitude of the base is equal to unity, approximately.

There are, in addition to small-base signals, those with large bases. These signals, because of additional modulation, accomplished inside the pulse, provide for distribution of useful signal energy in a band of frequencies greatly in excess of that needed simply for undistorted transmission of signal shape. There is a definite excessiveness, the magnitude of which is determined by the "band expansion factor." It is this excess that makes it possible to improve the quality of system operation, and, in particular, to increase its noise resistance.

Given this approach, the system bandwidth is not determined by the absolute values of the magnitude of the frequency band used, but by the relationship between the communication spectrum (it is determined by the data flow rate, and coincides with the magnitude necessary for undistorted transmission of signal shape) and own signal spectrum, the magnitude of which is determined by the type of modulation selected [120].

Let $\Delta F$ be the width of the communication spectrum, W be the width of the signal spectrum, and T the signal width. We now can distinguish the wide-band system from the conventional narrow-band system by the magnitude of its base. The narrow-band system, in accordance with our definition, can be characterized by the relationships /33

$$W = \Delta F \text{ and } TW = T\Delta F \approx 1,$$

and the wide-band system by the relationships

$$W \gg \Delta F \text{ and } TW \simeq 100\text{-}1000.$$

Wide-band signals with a large base are propagated in communication systems in which it is necessary to achieve a high degree of noise resistance, or to attain effective use of the frequency spectrum in an overloaded frequency band. It also is possible to sound the ionosphere with wide-band signals. The primary gain by so doing is the significant improvement in the ionospheric sounder's resistance to noise.

There are a number of methods for obtaining large-base signals [120]. We shall consider, briefly, only those that can be used in ionospheric equipment. One such is the subdivision of the information parcel of width T into binary elements of width $\tau$ with the same amplitude as the fundamental signal, but with

different signs. This subdivision provides a signal of width $\tau$ and bandwidth $W = 1/\tau$. The number of elementary pulses in the parcel, $N = T/\tau$, determines the value of the signal base.

It should be pointed out that few subdivisions of the original information parcel into binary elements will yield a signal that can be used effectively in a wide-band system. Because the sounding signal is quite wide, and because the ionospheric sounder must provide high resolution and accuracy in the recording of the height coordinate, it is necessary to have signals that can be spatially separated even when they overlap. This requirement can be met if the signals have a correlation function with a single maximum of considerable amplitude and narrow width (coinciding with the width of an elementary pulse that is a component of the total parcel). Noise segments with band W characterize this type of correlation function. By analogy, all other signals with a correlation function of similar form are called pseudonoise, or noise-like, sequences equivalent to the pulse. They assume the shape of a pulse with width $\tau$ and amplitude NA after processing in a correlation receiver. Here $\tau$ is the width of an elementary pulse, A is its amplitude, and N is the number of elementary pulses in the parcel.

Wide-band signals also can be obtained by using so-called multiphase coding. The phase of the carrier oscillation in the elementary pulses of the information parcel is changed in accordance with some specially selected law, one providing signals with good correlation properties. The number of different phases can vary from 3 to 10, and more. These signals usually coincide with pseudonoise sequences when the number of phases is two (0 and $\pi$).

There is, in addition, a method for providing a wide-band signal by modulating the phase of the carrier in accordance with the Barker code. Here the original signal, of width T, is subdivided into N elementary parcels of width $\tau$. Their carrier phase can coincide completely, or differ by $\pi$. The mutual correlation function for these parcels is -1 when there is no time shift. /34
Signals such as these provide maximum noise resistance for the transmission of discrete messages.

The number of elementary parcels, N, in the original signal modulated by the Barker code cannot be arbitrary because the correlation function has a

clearly expressed maximum only for completely definite values, N = 3, 7, 11, 13. Reference [98] proves that the Barker code does not exist when N > 13. So, even if filtering is optimum, it is impossible to obtain an excess of the correlation function main maximum modulus over the side lobes by a factor of more than 13.

Systems in which the signal has pseudorandom phase shift keying have much better potential in this plan. These systems provide extremely good height resolution. But pseudorandom sequences are periodic [98] in nature, so continuous radiation is required if they are to be used to obtain a correlation function with a clearly expressed main maximum and small side lobes. Moreover, the engineering solution to the problem of reliable decoupling of transmitter and receiver is greatly complicated. It is possible to select segments of a pseudonoise sequence of finite length with good correlation properties, but it nevertheless must be long enough (with N of the order of thousands), and this requires a complicated delay line. Moreover, there is still no reliable method for selecting this segment.

Recapping, it can be asserted that the realization of systems such as these in general, and their use in equipment for investigating the ionosphere in particular, is attended by substantial difficulties, in principle, as well as from an engineering standpoint. Thus, the simplest way to obtain wide-band signals to investigate the ionosphere is to modulate the phase of the carrier frequency with the Barker code. The necessary phase-shift keying of the signal by $\pi$ can be done with a balanced modulator supplied from a high-frequency oscillator and modulated by a sequence of code pulses. The code sequence is obtained by the algebraic summing of pulses taken from a sectioned delay line with total width $(N - 1)\tau$, the input to which is a pulse of width $\tau$. The summing incorporates weight factors corresponding to the values of the code terms [74, 98]. Figure 1.6a is a block diagram of the device and its operating principle for N = 7.

The sounder receiver should include more units than are found in a standard /35
receiver if it is to receive phase-shift keyed signals and provide for efficient detection of those signals. The detector stage should be responsive to the phase of the incoming signal. The two inputs to the stage are the echo received by

the receiver, and the reference signal from the synchronizing local oscillator. A sine (or rectangular) voltage, the frequency and phase of which should match the frequency and phase of the received signal, can be used as the reference voltage. A sequence of pulses of different widths, with constant amplitudes but different polarities, is formed at the phase detector outlet after the input voltages have been multiplied, low-pass filtered and clipped. This signal then is fed into a matched filter, the purpose of which is to form the autocorrelation function of the rectified signal.

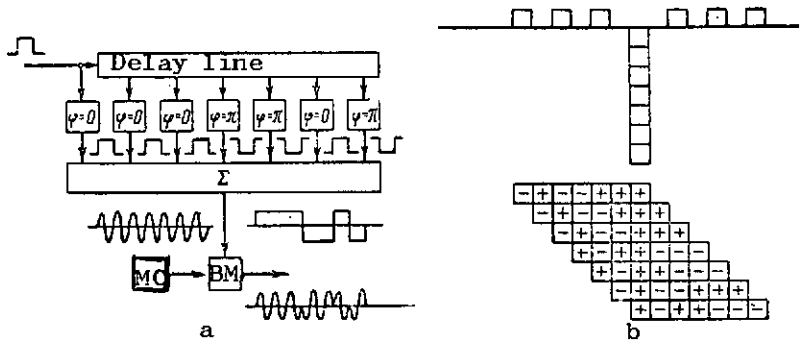


Figure 1.6. A wide-band system for sounding the ionosphere.
a - block diagram of a device generating a Barker code;
b - diagram of the structure of the correlation function by a matched filter. MO - master oscillator; BM - balanced modulator.

The filter is matched with respect to a signal of definite shape (coinciding with the shape of the signal from the transmitter). The autocorrelation function thus formed will have one large, main maximum only when the actual echo enters the receiver input. In all other cases the signal amplitude at the output of the matched filter will be small. Thus, we can decide on the presence of an echo by comparing the output voltage from the filter with some threshold value, and feed this signal into the recorder only when the echo is in fact that of the signal we have radiated from our transmitter. Figure 1.6b shows the diagram of the structure of the correlation function in a matched filter designed to process a Barker code modulated signal in accordance with Figure 1.6a. The received signal is shifted 7 times in an interval equal in width to a single code parcel, and the result of such shift is constantly summed in the adder.

It is possible to separate the useful signal at an intermediate frequency (prior to detection) by using analog devices [172], and this is in addition to the method described in which the signal is filtered after detection. Here, in addition to time of arrival, the amplitudes of the received signals can be recorded.

The Partial Reflections Method

When the sounder receiver locates signals reflected from the ionosphere, these signals, in complete accord with the theoretical assumptions made, are signals reflected from a region with a concentration determined by Eq. (0.26). But if the radiated power is very high it is possible to detect very weak signals (smaller in amplitude than ordinary reflections from regular layers by a factor of $10^5$) arriving from heights of 50 to 90 km. The method that will be described briefly in what follows is called the partial reflections method.

The amplitude of partially reflected waves is determined by the scattering processes responsible for their return to the point of reception as well as by the passage of these waves through the region below the scattering level. Study and comparison of the amplitudes of waves of both components (ordinary and extraordinary) scattered by discrete irregularities provide us with information on the concentration and frequency of electron collisions in the D region.

Pulse transmitters with pulse powers of 100 kW and higher are used in the equipment. A frequency of 2.66 MHz is used to study the normal D region. Certain results concerning the base of the E layer, as well as certain results with respect to disturbed conditions when 2.66 MHz pulses cannot penetrate the /36
scattering region because of heavy absorption, have been obtained at a higher frequency (6.25 MHz).

The significant feature of the partial reflections method is the use of high radiated power and highly responsive receivers with signal accumulation (of the type used in the case of incoherent scattering). The installation described in [26] radiates main pulses with an equivalent frequency of 12.5 Hz, and measurement results are recorded every 2 seconds. Figure 1.7 shows the results of one of the experiments.

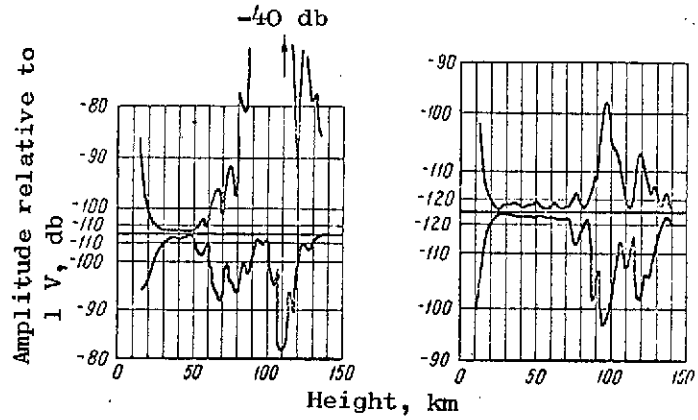


Figure 1.7. Oscillograms illustrating the partial reflections method. The upper trace in each oscillogram is the ordinary component, the lower the extraordinary.

The ratio of the amplitudes of the reflected ordinary and extraordinary components, $A_x/A_0$, slightly scattered at height h and received on the ground, depends on the ratio of the reflection factors, $R_x/R_0$, and the summed differential absorption $(k_x - k_0)$ below the scattering level. $A_x/A_0 = R_x/R_0$ at low heights, where the differential absorption is slight. We can write the dependence of $R_x/R_0$ on the wave frequency, gyrofrequency, and mean frequency of collisions between electrons and molecules of air by using the generalized Appleton-Hartree formula after making some simplifying assumptions. The electron concentration then can be calculated from the known collision frequency values.

Ionospheric Sounders on Satellites

The pulse sounding method, with reception of signals reflected from the ionosphere and analysis of the properties of these signals, provides for investigating the ionosphere, but only those sections in which the electron concentration increases with height. Hence, it is impossible to investigate the distribution of the electron concentration above the main ionization maximum with equipment located on the terrestrial surface. Moreover, the nonuniformity in the network of ground ionospheric sounders results in vast regions for which the network provides no information at all on the behavior of the ionosphere. Certain reference data on the condition of the ionosphere for the whole of the terrestrial surface are essential in order to make global maps of the planetary

distribution of the ionospheric parameters.

Therefore, when the possibility arose of assigning scientific experiments involving the use of equipment installed on artificial earth satellites there was posed the question of how to sound the ionosphere with an installation on the satellite. The path of this type of satellite would have to be above the main ionization maximum ($\geq$ 1000 km). This height was selected so as to record as large a section of the height profile as possible. It also was desirable to /37 select the orbital inclination as large as possible (close to 90°) in order to observe as much of the earth as possible, including the polar regions, knowledge of the behavior of the ionosphere over which is of great interest.

The equipment installed in satillites must meet many specific requirements because of the operating conditions encountered. The limited working space and power resources require that the set be small, and consume very little power. Corresponding requirements are imposed on structural solutions by the conditions under which the satellite is placed in orbit (high accelerations, vibration), and the selection of components used is limited. The sounder should be fully automatic and capable of being controlled by telemetry. Souding data must be obtained in a form such that they can be transmitted by telemetry. Finally, all components must be highly reliable because experiments are expensive and because it is impossible to make repairs. Operating modes should be the subject of particular design attention because of this latter fact. Redundancy of individual, more vital, circuit components should be planned.

It also should be mandatory to consider the specifics of the operation of the ionospheric sounder as developed when selecting what are strictly the sounder's radio engineering parameters (frequency range, main pulse repetition frequency, rate of change in frequency, radiated power, main signal width). The first thing to be considered here is that the satellite carrying the sounder will be hurtled into space at a rate of the order of 8 km/sec. Then too, the sounder will not be in the neutral environment found in ground stations, but will be in a region in which the concentration of free electrons is different from zero. This factor, in particular, is significant for the main pulse repetition frequency because long group delays are observed in high orbits where the electron concentration gradient is shallow. The upper limit of sounding frequencies is determined by the maximum values of critical F region frequencies

for unusual components during the experiment (this requirement is similar to that imposed for ground stations).

The upper frequency limit should be even higher if the investigations assume that reflections from the terrestrial surface will be analyzed. The minimum frequency should be lower than the frequency at which reflection of the Z-component of the signal near the satellite occurs so as to provide maximum accuracy when measuring low electron concentrations.

The United States built the first ionospheric sounder to study the ionosphere above the main ionization maximum. Alouette 1, which carried the sounder, was launched on 20 September 1962, and went into an almost circular orbit at a height of 1000 km. The inclination was 80.5°. The main purpose of this launch was to measure electron concentration in the ionosphere at heights from 300 to 1000 km [148, 179].

The sounder carried by Alouette 1 operated on the principle developed for conventional ionospheric sounders. The radiated pulse was 100 μsec wide, the repetition frequency was 62 Hz. Each session lasted 12 seconds. The carrier radiated by the transmitter changed from 1.6 to 11.5 MHz during this time. Radiated pulse power was approximately 100 watts. The sounder was used under low noise level conditions, so this power was sufficient to obtain stable reflections over the entire frequency range. Sessions were repeated every 18 seconds, and this was equivalent to a distance of some 125 km when converted to path length.

The circuit makes use of the single-frequency conversion principle. Change /38
in the carrier frequency within specified limits is achieved by mixing the oscillations from the 19.0 MHz frequency generator and from the continuously-functioning generator, which changes its frequency in the limits from 19.5 to 32.0 MHz. This is the generator used as the first local oscillator in the receiver section. The entire electrical circuit is made up of semiconductors to meet the requirements imposed for power consumption and weight, as well as those concerned with increasing operational reliability and service life.

An outstanding feature of the experiment described was the direct transmission of soundings over telemetry channels to the ground as the measurements were being made. An extensive network of ground tracking telemetry stations was

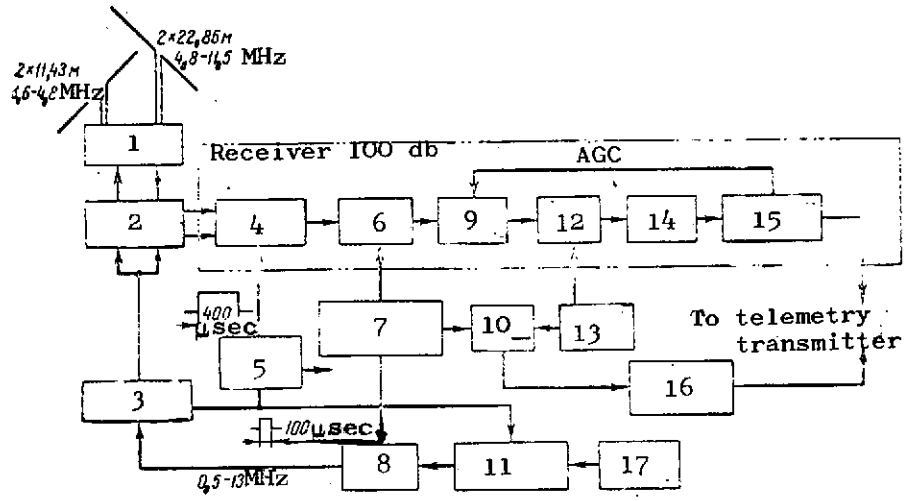


Figure 1.8. Block diagram of the Alouette ionospheric sounder.

LEGEND FOR FIGURE 1.8.

1 - matching circuits; 2 - T-R switch; 3 - impedance transmitter 100 watts; 4 - preamplifier; 5 - timing generator 67 Hg; 6 - mixer; 7 - sweep generator 19.5-32 MHz; 8 - mixer; 9 - I-F amplifier 19 MHz; 10 - mixer; 11 - strobe frequency doubler; 12 - mixer; 13 - generator 18.5 MHz; 14 - I-F amplifier 0.5 MHz; 15 - detector; 16 - frequency sweep monitor; 17 - generator 9.5 MHz.

set up for data reception [180]. Despite the fact that this network was quite extensive (it included 18 regularly used stations in Canada, the United States, South America, Australia, and in other areas), the task of obtaining data on the behavior of the electron concentration above the main ionization maximum over the entire surface of the globe through this experiment was not fully carried out. To do so would have required the incorporation in the sounder design described of a storage device to record soundings during the time interval the satellite was not in communication with ground stations.

This type of storage device was used with the ISIS-1 satellite [179]. Data could be recorded on magnetic tape directly from the sounder receiver output. The signal was recorded in analog form, and the storage volume was such that signals could be recorded for 66 minutes with the magnetic tape traveling at a rate of 12.7 cm/sec.

Figure 1.8 is the block diagram of the Alouette ionospheric sounder. Note that the telemetry transmitter transmits a signal that monitors the frequency

at which the sounding is being made, a unique frequency marker, as well as the direct results of sounding.

The unique feature of Alouette was the moving sounding antennas [199]. They were made of coiled steel tape 0.1 mm thick, 10 cm wide, which, as a result of annealing resembled cylindrical tubing 2.5 cm in diameter. The tubing then was straightened into a band and wound onto a drum located inside the satellite. Once the satellite was in orbit a special command caused the antennas to uncoil from a motor-driven drum to form with the help of rubber friction tapes, two rigid crossed dipoles 46 and 23 meters long. The planning and launching of Alouette II, designed for a broad frequency range (from 0.2 to 13.5 MHz), included a 73 meter long dipole as the larger one. /39

All electronic equipment was supplied from nickel-cadmium cells connected into a 15.5 volt battery capable of withstanding many recharging cycles (almost 6500). Silicon solar p-n cells were connected in parallel with the other cells. Maximum power demand by the electronic equipment was 30 watts. Four direct current converters provided the different voltages needed to supply all units in the electronic equipment.

The telemetry transmitter used to transmit sounding data to the ground (to transmit the receiver output voltage) operated in the 136 MHz band and had an output power of 2 watts.

Explorer 20, the second generation of ionospheric sounder satellites [209], was launched by the United States on 25 August 1964. This sounder had to face a different physical task than that planned for Alouette. It was to study the structure of the horizontal gradients of the electron concentration and of localized irregularities with a horizontal extent of 100 km and less. This is why the design and operating conditions for Explorer 20 differed from those of Alouette. Explorer 20 radiated sounding pulses on six fixed frequencies: 1.5, 2.0, 2.85, 3.72, 5.47, and 7.22 MHz. All six frequencies were radiated in sequence for 0.1 second. Sessions could be repeated practically continuously. It was possible to arrive at spatial resolution of small-scale discontinuities in the electron concentration gradients under those operating conditions because the region for which it was necessary to take a single measurement thus was limited to a few hundred meters.

Design-wise, Explorer 20 was a combination of three two-frequency transceivers operating one after the other. Radiated pulse power was 100 watts. The sounding pulse repetition frequency was 67 Hz. Three dipoles, 60° apart in the middle of the spacecraft and perpendicular to the axis of its rotation, made up the antenna system.

Sounding data were transmitted by telemetry to the ground and recorded on magnetic tape. It then was necessary to present these data in the form customary for ionograms to make it convenient to analyze and process the data. Used for the conversion was a complex consisting of a reproducing tape recorder, an oscillograph, a motion picture camera, and several auxiliary control units, such as height marker circuits, and a number of others. The authors tell us that this task was quite a complicated one, and had to be considered as a complex problem that included operation of the satellite's ionospheric sounder, the command-telemetry communication lines, ground stations, and the data processing center.

## Limits and Principal Drawbacks of the Pulse Method

Pulse sounding of the ionosphere, just as any other concrete research method, can be characterized by its limits. We have, above, repeated that the present basic limitation to pulse sounding is the inability to record reflections from those sections of the height profile of the electron concentration that /40
characterize the negative values of the height gradient. A second, equally important limitation stems from the fact that this method uses pulse signals to investigate the ionosphere. Obviously, then, panoramic vertical sounding will not record reflected signal parameters other than carrier frequency and delay time. The result is loss of data containing information on the high-frequency phase of the signal, its amplitude, and shape. But we do not consider the loss of this information to be the chief drawback of the pulse method of studying the ionosphere because the task of recording these parameters of a reflected signal simply was not within the framework of panoramic soudning as we reviewed it. The chief drawback stems from the fact that the time coordinate of ionospheric reflection can be determined with finite accuracy only, even theoretically. What follows from an analysis of the processes involved in detecting signals in noise, as cited in reference [34] in particular, is that in the low noise level case, $\mu \gg 1$, the expression

$$\Delta t = \frac{1}{2\pi\delta_s f \sqrt{\mu}} \tag{1.3}$$

is applicable when estimating the error in determining the signal arrival time, or, converting to a height reading in accordance with Eq. (1.2)

$$\Delta h' = \frac{c}{4\pi\delta_s f \sqrt{\mu}}, \tag{1.4}$$

where

$\mu$ is the signal/noise ratio;

$\delta_s f$ is the frequency band occupied by the signal spectrum;

$\Delta t(\Delta h')$ is the unknown error in fixing the time of arrival (of the height of the reflection).

A pulse of predetermined shape and width must therefore be used to achieve the specified accuracy in recording the height coordinate because the width of the pulse spectrum is closely linked with these signal characteristics. At the same time, it is quite obvious that regardless of how broad the band may be, the pulse signal used for sounding is not described. Its width is finite, so increase in the accuracy with which the height coordinate of the pulse reflected from the ionosphere can be recorded has a limit.

Let us consider the main technical variant of realization of the pulse method of investigating the ionosphere; an installation for vertical panoramic sounding that uses a continuously-functioning master oscillator.

A pulse, the shape and width of which have been completely defined, must be used to achieve specified accuracy in recording the height coordinate. Here the determining factor will be the steepness of the fronts. We know [144] that the width of the pulse spectrum, $\delta_s f$, is closely linked with these signal characteristics. But distortionless recording of such a pulse requires a reception channel with a band $\delta_n f$, or in any case at least $\delta_s f$. In other words, the inequality

$$\delta_n f \geqslant \delta_s f. \tag{1.5}$$

must be satisfied. Expansion in the receiver band (given the condition that a pulse with constant parameters is used) will not reduce the accuracy with which

the reflection height is recorded, but reduction in $\delta_n f$ to some value below that of the spectral band of the signal used, that is, inequality (1.5) will be affected, will result in a reduction in the accuracy with which the height is recorded (in distortion of the shape of the incoming pulse).

The value of the carrier frequency on which the sounding is taking place at /41
each given moment can be isolated with an accuracy equal to the value for the receiving channel band without the need for special measures, if the carrier frequency is changed continuously and smoothly during the experiment (when a continuously-functioning master oscillator is used in the sounder circuitry). We therefore can state that we can take the value $\delta_n f \simeq \delta_s f$ as the upper limit of the accuracy in determining the frequency coordinate of the recorded reflection, and the magnitude $\Delta h'$, found from Eq. (1.4) can be used as the limit of accuracy in determining the reflection height. What follows from Eq. (1.4) is that the product $\Delta h' \cdot \Delta f$ = constant, and this means that the simultaneous increase in the accuracy in reading both parameters of a reflected signal as determined using the panoramic vertical sounding method to above some limit is, in principle, impossible. An increase in the accuracy in reading one characteristic will inevitably reduce the accuracy in reading the other, and vice versa. This result, obtained in reference [47], is in complete agreement with the basic conclusions of information theory (see reference [30], for example). Bear in mind that the conclusion just formulated refers to the evaluation of definite parameters associated with other than modern equipment, the presence of subjectivism, and the like.

Let us, in concluding this section, present our summarizing assessments of variations in the principal parameters of ionospheric sounders used until recently and now in the world's network of stations.

Pulse power ranges from several tens of watts to tens of kilowatts, depending on the nature of the assigned task. The maximum frequency range is from 0.5 to 35 MHz. Ionospheric sounders used for oblique and back-oblique sound have an even higher carrier frequency upper limit, approaching 64 MHz. The circuitry usually includes the possibility of operating on expanded bands (there are two such bands, 1-10, or 1-18 MHz, in the AIS). The switch from one band to the other is done manually.

The temporal frequency change scale can be linear, or logarithmic. The time required to cover the band varies from seconds to several minutes (in the old models). Frequency markers most often show every 1.0 MHz, but sometimes every 0.1 MHz.

The height band varies over broad limits, from 100 to 4000 km and, as in the case of the carrier frequency, can be broken down into subbands (0-250, 0-750, 0-1500 km in the AIS). Bands are shifted in steps, and usually manually. Plans sometimes call for continuous adjustment. Height markers appear at 50 or 100 km intervals. The spacing can be increased to 500 km at greater heights.

The sounding pulse repetition frequency (most often 50 Hz) can vary from 10 to 120 pps. Some sounders include continuous adjustment.

The width of the pulse radiated by the transmitter can be changed from 30 to 150 μsec, and continuous adjustment within certain limits is possible in each concrete case. Synchronous tuning of the sounder's receiving and transmitting sections is provided for in modern sounders by the use of a common master oscillator. Earlier models used blocks of variable condensers for this purpose. The condensers changed their capacitance in synchronism because their rotors were mounted on the same shaft.

The question of indicators was reviewed above, and the most widely used type still is the type B panoramic indicator with a cathode-ray tube and subsequent photographing of the image on 35-mm motion picture film.

The antenna arrays usually used are vertical crossed deltas, vertical rhombuses. Antenna resistance is about 600 ohms. The same antenna is used to receive and transmit and switching takes place during the transition from low carrier frequencies to high. The receiving and transmitting functions sometimes are separate. /42

Reference [121] contains technical characteristics of some ionospheric sounders.

### 1.1.2. Physical interpretation of height-frequency curves

Experimental data indicate that the electron concentration changes very rapidly with height at the beginning of the layer (counting from its lower boundary). The magnitude dN/dh is characterized by high values. The rate of rise in N decreases with penetration into the layer. The closer to the maximum,

the smaller these changes, and dN/dh vanishes in the region of the electron concentration maximum. These reasons tend to explain the characteristic configuration of the height-frequency curve for the ionosphere, a curve obtained experimentally and fixing the height of reflection of a radio pulse as a function of its carrier frequency. The reflection initially moves from the lower edge of the layer. Here the electron concentration changes so rapidly with height that changes in h' are slight over quite a broad frequency interval. The height-frequency curve is parallel to the frequency axis over this section (Figure 1.9). The deeper within the layer the point of reflection, the longer the path the pulse must travel into the ionized medium. A pulse encountering an ionized medium will be propagated in that medium at group velocity $V_g = cn$. Group delay time therefore will rise because of penetration into the layer, as well as because of the reduction in the group velocity attributable to the change in the value of the index of refraction.

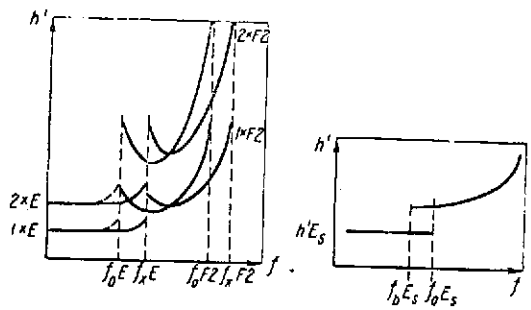


Figure 1.9. Schematic presentation of an idealized height-frequency curve.

If we designate the dependence of the electron concentration on the height by N(h), the delay time for a signal propagated in an ionized medium can be defined as

$$\tau = \frac{h}{V} = \frac{1}{c}\int_0^{h_0} \frac{dh}{n}, \qquad (1.6)$$

where

$h_0$ is the true height of the echo point.

Using the apparent height, h', concept introduced above, we can obtain the following expression for the link between the apparent and true echo heights. Since $h' = c\tau$, and considering the simplest case, that of absence of a magnetic field ($H_l = H_t = 0$), we will have an expression for n in the form

$$\sqrt{1 - \frac{4\pi e^2}{m\omega^2} N(h)},$$

and, substituting this value for n into Eq. (1.6), we obtain the following

expression for h'

$$h' = \int_0^{h_0} \frac{dh}{\sqrt{1 - \frac{4\pi e^2}{m\omega^2} N(h)}}. \qquad (1.7)$$

The Eq. (1.7) integral is improper. When $h = h_0$, in accordance with the conditions for the reflection of a vertically directed beam ($n = 0$), the expression under the integral sign becomes infinite. The integral nevertheless converges. This analysis shows that its convergence condition is not satisfied only in that region of the ionosphere in which the electron concentration gradient in terms of the height vanishes. This occurs in the region of the maximum. Consequently, the apparent echo height should increase sharply with approach to the layer's critical frequency, becoming infinite.

In fact, the apparent height does not increase to infinity. This can be explained by the fact that the propositions of geometrical optics no longer are applicable in the region near the echo point. A precise solution of the problem within the framework of wave optics shows that when $n \to 0$, the group path has a higher, albeit finite, value. This same picture is seen under real conditions, in that the height-frequency curve has an upward knee in the region of the layer maximum. The critical frequency can be established from the location of this knee on the curve, so the magnitude of the electron concentration at the layer maximum can be estimated. /43

Measuring the pulse signal delay time at those frequencies reflected from the reference layer, and using Eq. (1.2) for the recalculation, we obtain the values of the apparent height at which the layer begins. The delay caused by the propagation of the signal in the layer is slight in this case, so the height values obtained can be taken as the true heights of the lower boundary of the layer accurately enough for our purposes.

So-called multiple reflections often are noted on the ionograms when absorption of the propagating signal is slight. The physical reason for their occurrence is the secondary (sometimes multiple) reflection of the signal in the earth-reflection layer section. Figure 1.9 shows that the recorded values of the heights of these reflections on one frequency must necessarily be multiples of each other.

There are a number of different approaches to determining the height at which the layer maximum is located. The simplest is that suggested by Booker and Seaton [164]. This approach takes the value of the apparent height of the reflection at a frequency on the ionogram equal to 0.834 the critical as the true height of the ionization maximum, and is based on the assumption that the height distribution of the electron concentration near the layer maximum is close to parabolic, and does not include the influence of the external magnetic field. If the difference in apparent height of the reflection readings at frequencies 0.83 and 0.97 the critical are taken, the half-thickness of the layer from which the reflection took place can be estimated, assuming that change in the election concentration with height can be described by a parabolic equation.

A radio wave at a frequency higher than the critical for the particular layer pierces this layer and is reflected from higher layers characterized by higher electron concentrations. However, the effect of increase in apparent heights near the layer maximum appears at frequencies somewhat exceeding the critical. This is why the higher layer shows a gradual reduction in the delay at the beginning of reflections (see Figure 1.9). The height of the layer (the parameter is h') is determined from that section of the trace where the pulse experiences minimum delay.

Thus, a single branch of the height-frequency curve can be used to estimate the magnitude of a number of ionospheric layer parameters, such as its height, maximum electron concentration, true height at which the maximum is located, and the layer half-thickness, all based on the assumption that the layer is shaped /44 like a parabola.

The height-frequency curve obtained by experiment differs significantly from the one we discussed above. First of all, it is associated with the presence of an external magnetic field. The wave, influenced by that field, undergoes double refraction and is split into two components. The two signs of the root in the denominator of Eq. (0.16) for finding the index of refraction yield two values for these components. It is obvious that since the values of the index of refraction for the different components will be different, even if $\omega$ is constant, two components of the same carrier frequency will be reflected from regions of the ionosphere characterized by different electron concentrations. Both components are elliptically polarized and their field vectors have left and right

rotation. Reflection conditions, as in the no-field case, can be written $n_{1,\,2} = 0$.

The plus sign in front of the root determines the value of the index of refraction for the component referred to as the ordinary component. When $\omega = \omega_0$, the index of refraction, $n_2$, vanishes, just as it would if there were no external magnetic field. Reflection of the ordinary component takes place when the pulse carrier frequency coincides with the value of the plasma frequency, so the electron concentration at the point of reflection is

$$N = \frac{m\omega^2}{4\pi e^2}. \tag{1.8}$$

Extraordinary component reflection conditions, as analysis of Eq. (0.16) with a minus sign in front of the root will show, can be written

$$\omega^2 - \frac{\omega^2\omega_t^2}{2(\omega^2 - \omega_0^2)} \sqrt{\left[\frac{\omega^2\omega_t^2}{2(\omega^2 - \omega_0^2)}\right]^2 + \omega^2\omega_1^2} = \omega_0^2.$$

Introducing the notation $\omega_H^2 = \omega_t^2 + \omega_1^2 = (eH_0/m)^2$, and making the corresponding transformation, we find that the electron concentration at the point of reflection of the extraordinary component of the wave at frequency $\omega$ can be found from

$$\frac{4\pi Ne^2}{m\omega^2} = 1 \mp \frac{\omega_H}{\omega} = 1 \mp \frac{eH_0}{mc\omega}. \tag{1.9}$$

Eq. (1.9) is the formal statement that the extraordinary component will be reflected from two different levels of electron concentration

$$N_{1,2} = \frac{m\omega^2}{4\pi e^2}\left(1 \mp \frac{eH_0}{mc\omega}\right). \tag{1.10}$$

Only one of the values considered, the lesser, makes any physical sense because if total reflection of the extraordinary component took place in this region this component could not reach levels with high N values.

The ordinary and extraordinary components of a vertical beam are propagated over a common path, except for a segment between the points of reflection of both components. Their group velocities will differ because of the difference in the indices of refraction. So both components experience the same delay at

the beginning of the layer, and it is only during the approach to electron concentration maxima that the image of the height-frequency curve "bifurcates" /45 and these h'(f) sections of the curves for both components are recorded differently (see Figure 1.9). The magnitude of the magnetic field intensity, $H_0$, in the region of the electron concentration maximum can be found by using the critical frequencies $\omega_m^o$ and $\omega_m^x$ and Eqs. (1.10) and (1.8).

From Eq. (1.10)

$$\frac{4\pi e^2 N_m}{m\omega_m^{(x)2}} = 1 - \frac{eH_0}{mc\omega_m^{(x)}}.$$

In accordance with Eq. (1.8), $4\pi e^2 N_m/m = \omega_m^{(o)2}$, so

$$\frac{\omega_m^{(o)2}}{\omega_m^{(x)2}} = 1 - \frac{eH_0}{mc\omega_m^{(x)}}, \quad \omega_m^{(o)2} = \omega_m^{(x)2} - \frac{eH_0}{mc}\omega_m^{(x)},$$

from whence

$$H_0 = \frac{mc}{e\omega_m^{(x)}}(\omega_m^{(x)2} - \omega_m^{(o)2}). \tag{1.11}$$

Magnetic-ionic theory provides that in the case of quasi-longitudinal wave propagation, when the normal to its front makes small angles with the direction of the external magnetic field $H_0$, and the gradient of the electron concentration, dN/dh, is steep enough, an appreciable part of the energy of an ordinary wave penetrates above the region when $n_1 < 0$. The ordinary wave is propagated as an extraordinary wave in this region. It has electron concentrations satisfying the equation

$$N = \frac{m\omega^2}{4\pi e^2}\left(1 + \frac{eH_0}{mc\omega}\right), \tag{1.12}$$

and is reflected from this level. Now the height-frequency curve will have three branches. Each branch will be characterized by the corresponding critical frequency, $f^{(O)}$, $f^{(x)}$, $f^{(z)}$, satisfying the condition $f^{(x)} > f^{(O)} > f^{(z)}$. The $f^{(z)}$ branch is called the Z-component of the height-frequency curve.

So-called sporadic layers often are observed in the ionosphere, and these are in addition to the primary, regular, layer formations. Reflections from

them have a number of specific properties that distinguish them from the regular, the E, F1, and F2, layers. Specifically, the sporadic formations have high electron density compared to that for the regular layers. dN/dh values for them usually are higher than for the regular layers, so that reflections from the sporadic layers often do not have the characteristic upward knee at the high-frequency end of the trace.

Another feature that distinguishes the sporadic layers from the regular formations is that they frequently are semitransparent. In such case reflections from a sporadic layer and from a regular layer above it will be found to have the same frequency (see Figure 1.9). Here a significant feature of the sporadic layer is the screening frequency, $f_b$, that is, a frequency above which the layer becomes semitransparent, and below which it screens all ionospheric formations above the layer. The sporadic layer sometimes develops so as to screen the whole of the frequency band. Multiple reflections from the layer are observed most frequently in such case.

Sporadic formations occur in the E, as well as in the F, region. The E layer formations have long been studied in detail. Three main E types are distinguishable, according to their physical nature: thin layer; steep gradient /46
(or protuberance); and scattering centers (or disseminations). Determination of a series of layer parameters (height h', limit frequency $f_0E_s$, screening frequency $f_bE_s$, and classification according to the shape of the trace) is part of the standard processing of ionograms from sounders on a daily basis in accordance with international interpretation rules. A very great deal of attention is being given to the study of sporadic formations in the E region at this time.

Very little study has been given to sporadic formations in the F region. There still is no definite, accepted, standardized terminology dealing with the sporadic formation in the $F_s$ region. Different authors understand $F_s$ to mean diffuse (scattered) reflections in the F region, oblique reflections, reflections that resemble those from the regular F layer because of their configurations, but which have characteristically abnormally high critical frequencies, and the like.

Summarizing what has been said, one can imagine some idealized height-frequency curve for the ionosphere which should be observed in the course of vertical

sounding, and estimate that minimal set of parameters that could be taken for that ionogram (see Figure 1.9).

Selection of these parameters, as well as the formulation of the rules for reading them, is being given much attention because of the need for a valid comparison of data obtained at different points on the globe. If such comparison cannot be made, or if its validity is in doubt, the value of the results obtained by the vast network of ionospheric stations is virtually zero. The following list of parameters, taken from ionograms and offered for international exchange, has today won general acceptance.

1. Critical frequencies of an ordinary wave reflected from regular layers of the ionosphere, F2, F1, E, -$f_0F2$, $f_0F1$, $f_0E$.

2. Corresponding critical frequencies of an extraordinary wave, $f_xF2$, $f_xF1$, $f_xE$. These characteristics usually are determined to increase the reliability of the determination of the critical frequencies of the ordinary component.

3. $f_0E_s$, the limit (highest) frequency of an ordinary wave reflected from the $E_s$ layer. If it is impossible to distinguish, or establish, that what is reflected is in fact the ordinary component, $fE_s$, the apparanet $E_s$ limit frequency is determined.

4. $f_bE_s$, the highest frequency at which the $E_s$ layer screens the regular layer above it.

5. $f_{min}$, the lowest frequency at which the trace of reflections from the ionosphere can be seen on the ionogram.

6. h'F2, the minimum active height of the highest stable layer in the F region.

7. h'F, the minimum active height of the lowest layer in the F region.

8. h'E and h'$E_s$, the minimum active heights of the E and $E_s$ layers.

9. $h_pF2$, the active height of the F2 layer, read on the ionogram at frequency $0.834f_0F_2$. Numerically, it determines the height of the F2 layer ionization maximum, assuming a parabolic distribution of ionization near the maximum, and without consideration of wave delay in lower layers.

The physical tasks that can be carried out by analyzing the results obtained

from stations performing panoramic vertical sounding can be broken down into two large groups: (a) study of the general characteristics of the ionosphere and its changes on a planetary scale that depend on other phenomena; (b) investigation of the detailed structure of the ionosphere (during special ionospheric phenomena, in particular).

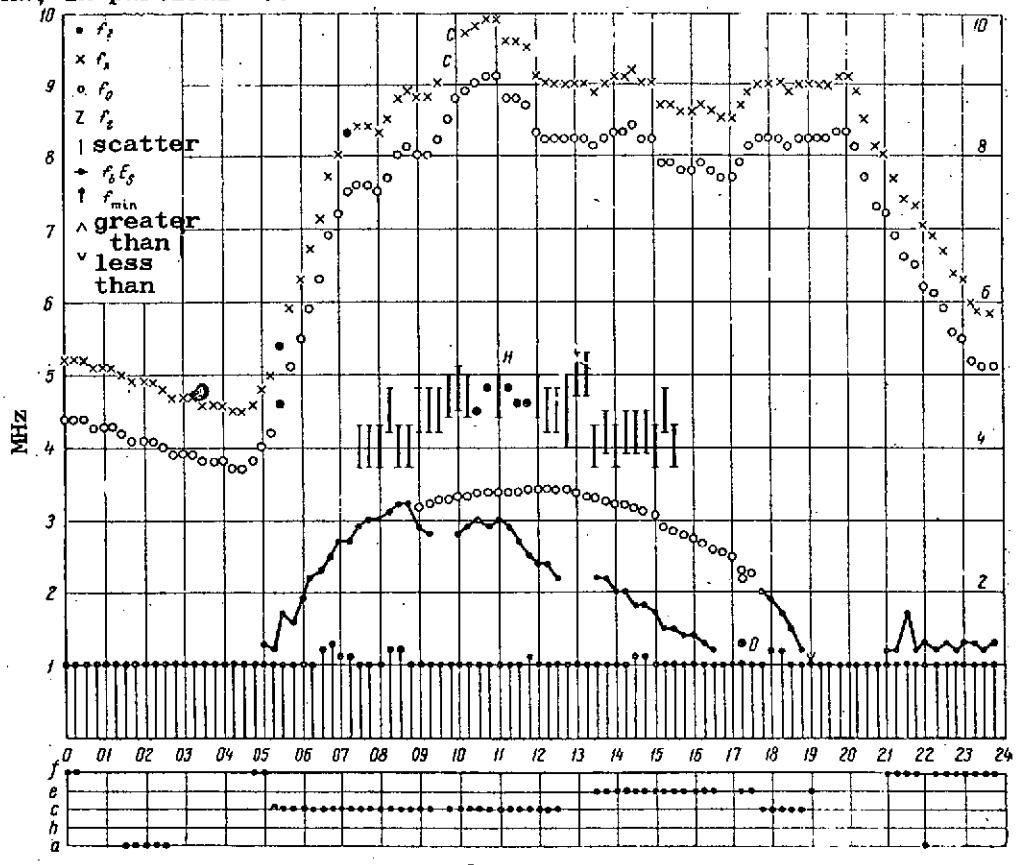


Figure 1.10. Sample f-curve.

The first group of tasks, which can be called standard ionogram processing, requires statistically representative data in the form of series as complete as possible, the accuracy of which should be very high, although this latter is not mandatory. Nevertheless, these data, obtained from different sounders, should be highly uniform. /47

Rules for identifying ionograms within the framework of the requirements imposed, and determination of the quantitative values of the parameters evaluated are described in a number of handbooks on how to interpret and process data from panoramic vertical sounding [122, 121]. These contain uniform rules for the

TABLE 1.

Read by ———— Hourly Values Date ————

Checked by ———— Vertical Ionospheric Sounding Station ————

| Zone | | | | F-region | | | | | | | | | | | | | | E-region | | | | | | | | | | | | | | | Notes | | |
|---|---|---|---|---|---|---|---|---|---|---|---|---|---|---|---|---|---|---|---|---|---|---|---|---|---|---|---|---|---|---|---|---|---|---|---|
| Hour | $f_{min}$ | Estimated | Descriptive | $foF2$ | $\frac{F2}{M3000}$ | Estimated | Descriptive | $h'F2$ | Estimated | Descriptive | $h'F$ | Estimated | Descriptive | $foF1$ | $\frac{F1}{M3000}$ | Estimated | Descriptive | $foE$ | Estimated | Descriptive | $h'E$ | Estimated | Descriptive | $F_0E_s$ | $FoE_s$ | Estimated | Descriptive | $h'E_s$ | Estimated | Descriptive | Type $E_s$ | | $h_pF2$ | |
| 00 | 010 | | | 044 | 285 | | *F* | | | | 270 | | | | | | | | | | | | | 017 | 020 | | | 100 | | | $f_2$ | | 350 | *F* |
| 01 | 010 | | | 043 | 285 | | | | | | 265 | | | | | | | | | | | | | *E* | | | *E* | | | *E* | | | 350 | |
| 02 | 010 | | | 041 | 290 | | | | | | 265 | | | | | | | | | | | | | *E* | 019 | | | 110 | | | $r_1$ | | 340 | |
| 03 | 010 | | | 039 | 285 | | | | | | 260 | | | | | | | | | | | | | *E* | | | *E* | | | *E* | | | 350 | |
| 04 | 010 | | | 038 | 285 | | | | | | 255 | | | | | | | | | | | | | *E* | | | *E* | | | *E* | | | 350 | |
| 05 | 010 | | | 040 | 300 | | | | | | 260 | | | | | | | | | | | | | 013 | 015 | | | 010 | | | $f_3$ | | 320 | |
| 06 | 010 | | | 055 | 320 | | | | | | 240 | | | | | | | | | *A* | 115 | | | 019 | 021 | | | 115 | | | *C2* | | 290 | |
| 07 | 011 | | | 072 | 335 | | | | | | 240 | | | | | | | | | *A* | 110 | | | 027 | 029 | | | 115 | | | *C2* | | 270 | |
| 08 | 010 | | | 075 | 335 | | | | | *L* | 225 | | | | | | | *L* | | *A* | 105 | | | 030 | 032 | | | 105 | | | *C2* | | 270 | |
| 09 | 010 | | | 080 | 335 | | | 250 | | | 225 | | | | | | | *L* | 315 | | 100 | | | 029*G* | 031 | | *G* | 105 | | | *C2* | | 270 | |
| 10 | 010 | | | 088 | 320 | | | 255 | | | 205 | | | | | | | *L* | 330 | | 100 | | | 028*G* | 030 | | *G* | 105 | | | *C2* | | 290 | |
| 11 | 010 | | | 091 | 320 | | | 255 | | | 200 | | | | | | | *L* | 335 | | 100 | | | 030*G* | 030 | | *G* | 105 | | | *C2* | | 290 | |
| 12 | 010 | | | 083 | 305 | | | 250 | | | 200 | | | | | | | *L* | 340 | | 100 | | | 021*G* | 024 | | *G* | 100 | | | *C2* | | 310 | |
| 13 | 010 | | | 082 | 315 | | | | | *L* | 205 | | | | | | | *L* | 335 | | 100 | | | *G* | | | *G* | | | *G* | | | 300 | |
| 14 | 010 | | | 083 | 315 | | | | | *L* | 225 | | | | | | | *L* | 320 | | 110 | | | 020*G* | 020 | | *G* | 100 | | | $l_1$ | | 300 | |
| 15 | 010 | | | 082 | 320 | | | | | *L* | 230 | | *H* | | | | | *L* | 305 | | 105 | | | 017*G* | 017 | | *G* | 105 | | | $l_1$ | | 290 | |
| 16 | 010 | | | 078 | 305 | | | | | | 235 | | | | | | | | 275 | | 105 | | | 014*G* | 014 | | *G* | 100 | | | $l_1$ | | 310 | |
| 17 | 010 | | | 077 | 315 | | | | | | 240 | | | | | | | | 250 | | 105 | | | *G* | | | *G* | | | *G* | | | 300 | |
| 18 | 012 | | | 082 | 320 | | | | | | 240 | | | | | | | | | *A* | 130 | | | 019 | 019 | | | 135 | | | *C2* | | 290 | |
| 19 | 010 | | | 082 | 305 | | | | | | 240 | | | | | | | 100 | *E* | *E* | | | *E* | *G* | 011 | | | 120 | | | $l_1$ | | 310 | |
| 20 | 010 | | | 083 | 315 | | | | | | 240 | | | | | | | | | | | | | *E* | | | *E* | | | *E* | | | 300 | |
| 21 | 010 | | | 072 | 305 | | | | | | 240 | | | | | | | | | | | | | 012 | 013 | | | 100 | | | $f_1$ | | 310 | |
| 22 | 010 | | | 062 | 305 | | | | | | 240 | | | | | | | | | | | | | 013 | 019 | | | 100 | | | $r_1$ | | 310 | |
| 23 | 010 | | | 055 | 280 | | | | | | 245 | | | | | | | | | | | | | 113 | 017 | | | 100 | | | $f_2$ | | 360 | |

TABLE 2.

F km September 1969

(Characteristic) (Units) (Month) (Year)

SibIZMIR SO AN SSSR*

Station Irkutsk — Ionospheric Data — Compiler

Longitude 104°0.' Latitude 52°28' — Zone Time 105°E — Calculator

| Day | 00 | 01 | 02 | 03 | 04 | 05 | 06 | 07 | 08 | 09 | 10 | 11 | 12 | 13 | 14 | 15 | 16 | 17 | 18 | 19 | 20 | 21 | 22 | 23 |
|---|---|---|---|---|---|---|---|---|---|---|---|---|---|---|---|---|---|---|---|---|---|---|---|---|
| 1 | 300 | 305 | 280 | 250 | 270 | 260 | 250 | 240 | 220 | 210 | 200 | 230 | 1230C | 225 | 210 | 1220C | 235 | 245 | 250 | 250 | 250 | 250 | 235 | 270 |
| 2 | 265 | 270 | 265 | 250 | 250 | 255 | 240 | 225 | 205 | 230 | 225 | 230 | 210 | 240 | 200 | 210H | 225 | 240 | 250 | 240 | 225 | 240 | 250 | 255 |
| 3 | 255 | 260 | 260 | 250 | 245 | 250 | 235 | 225 | 240 | 250 | 225 | A | A | 250 | 220 | 240 | 230 | 235 | 250 | 245 | 250 | 240 | 240 | 240 |
| 4 | 250 | 275 | 290 | 265 | 250 | 260 | 240 | 240 | 225 | 230 | 230 | 225 | 230 | 225 | 245 | 240 | 240 | 240 | 240 | 230 | 1240C | 245 | 240 | 255 |
| 5 | 255 | 265 | 260 | 250 | 240 | 255 | 240 | 240 | 1230A | 215 | 225 | 220 | 215 | 230 | 250 | 225 | 225 | 250 | 245 | 245 | 250 | 250 | 265 | 290 |
| 6 | 320 | 250 | 265 | E 290.1 | 300 | 310 | 275 | 250 | 1250A | 250 | 250 | 250 | 240 | 220 | 210 | 225 | 240 | 250 | 245 | 245 | 250 | 250 | 250 | 250 |
| 7 | 260 | 280 | 255 | 255 | 270 | 250 | 255 | 240 | 250 | 240 | 240 | 235 | 215 | 210 | 205H | 210 | 235H | 240 | 250 | 240 | 240 | 240 | 250 | 250 |
| 8 | 250 | 270 | 290 | 290 | 280 | 250 | 260 | 240 | 210 | 240 | 250H | 220 | 200H | 210H | 205H | 225 | 250 | 250 | 245 | 240 | 250 | 250 | 250 | 260 |
| 9 | 275 | 275 | 245 | 250 | 250 | 255 | 245 | 235 | 235 | 225 | 220 | 200 | 200 | 200 | 215H | 225 | 235 | 245 | 250 | 240 | 235 | 240 | 250 | 270 |
| 10 | 280 | 270 | 255 | 250 | 250 | 250 | 250 | 240 | 255 | 240 | 205 | 200 | 200 | 200H | 240 | 235 | 240 | 245 | 245 | 240 | 240 | 230 | 240 | 250 |
| 11 | 295 | 290 | 290 | 275 | 245 | 245 | 240 | 240 | 225 | 220 | 240 | 200 | 205 | 200H | 220 | 1220A | 225 | 245 | 245 | 240 | 240 | 225 | 235 | 250 |
| 12 | 260 | 265 | 275 | 255 | 250 | 250 | 240 | 240 | 235 | 200H | 200 | 195 | 200 | 220H | 215H | 240 | 240 | 240 | 1245A | 250 | 240 | 225 | 225 | 240 |
| 13 | 270 | 265 | 265 | 260 | 255 | 260 | 240 | 240 | 225 | 225 | 205 | 200 | 200 | 205 | 225 | 230H | 235 | 240 | 240 | 240 | 240 | 240 | 240 | 245 |
| 14 | 250 | 250 | 255 | 250 | 250 | 250 | 250 | 240 | 235 | 220 | 210 | 200 | 200 | 200 | 200H | 210H | 240 | 240 | 230 | 235 | 240 | 240 | 240 | 250 |
| 15 | 255 | 250 | 255 | 250 | 265 | 250 | 235 | 245H | 210 | 225H | 225 | 215 | 250 | 230 | 215 | 220 | 220 | 250 | 260 | 250 | 250 | 250 | 250 | 260 |
| 16 | 300 | 305 | 310 | 270 | 275 | 270 | 245 | 245 | 240 | 215 | 210 | 210 | 200 | 195H | 220 | 235 | 240 | 250 | 235 | 220 | 240 | 1240C | 245 | 240 |
| 17 | 260 | 270 | 250 | 270 | 250 | 240 | 230 | 230 | 215 | 215 | 230 | 205 | 210 | 210 | 220 | 200 | 240 | 245 | 240 | 230 | 235 | 250 | 245 | 270 |
| 18 | 270 | 280 | 320 | 300 | 280 | 275 | 245 | 240 | 245 | 230 | 215 | 200H | 200H | 200H | 240 | 250 | 220 | 245 | 240 | 240 | 240 | 250 | 250 | 280 |
| 19 | 270 | 280 | 320 | 300 | 255 | 255 | E 270A | 250 | 210 | 240 | 235 | 200H | 210 | 235 | 240 | 230 | 240 | 245 | 240 | 250 | 240 | 240 | 245 | 275 |
| 20 | 275 | 275 | 265 | 260 | 250 | 245 | 240 | 240 | 240 | 215 | 235 | 205 | 230 | 200 | 205 | 200 | 235 | 240 | 240 | 220 | 235 | 235 | 250 | 280 |
| 21 | 300 | 300 | 275 | 250 | 250 | 240 | 245 | 235 | 210 | 205 | 205 | 200 | 205 | 215 | 205 | 200 | 215 | 245 | 235 | 230 | 240 | 250 | 230 | 250 |
| 22 | 260 | 280 | 255 | 250 | 250 | 250 | 240 | 230 | 230 | 220 | 230 | 210H | 200 | 210 | 225 | 200 | 245 | 245 | 225 | 225 | 230 | 240 | 250 | 255 |
| 23 | 255 | 250 | 260 | 260 | 260 | 245 | 240 | 235 | 240 | 225 | 210 | 205 | 205 | 215H | 200H | 240 | 225 | 245 | 240 | 225 | 230 | 245 | 250 | 280 |
| 24 | 270 | 270 | 275 | 270 | 255 | 250 | 270 | 235 | 210H | 230H | 230 | 215 | 205 | 200 | 200H | 240 | 240 | 240 | 235 | 220 | 235 | 245 | 250 | 250 |
| 25 | 250 | 260 | 250 | 260 | 250 | 250 | 230 | 230 | 225 | 235H | 235 | 220 | 205 | 215 | 215 | 235 | 230 | 240 | 235 | 230 | 235 | 250 | 250 | 275 |
| 26 | 290 | 285 | 250 | 250 | 250 | 275 | 245 | 235 | 225 | 235 | 235 | 240 | 215 | 225 | 220 | 220 | 240 | 230 | 230 | 220 | 230 | 245 | 245 | 250 |
| 27 | 270 | 270 | 265 | 260 | 250 | 250 | 225 | 240 | 235 | 215 | 210H | E240P | 235 | 230 | 215 | 225 | 240 | 235 | 225 | 240 | 240 | 230 | 250 | 255 |
| 28 | 265 | 255 | 265 | 250 | 250 | 250 | 230 | 225 | 220 | 225 | 225 | 210 | 240 | 225 | 225 | 225 | 245 | 240 | 245 | 255 | 250 | 255 | 260 | 250 |
| 29 | 250 | 275 | 300 | 295 | 275 | 275 | 250 | 250 | 240 | 250 | 240 | 230 | 220 | 240 | 225 | 215 | 250 | 245 | 245 | 245 | 250 | 210 | 280 | E 360.4 |
| | | 340 | 315 | 300 | 300 | 200 | 270 | 250 | 250 | 225 | 220 | 215 | 205 | 210 | 230 | 250 | 250 | 245 | 230 | 220 | 255 | 250 | 280 | 240 |
| Quart. Median | E390A | 270 | 265 | 260 | 250 | 250 | 240 | 240 | 230 | 225 | 225 | 210 | 205 | 215 | 220 | 225 | 240 | 245 | 240 | 240 | 240 | 240 | 250 | 250 |
| Consid. Quart. range | 270 30 25 | 30 | 30 | 30 | 30 | 30 | 30 | 30 | 30 | 30 | 30 | 29 | 29 | 30 | 30 | 30 | 30 | 30 | 30 | 30 | 30 | 30 | 30 | 30 |
| | | 20 | 25 | 20 | 20 | 10 | 10 | 5 | 20 | 20 | 25 | 25 | 25 | 25 | 20 | 20 | 10 | 5 | 10 | 15 | 15 | 10 | 10 | 20 |

Time to cover frequencies from 1 to 18 MHz 20 seconds. Automatic station.

* Siberian Institute of Terrestrial Magnetism, the Ionosphere and Radio Wave Propagation, Siberian Branch, Academy of Sciences of the USSR.

presentation of the data obtained and specify the makeup of f-curves, and the daily and monthly tables for plotted parameters (Figure 1.10 and Tables 1 and 2). Standard processing is complicated by the fact that the ionograms obtained by the stations are located in different parts of the world, each of which has its own peculiarities, so that uniform interpretation and plotting of the numerical values is difficult (see references [159, 213], for example).

Ionograms obtained by the middle-latitude stations are closest to the "theoretical" shape of the height-frequency curve. Figure 1.11a is an example of such ionogram. The trace configuration is extremely close to the idealized height frequency curve, it is light, and the quantitative values are easy to read. Nevertheless, here too we find the complications associated with the dynamics of the development of ionospheric layers (occurrence and disappearance of the F1 layer, classification of the sporadic formations, screening of the regular layers by the sporadic, development of ionospheric disturbances, that put in an appearance in the strongly developed lowest of the regular regions of the ionosphere, the D region, as well in the anomalous change in electron concentration in the regular layers and appearance of sporadic formations, and others). We need not deal with these phenomena in this text, but we invite the attention of those interested to special manuals on the subject that deal with these questions in detail [121, 122]. 50

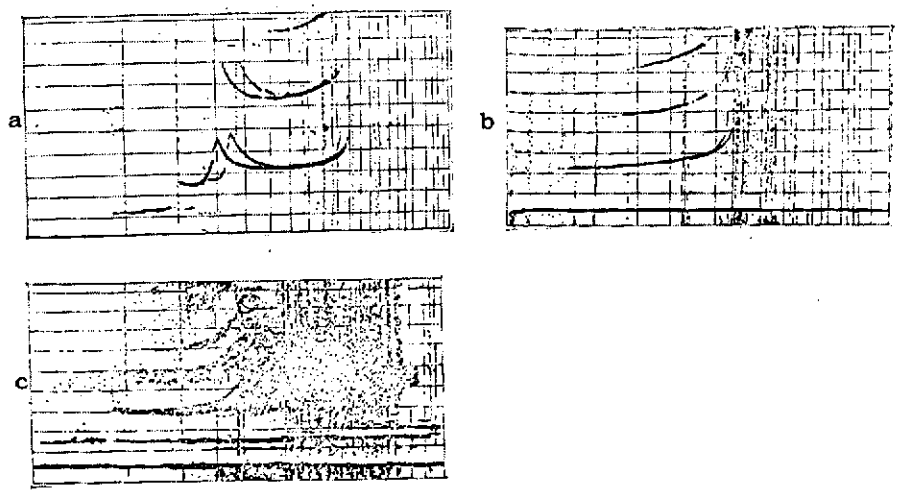


Figure 1.11. Typical height-frequency curves. a - middle-latitude day ionogram; b - low-latitude night ionogram; c - high-altitude ionogram.

Interpretation of low-altitude ionograms is somewhat more complicated.

Taken individually, the configuration of each of the height-frequency curves is no different from that obtained in the middle latitudes. The difference is in the quantitative values of the parameters, but this is explained in its entirety by, in particular, the magnitude of the sun's zenith angle. The nature of time variations (diurnal and seasonal changes) also differs. Moreover, the frequency of observation of sporadic formations of different types changes with the geographic latitude. The appearance of an equatorial type sporadic layer is more characteristic of the regions close to the equator for example. Typical of this type is a sharply outlined flat lower edge and diffusivity in the upper part, reaching a maximum in the middle of the trace (along the frequency scale) and diminishing toward the edges. Figure 1.11b is an example of a low-latitude ionogram.

The ionograms obtained in the polar regions are much more difficult to interpret. The high degree of changeability in the high-latitude ionosphere, the existence of additional sources of ionization, result in the appearance on these ionograms of oblique reflections, reflections from sporadic formations, anomalous absorption, strong diffusivity of the reflected signal, and other phenomena, materially complicating decoding and appearing much more frequently than is the case in other regions. Moreover, the type of recording on high-latitude ionograms changes within a short time span, and this makes it difficult to apply the sequence principle to ionogram interpretation. Practice in analyzing the results of processing data from the network of high-latitude stations has shown that the divergence in the interpretation of the data sometimes is so great that the result can be completely different conclusions for comparatively nearby geographic regions for which one should, a priori, expect approximately identical behavior patterns.

The following groups of questions causing differences of opinion in interpretation can be distinguished: (a) classification of sporadic formations; (b) /51 determination of the numerical values of the critical frequencies for the F2 layer when reflections are diffused; (c) selection of the main trace of reflections from the F region when oblique reflections are present, or when a series of intermediate formations appear. There are special handbooks dealing with questions of the interpretation of high-latitude ionograms (references [44, 107], for example). Figure 1.11c is an example of a high-altitude ionogram.

Identity of interpretation, processing, and presentation of observation data, as well as their completeness and reliability, are of primary importance. A satisfactory solution to this problem depends on strict observance of interpretation rules by the operators-processers, as well as on the manner in which equipment performs. Experience in the operation of numerous ionospheric sounders, special investigations, and physical prerequisites have developed the fact that determination of quantitative data on many ionospheric parameters, and even the very possibility of obtaining these data, is very much dependent on how the equipment making the observations performs. It is common knowledge that $f_{min}$ (the minimum sounding frequency), for example, depends on the power radiated by the sounder's transmitter. Receiver response plays an extremely important part in obtaining quality ionograms, and here the absolute value of the response, and the uniformity of the response of the receiver channel in the sounder over the entire frequency range, are of equal importance. If response is too low the ionogram will not show those sections where reflected signal power drops as a result of selective absorption. This effect is observed most often in the critical frequency region, that is, precisely where the need to record the trace is particularly great. But if receiver sensitivity is too high the image of the height-frequency curve on the oscilloscope can be completely covered by noise, resulting in the loss of useful information.

Nonuniformity in the receiving channel frequency curve can result in "troughs" appearing on the height-frequency curve, resulting in a poorer quality image (an interrupted trace) and in complications in interpreting the data, sometimes to the point where interpretation is impossible. This is why maintenance is extremely important when making ionospheric investigations (particularly in accordance with an agreed program in different parts of the world) because it provides the means for judging the performance of equipment.

The question of how to interpret height-frequency curves for the outermost ionosphere arose with the appearance of sounders installed on rockets and satellites [139]. Figure 1.12a is a schematic image of an ionogram obtained from topside sounding, and Figure 1.12b is a typical ionogram obtained by the Alouette sounder. The structure of the main trace of the "outer" h'(f) curve can be fully explained in terms of the magnetic-ionic theory and is similar to the /52

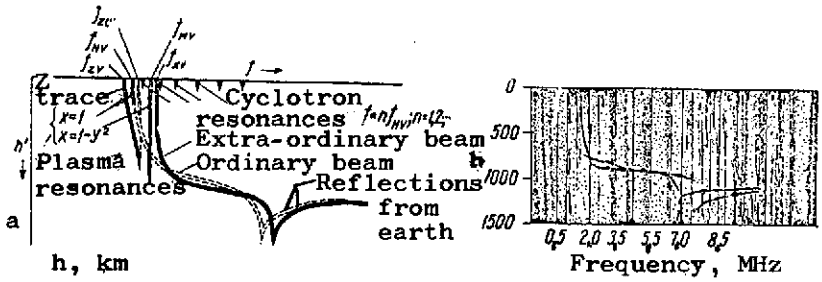


Figure 1.12. Results of ionospheric sounding by sounders installed in artificial earth satellites. a - Schematic image of an ionogram of the upper half of the ionosphere; b - example of a high-frequency curve obtained by Alouette.

explanation given for the configuration of ordinary "ground" high-frequency curves. But the outside ionograms can be characterized by yet other peculiarities that are typical only of outside sounding. Resonance phenomena should be recalled first. Resonances are the result of satellite sounders being in a medium in which the concentrations of free electrons differ from zero. If the frequency of the signal radiated by the sounder is a coincident, or multiple, characteristic frequency of the environment, natural resonance oscillations will be produced in the environment and will be recorded by the sounder's receiver. The oscillations occur in direct proximity to the satellite, so they will be recorded on the ionograms as vertical traces beginning immediately after the restoration of the receiver's normal response. The greater the development of these phenomena, the higher the peak. Most ionograms show three peaks. They can be observed at the plasma frequency, $f_N$, proportional to the square root of the electron concentration near the satellite, at the gyro frequency, $f_H$, the value of which is determined by the strength of the magnetic field in the orbit, H: $f_H = (He)/2\pi m)$. The frequency of the third peak, $f_T$ (the upper composite frequency), can be found from

$$f_T = \sqrt{f_N^2 + f_H^2}.$$

Peaks at multiple frequencies $2f_H$, $3f_H$, and $2f_T$ will be observed, and these are in addition to the fundamental peaks. A $2f_N$ peak will be found occasionally, but $3f_N$, $4f_N$, etc., as well as $3f_T$ and $4f_T$ peaks will never be found. On the other hand, peaks of harmonics of the cyclotron resonance, $f_H$, were observed on

Alouette 1 ionograms at high $f_0F2$ magnitudes when the sounding antennas were parallel to the earth's magnetic field, right up to the 22nd harmonic [183]. The plasma frequency, $f_N$, is measured in terms of the location of the peak, regardless of object potential, its photoemission rate, or other attendant phenomena, so its value is accurate and is an absolute measure of the electron concentration near the satellite. This is why we have equipment developed specially for the investigation of plasma resonances (see reference [190], for example). This transmitter has a frequency range from 0.1 to 3.0 MHz, a main pulse repetition frequency of 500 Hz, and a receiver passband of 30 kHz, so that several signals can be obtained within the limits of each resonance.

Both types of sounders should be carried by the satellite in order to obtain more complete data, because one will provide smooth coverage of the band for a long period of time, while the other, the sounder, will operate at fixed frequencies [195].

The American satellite ISIS-1, launched 30 January 1969, and placed in a polar orbit (apogee 3523 km, perigee 574 km, inclination 88.4°) uses this program. It sounds by changing frequencies from 0.1 to 20 MHz, as well as on six fixed frequencies: 0.25; 0.48; 1.0; 1.95; 4.0 and 9.303 MHz.

The rules by which ionograms are identified must be followed identically, as must the requirements for accuracy in reading the quantitative values of parameters, and the like, in order to obtain the data for the primary processing of the ionograms in the form that will permit them to be used for a valid comparison with each other. This is the only way that data obtained by the network of stations will be sufficiently uniform to permit conclusions to be reached that will be on solid ground when comparisons are made. One thus can try to reduce the primary processing of ionograms to a clearly formulated set of uniquely realized rules. In other words, it is possible to compose an algorithm /53 for standard processing of ionograms that will simplify the introduction of electronic digital computers into the practice of ionospheric investigations.

The first step in automating the gathering and processing of ionospheric data should be to obtain panoramic vertical sounding data in a form such that they can be fed directly into the computer. A great deal of effort has been devoted to this question, in the course of which the general procedural aspects of the particular trend [49, 197], as well as concrete variants of constructive

solutions designed to provide a solution to the problem as posed [15, 202, 228], were considered. If the results of sounding the ionosphere can be recorded on magnetic tape in discrete form with practically no preliminary filtering directly from the sounder output such that they can be fed directly into the computer [45, 228], the second step could be the identification of the ionogram; that is, separate by machine (algorithm-aided) the authentic main portions of the high-frequency curve from the total volume of recorded information. Reference [49] set forth, for the first time, the general principles of composing the algorithm for the realization of this particular task. Reference [48] contains a detailed description of the algorithm and of the program.

The first experimental results obtained by an AIS sounder using the equipment [45] and the BESM-2 computer were included in the candidate dissertation written by one of the authors of this monograph [47]. Analogous results are contained in reference [228], from which we have borrowed Figure 1.13, which illustrates the computer construction of an ionogram. Reference [48] describes a variant of the sequence of operations proposed for use when composing the algorithm for the standard processing of ionograms.

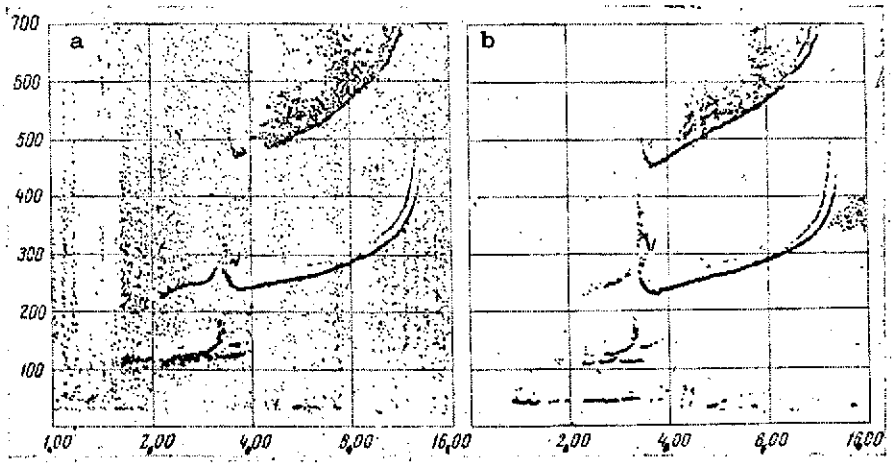


Figure 1.13. Height-frequency curves constructed by an electronic digital computer using a recording of sounding results in digital form on magnetic tape. a - without noise suppression; b - with preliminary noise filtering.

Study of the distribution of ionization with height is one of the main tasks of ionospheric research. Information on the temporal and spatial changes in these distributions is needed to solve practical problems of the propagation of radio waves, as well as the majority of problems concerned with the structure of

the upper atmosphere and with the physical processes that take place there.

The height-frequency curves obtained from panoramic vertical sounding are used to establish the apparent heights of reflections of radio pulses, h', calculated on the assumption that the rate of propagation of radio waves is constant, and does not depend on the characteristics of the medium. The divergence between h' values and the true heights at which reflections occur is reached upon approaching maximum electron concentrations in the layer of quite high values. 54

A transition must be made from apparent to real reflection heights in the recalculation process in order to obtain the true distribution of ionization with height (the so-called N(h)-profile of the ionosphere).

Today the N(h)-profile of the ionosphere can be obtained by rockets when the profile is constructed using the results of direct measurements of electron concentration as the rocket penetrates the ionospheric depths.

Rocket measurements have a number of advantages that distinguish them from the indirect methods used to determine the true distribution of the electron concentration in terms of height, among which one should point out the obtaining of the N(h)-profile from the results of panoramic vertical sounding. Rocket measurements cannot, however, completely replace the indirect methods. This is so primarily because rocket measurements are made sporadically, at individual moments in time, and at a few points. Since data on temporal and spatial variations in the N(h)-profile are highly important to the solution of any applied, as well as purely scientific, problems, and since such data can be obtained only from an extensive network of sounders operating on a regular basis, it is clear that the task of converting the results of panoramic vertical sounding into curves of the true distribution of the electron concentration in terms of height is one of extreme importance. The task of obtaining the N(h)-profile of the outermost ionosphere too has recently become a current one in connection with the obtaining of height-frequency curves above the main maximum. At the same time, a new task arose, that of making mosaics of profiles obtained by ground-based sounders and sounders carried by a satellite. This should provide a unified curve of the electron concentration distribution in terms of height.

Clearly, obtaining the height profile of the electron concentration from the height-frequency curves is being given very serious attention indeed at this time.

The solution of the corresponding problem in its fully stated form has difficulties associated with it that are the result of the complexity of the expression for the ionosphere's index of refraction, and of the formula for group velocity attributable to the influence of the terrestrial magnetic field. Disregard of the magnetic field greatly simplifies the calculations and in many cases provides a height profile that is quite close to reality. However, the accuracy of this type of an approximation is not satisfactory in many cases, either for research or practical purposes. Moreover, two difficulties arise in almost identical fashion in approximate, as well as precise, calculation methods.

First of all, there is a definite error in the determination of the initial height profile, N(h). This error occurs because practically speaking the height-frequency curves begin with quite high frequency values, so there is no experimental information on what the configuration of height-frequency curves is at frequencies below $f_{min}$. Second, the transition through the electron concentration maximum often is associated with a discontinuity in the height-frequency curve, or with steep rise in its branches. This leads, in turn, to a discontinuity in calculated curves that makes the position of the origin of each section of the curve beyond the electron concentration maximum in the layer ambiguous. Interlayer ionization, that is, those sections of the height-frequency curve not recorded directly on the ionogram, has a definite influence on the /55
heavior of the N(h)-profile, because it is associated with the decrease in values as height increases.

It is precisely for this reason that the problem of calculating the true distribution of electron concentration in terms of height can be solved when the information needed for its unambiguous solution is insufficient. Consequently, in accordance with generally accepted definitions, what must be done here is to determine just how mathematically incorrect the solution is, assuming that the basic physical causes of the incorrectness are: (a) lack of experimental information on lower-lying (at frequencies below $f_{min}$) and interlayer (where

the monotonic growth in N with height is interrupted) ionization; (b) ambiguity of the phsyical interpretation of those sections of the height-frequency curve where discontinuities of the first and second kind occur.

Stated in general terms, determination of N(h) in terms of the height-frequency curve reduces to the approach of geometrical optics to the conversion of the integral

$$h'(\omega) = h_0 + \int_{h_0}^{h} \frac{c}{u} dh = h_0 + \int_{h_0}^{h} n(\omega, N)\, dh', \tag{1.13}$$

where

n(ω, N) is the group index of refraction;

u is the group velocity,

into an integral of the form

$$h(\omega) = h_0 + \int_{0}^{\omega} F(\omega, h')\, d\omega, \tag{1.14}$$

The function F(ω, h') can be obtained from the corresponding transformation of Eq. (1.13) into Eq. (1.14). Eq. (1.14) also determines the shape of the profile because h(ω) is the inverse function h(N), in as much as ω and N are associated with the condition of reflection of a wave by equating the coefficient of refraction to zero.

There are a great many methods available today for solving this problem with some particular degree of approximation. The methods can be broken down into four [105] groups based on the principle of approach of the integral equation to inversion. The first group includes modeling methods, the principles of which involve an evaluation of profile parameters by comparing experimental height-frequency curves with a set of standard curves constructed in terms of a definite law. The model distributions most often used are:

(a) the parabolic layer $N(h) = N_m\left[1 - \left(\frac{h}{Y_m}\right)^2\right]$,

where

$Y_m$ is the layer's half-thickness;

(b) the cosinusoidal layer $N(h) = N_m\left[\frac{1}{2}\left(1 - \cos\frac{3\pi h}{4Y_m}\right)\right]$;

(c) the Epstein layer $N(h) = N_m \frac{4\exp(3h/Y_m)}{[1+\exp(1+3h/Y_m)]^2}$;

(d) the Chapman layer $N(h) = N_m \exp\left[\frac{1}{2}\left(1 - \frac{h}{Y_m} + \exp\frac{h}{Y_m}\right)\right]$.

The latter distribution is considered to be closest to the true distribution.

The second group of calculation methods assumes subdivision of the height-frequency curve into intervals along the frequency scale. The subdivision can be uniform, or nonuniform. Mathematically, subdivision of the profile into sections subdivides the Eq. (1.13) integral into /56

$$h'(\omega) = h_0 + \int_{h_0}^{h} n(\omega, N, \bar{H})\, dh = h_0 + \int_{0}^{\varphi_0(N_n)} n \frac{dh}{d\varphi} d\varphi = \\ = h_0 + \sum_{i=1}^{n} \frac{\Delta h_i}{\Delta \varphi_i} \times \int_{\varphi(N_{i-1})}^{\varphi(N_i)} n d\varphi. \tag{1.15}$$

Let us designate

$$M_{in} = \frac{1}{\Delta\varphi_i} \int_{\varphi(N_{i-1})}^{\varphi(N_i)} n d\varphi. \tag{1.16}$$

The introduction of $M_{in}$, the mean parameters of the group delay for each particular section, results in the set

$$h_n' = h_0 + \sum_{i=1}^{n} M_{in}(h_i - h_{i-1}), \tag{1.17}$$

the solution of which will be $h_i = \sum_{k=1}^{n} N_{ki} h_k'$.

The elements of the matrix of group indices, $M_{in}$, and the elements of the matrix $N_{ki}$, which is the inversion of the $M_{in}$ matrix, must be calculated to calculate the profile by this method. These matrices are calculated once only for a sounder with the specified magnetic coordinates.

The methods most widely used are those proposed by Budden [169] and Titheridge [224]. The inversion in Titheridge's method does not result in inversion of the matrix, but rather in successive steps. The solution finds $\Delta h$, the increment of the true heights, rather than the true heights, h, and this

requires their increments, $\Delta h'$, rather than the absolute values of the actual height, h', when making the calculations. This method is, in our view, more convenient because $\Delta h'$ can be determined with somewhat greater accuracy than the heights themselves. It is described in great detail in references [154, 155], which include discussion of the algorithm and its programmed realization using a "Strela" computer.

The distinguishing feature of the methods combined into the second group is that the gradient dh/dN is a constant within the limits of each of the individual intervals into which the height-frequency curve is subdivided to make the calculations, and that it changes stepwise upon transition from one section to another; that is, we have discontinuities of the first kind.

The third group of methods can be defined as a group of polynomial methods for making a calculation. The fundamental principles involved in the construction of these methods reduce to the use of the following assumptions: continuity of the h(N) curve, and its presentation in the form of a step series (polynomial) of the type

$$h(N_i) = \sum_{k=0}^{n} a_k \psi^k (N_i). \tag{1.18}$$

This reduces to the assignment of heights $h_1$, $h_2$, ..., $h_n$ for the corresponding frequencies $f_1$, $f_2$, ..., $f_n$ in the form of a system

$$\begin{aligned} h_1 &= a_0 + a_1\varphi(f_{N_1}) + a_2\varphi^2(f_{N_1}) + \ldots + a_n\varphi^n(f_{N_1}), \\ h_2 &= a_0 + a_1\varphi(f_{N_2}) + a_2\varphi^2(f_{N_2}) + \ldots + a_n\varphi^n(f_{N_2}), \\ &\cdots\cdots\cdots\cdots\cdots\cdots\cdots\cdots \\ h_n &= a_0 + a_1\varphi(f_{N_n}) + a_2\varphi^2(f_{N_n}) + \ldots + a_n\varphi^n(f_{N_n}). \end{aligned} \tag{1.19}$$

The second group, as distinguished from the laminar methods, assumes that the gradient, dh/dN, is a continuous magnitude when polynomials are used. /57

The gradient $dh/d\varphi$ $(f_N)$ is substituted into the basic integral equation in the form of the sum $\sum_{k=1}^{n} k a_k \varphi^{k-1}(f_N)$. to find the association between the $a_k$ parameters and the experimental h' values. After substitution and interchanging the sites of summing and integration, we obtain

$$h'(f_i) = h_0 + \sum_{k=1}^{n} k a_k \int_0^{f_i} n(f, f_N, H)\, \varphi^{k-1}(f_N)\, d\varphi(f_N). \tag{1.20}$$

Introduction of the coefficients

$$b_{ik} = k \int_0^{f_i} n(f, f_N, H) \varphi^{k-1}(f_N) d\varphi(f_N) \tag{1.21}$$

leads to a set of equations with respect to $a_k$

$$h'(f_i) = \sum_{k=1}^{n} b_{ik} a_k. \tag{1.22}$$

In this system the coefficients of $b_{ik}$ can be calculated by using Eq. (1.21) once for the particular sounder and for the specified series of frequencies. The difference in the concrete variants of the polynomial methods can be determined by the diversity in the selection of the form of the polynomial $\varphi(f_N)$. Titheridge's method, suggested in 1961 [223], can be said to be the principal variant of the polynomial method.

The big advantage of this group of methods is the possibility of achieving a high degree of accuracy for a very much fewer number of experimental points (comparison can be made with laminar methods). The needed number of experimental readings taken from the height-frequency curve is determined by the degree of the polynomial.

The degree of the polynomial can be no higher than 4 if the curve has no discontinuity. Several polynomials can be used for multilayer ionograms (recorded in the daytime when several layers are recorded on them), one for each layer. It is possible, generally speaking, to limit the number of polynomials to one that writes the ionogram as a whole, but if this is done the degree of the polynomial must be selected high, so high that the solution is unstable.

A modification of the principal variant considered is the overlapping polynomials method wherein the original height-frequency curve is broken down into several intervals along the frequency scale so that the boundaries of these intervals overlap.

The fourth group includes the so-called manual methods, although if they are to be carried out machine calculations must be done first (determination of values of frequencies at which the height readings at which the reflection occurred must be taken). Today this group combines those methods requiring a minimum

number of operations and which reflect the true heights, or other parameters of the ionosphere directly by reading h' values off the ionogram. The most modern example of this method is Schmerling's [217].

Kelso [196] has demonstrated that if the influence of the magnetic field is disregarded one can, in order to determine the true height at which the reflection of frequency f occurred, take the arithmetic mean of ten values of apparent height from the ionogram at frequencies definable as 0.997; 0.972; 0.924; 0.853; 0.760; 0.649; 0.523; 0.383; 0.233; 0.078 of the f value.

Subsequently, papers have shown that these coefficients must be modified to 58
calculate the influence of the magnetic field, and that the degree of modification will depend on the ratio of the frequency considered, f, to the gyro frequency, and on the magnitude of the magnetic declination at the sounder. The correction factors are relatively small, and change very slowly with the magnetic declination, so can be taken as some family of a series of coefficients of the type presented above. Each of these series can be applicable to some range of frequencies, f, for which determination of the true reflection height can be made, and to some range of magnetic inclination to the gyro frequency. Tables of these series containing data sufficient to use over almost the entire globe will be found in a handbook for interpreting and processing ionograms [122]. All that need be known to use these tables is the magnetic inclination and the magnitude of the gyro frequency for the particular sounder. Knowing f, one finds the concrete values of the coefficients to use to select the points at which one must take the values of the apparent reflection heights, and these then are averaged. Ionograms constructed using these tables can be used to simplify the readings. The ionograms are particularly convenient when the frequency scale of the ionograms obtained by the sounder are logarithmic.

The following difficulties can arise in the practical application of this method. Some number of frequencies read (minimum values) can be below $f_{min}$, where experimental data on reflection heights, h', are lacking. Also possible is the fact that ionization density between layers will be less than the density at the maximum for the lower lying layer when there are several layers in the ionosphere; that is, the monotonic shape of the height-frequency curve is broken.

These two complications are, generally speaking, characteristic of practically any calculation method, regardless of which one of the four classifications of the groups mentioned includes the method. As we already have said, the lack of experimental information on the underlying (at frequencies below $f_{min}$) and interlayer ionization is one of the reasons why the task of constructing the N(h)-profile from the height-frequency curve has no unique solution; that is, it is in the mathematically incorrect class of solutions.

Information supplemental to that combined in the section of the height-frequency curve initially used to construct the profile must be used to obtain a unique solution.

The original basis for constructing the profile is the reflected trace of an ordinary wave on the height-frequency curve. The trace of the extraordinary component, the phase heights, measurements of absorption, and other experimental data, can be used as this supplemental data. The introduction of additional data has led to the use of the least squares method to minimize divergences in the calculated magnitudes and in the magnitudes belonging to the additional data. A detailed consideration of the question of the construction of the N(h)-profile using the different methods is beyond the scope of strictly ionospheric measurements, so we shall merely invite the attention of those interested to the literature that devotes special attention to a survey of calculation methods cited in references [105, 153].

The problem of how to obtain height profiles of electron density has been the subject of a great many papers, and there are several ways to find the solution. Of unquestioned interest is the calculation of the true distribution of the electron concentration with height based on the height-frequency curve obtained using ionospheric sounders carried by satellites. This task is analogous to the basic task of calculating the ground-based profile, but does /59
have a series of specific features not found when analyzing data obtained from ground-based soundings.

First, because the satellite is moving in plasma, all actual heights (depths) are measured from a region in which the plasma frequency has a finite value other than zero, rather than from the boundary of the layer (from a point at which the plasma frequency equals zero). None of the methods developed

to analyze ground-based sounding data can be used without loss of accuracy if the value is very different from zero because the lower limit of the original interval is equal to zero in all these methods. The lower limit of the interval in Eq. (1.14) is not equal to zero when data obtained by topside sounding are analyzed and can be determined by the value of the electron concentration near the ionospheric sounder.

Second, the magnitude of the gradient dh/df too is finite and not equal to zero at the location of the satellite, just as it is in the case of ground-based sounding.

All methods for calculating the N(h)-profile, without exception, assume vertical sounding. Topside sounding shows a deviation from vertical propagation. The higher the satellite's trajectory the greater the possible error.

Practically all the methods previously developed can be used to calculate the profiles of the outermost section of the ionosphere if the peculiarities listed are taken into consideration. Reference [193] describes the use of the laminar method and, analyzes the part in which errors occur as a result of the conversion of apparent reflection heights into true heights, in detail. It is demonstrated that satisfactory accuracy can be obtained by using 10 to 20 values taken from the height-frequency curve. Reference [138] describes the polynomial method. It is assumed that this method is more efficient for processing the "outermost" ionograms, recognizing that the number of experimental points will be fewer than required for optimum use of the laminar method when discrete frequencies [209] are used for sounding.

Divergence in experimental results was found when data obtained by Alouette 1 were compared with data obtained by ground-based sounding, as well as by other methods (incoherent scattering, rocket experiments). The profiles obtained from the satellite lay below the corresponding profiles obtained using other methods. Reference [194] contains a special analysis of this question. It is demonstrated that the recorded divergence can be explained, in part, by the systematic errors in the height marks in the satellite equipment. These errors can be corrected by the analysis of the heights of reflection from the terrestrial surface at frequencies higher than the critical. Reasons for the divergence also

can include the horizontal gradients of the electron concentration and deflections from the vertical of the trajectory over which radiated pulses are propagated.

Efforts are afoot to set up a special system providing for taking the coordinates from the ionograms and using computer-aided calculation of the N(h)-profile to cope with the increased flow of data resulting from topside sounding of the ionosphere, and because of the need to convert ionograms into profiles on a massive scale [198]. The system consists of a small computer connected to a cathode ray tube indicator and a big, the main, electronic computer. The ionogram, recorded in analog form on magnetic tape, is fed into an amplitude-code converter. These data are converted into digital form (reflected signal amplitude and delay time) and fed into the small computer. This machine provides a constant ionogram output, as well as other data, in digital form for the cathode ray tube screen. The operator picks the coordinates off the height-frequency curve on the screen with a light pencil and these data are fed into the all-purpose computer so the N(h)-profile can be calculated. This computer performs the following sequence of operations. It /60
constructs the N(h)-profile from one of the components of the height-frequency curve (the operator ordinarily uses the extraordinary branch of the height-frequency curve for this purpose), then, using this profile, the machine calculates the second branch of the curve and returns it to the small computer for comparison with the experimental data. The operation is repeated if the calculated ionogram does not coincide with the original. This system is very convenient for interpreting structurally complex ionograms because it has "feedback" lines that show up operator errors if the latter incorrectly selected the coordinates of the main reflection for computer input.

### 1.1.3. Measurement of the parameters of a heterogeneous structure

Numerous experimental investigations lead to the conclusion that the ionospheric layer is a heterogeneous medium consisting of ionized formations, heterogeneities of different scale. The principal methods for studying a heterogeneous structure, given the present level of research, suggest that the spectra of the linear dimensions of the heterogeneities of the electron concentration in the ionosphere are extremely broad, from a few score meters to hundreds of kilometers. We shall classify heterogeneities in terms of horizontal

dimensions in accordance with the nature of the phenomena caused when radio waves are propagated in the heterogeneous ionosphere. The principal classes to be distinguished are:

1. $l > 500$ km. Heterogeneities known in the literature as sporadic formations and traveling disturbances;

2. $l < 500$ km. Large-scale heterogeneities, usually studied using the long-base, spaced-reception method;

3. $2 > l > 20$ km. Heterogeneities causing F-scatter and radio star scintillation;

4. $l < 2$ km. Small-scale heterogeneities causing distortion of radio pulses and damping of reflected signal amplitude.

Bear in mind that the term "ionospheric heterogeneity" always is understood to mean a region with increased, or decreased, ionization as compared to the surrounding "background" density. This heterogeneity is of the magnitude of the index of refraction in spatial distribution, looked at from the standpoint of radio wave propagation.

Ionospheric heterogeneities are in a state of continuous motion. Reference [66] contains a survey of the theory of their motion. They can be depicted as ionized "clouds" appearing and disappearing, moving chaotically in different directions inside some region, or found in a state of ordered drift in a definite direction. The moving front of these heterogeneities is readily depictable. The experimental data favor the existence of chaotic, as well as of regular, motion. Moreover, study of the horizontal drift of small-scale ionization heterogeneities makes it possible to investigate the wind regime at the level of the ionosphere. Thus, ionospheric heterogeneities are unique "bench marks."

It should be pointed out that the existence in the ionosphere of ionized "clouds," that is, of regions of increased, or decreased, ionization, is a sufficient, but not necessary, condition for arriving at an explanation of the phenomena observed when studying the ionosphere by radio-physical methods. The assumption made with respect to them simply is a graphic approach to the concept of speed of movement, dimensions, and life of heterogeneities. It is possible that the scattering of radio waves takes place in regions in which

longitudinal plasma oscillations are excited. At the same time, the field of incoming radio waves will be satisfied by a statistical law; that is, these waves /61 are coherent with respect to each other. The dimensions of the heterogeneities should be understood to mean the wavelength for longitudinal plasma waves, and the life to mean the extinction time.

This does not preclude any other interpretation of the form of the existence of ionization heterogeneities.

References [3, 115] contain a survey of a number of hypotheses and theories concerning the mechanism involved in the formation of heterogeneities in the ionosphere, the nature of their space-time distribution. References [3, 115, 151, 161, 211] discuss the theoretical principles of radiophysical methods for investigating heterogeneities. This section will review questions concerned with the measurement of the principal magnitudes characterizing the heterogeneous structure of the ionosphere.

The principal methods used today to study the heterogeneous structure of the upper ionosphere are based on investigation of the structures of the field of the radio signal reflected from the ionosphere, or passing through it. Primary to these methods is investigation of the fading of short radio waves during vertical, or oblique, sounding of the ionosphere, including space-spaced and frequency-spaced reception, investigation of the structure of the radiation fields of radio stars, or of artifical earth satellite signals, and, finally, study of F-scatter on the ionograms of vertical pulse sounding. All these methods make it possible to definitely establish the fact of the presence of ionization heterogeneities, and to estimate their intensity, localization, shape, and motion parameters. Physical information concerning small-scale heterogeneities can be obtained by studying time variations in amplitude, phase, or angle of arrival of a radio wave reflected from the ionosphere during pulse sounding.

Suppose we sound on a fixed frequency with wave incidence normal to the layer. The wave incident on the layer obviously will, at least in part, pass through the heterogeneity of the electron concentration and will be reflected at a point where the index of refraction, n, becomes zero [3]. Given these reflection conditions, some diffraction pattern showing the shape, size, and

mutual positioning of the scattering centers, the ionization heterogeneities, will be observed at the terrestrial surface. The ionization heterogeneities are in constantly chaotic and ordered motion, so the diffraction pattern at the terrestrial surface will change continuously, in time, and in space.

Part of the energy reflected when n = 0 will yield the field component, the "mirror" image wave, arriving at the point

$$E_0 \cos(\omega_0 t - \varphi_0) \tag{1.23}$$

of observation at angle $\alpha_0 = \pi/2$. Part of the energy scattered by the heterogeneities, forms the field component

$$\sum_s E_s \cos(\omega_s t - \varphi_s), \tag{1.24}$$

that is, a bundle of scattered waves with random amplitudes $E_s$ and phases $\varphi_s$.

Each of the elementary waves of (1.24), because of the movement of the scattering centers, has a Doppler frequency shift

$$\Delta f = f_s - f_0 \tag{1.25}$$

and angular displacement

$$\theta_s - \alpha_0. \tag{1.26}$$

Thus, the electromagnetic field, E(t), of each of the individual signals at some point on the terrestrial surface can be represented as the superposition of the (1.23) regular wave and of a great many (1.24) elementary waves /62

$$E(t) = E_0 \cos(\omega_0 t - \varphi_0) + \sum_s E_s \cos(\omega_s t - \varphi_s), \tag{1.27}$$

The following expression for the reflected signal amplitude results when we designate $\Omega_s = \omega_s - \omega_0$

$$R(t) = \sqrt{\left[E_0 + \sum_s E_s \cos(\Omega_s t - \varphi_s)\right]^2 + \left[\sum_s E_s \sin(\Omega_s t - \varphi_s)\right]^2}. \tag{1.28}$$

It should be pointed out that when the nature of the diffraction pattern at the terrestrial surface is taken into consideration we have

$$R = R(x, y, t), \tag{1.29}$$

where

x, y are the coordinates of the observation point on the terrestrial surface.

Study of the diffraction pattern at the terrestrial surface yields information as to the structure of a heterogeneous screen.

R(t) Characteristics

Variations in the amplitude, R, of a reflected signal are in the nature of a random process. It is a well known fact that conditions for the reflection of radio waves from the ionospheric layer are very much dependent on time of day, season of year, and conditions in the ionosphere. R(t) variations therefore are nonsteady-state random processes [115].

Calculations that consider R(t) for a short time span (a few minutes) usually are made because of the great complexity involved in analyzing a nonsteady-state random process. This enables us to use mathematical analysis apparatus developed as applicable to steady-state processes while, at the same time, making it possible for us to study time variations (diurnal, seasonal, and the like) in the parameters of the heterogeneous structure. Special measures that include the nonsteady-state nature of the process sometimes are used.

Thus, let the values of the amplitudes R(kδ) of a reflected signal for a time interval T be known from observation data (Figure 1.14).

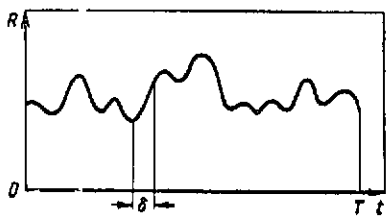


Figure 1.14. Temporal variation in the amplitude of a reflected signal, R(t).

1. The mathematical expectation (mean value) of the process discussed can be calculated from

$$R_m = \frac{1}{N_T} \sum_{k=1}^{N_T} R(k\delta), \tag{1.30}$$

where

δ is the integration step

$$\delta = \frac{T}{N_T}, \tag{1.31}$$

and $N_r$ is the total number of readings [99].

The integration step, $\delta$, is selected small enough so that changes in the R(t) curve over the time interval $\delta$ can be disregarded. Reference [128] contains more detailed consideration of the $\delta$ selection. /63

The mathematical expectation of the $R(k\delta)$ process is the mean value of the amplitude of the reflected signal for the period of observation, T. The magnitude $R_m$ can be used to find many ionospheric characteristics.

2. The amplitude distribution function can be derived as

$$P(R) = \frac{1}{\Delta R} \cdot \frac{N_i}{N_r}, \tag{1.32}$$

where

$N_i$ is the number of readings with amplitude in the interval from R to R + + $\Delta$R.

The type of distribution function for the R(t) process can be described by Eq. (1.28) according to the ratio of the energies of the regular and scattered components [3, 115]

$$\beta = \frac{E_0^2}{\sum_s E_s^2}. \tag{1.33}$$

The values of $E_0$ and $\sum_s E_s^2$ must be determined from the experimental data, therefore, if we are to discuss the P(R) curve and compare it with the theoretical amplitude distribution curve. This can be done as follows. Reference [3] obtained a graphical relationship (Figure 1.15a).

$$\frac{[R^2]_m}{R_m^2} = f(\beta).$$

We can, therefore, find $\beta$ from the curve (Figure 1.15a) once we have found $[R^2]_m/R_m^2$ from the experimental data /64

$$\frac{[R^2]_m}{R_m^2} = \frac{1}{N_r} \frac{\sum_{k=1}^{N_r} R^2(k\delta)}{R_m^2}, \tag{1.34}$$

Considering that

$$[R^2]_m = [E_0^2]_m + \sum [E_s^2]_m, \tag{1.35}$$

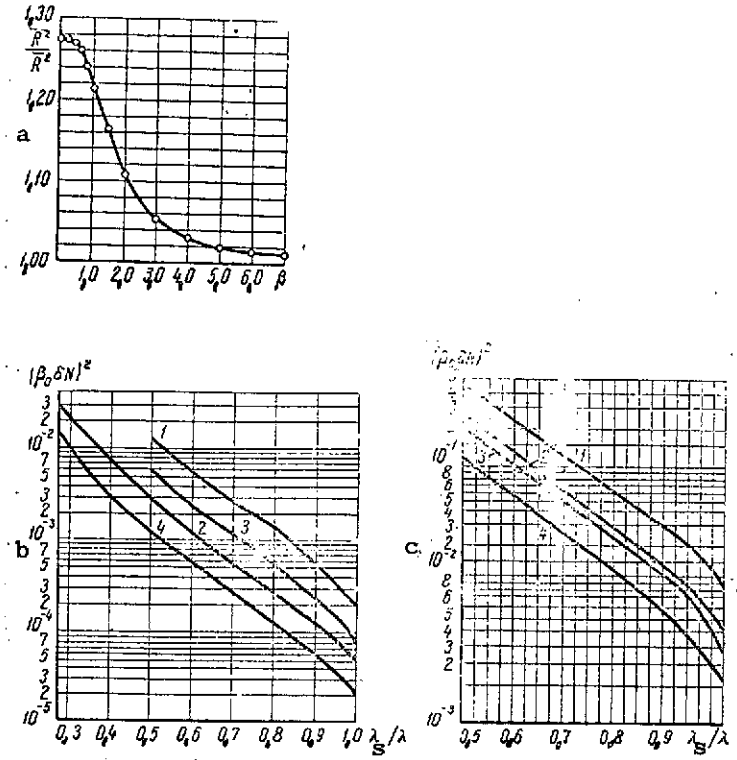


Figure 1.15. Parameters of the heterogeneous structure of the ionosphere. a - dependence of the ratio $\overline{R^2}/\overline{R}^2$ on $\beta$ (R is signal amplitude) [3]; b - theoretical dependence of $(\beta_0\delta N)^2$ on $\lambda_s/\lambda$ for $\xi_0$ = 200 m and h = 250 km. Curves 1 and 2 are for $h_m$ = 100 km, $\lambda_s$ = 50 and 25 m, curves 3 and 4 for $h_m$ = 20 km and the same $\lambda_s$ values [3]; c - theoretical dependence of $(\beta_0\delta N)^2$ on $\lambda_s/\lambda$ for $\xi_0$ = 200 m and h = 110 km. Curves 1 and 2 are for $h_m$ = 10 km and $\lambda_s$ = 75 and 100 m, curves 3 and 4 for $h_m$ = 20 km and the same $\lambda_s$ values [3].

we can calculate $E_0$ and $E_s^2$.

The data obtained being available, we can compare the experimental and theoretical reflected signal amplitude distribution curves and check the correctness of Eq. (1.28).

It must be pointed out that presentation of the E(t) field in the Eq. (1.33) form imposes known limitations on the $[R^2]_m/R_m^2$ ratio. Specifically, as reference [3] has demonstrated

$$\frac{4}{\pi} \leqslant \frac{[R^2]_m}{R_m^2} \leqslant 1. \tag{1.36}$$

So the calculations set forth above can be made only for those recordings of variations in the amplitude, R(t), satisfying the (1.36) condition. Analysis

of

$$\frac{[R^2]_m}{R_m^2} > \frac{\pi}{2}$$

cases requires investigation of the scattered component. Methods for making such measurements are discussed in what follows.

3. The normalized autocorrelation function is one of the important characteristics of the random process involved in amplitude R(t) variations. This function can be calculated as follows [99]

$$K(\tau) = \frac{[R(t) \cdot R(t+\tau)]_m - [R(t)]_m^2}{[R^2(t)]_m - [R(t)]_m^2}, \tag{1.37}$$

and the mean product

$$[R(t) \cdot R(t+\tau)]_m = \frac{1}{N_r} \sum_{k=1}^{N_r} R(k\delta)\ R(k\delta + \tau) \tag{1.38}$$

can be found directly from the experimental data.

The Eq. (1.37) autocorrelation function, since it is a temporal function, characterizes the degree of the statistical connection between the signal amplitude and time.

The space correlation function, defined as follows, can be calculated similarly

$$K(x) = \frac{[R(a, t)\ R(a+x, t)]_m - [R(a, t)]_m^2}{[R^2(a, t)]_m - [R(a, t)]_m^2}, \tag{1.39}$$

where

R(a, t) and R(a + x, t) are the signal amplitude, measured at points with coordinates a and a + x (the one-dimensional case) simultaneously.

The Eq. (1.39) function characterizes the degree of the statistical connection of the signal amplitude along the x direction. As follows from Eq. (1.37), or Eq. (1.39), /65

$$K(\tau) = 1 \quad \text{when} \quad \tau = 0,$$
$$K(x) = 1 \quad \text{when} \quad x = 0,$$

so it frequently is convenient to introduce for consideration the value of the

time interval $\tau$ for which $K(\tau) = 0.5$ (or the corresponding distance x for which $K(\tau) = 0.5$).

Parameters of the Heterogeneous Structure of the Reflecting Layer

1. Degree of turbidity of the ionosphere. The parameter $\beta$, introduced above in Eq. (1.33), characterizes the reflecting screen as a semiopaque medium. It is more convenient to introduce the turbidity factor, $\alpha$, defining it as the ratio of the energy of a bundle of scattered waves to the total energy of a reflected wave

$$\alpha = \frac{\sum_s E_s^2}{\sum_s E_s^2 + E_0^2} = \frac{1}{1+\beta^2}. \tag{1.40}$$

in place of $\beta$, which changes from zero to infinity. $\alpha$, since it is a measure of the degree of the heterogeneity of the reflecting region, changes from 1 to 0.

2. Root-mean-square velocity of chaotic motions. The expression for calculating the root-mean-square velocity of chaotic motions of the scattering centers was derived in reference [3] by analyzing the normalized correlation function of the R(t) process. It was found that

$$V_0 = \frac{\lambda R_m \| \Delta R_\tau \|_m}{2\pi\tau \sum_s E_s^2 \sqrt{2+2\beta}}, \tag{1.41}$$

where

$\Delta R_\tau = R(t) - R(t+\tau)$ is the difference in the amplitude of the reflected signal at times t and $t + \tau$;

$\lambda$ is the wavelength of the sounding radiation.

Eq. (1.41) will take the following form in the special case of $E_0 = 0$

$$V_0 = \frac{\lambda \| \Delta R_\tau \|_m}{8\sqrt{2}\tau R_m}. \tag{1.42}$$

3. Root-mean-square value of the scatter of a bundle of waves. The expression for finding $\theta_0$ for a bundle of scattered waves was derived in reference [3] by analyzing the space autocorrelation function for the process involved in the fading of the reflected signal amplitude along the x axis. It

was found that

$$\theta_0 = \frac{\lambda [| \Delta R_\xi |]_m}{4 \sqrt{4 - \pi \xi R_m}}, \tag{1.43}$$

where

$\Delta R_\xi = R(x, t) - R(x + \xi, t)$ is the difference in amplitudes of the reflected signal at time t at observation points at distance $\xi$ from each other along the x direction.

4. Linear dimensions of ionization heterogeneities can be found from

$$l_0 = \frac{\lambda}{2\pi\theta_0}, \tag{1.44}$$

and the linear dimensions of the region forming the reflected signal from <66

$$\rho_0 = \theta_0 h, \tag{1.45}$$

where

h is the height of the reflecting region.

5. Electron density fluctuation. The electron density fluctuation $(\delta N)^2$ can be found when the experimental data mentioned above are available. Reference [3] calculated the theoretical relationship between the product $\beta(\delta N)^2$ and the ratio of the working frequency, $f_0$, to the critical frequency, $f_c$

$$\frac{f_0}{f_c} = \frac{\lambda_c}{\lambda_0}$$

for several typical $t_0$ values and layer half-thicknesses, $h_m$ (for the E and F regions of the ionosphere). Figure 1.15 shows the corresponding curves and, using these curves and $\beta$, $f_0$, and $f_c$ values from the experimental data, we can find $(\delta N)^2$.

Fluctuation in the electron density, $\delta N$, that is, the deviation of the electron density for small-scale heterogeneities from the mean value, $N_m$, is an important physical characteristic of the ionosphere layer.

The complexity of the calculation of the parameters of a heterogeneous structure sometimes forces researchers to use different approximate fading characteristics (fading "indices," fluctuation rate, and the like) which, while they have the same physical meaning, fail to provide any more physically valuable

data than that already obtained from the characteristics considered. We shall not dwell on them here.

Analysis of the diffraction pattern at the terrestrial surface provides data on screen structure, that is, on the effective dimensions, shape, and all possible motions of the scattering centers (ionization heterogeneities). But the inevitable question arises. To what level of the ionosphere layer (to what height) should the results be equated? It is customary where reflection of radio waves is involved, to understand the ionosphere diffraction screen to mean a comparatively narrow region of the layer directly adjacent to the reflection region. The data obtained thus refer to the corresponding reflection heights.

The ionization heterogeneities that exist throughout the layer cause fluctuations in the index of refraction, n. The index of refraction differs little from unity at a distance from the reflection region, and fluctuations in $\delta N$ do not result in any marked changes taking place in the wave field. But conversely, even slight fluctuations in $\delta N$ can cause extensive changes to take place in the field structure at the reflection level where $n \to 0$. This is the basis for the assumption that the diffraction pattern observed on the ground is formed at the reflection level.

The arguments cited are purely qualitative in nature, and are not shared by all researchers.

## Measuring Installation for Recording R(t) at one Point on the Terrestrial Surface During Vertical Sounding

General information. (a) The installation is a pulse-type ionospheric sounder for vertical sounding, operating on a fixed frequency. (b) The installation is stationary. (c) The range of working frequencies is 1.5-20.0 MHz, selected from considerations of the possibility of investigating the E and F regions of the ionosphere. (d) The power supply is from the 50 Hz, AC net. (e) Operating mode is constant, continuous.

Figure 1.16a is the functional diagram of the installation.

The pulse center, 4, which generates the following primary voltages, controls the operation of the entire installation: (a) rectangular command pulses with a width of 50-300 μsec and a repetition frequency of 25 or 50 Hz for controlling the transmitter; (b) sawtoothed pulses with a frequency of 25 or 50 Hz /67

for creating the height sweep on the indicators. The sweep width usually is selected of the order of 7000 μsec, providing a height sweep of up to 2000 km, and providing for observations of multiple reflections from the F region; (c) rectangular pulses with a width of the order of 10 μsec and a repetition frequency of 1500 or 3000 Hz for obtaining height markers on the indicators. Pulses at these frequencies provide marker divisions at 50 or 100 km, respectively.

Transmitter 2, controlled by modulator 3, radiates short pulses of radio waves from antenna 1 upon command from the pulse center. The height sweep sawtooth voltage is supplied to indicator 7 simultaneously. The reflected signal, received and separated in the receiver channel (5, 6), is seen on cathode ray tube indicator 7. The reflected signal is fed into the recorder, 8, at the same time so the R(t) process can be recorded.

Transmitter

Installations such as these require a pulse transmitter operating with an off-duty factor of 50-400. The transmitter power rating will depend on the intensity of radio frequency noise at the measuring installation site. Experience in pulse mode operation has demonstrated that a transmitter with a power rating of several tens of kilowatts is needed for reliable recording of the R(t) process.

The transmitter can be designed to use a self-excited oscillator with grid or plate modulation. Figure 1.17 shows the circuitry for an oscillator such as this using type G-481 tubes [79, 94] with a pulse rating of 25-30 kW. A push-pull oscillator comprising self-excited tubes $T_1$ and $T_2$ is used here. The transmitting antenna array is connected to the oscillatory circuit $T_2C_1$ through separation condensers $C_2$ and $C_3$. Condenser $C_1$ provides smooth transmitter tuning. The whole frequency band is covered by shifting coils $L_1$ and $L_2$. The transmitter is grid-modulated. Tubes $T_1$ and $T_2$ are blocked by negative grid voltage for the greater part of the time. The grids of the oscillator tubes /68 are supplied with a positive pulse of 500-600 volts from the modulator. The grids are supplied with a small positive voltage with respect to the cathode during the time this pulse is flowing and this provides an adequate plate current flow in the oscillatory mode. Reference [108] describes a similar

transmitter with plate modulation.

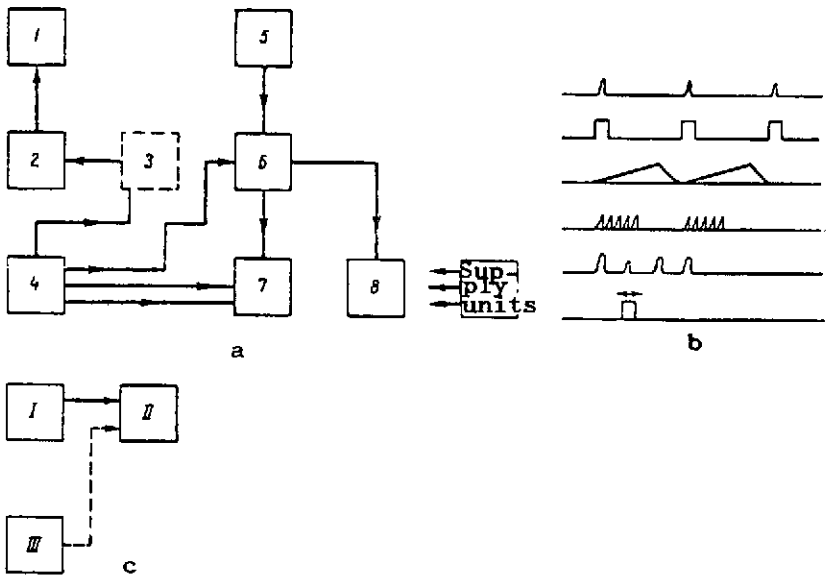


Figure 1.16. Measuring installation for recording R(t).
a - functional diagram of R(t) recording at one point;
b - voltage diagrams at the main units in the installation;
c - functional diagram of a broadband transmitter.

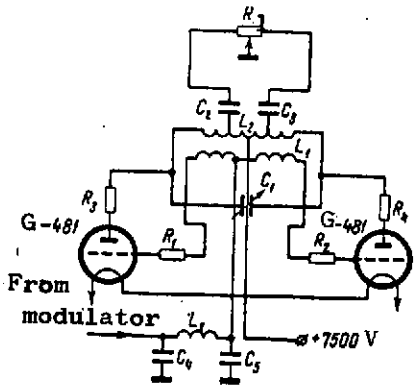


Figure 1.17. Wiring diagram of transmitter with type G-481 tubes.

Another type of transmitter frequently found in use consists of a low-powered master oscillator and a broadband power amplifier [40].

The transmitter is tuned to the required frequency by tuning the master oscillator (see Figure 1.16c) operating in the pulse mode. The high-frequency pulse voltage then is supplied to a multistage broadband amplifier, II, the load on which is the last stage of the transmitting antenna system. This amplifier is, in essence, similar to the amplifiers used in automatic ionospheric sounders (see 1.1.1).

Special oscillators, or mass-produced components of the GSS-6 type [154], can be used as the master oscillator. The operator, simply for convenience, sometimes matches master oscillator and receiver tuning mechanically [40].

Type GMI-90 tubes are used to obtain 30-50 kW at the output of amplifier II (see Figure 1.16c). Corrections must be introduced into the system to ensure uniform amplification in the specified range in these amplifiers (see 1.1.1). It should be pointed out that even the use of a complicated correction circuit will not provide constancy of amplification on all frequencies, so power drops to 1-3 kW at the end of the band [40].

The advantage of this transmitting system is that several master oscillators can be connected to the input of broadband amplifier II (two, units I and II, in Figure 1.16c, for example) controlled by pulses shifted along the time line with respect to each other. This provides for the simultaneous operation of the installation on several frequencies (using the corresponding receiving-recording devices, naturally).

Transmitting Antennas

Standard transmitting antennas for vertical sounders can be used for this measuring installation. Two mutually perpendicular antenna systems fed through /69
a phase-shifting four-terminal network can be used when polarized transmitting antennas are used (vertical rhombic antennas, for example).

Receiver

A standard superheterodyne receiver usually is used to amplify incoming signals, but with the following changes made in the circuitry: (a) the entire automatic gain control (AGC) circuit is removed; (b) the magnitudes of the time constants for all cirucits are normalized according to the nature of the incoming signals (see 1.1.1).

The first change is required for undistorted reproduction of R(t) at the receiver output.

The second change stems from the fact that the signal, which is distorted as it is reflected from the ionosphere, has a width of $\tau$ = 150-400 μsec. In this case the time constant for any circuit should be less than $\tau$. Under these conditions a pulse signal is amplified without distortion and, what is more significant, is not distorted when the receiver is overloaded by the powerful radiation of its own transmitter.

Planned, in addition to the basic changes in the standard receiver indicated, is attenuation of receiver response when the transmitter is radiating by feeding a negative pulse to some of the stages, manual receiver gain control (and mandatory monitoring of this control), and expansion of the pass band.

A pass band of $\Delta f$ = (18-20) kH is needed for undistorted transmission of a pulse signal. The necessary pass band is obtained by the corresponding tuning of the IF-amplifier circuits. Moreover, all circuits are shunted by 40-60 kΩ resistors to reduce the natural oscillations of the circuits affected by pulses with steep fronts, and to increase $\Delta f$.

The signal, after detection, is fed to indicator 7 and recorder 8 (see Figure 1.16a).

The following production receivers can be used: R-250, R-250M, Volna-K, US-9, R-311 [133-135]. The type AR-88 and VS-342 receivers among the older models can operate satisfactorily.

Let us single out the changes that must be made by, taken as a concrete example, the R-250 receiver (the designations, and the numbers of the circuit components, are in accordance with [133]). They include the following.

1. The multicircuit filters in the first IFA-2 [intermediate-frequency amplifier], and in the second IFA-2, are disconnected. The remaining individual circuits for expanding the pass band are shunted by 30 kΩ resistors.

2. 100 pF condensers are installed in the circuit to provide the coupling between the second mixer IF plate circuit (409, 410) and the first IFA-2 grid circuit, as well as between the first IFA-2 plate circuit and the second IFA-2 grid circuit (Figure 1.18).

3. The AGC system in all receiver stages is disconnected (condensers 135, 303, and 291 are shorted; see the receiver circuit diagram in [133]).

4. The "LF band" filter in the first stage of the low-frequency amplifier (LFA) is disconnected (condenser 561 is unsoldered from resistor 603). Condenser 587 is disconnected from resistor 588 and is used to supply a signal from the first LFA to the indicator and photorecorder.

5. Voltmeters, connected to the slide of the potentiometer used as the manual gain control, the MGC, for the receiver, are used as the reading meters when the required receiver gain is set.

6. A pulse is fed to the suppressor grid of the second IFA-2 to block the receiver while the transmitter is radiating. A filter consisting of a 91 pF condenser and a 20 kΩ resistor (see Figure 1.18) is connected in the suppressor grid circuit to make the conditions under which the tube in this stage must function less arduous. /70

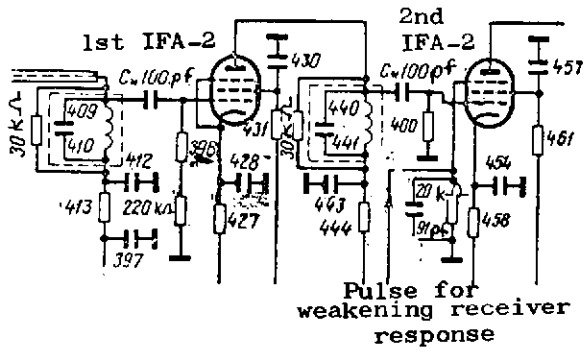


Figure 1.18. Modified circuitry for the intermediate-frequency amplifier for the type R-250 receiver.

Pulse Center

The pulse voltages generated by the pulse center for normal installation operation were listed above. If this unit is built independently, its purpose is to shape the main sync pulse from the 50 Hz commercial alternating current by using an overloading amplifier and trigger, with the sweep voltage obtained from a phantastron. It is more desirable to have this unit built of commercial components. The type GIS-2 delayed pulse generator can be used as the main pulse generator, for example. The sweep voltage can be obtained from type Br-1 sweep unit, or an indicator (oscillograph) with the corresponding sweep band, the type ENO-1, or S-1-34, for example, can be used. The question of calibrating the sweep line is solved automatically in the latter case.

Receiving Antennas

Any antenna with a pattern in the vertical differing from zero can be used as a receiving antenna. This includes all types of antennas used for panoramic ionospheric sounders, such as vertical rhombic antennas (Figure 1.4), and Delta and Chevron type antennas. These types of antennas can be used if their linear dimensions do not influence measurements. There are times, such as when measuring the velocities and directions of drifts of small-scale irregularities,

for example, when the linear dimensions of the receiving antennas must be small compared to the distance between them (the base). Here small antennas, such as loop antennas, must be used. As we know [41], the effective height, $h_e$, of a loop antenna is equal to

$$h_e = \frac{2\pi NS}{\lambda}$$

where

N is the number of turns;

S = hd, the area.

The loop antenna uses the difference in emfs induced in two opposite arms, the shift in phase between which at small $d/\lambda$ is slight, so the effective height of a loop antenna is much less than the geometric dimensions of its arms. This is why the use of tuning loop antennas makes sense. Here the voltage across the input circuit increases by a factor of Q (Q is loop antenna quality). The number of turns for specified area and loop shape should provide inductance governed by the band of working frequencies and by the data on the other components in the input circuit. One possible way to increase the effective height /71 of a loop antenna is to use loops with cores made of a magnetic dielectric. A ferrite, carbonyl iron, and other materials may be used as the magnetic dielectric.

The effective height of this loop is

$$h_e = \mu_e \frac{2\pi SN}{\lambda}$$

where

$\mu_e$ is the effective permeability of the magnetic dielectric.

The drawbacks of loop antennas include the tuner and the complexity involved in feeder padding. It obviously is convenient to use an antenna amplifier located directly beside the loop and loading the feeder.

An analysis of the formulas describing the index of refraction in the ionosphere [3] makes it apparent that double refraction takes place in the ionosphere because of its magnetically active properties. The reflected signal contains two different waves, the ordinary, and the extraordinary. Both

are polarized, and their field vectors have right and left rotation, respectively. The interaction between these waves can cause polarization fading, distorting the diffraction pattern. This type of fading must be eliminated in order to investigate the diffraction pattern in its pure form. There are two ways to eliminate polarization fading. One involves having the R(t) processes take place on one frequency only, and that near the gyromagnetic frequency. This causes substantial attenuation of the extraordinary component, and it can be taken that only one component is being investigated.

The second involves the use of special antennas called polarization antennas. They work as follows [105]. Two identical antennas are arranged perpendicular to each other, so the emfs induced in them by the ordinary and extraordinary waves will differ in phase by ±90°. If the sum of the emfs from both antennas now is fed into the receiver input after one emf has been shifted ±90° in phase, one of the waves will be suppressed.

A six-terminal network (Figure 1.19a) consisting of two four-terminal networks with natural frequencies $f_{01}$ and $f_{02}$ [105], is used to obtain the necessary shift in the phase of the emfs. Each section of the four-terminal network is its own bandpass filter with the phase curve shown in Figure 1.19b. The phase shift for this filter is equal to

$$\psi = \operatorname{arc\,tg} \frac{f}{f_0},$$

where

f is the working frequency.

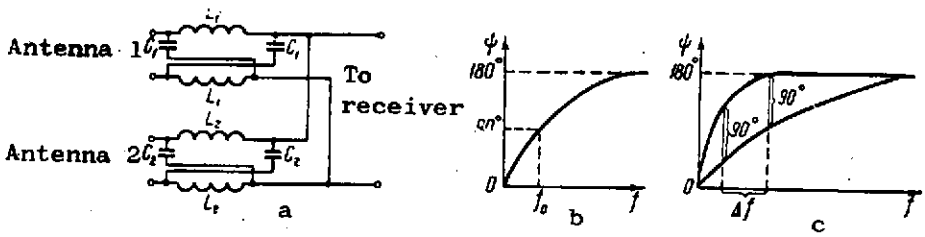


Figure 1.19. Diagram of a phase-shifting six-terminal network. a - principal schematic; b - phase curve for a single four-terminal network; c - phase curves for a six-terminal network.

The $\psi = 90°$ shift will take place only at the four-terminal network's natural frequency, $f_{k0}$. Two four-terminal networks (Figure 1.19a), selected /72

such that their phase curves differ by ±90° within the required frequency band (Figure 1.19c), must be connected for operation within the specified frequency band, $\Delta f$; that is, in order to have

$$\psi = 2\left(\text{arc tg}\,\frac{f}{f_{01}} - \text{arc tg}\,\frac{f}{f_{02}}\right) = \pm 90°.$$

The practical accomplishment of systems such as these has shown that the ratio of suppressed to passed waves is no worse than 1/10. Much better results can be obtained when transmitting and receiving polarization antennas are used simultaneously [108].

Naturally, the filter circuit (Figure 1.19) can include a switch to transfer from one type of polarization to the other.

References [14, 105] discuss the procedure for calculating the filter components.

The site of receiving antennas in a particular locality must be selected to avoid having them near large metal objects (communication lines, electrical networks, antenna arrays, and the like) because they are reradiators of electromagnetic energy and thus can seriously distort the diffraction pattern under study. The requirements for choosing radio direction finder sites [41] can serve as a guide for the selection of the antenna field.

Indicator

Reflected signals are observed visually on the screen of a cathode ray oscillograph. The sweep voltage is supplied to one pair of plates in the tube, and the receiver output voltage is supplied to the other pair. The pulse voltage for the height markers can be supplied to the cathode, or to the control electrode in the cathode ray tube to modulate beam brightness. Type S-1-1, ENO-1, S-1-15, S-1-34, and the like, instruments can be used as indicators [154].

Recorder

Camera attachments can be used to record variations in the amplitude of a reflected signal on motion picture film. The attachment can be mounted directly in front of the screen of the visual indicator, or of the auxiliary

indicator added to the measuring installation especially for recording purposes. The film moves continuously in a direction perpendicular to the beam deflection caused by the reflected signal. Film speed can be selected in the 1.5-3.5 mm/sec range.

Loop oscillographs, the type K-105, for example, can be used to record temporal variations in signal amplitude.

The methods described as in use to record on motion picture film are simple and descriptive, but are ineffectual when computers must be used to process incoming information. In the latter case the recording must be made directly in a form suitable for computer input (a digital recording on punched tape, punched cards, or magnetic tape), or special converters can be used to convert the graphic R(t) recording into analog or digital form (the "Siluet" installation, for example [136). Reference [228] describes recorders that can be used in conjunction with computers.

There are several signals corresponding to the radiated and received pulses present at the receiver output, but their recording requires that they be distinguished from each other in some fashion. Time gating can be used for this purpose, that is, the required signal is separated by an auxiliary gating pulse. The gating pulse should have the same repetition frequency as the command pulses, a width of 250-400 μsec, and a regulated time delay between 0-7000 μsec /73 (see Figure 16.b). The required signal is separated because some stage in the receiver is blocked by the permanent negative bias. This stage can be enabled only by the gating pulse, the time delay for which corresponds to the time of arrival of the required signal. Gating can take place in any receiver or indicator stage [108].

If the recording is made on motion picture film from the screen of a cathode ray tube, it is rational to gat the electron beam of the recording oscillograph directly.

### 1.2. The Coherent Frequency Method

Measurement of the difference in the coherent frequency Doppler shift has been widely used in recent years in ionospere research with rockets and satellites to establish the electron concentration.

The idea of using coherent frequencies to study the ionosphere came into being long before the appearance of rockets and satellites. L. I. Mandel'shtamm and N. D. Papaleksi used the method for the first time in 1936 to study the ionosphere during the solar eclipse.

The method is referred to as the dispersion interferometer method, the Doppler frequency difference measurement method, and the like, depending on the conditions under which the method is used. The general arrangement, explained in particular in references [3, 4], reduces to the following.

We know that the complete change in the phase of wave $\varphi$ over some section of path $l$ can be defined as the product of the frequency of the wave, $\omega = 2\pi f$ for each oscillation, by the time it takes the wave front to traverse this section. The value of the phase velocity, $v_p = c/n$, where n is the index of refraction, is taken to find the time interval because we are discussing phase relationships. If the medium is homogeneous

$$\varphi = \frac{2\pi f}{c} nl.$$

The index of refraction is a variable in the ionosphere, so the interval along the propagation path must be taken to evaluate the change in phase of a radio wave propagating in the ionosphere. Now the phase is

$$\varphi = \frac{2\pi f}{c} \int_0^l n(l)\, dl. \tag{1.46}$$

A transmitter radiating coherent waves with frequencies $f_1$ and $f_2$ is at point A. $f_1 = pf_2$, where $p = m/k > 1$, and m and k are integers. These radio waves are received and their phase difference, $\Delta\varphi$, is recorded at point B. The phase difference results in a higher frequency, such that $\Delta\varphi = \varphi_1 - p\varphi_2$. The following expression for $\Delta\varphi$ can be obtained by using Eq. (1.46)

$$\Delta\varphi = \frac{2\pi p f_2}{c} \left( \int_0^l n_1(l)\, dl - \int_0^l n_2(l)\, dl \right). \tag{1.47}$$

Integration takes place along the path from the receiving to the transmitting antenna, with $n_1(l)$ and $n_2(l)$ the indices of refraction for the radio waves for frequencies $f_1$ and $f_2$, respectively.

As has been pointed out more than once, if electron collisions and the influence of the earth's external magnetic field are disregarded, n can be written in the following form as a function of the radio wave frequency 74

$$n = 1 - \frac{e^2}{2\pi m f^2} \cdot N, \tag{1.48}$$

where

N is the electron concentration.

Using Eq. (1.48), Eq. (1.47) can be rewritten in the form

$$\Delta\varphi = \frac{e^2}{cmf_2}\left(\frac{p^2-1}{p}\right)\int_0^l N(l)\,dl, \tag{1.49}$$

making it apparent that the difference in the phases of two coherent frequencies is proportional to the content of free electrons along the path over which these oscillations are propagated.

Let us follow reference [3] in considering the limit case, when the radiator is moved in the ionosphere in a direction coinciding with the direction of radio wave propagation. This variant can be realized in particular by a rocket ascending absolutely vertically.

Let us measure $\Delta\varphi$, the incremental phase difference over the interval $\Delta h$. Using Eq. (1.49), in which l is replaced by h, we can evaluate the mean value of N in the interval $\Delta h$ as

$$\int_h^{h+\Delta h} N(h)\,dh = N(h,\ h+\Delta h)\,\Delta h,$$

from whence

$$N(h,\ h+\Delta h) = \frac{\Delta\varphi}{\Delta h} \cdot \frac{cm}{e^2} \cdot f_2 \cdot \frac{p}{(p^2-1)}. \tag{1.50}$$

If phase difference measurements are continuous this approach will provide the height behavior in the electron concentration distribution. Reference [57] contains a detailed analysis of the case of a radiator moving vertically.

Now let us take the case when the radiator is moving over a more involved path. Let the radius vector connecting the point of reception of the oscillations with the moving radiatior at height h(t), and which is changing

with respect to time, equal r(t), and let the radial, horizontal, and vertical components of the velocity at which it is moving equal $\dot{r}(t)$ along a straight line of sight, $\dot{x}(t)$ and $\dot{h}(t)$, respectively. Here, and in what follows, the dotted symbol signifies a temporal derivative.

The oscillations received at the observation point will be proportional to $\sin[\omega_1 t - \varphi_1(t)]$ and $\sin[\omega_2 t - \varphi_2(t)]$, respectively, where phases $\varphi_1(t)$ and $\varphi_2(t)$ can be found, as has been pointed out above, from

$$\varphi_1(t) = \frac{\omega_1}{c}\int_1^{r(t)} n_1(r)\,dr, \qquad \varphi_2(t) = \frac{\omega_2}{c}\int_0^{r(t)} n_2(r)\,dr.$$

The origional oscillations are coherent, so the cited difference in the instantaneous values of the frequencies of the received oscillations can be defined by

$$\Delta\dot{\varphi} = \dot{\varphi}_1(t) - p\dot{\varphi}_2(t) \tag{1.51}$$

and is the instantaneous difference in the Doppler frequencies of the incoming waves. Taking N = N(h) as before, and using the expression for the index of refraction in the Eq. (1.48) form, we obtain

$$\dot{\varphi}(t) = \frac{\omega_1}{c}\dot{r} - \frac{2\pi e^2}{m\omega_1 c}\cdot\frac{d}{dt}\int_0^{r(t)} N(h)\,dr,$$

from whence, assuming that h = r cos $\alpha$ (where $\alpha$ is the angle between the radius vector r and the vertical), we have the following expression for $\dot{\varphi}$ /75

$$\dot{\varphi}(t) = \frac{\omega_1}{ch}\dot{r}\left(1 - \frac{2\pi e^2}{\omega_1^2 m}\cdot\frac{N_n}{h}\right) + \frac{\omega^2_1}{c}\cdot\frac{h}{\cos\alpha}\left(N_0 - \frac{N_n}{h}\right)\frac{2\pi e^2}{m}, \tag{1.52}$$

where

$N_n = \int_0^h N(h)dh$ is the total number of electrons in a column with a section of 1 $cm^2$.

Substituting Eq. (1.52) into Eq. (1.51) we obtain the following expression

$$\Delta\dot{\varphi} = \frac{2\pi e^2}{mc\omega_1}(p^2-1)\left\{\frac{N_n}{h}(\sin\alpha\cdot\dot{x} + \frac{\sin^2\alpha}{\cos\alpha}\cdot\dot{h}) - \frac{N_0}{\cos\alpha}\dot{Z}\right\}, \tag{1.53}$$

connecting the measured phase difference with the parameters of the path over which the satellite is moving, and with the magnitude of the electron concentration.

Eq. (1.53) makes it apparent that the relationship between the magnitude $\Delta\dot{\varphi}$ and the concentrations is a complex one, and that it is difficult to establish that relationship from Doppler frequency measurements in the general case. Two limit cases can be considered. One is when the path is along a straight line, or, in the case of more involved paths, when the radiatior passes through the zenith. Here $\dot{r} = \dot{h}$ and $\cos \alpha = 1$. Eq. (1.52) now yields $N_0$ at satellite height h directly. It may be seen that Eq. (1.53) becomes Eq. (1.50), which we obtained for rocket height. The second case corresponds to that of a quasi-horizontal trajectory (a quasi-circular satellite orbit). Here $\dot{h} \ll \dot{x}$, so, ignoring terms containing $\dot{h}$, we can use Eq. (1.53) to obtain an expression for making a direct determination of the integral concentration

$$\Delta\dot{\varphi} = \frac{2\pi e}{mc\omega_1}(p^2 - 1)\frac{N_n}{h}\sin\alpha, \qquad (1.54)$$
$$N_n = \frac{\Delta_T\, mc\omega_1 h}{2\pi e\,(p^2 - 1)\sin\alpha}.$$

The radio frequencies at which the measurements are made clearly should be higher than the maximum critical frequencies encountered to ensure uninterrupted communication between rocket, or satellite, and the ground at all heights. The use of radio waves in the ultrashort wave range makes it possible to use highly directional antennas and thus increase the resistance of the method under consideration to noise. These waves did not produce spurious reflections from the regions of the ionosphere above the radiator, and this too increases noise resistance. Moreover, their use provides ionospheric charactistics averaged for fewer regions than is the case when longer waves are used because the size of the region participating in the formation of the signal is, in the first approximation, proportional to the size of the first Fresnel zone (of the wavelength). These considerations have led to the selection of working frequencies of $f_1$ = 144 MHz, $f_2$ = 48 MHz, and $f_3$ = 24 MHz for the equipment used for these investigations by the Soviet Union.

The set of equipment used for rocket measurements [56] comprises (a) the set of radio transmitters and transmitting antennas installed on board the rocket, (b) the ground antennas, (c) the receivers and phasometers, and (d) the recording and auxiliary equipment.

The set of radio transmitters carried by the rocket generates coherent

oscillations with three frequencies, $f_1$, $f_2$, $f_3$. Each frequency has its individual output, designed for a symmetrical load. Output powers are $P_1$ = = 15 W, $P_2$ = 8 W, and $P_3$ = 3 W, respectively. Coherency of the radiated frequencies is ensured because all oscillations are the results of the sequential multiplication of the frequency of the oscillations generated by the common /76 master oscillator. The master oscillator is a crystal-controlled oscillator installed in a thermostatically controlled housing.

The transmitting antennas are symmetrial linear dipoles. A common dipole is used to radiate radio waves with frequencies $f_1$ and $f_2$. The dipole is excited by two oscillations simultaneously. A separate dipole is used to radiate the third frequency.

The use of a single antenna system to simultaneously radiate two frequencies is necessary to reduce possible errors in measurements caused by rocket rotation. If the transmitting antennas are spaced, arbitrary rotation of the rocket in flight causes random changes in the difference in the geometric distances between transmitting and receiving antennas and this causes random changes in the recorded phase differences. The use of a superposed antenna eliminates errors attributable to change in distance, but there still are certain errors associated with possible differences in phase-space antenna characteristics for each of the frequencies.

Filters are used for decoupling to do away with the mutual effect of the outputs of frequencies $f_1$ and $f_2$ when working with a common dipole.

The ground-based equipment, which is located near the point where a projection from the apex of the rocket trajectory intersects the earth, receives the signals radiated from the rocket, and then converts and records them. The ground-based equipment (1) receives and measures change in the difference in phases of waves with frequencies $f_1$ and $f_2$, as well as $f_2$ and $f_3$, (2) measures the high-frequency oscillation voltages across the receiver input, and (3) records on motion picture film simultaneously changes in the differences in the phases of two pairs of incoming signals, the voltages of these signals at the corresponding receiver inputs, and the time markers. Figure 1.20 is a block diagram of a ground-based receiver.

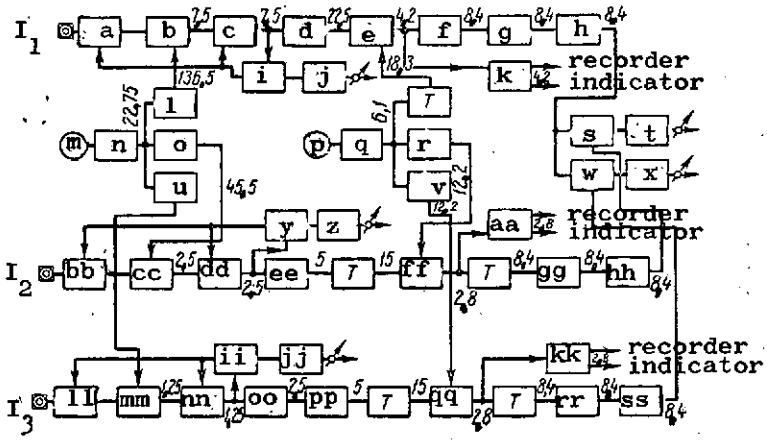


Figure 1.20. Block diagram of a receiver. $I_1$, $I_2$, $I_3$ - inputs for frequencies $f_1$, $f_2$, $f_3$, respectively; $H_1$, $H_2$ - first and second heterodynes; D - doubler; T - tripler; M-6 - factor of 6 mutiplier; 1M, 2M - first and second mixers; $C_1$ and $C_2$ - crystals; 1CF, 2CF, 3CF - cathod followers; De - AGC detectors; FD - phase detectors.

LEGEND FOR FIGURE 1.20.

a - HFA-1; b - 1M; c - 1FA; d - T; e - 2M; f - D; g - L; h - 2CF; i - De; j - 1CF; k - 2CF; l - M-6; m - $C_1$; n - $H_1$; o - D; p - $C_2$; q - $H_2$; r - D; s - FD; t - 3CF; u - D; v - D; w - FD; x - 3CF; y - De; z - 1CF; aa - 2CF; bb - HFA-2; cc - 1M; dd - 1FA; ee - D; ff - 2M; gg - L; hh - 2CF; ii - De; jj - 1CF; kk - 2CF; ll - HFA-3; mm - 1M; nn - 1FA; oo - D; pp - D; qq - 2M; rr - L; ss - 2CF.

Each of the ground receiving antenna installations is designed to receive signals at one of the frequencies and consists of two electrically independent, but structurally coupled antennas with mutually perpendicular linear polarization. This was done to specifically separate polarized changes in signal levels, as well as to keep from losing data when one of the antennas is in a "polarized null." The antenna for each polarization is connected to its individual receiver. /77

Signals received by the antennas are fed into the receiver, a 3-channel, superheterodyne receiver capable of simultaneously receiving and measuring changes in differences in phases of oscillations with frequencies $f_1$, $f_2$, and $f_3$. Mixers convert the frequencies twice in each channel. The corresponding heterodyne voltages are obtained by multiplying the frequencies of the two crystal-controlled heterodynes common to the three channels. The use of common heterodynes eliminates errors in phase measurements caused by

instability in heterodyne frequencies.

Frequencies at the output of each channel are reduced to a single frequency by multiplying the frequencies in the $f_2$ and $f_3$ channels. The intermediate frequencies in all three channels are additionally increased by a factor of 6. So too are the phases of the intermediate frequencies, simplifying measurement of changes in phase differences.

The oscillations, reduced to one frequency at the channel outputs, are paired and, after summing, are detected by separate detectors to yield two envelopes of summed oscillations (interference frequencies) at the detector outputs.

The summed voltage across the detector output can be described by the equation

$$u = U\sqrt{1 + \cos\Delta\varphi}, \qquad (1.55)$$

where

U is the voltage across the detector output when the voltage across one of the channel outputs is detected;

$\Delta\varphi$ is the difference in the phases of the summed oscillations.

This method requires that the voltages across all three channel outputs be constant with respect to time, and equal to each other. The limitation mode for the series of stages and AGC must be used to satisfy this requirement.

The intermediate frequencies are different in each of the channels (frequency equalization occurs at the channel output, before the signal is fed to the phase detectors) so there is yet another method that can be used to measure phase difference, that of recording shifts in the characteristic points of the Lissajous figures. Here the receiver circuitry includes a tap to bring out voltages with the corresponding intermediate frequencies. These voltages are supplied to form the figures on the cathod ray tube.

The measurements are recorded on motion picture film. Figure 1.21 is an example. The interference frequency current and the currents that depend on the voltages across the receiver inputs, are recorded when a loop oscillograph type MPO-2 is used to record the voltages across the outputs of the phase detectors.

This is necessary to monitor the temporal constancy of U [see Eq. (1.55)]. Time markers too are recorded.

The positions of two adjacent maxima on the interference curve obtained using Eq. (1.55) determine the interval over which the difference in phases of the summed coherent oscillations succeeds in changing by the magnitude $2\pi$. The corresponding time markers can be used to evaluate the magnitude of this interval, and to determine the speed and height of the rocket for that interval by using available trajectory measurement data. With such data available, and observing the above limitations (conditions), Eq. (1.50) can be used to calculate the value of the electron concentration averaged for the particular segment of the trajectory, $\Delta h$, and reduced to the middle of this segment.

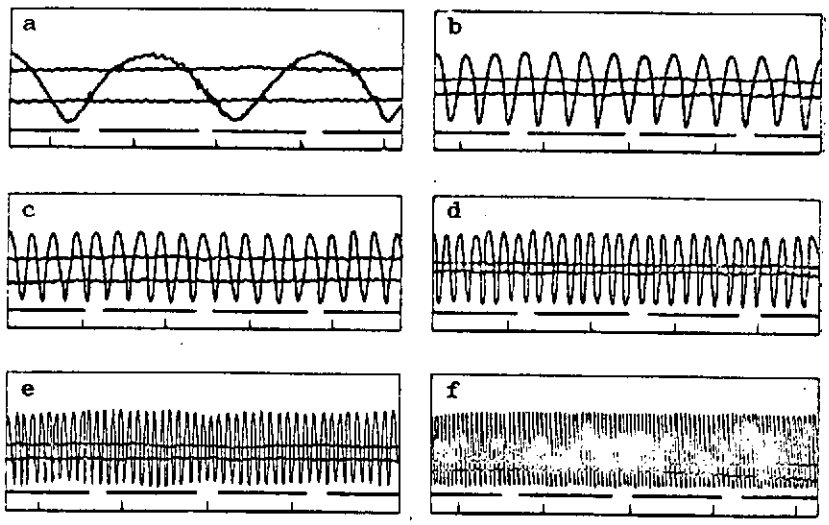


/78

Figure 1.21. Sample recordings at the output of a receiver using the coherent frequencies method. The different oscillograms (a-f) are for different sections of the trajectory (different rocket speeds and different electron density values).

The second method of recording changes in phase difference is, as has been pointed out above, based on recording the characteristic points of Lissajous figures on moving film. These figures are formed on the screen of a cathode ray tube if voltages from the outputs of two receiver channels are supplied to the deflection plates. These changes are uniquely associated with changes in $\Delta\varphi$. The phase difference, $\Delta\varphi$, changes continuously while the rocket is in flight so the change in the shape of the figures will also change continuously.

The characteristic points of these figures will move across the screen in unique fashion. The shape of the recording will determine the difference in signal phases for any moment in time. The interval on the recording between two successive points corresponding to the limits of the Lissajous figures will correspond to $\Delta\varphi = \pi/2$ for the higher frequency, and to $\pi/3$ for the lower. What must be taken into consideration, however, is the fact that the values of the intermediate frequencies used are 22.5 and 15.0 MHz, as follows from the block diagram of the receiver.

As in the first case, the time markers are recorded at the same time as are the characteristic points. The time markers can be used along with the coordinate data to convert to N values and to their spatial localization.

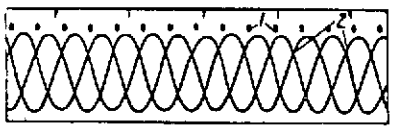

Figure 1.22. Recording of changes in the positions of the characteristic points of Lissajous figures. 1 - time points; 2 - points corresponding to figure limits.

Figure 1.22 is a portion of one of the recordings. The limits of the figures can be determined from the intersections of the lines. The distance between two points of intersection covered by one position on the screen (in the vertical) corresponds to a definite phase difference value. Evaluating it with respect to the time scale (time markers are recorded on the same film), we can convert to rate of change values.

Reference [56] reviews the errors contributed to the measurements considered by the equipment used, and suggests that they are no more than 5% of the measured magnitude.

The equipment used to make earth artificial satellite-aided measurements is, for all practical purposes, no different from that used in the rocket experiments (see [5, 7], for example).

Much like the coherent frequencies method is that for determining the electron concentration based on the recording of changes in the angle of rotation of the plane of polarization of the waves radiated by the satellite [57]. The cause of these changes is the Doppler rotational effect (the Faraday effect). /79

We know that the two components of a radio wave that result from the wave being split by the earth's magnetic field are propagaged at different phase

velocities. Therefore, the plane of polarization of waves radiated from the ionosphere will be rotated through angle $\Theta$ at the reception site if they were polarized linearly initially. Readily shown is the fact that when the direction of propagation of radio waves with respect to the magnetic field vector is arbitrary, the plane of polarization will be rotated as the wave covers distance $\Delta L$ along the beam through an angle determined by the magnitude

$$\Theta = \frac{e^3 2\pi}{c^2 m^2 \omega^2} \int_L^{L+\Delta L} H_L N(l)\, dl, \tag{1.56}$$

where

$H_L$ is the component of the magnetic field along the beam of propagation;

$\omega$ is the frequency.

The frequency should be high enough so that absorption can be ignored and that the coefficient of refraction can be taken as near unity.

Voltages at the inputs to receivers with antennas with linear polarization are recorded when receiving radio waves radiated from a rocket. The rotation of the plane of polarization caused by the Faraday effect in this case is recorded in the form of periodic signal fading (Figure 1.23). The distance between two minima corresponds to a $\pi$ change in angle $\Theta$.

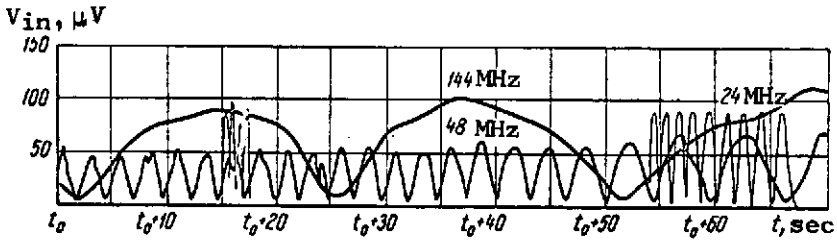


Figure 1.23. Amplitude feeding of radio signals of different frequencies received from a rocket, the Faraday effect. The curve for $f_3$ = 24 MHz is incomplete.

What follows from Eq. (1.56) is that is $\Theta = \pi$, taking it that $H_L$ is known and equal to the temporally constant vertical field component, and substituting $\Delta h$ for $\Delta L$ (the rocket is ascending vertically), the mean electron concentration /80 over the section of the path corresponding to a $\pi$ change in angle $\Theta$ can be

defined as

$$N(h,\ h+\Delta h)=\frac{c^2m^2\omega^2}{2e^2H\Delta h}. \qquad (1.57)$$

The magnitude ΔH is determined in terms of $t_i$ and $t_{i+1}$, corresponding to the recording of the π change in the angle (two adjacent polarization minima).

This method, when compared with the coherent frequencies method, has less resolution, but is simpler because radio waves with one frequency can be avoided when making the measurements.

## 1.3. The Incoherent Scattering of Radio Waves in the Ionosphere Method

### 1.3.1. Theoretical premises

Reviewed in the preceding sections were methods for measuring the electron concentration in the ionosphere, the theoretical bases of which were the phenomena of refraction and reflection of radio waves in the ionosphere, interpreted within the framework of geometric optics. However, the reaction between charged particles of ionospheric plasma and radio waves actually is a very involved physical process. Each free electron, reacting with an incident radio wave, scatters some of the energy, and this phenomenon can be described by a magnitude known as the effective scattering cross section. Waves scattered by an ionized medium containing many free electrons, as well as fluctuations in electron density, can be coherent, limited coherent, or incoherent, depending on the concrete relationships between the wavelength used, plasma parameters, and scattering geometry. Coherent scattering occurs when vertical sounding of the ionosphere takes place at frequencies, f, below the critical frequency for the F2 layer, $f_0F2$.

If sounding frequency is increased such that $f \gg f_0F2$, the ionosphere becomes a source of inchoherent scattering of reradiated energy that can be recorded by using high-response radar receivers (the power radiated by the radar too must be quite high, naturally). The following physical parameters of the ionosphere in the scattering volume can be evaluated by measuring the intensity of the reflection and establishing the features of the scattered signal spectrum, as will be shown in what follows: electron concentration, $N_e$;

electron temperature, $T_e$; ion temperature, $T_i$; and ionic composition. Then too, the scattered signal contains information on the charged particle drift rate, on streams of fast electrons with energy E < 25 eV, and on the orientation of the magnetic field vector at the heights under study.

Briefly then, let us review (without mathematical calculations) the results presented in the theoretical papers while limiting ourselves to those of them with practical application for ionospheric research. Our discussion will take place primarily within the context of reference [175].

The phenomenon of the scattering of the energy contained in electromagnetic waves by charged particles was studied at the beginning of the century by J. J. Thomson [222], hence the frequent use of the term "Thomson scattering" in the scientific literature to describe the results of measurements using this effect. The effective scattering cross section by a free electron ($m^2$) is

$$\sigma_e = \left(\frac{4\pi e^2}{m_e c^2}\sin\psi\right)^2 \cong 8{,}1\cdot 10^{-30}\sin^2\psi, \tag{1.58}$$

where

/81

e amd $m_e$ are charge and electron mass, respectively;

$\psi$ is the polarizing angle, the angle between the direction of the electric vector for the incident radio wave and the direction from the scattering volume to the receiver.

In this particular case the electron can be considered an ideally conducting and isotropically scattering sphere. If the electrons in the volume illuminated by the radar antenna are distributed uniformly, with concentration N, the total effective cross section is

$$\sigma = N\sigma_e. \tag{1.59}$$

In this simplest of all cases only the thermal disordered motion of the electrons, when the percentage of the energy scattered by the individual electrons is simply added, is considered. This is, in essence, the classical case of <u>incoherent</u> scattering, as distinguished from <u>coherent</u> scattering, when the section will be proportional to $N^2\sigma_e$.

Practically speaking, scattering of radio waves in the ionosphere takes place, as is obvious, at nonuniformities in electron density associated with fluctuations in the permittivity, $\Delta\epsilon$, such that [163, 170]

(1.60)

where

$\epsilon$ and N are the mean values of the permittivity and the electron concentration in the volume under consideration, respectively;

$\Delta\epsilon$ and $\Delta N$ are the deviations from the means;

f is the radar working frequency;

$f_N = ((Ne)^2/(\pi m)^{1/2}$ is the plasma frequency.

When $f \gg f_N$

$$\left|\frac{\overline{\Delta\varepsilon}}{\varepsilon}\right|^2 = \left|\frac{\overline{\Delta N}}{N}\right|^2\left(\frac{f_N}{f}\right)^4 = \left(\frac{e^2}{\pi m}\right)^2\overline{[\Delta N]^2}\,\frac{1}{f^4}. \tag{1.61}$$

It can be shown [163] that the effective backscattering cross section ($\psi = \pi/2$) is

$$\sigma = \frac{4\pi^3}{c^4}\left|\frac{\overline{\Delta N}}{N}\right|^2 f_N^4 (2\pi)^{3/2} L^3 \exp\left[-\frac{8\pi L^2}{\lambda^2}\right]. \tag{1.62}$$

if the irregularities in the plasma are spherical and symmetrical and can be described by a Gaussian autocorrelation function with scale L. It is perfectly obvious that the effective scattering cross section, and, as a result, the strength of the received signal, depend significantly on the $L/\lambda$ ratio. The scattering cross section therefore will be very small for all wavelengths $\lambda \leq 1$ m, and particularly for the irregularities with $\Delta N/N \sim 1\%$ and scale $L \geq 1$ km always present in the ionosphere. Yet it will be large enough (for the technical accomplishment of reception of scattered energy) if what we are talking about are irregularities caused by disordered thermal motion of charged particles, the scale of which we can compare with $\lambda$. The backscattering cross section for these fluctuations [163] is

$$\sigma = \left| \frac{\Delta\varepsilon}{\varepsilon} \right|^2 \frac{4\pi^3}{\lambda^4} P(2kl,\ 2km,\ 2kn), \tag{1.63}$$

where

k = $2\pi/\lambda$ is the wave number;

l, m, n are unit vectors characterizing the direction of radio wave incidence;

P(2kl, 2km, 2kn) is a function describing the spatial distribution of density fluctuations.

Substituting here the value $\left| \overline{\Delta\varepsilon}/\varepsilon \right|^2$ from Eq. (1.61), we obtain

$$\sigma = 4\pi \left( \frac{e^2}{m_e c^2} \right)^2 \overline{[\Delta N]^2} P(2kl,\ 2km,\ 2kn) = \sigma_e \overline{[\Delta N]^2} P(2kl,\ 2km,\ 2kn). \tag{1.64}$$

Fejer [178] has shown that for thermal equilibrium /82

$$\overline{[\Delta N]^2} P(2kl,\ 2km,\ 2kn) = N, \tag{1.65}$$

that is,

$$\sigma = \sigma_e N. \tag{1.66}$$

Thus, the microscopic (free electrons) and the macroscopic (density fluctuations) approach arrives at the same $\sigma$ values. This is the basis for considering that the scattered signal intensity is a measure of the electron concentration in the scattering volume.

Continuous motion of the charged particles in the scattering volume should lead to a Doppler shift in the frequency of the radio wave when the scattering process is used. If this process is looked at with only free electrons moving at thermal velocities in mind, the scattered signal spectrum should be purely Gaussian, and the halfwidth of this spectrum, which is proportional to the thermal velocity of the electrons, will equal

$$\Delta f_e = \frac{1}{\lambda} (8kT_e/m_e)^{1/2}. \tag{1.67}$$

The width of the scattered signal spectrum thus can be a measure of the temperature of charged particles in the scattering volume.

In fact, however, the scattered signal spectrum has a much more complicated configuration than a Gaussian curve. This is explained by the fact that the scattered signal strength and spectrum configuration depend on the relationship between the radio wave frequency and the plasma parameters, on the nature of the electrostatic interaction between the electrons in the ionospheric plasma and the positive ions, on the nature of collisions between charged particles, and with neutral particles, on the ion composition, thermal equilibrium, or lack thereof, between ions and electrons ($T_e = T_i$, or $T_e \neq T_i$), nature of particle drift, magnetic field orientation, and other factors.

A theoretical consideration of this problem [178] has revealed that it is important to distinguish between two principally different cases: $\lambda \gg D$ and $\lambda \ll D$ (D is the Debye radius of the ionospheric plasma)

$$D = (kT_e/4\pi Ne^2)^{1/2} \cong 6.9\,(T_e/N)^{1/2}, \tag{1.68}$$

where

$k = 1.38 \cdot 10^{-16}$ erg/°K (the Boltzmann constant).

The magnitude of D in the ionosphere depends on height, time of day, season of year, and solar activity. The mean D for heights up to 300 km is 0.3-1 cm, and $\sim$ 6 cm at heights of the order of 2000 km.

Scattering can be considered purely electron, and the spectrum Gaussian, if $\lambda \ll D$. But it is readily apparent that in this case the spectrum will become so broad that the energy contained in the scattered signal arriving per spectral interval unit will be too low to be detected by modern electronic equipment. In fact, if we substitute $\lambda = 1$ cm ($\approx D$) and $T_e \approx 1600$°K in Eq. (1.67), we obtain a Doppler shift equal to $0.71\,\Delta f_e$ at the half-power level of 31 MHz. Thus, the $\lambda \ll D$ case, while it can be brought about in experiments with laboratory plasma and laser radiation, still has no practical application in ionospheric measurements.

If $\lambda \gg D$, in the general case the function $W(\Delta f)$ describing the spectrum configuration is the sum of two parts which can be called the "electron component," and the "ion component." Let us introduce the parameter $\alpha = 4\pi D/\lambda$. The relative contribution of both components to the total energy of the scattered signal will be determined by the magnitude of this parameter. If $\alpha = 0.5$-2,

the components make approximately the same contribution, and if there is a reduction in $\alpha$ the contribution of the ion component increases, and the signal spectrum is narrowed. Figure 1.24 shows the configuration of the ion component spectrum for the thermal equilibrium case ($T_e = T_i$). The spectrum is a double-humped curve when $\alpha \to 0$, symmetrical with respect to the carrier frequency (the figure is of half the spectrum corresponding to the positive shift). The Doppler shift is determined by the thermal velocity of the ions; that is

/83

$$\Delta f_i = \frac{1}{\lambda} (8kT_i/m_i)^{1/2}. \tag{1.69}$$

$\Delta f_i$ = 2.6 kHz for elemental oxygen, $O^+$, when $\lambda$ = 1 meter and $T_i$ = 1600°K.

Reflection energy thus is concentrated in a very much narrower spectral interval than in the case of purely electron scattering, making detection of a scattered signal a technical possibility.

The total reflection energy, proportional to the area under the $W(\Delta f_i)$ curve, when $T_e = T_i$, will depend on $\alpha$ in the following manner

$$\sigma = \sigma_e \left[1 - \frac{1}{1+\alpha^2} + \frac{1}{(1+\alpha^2)(2+\alpha^2)}\right]. \tag{1.70}$$

The first two terms in this equation reflect the action of the electron component, the third that of the ion component. Readily shown is the fact that the scattering cross section is $\alpha \to 1/2\sigma_e$ when $\alpha \to 0$; that is, it is halved as compared to the simple theory of Eq. (1.59). This reduction in the reflection energy was noted experimentally as well in the first measurements of incoherent scattering from the ionosphere at 41 MHz [165].

Ion and electron velocities are subordinate to Maxwellian distribution if the thermal equilibrium is upset; that is, $T_e \neq T_i$. If $T_e/T_i \leq 3$

$$\sigma = \sigma_e \left[1 - \frac{1}{1+\alpha^2} + \frac{1}{(1+\alpha^2)(1+\alpha^2+T_e/T_i)}\right]. \tag{1.71}$$

The effect of the influence of nonequilibrium on spectrum shape is demonstrated in Figure 1.25. Let us designate $T_e/T_i$ when $\alpha = 0$ by $\beta$. The relationship that does in fact exist is

/84

$$\frac{T_e}{T_i} = \frac{1}{1+\alpha^2}\beta. \tag{1.72}$$

and

$$\sigma = \frac{2\sigma_r}{1+\beta}. \qquad (1.73)$$

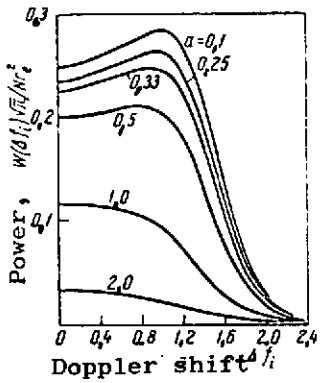


Figure 1.24. Signal ion component spectra for $T_e = T_i$ for different $\alpha = 4\pi D/\lambda$ values.

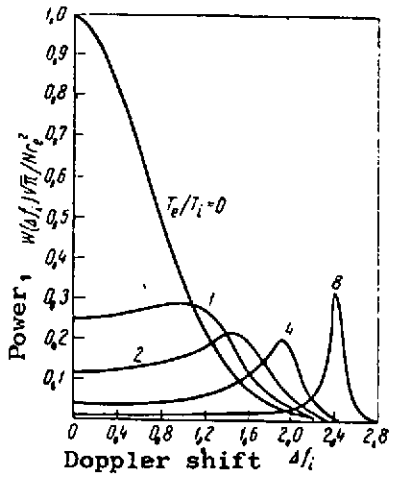


Figure 1.25. Ion component spectra for $\alpha = 0.1$ for different $T_e/T_i$ values.

$\beta$ is thus immediately determinable from the observed spectrum shape. Eq. (1.73) then can be used to calculate $\sigma$ and determine N. $T_i$ can be calculated from the magnitude of the shift at the half-power level, D can be estimated, $\alpha$ can be calculated, and Eq. (1.72) will yield $T_e$. It is quite obvious that the spectrum must have two "wings" if these calculations are to be made, because $\beta$ is estimated from the relationship between the "wings" and the center of the spectrum (Figure 1.25). But, as may be seen from Figure 1.24, the spectrum takes this shape only when $\alpha \leq 0.5$, and this means that the lower limit for the working wavelength needed to support measurements is $\lambda \geq 25D$. Table 3 lists certain of the characteristics of the ionosphere for different conditions, as well as the minimum wavelengths and spectrum width for $\lambda = 1$ meter.

Uniqueness in the determination of the spectrum is difficult to establish when several kinds of positive ions are contained in the ionospheric plasma. Figure 1.26a ($T_e/T_i = 1.5$) shows variations in the spectrum shape for a mixture of $O^+$ and $He^+$ ions. The slope of the curve at the scattering half-power point is a measure of the percentage relationship of concentrations. Figure 1.26b is

a schematic presentation of a series of spectra for a three-component mixture of $O^+$, $H^+$, and $He^+$ ions for the case when $T_e/T_i = 2.0$ [204]. The spectra for 100% content of ions of one kind are placed at the apex of the triangular diagram, the spectra containing two kinds are placed along the sides of the triangle, and those for three kinds of ions are inside the triangle. Keep in mind that it is, in general, impossible to arrive at a unique interpretation of the spectrum as measured if $T_e/T_i$, $\alpha$, and the ion composition are unknown. In practice, the task usually reduces to a determination of $T_i$ and of the percentage content of ions, assuming the other parameters to be known, or finding them by using independent methods.

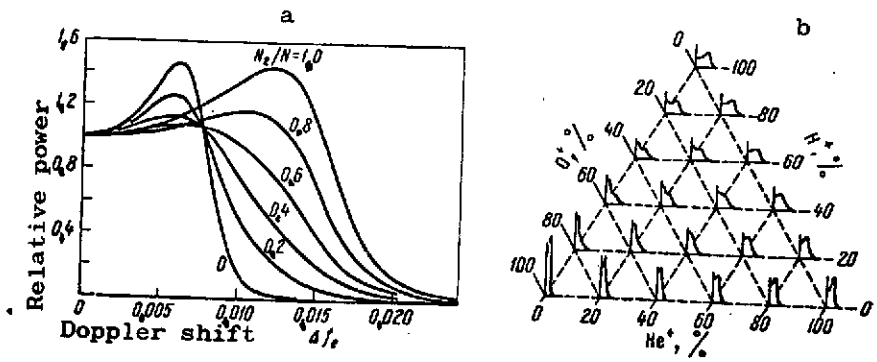


Figure 1.26. Influence of ion composition on spectrum shape. a - change in the shape of the ion spectrum for a mixture of $O^+$ and $He^+$ ions, $N_2$ is ion concentration, N is electron concentration. $\alpha \to 0$, $T_e/T_i = 1.5$; b - diagram of spectrum shape for the $O^+$, $He^+$, $H^+$ ion mixture when $\alpha \to 0$, $T_e/T_i = 2.0$.

Electron and ion collisions with neutral particles should, in principle, also have an influence on the scattered signal spectrum shape and should make it difficult to determine $T_e$ and $T_i$ separately. The length of the free path for electrons ($l_e$) and for ions ($l_i$) can be expressed as

$$l_{e,i} = (\nu_{e,i}\sqrt{m_{e,i}/2kT_{e,i}})^{-1}, \qquad (1.74)$$

where

$\nu_e$ and $\nu_i$ are frequencies of collisions with neutral particles.

/86

TABLE 3. TYPICAL CHARACTERISTICS OF THE IONOSPHERE

| Region of the ionosphere | Height, km | Time of day, season, level of solar activity, S | Concentrations, $N$, cm$^{-3}$ | Electron temperature $T_e$, °K | Ion temperature $T_i$, °K | Ion mass (mean), $m_i$, au | Debye radius $D$, cm | Geomagnetic field strength $H \cdot 10^{-3}$, a/m | Ion gyroradius, $R_i$, cm | Electron gyroradius $R_e$, cm | Minimum wavelength, $\lambda_{min}$, cm | Spectrum width for $\lambda = 1$ m $2\Delta f$, kHz | Maximum wavelength, $\lambda_{max}$, m |
|---|---|---|---|---|---|---|---|---|---|---|---|---|---|
| *E* | 120 | winter night $S_{min}$ | $10^4$ | 300 | 300 | 30 | 1 | 5,90 | 171 | 0,73 | 25 | 1,65 | 8,5 |
| | | summer day $S_{max}$ | $10^5$ | 300 | 300 | 30 | 0,4 | | | | 10 | 1,65 | |
| *F1* | 200 | winter night $S_{min}$ | $10^5$ | 2000 | 750 | 25 | 1 | 5,84 | 169 | 1,92 | 25 | 2,8 | 8,5 |
| | | summer day $S_{max}$ | $5 \cdot 10^5$ | 3000 | 1500 | 25 | 0,6 | | 285 | 2,36 | 15 | 3,8 | 14,3 |
| *F2* | 300 | winter night $S_{min}$ | $10^5$ | 2500 | 1000 | 16 | 1 | 5,78 | 235 | 2,18 | 25 | 4,3 | 11,7 |
| | | summer day $S_{max}$ | $10^6$ | 2500 | 2000 | 16 | 0,3 | | 332 | 2,18 | 7,5 | 6,0 | 16,6 |
| Upper part F2 | 1000 | — | $10^4$ | 3000 | 2500 | 4 | 3,8 | 5,40 | 199 | 2,55 | 95 | 14,3 | 10,0 |
| Lower part exosphere | 2000 | — | $5 \cdot 10^3$ | 3000 | 3000 | 1 | 5,6 | 5,03 | 117 | 2,75 | 140 | 28,6 | 5,85 |

Let us introduce the parameter $\psi_{e,i} = \lambda/4\pi l_{e,i}$. Figure 1.27 shows ion component spectra in terms of $\psi_i$ for $T_e = T_i$. Note that when the length of the free path for the ions becomes short compared with $\lambda/4\pi$, the spectrum narrows and the hump disappears. It should be pointed out that the total reflection energy remains constant and does not depend on collision frequency.

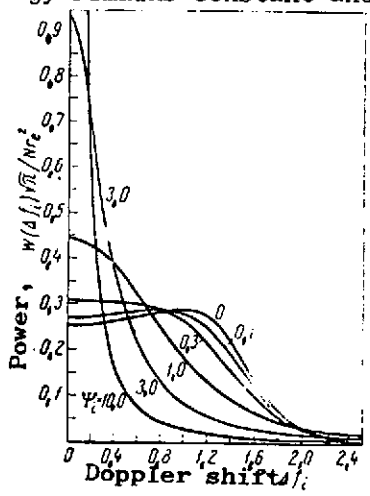

Figure 1.27. The influence of collisions of the ion component of the spectrum when $\lambda \gg 4\pi D$ and $T_e/T_i = 1$; $\psi_e = 0.1\psi_i$.

Practically speaking, $\psi_e \approx 0.1\psi_i$ at all heights in the ionosphere, and electrically neutral collisions can be disregarded. Ion neutral collisions are important below 120 km only (for $\lambda \geq 0.2$ m). There is every reason to say that in this region of the ionosphere (100-120 km) $T_e = T_i = T_n$ ($T_n$ is the temperature of the neutral particles) and that the collision frequency ($sec^{-1}$) is

$$\nu_i \cong 0{,}9 \cdot 10^{-15} N(N_2), \qquad (1.75)$$

where

$N(N_2)$ is the density of neutral nitrogen in the E region of the ionosphere.

Consequently, the neutral density in the range of heights under consideration can be found directly by finding $\psi_i$ from the spectra of the type shown in Figure 1.27, and assigning values to $T_i = T_e = T_n$. It should be pointed out that the characteristics of this region are very important to the building of models of the atmosphere (they are the lower boundary conditions) and yet the majority of the meterological rockets do not reach this level, while artificial earth satellites fly well above them. Hence, the method of incoherent scattering is highly valuable for evaluating the parameters of the lower ionsphere.

It has already been pointed out that directional motions such as the drift of electrons and ions (if there is no magnetic field the electrons and ions will move in the same direction), as well as currents, that is, motion of electrons with respect to ions, can exist in the ionosphere in addition to chaotic thermal motion of charged particles. Directional motion of particles relative to the radar should influence the scattered signal spectrum. If the

whole of the plasma drifts with respect to the receiver at speed $V_d$ m/sec, the whole spectrum should shift by

$$\Delta f_d = \pm \frac{2|V_d|}{\lambda} \text{ Hz}, \qquad (1.76)$$

in which the plus sign is for motion toward the receiver, the minus sign away from the receiver. Spectrum shape does not change for this shaft [175].

If there is a current flow (but the ions do not move relative to the radar) the spectrum, not shifting as a whole, will become asymmetrical. How much so will depend on the ratio of the rate of directional drift, $\bar{V}_d$, to the thermal velocity of the electrons, $\bar{V}_e = (2kT_e/m_e)^{1/2}$ and on the magnitude $T_e/T_i$. Figure 1.28a shows that the degree of asymmetry increases with increase in the electron drift rate toward the receiver, providing that the radiation is from a direction normal to $\bar{V}_d$ (spectrum width is narrower by a factor of $\sqrt{2}$ as compared to purely back scatter). Figure 1.28b illustrates the effect of change in $T_e/T_i$, for fixed $\bar{V}_d = 0.5\ \bar{V}_e$ and the above-cited scatter geometry ($\alpha = 10^{-2}$). The spectrum actually occurs and shifts asymmetrically with respect to the frequency. So careful measurement of the position of the center of the spectrum and of the relationship between the magnitudes of its "wings" makes it possible to estimate the rate of ion drift relative to the radar and electron drift relative to the ions. Estimates show that, in principle, when the accuracy with which elements of the spectrum are measured is within 1%, we can estimate $\bar{V}_d$ within 0.36-0.9 m/sec, and the rate of electron motion at no worse than $0.01\bar{V}_e$ [175]. /87

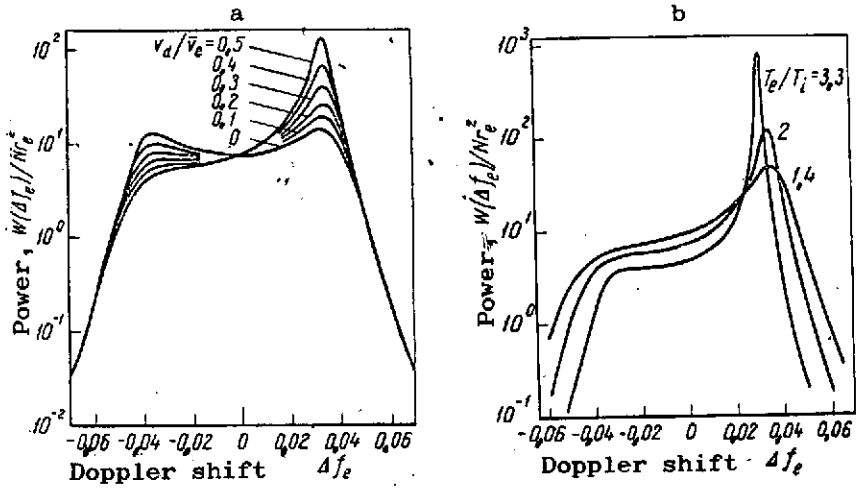


Figure 1.28. Effect of drift motions. a - influence of drift of electrons on the ion components of the spectrum. $T_e/T_i = 2.0$, $\alpha = 10^{-3}$; b - influence of increase in $T_e/T_i$ when drift is present $V_d/V_e = 0.5$, $\alpha = 10^{-2}$.

Real ionospheric plasma always is present in the terrestrial magnetic field. A theoretical consideration of the influence of the geomagnetic field on the strength of the scattered signal and on its spectrum [177, 215] shows that when waves are propagated along the geomagnetic field there are no changes in intensity and spectrum. At the same time the maximum effect takes place in the case of orthogonality of the magnetic field and of propagation direction. The nature and effectiveness of the influence of the geomagnetic field also can be determined by the degree of thermal equilibrium in the ionospheric plasma and by the relationships between the wavelength and the gyrofrequency of the charged particles; that is, by the frequency of their rotation about the magnetic lines of force attributable to the action of the Lorentz force. Ion gyrofrequency is

$$f_H = \frac{eH}{2\pi m_i c}, \tag{1.77}$$

where

H is geomagnetic field strength.

The $O^+$ ions will have a gyrofrequency of the order of 50 Hz in the middle latitudes at F region heights. Ions moving along a normal to the field lines of force appear periodically in the same places with frequency $f_H$, and this, naturally, should lead to the superposition on the spectrum of a signal, the direction of scattering of which is perpendicular to the field, of characteristic fluctuations. Let $\phi$ be the angle between the radio wave and the normal to the direction of the field, and $R_e$ and $R_i$, the so-called gyroradii of the electron and ion, be such that

$$R_e = \frac{c\,(m_e k T_e)^{1/2}}{eH}, \tag{1.78}$$

$$R_i = \frac{c\,(m_i k T_i)^{1/2}}{eH}. \tag{1.79}$$

Table 3 lists the numerical values of $R_e$ and $R_i$. There are two cases that are of practical interest: $\lambda \sim R_i > R_e$ and $R_i > \lambda > R_e$.

In the first case, when $T_e = T_i$ and $\sin \Phi \leq \lambda/35R_i$, modulation of the ion gyrofrequency spectrum occurs. Figure 1.29 shows such a spectrum for $\lambda = 7.5$ meters, for $O^+$ ions, and for $\Phi = 2°$ [171]. It should be pointed out that modulation amplitude is extremely small in the range of angles $90° < \Phi < 5°$, but

/88

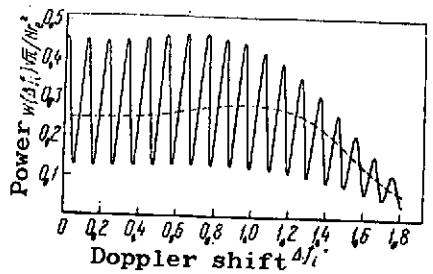


Figure 1.29. Appearance of gyroresonance lines for the $O^+$ ion in the ion composition of the spectrum. $\lambda/R_i = 1.8$; $\Phi = 2°$; $T_e = T_i$; $\alpha \to 0$. The dashed line is for the spectrum when $\Phi = 90°$, or for the case when there is no magnetic field.

increases sharply for $\Phi < 2°$. At the same time, the spectrum is compressed, and degenerated into a line at the sounding frequency when $\Phi \to 0$. Also to be emphasized is that in the case under consideration ($T_e = T_i$) modulation does not change the overall signal strength; that is, the area under the $W(\Delta f_i)$ curve. The range of $\Phi$ angles in which gyroresonance can be observed expands with increase in $\lambda/R_i$, but there is a drop in the modulation amplitude at the same time and only the spectrum width remains as a function of $\Phi$, sensitive to changes in $\Phi$. If $Te/T_i > 1$, reflected signal strength will increase when $\Phi \to 0$. The effect of collisions (ion-ion collisions) is to lessen spectrum modulation. Investigation of ionospheric conditions reveals that modulation vanishes completely at almost all heights below 1000 km, but that above this level proton gyroresonances can be observed.

In the second case, that is when $R_i > \lambda > R_e$, because of decrease in $\Phi$ the spectrum is constricted and approaches Gaussian in shape without change in the overall scattering intensity (Figure 1.30). Application of a magnetic field usually causes an increase in overall intensity as $\Phi \to 0$ when $T_e/T_i > 1$. The scattering cross section increased monotonically with increase in $T_e/T_i$ for $\Phi \leq 0.3°$. This permits the determination of $T_e/T_i$ by scanning the radar beam near $\Phi = 0°$.

Up to this point our discussion of the different effects with an influence on spectrum shape has included only the ion component. The electron component in the spectrum when $\lambda \gg 4\pi D$, that is, when $\alpha \to 0$, appears in the form of two radar lines symmetrical with respect to the carrier frequency. The position of these lines in the spectrum depends on $\alpha$, and in the absence of a magnetic field are away from the carrier frequency by the magnitude

$$f_r = \pm f_N (1 + 3\alpha^2)^{1/2}, \qquad (1.80)$$

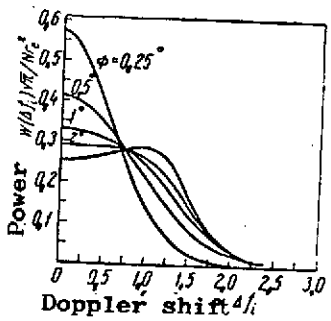

Figure 1.30. Influence of magnetic field on spectrum. $R_e \ll \lambda/4\pi \ll R_i$; $\alpha \leq 0.1$; $T_e = T_i$.

near the plasma frequency $f_N$ [175]. The width of these so-called plasma lines increases with increase in $\alpha$. The energy of the reflected signal associated with these lines, is two to three orders of magnitude less than the energy associated with the ion component of the spectrum, even when $\alpha = 1.0$. So it is very difficult to detect at night, and plasma lines usually are observed in the daytime and then at those heights where their intensity increases because of the streams of fast photoelectrons in the ionosphere with energies of from 1 to 25 ev [191].

The presence of plasma lines in the spectra of a scattered signal can be explained by the scatter by weakly attenuating longitudinal oscillations of plasma with frequency $f_r$, wavelength $\lambda/2$, and phase velocity $V_p = 0.5 f_r \lambda$. These plasma oscillations are small deviations from strict neutrality, and are possible because of the finality of $\lambda/4\pi D$. Photoelectrons moving at this wave velocity and having energy $E_p = 1/2 m_e V_p$ interact with the wave. If their energy is $E > E_p$, they impart their energy to the wave as they overtake it. The reverse is true when $E < E_p$ (Landau attenuation). This process determines the minimum plasma frequency at which the intensified plasma line can be observed ∠89

$$f_{N\ min} \approx 2/\lambda \text{ MHz}, \tag{1.81}$$

where

$\lambda$ is the radar wavelength, m.

Maximumm plasma frequency is determined by ion-electron collisions, and its magnitude is

$$f_{N\ max} \approx 6/\lambda \text{ MHz}. \tag{1.82}$$

What follows then is that by selecting the corresponding wavelength we can investigate the dependency of electron concentration on height, shifting receiver frequency by $f_r$ and finding the height at which the plasma frequency is equal to $f_N$. This approach permits us to find the profile of the electron concentration

in much of the F region in the special case when $f_0F2 \leq f_N$.

The geomagnetic field makes the interaction between electrons in the medium and the wave easy in a wide range of values of angle $\Phi$ because rotation of electrons about the lines of force with period $m/f_N$ sec helps them retain their position relative to the wave crest. This effect brings with it some increase in minimum energy at which the plasma line is intensified. Now

$$f_{N\min} = \frac{3}{\lambda} \tag{1.83}$$

and the interval of plasma frequencies narrows from 3:1 with inclusion of the geomagnetic field to 2:1 with its inclusion.

Let us now consider the basic principles that should form the basis for an experimental installation for studying the ionosphere by the method that involves the incoherent scattering of radio waves. First of all there is the question of selecting the radar wavelength. Quite obviously, the wavelength should be determined by the parameters of the unknown ionospheric plasma. The lower limit, $\lambda_{min}$, can be established as already noted, by the condition that $\lambda \geq 25D$. The upper limit, $\lambda_{max}$, is established such that when $\lambda \gg R_i$ the spectrum will become too sensitive to variations in angle $\Phi$, and this is undesirable. Estimates show [175] that from this point of view

$$\lambda_{max} \geq 5R_i. \tag{1.84}$$

Moreover, the condition

$$\lambda_{max} \geq f_N \tag{1.85}$$

should be satisfied. Table 3 lists $\lambda_{min}$ and $\lambda_{max}$ values corresponding to the ionospheric conditions cited here. It may be seen that wavelengths $\lambda$ = 2 to 6 cm /90 can be used for study at all heights, but below 300 km $\lambda$ = 25 cm to 8.5 m can be used. Collisions between ions and neutrals, as we have seen, have a significant effect on the spectrum when $\psi_i = \lambda/4\pi l_i \approx 0.3$. The wavelength must be shortened in order to reduce the height, beginning at which we can study the properties of a neutral atmosphere by observing collision effects. For example, this height will be $\sim$ 110 km when $\lambda$ = 150 cm, and is $\sim$ 95 km when $\lambda$ = 25 cm.

A number of other factors must be taken into consideration when selecting the wavelength. Included are the need to have the useful signal level exceed the noise level, height resolution, frequency resolution, and resistance to interference.

The incoherent scattering method can be used for oblique propagation of radio waves throughout the ionosphere (continuous radiation or pulse sounding), or for vertical pulse sounding using short pulses. In the latter case the power of the reflected signal (in watts), measured at the receiver output, will equal [175]

$$P_s = \frac{P_t L N \sigma c \tau \lambda^2}{128 \pi^3 R^2} \iint_{\theta \psi} G^2(\theta, \psi) \sin \theta d\theta d\psi, \tag{1.86}$$

where

$P_t$ is transmitter pulse power, watts;

L is the ohmic loss factor in the transmission lines from antenna to receiver and transmitter;

N is the electron concentration, which we assume as constant in the height interval $c\tau/2$, covered by the pulse;

$\sigma$ is the effective scattering cross section, found using Eq. (1.71);

c is the speed of light;

$\tau$ is the pulse width;

R is the distance to the scattering volume;

$G(\theta, \psi)$ is the antenna directive action factor, with $\theta$ the angle measured from the axis of the cone of radiation;

$\bar{\psi}$ is the azimuth angle, measured with respect to the vertical plane containing the axis.

Eq. (1.86) can be integrated with respect to $\psi$ if the radiation pattern is cylindrically symmetrical such that

$$P_s = \frac{P_t L N \sigma c \tau \lambda^2}{64 \pi^2 R^2} \int_{\theta} G^2(\theta) \sin \theta d\theta. \tag{1.87}$$

In the case of a conventional parabolic antenna reflector

$$P_s = \frac{0{,}76 P_t L N \sigma c \tau \lambda^2}{64\pi^2 R^4} G(0), \tag{1.88}$$

where

G(0) is the antenna gain along the axis of radiation.

If we convert from G(0) to the effective antenna area, $A_0$, and if we recognize that

$$A_0 = \frac{G(0)\lambda^2}{4\pi}, \tag{1.89}$$

we obtain

$$P_s = \left[\frac{0{,}76 P_t A_0 L c \tau}{16\pi}\right] \cdot \left[\frac{N\sigma}{R^2}\right], \tag{1.90}$$

in which the first multiplier contains the radar characteristics, the second the characteristics of the scattering medium.

$P_s$ must be increased substantially above the noise level in order to measure the useful signal power. Noise power at the receiver output is

$$P_N = kT_s b, \tag{1.91}$$

where

k is the Boltzmann constant;

$T_s$ is the equivalent system temperature;

b is the receiver passband.

Noise power is the sum of the internal receiver noise and external noise, such that

/91

$$T_s = T_A + T_R + T_L, \tag{1.92}$$

where

$T_A$ is antenna noise temperature;

$T_R$ is receiver effective noise temperature;

$T_L$ is noise associated with losses in the antenna, waveguides, and the like.

Special research has shown that $T_A$, which makes the principal contribution to $T_s$, is a minimum near a frequency of $10^3$ MHz, remains virtually constant to $10^4$ MHz, and then begins to increase once again. Therefore, if $T_s$ is to be reduced to a

minimum we must select $\lambda \leq 30$ cm, and use low-noise antennas and receivers. $P_N$ can be reduced by compressing b, the receiver passband. However, the band cannot be made less than the width of the scattered signal spectrum. Further, if the transmitter radiates a rectangular pulse with a width of $\tau$ seconds the spectrum of the transmitted signal will be $1/\tau$ Hz wide. The optimum signal/noise ratio (disregarding the influence of the medium) should, in this case, occur when $b = 1/\tau$ Hz. Obviously, then $P_s/P_N \sim \tau^2$. Eq. (1.90) shows that $P_s$ does not depend directly on the wavelength, and when installation parameters are selected one should obtain an optimum $P_i A_O$ value and properly select $\tau$. Suppose we assign the following parameters to the radar: $P_t = 3 \cdot 10^6$ W; $A_O = 1.6 \cdot 10^3$ m$^2$; $L = 0.81$; $T_s = 300°K$; $\tau = 50$ μsec; $b = 20$ kHz. Let us find $\sigma$ from

$$\sigma = \frac{1}{1 + T_e/T_i} 10^{-28} \text{ m}^2, \tag{1.93}$$

Now, using the data listed in Table 3, we can estimate $P_s/P_N$ for different heights and ionospheric conditions. At night $P_s/P_N < 1$ at all heights (and $P_s/P_N \ll 1$ at heights above 1000 km), and during the daytime $P_s/P_N > 10$ at all heights, so signal storage devices of different types must be used. The pulse is stretched to make measurements above the F2 layer maximum, and this causes a deterioration in the installation's height resolution.

In the case of the use of oblique propagation (the so-called bistatic radar), when two beams (the antenna transmitting and receiving patterns) intersect at angle X, the power of the scattered signal depends on the position and the characteristics of both antenna beams. If we assume that the transmitter is operating in a continuous radiating mode with mean power $P_m$ and that the area in which the beams, which are cylindrically symmetrical, intersect has an orthogonal system of coordinates, x, y and z, we have the following expression [175] for scattered signal power

$$P_s = \frac{P_m L N \sigma}{4\pi R_1^2 \cdot 4\pi R_2^2} \int_{-\infty}^{\infty} \int_{-\infty}^{\infty} \int_{-\infty}^{\infty} G_1(\theta_1) A_2(\theta_2)\, dx dy dz, \tag{1.94}$$

where

$R_1$ and $R_2$ are the distances from the center of the scattering volume to the transmitter and receiver, respectively, at the same time that this volume is small compared to $R_1$ and $R_2$; that is, the antennas have narrow patterns.

For conventional parabolic antennas with the same pattern

$$P_s = 5{,}7\,\frac{P_{cp}LN\sigma\lambda A_{20}^{1/2}}{16\pi^2 R_2 \sin\chi}. \qquad (1.95)$$

Eq. (1.95) shows that the signal power is inversely proportional to distance $R_2$ from the scattering volume to the receiving antenna (and not to the square of the distance, as is the case for the pulsed radar) and proportional to the square root of the effective area of the receiving antenna. The advantage of the bistatic radar is that its height resolution is not determined by pulse width, but only by the width of the antenna patterns, the distance between them, and the scattering geometry. The disadvantage is the complexity in matching operation of installations several hundred kilometers apart, as well as great difficulties in measuring the electron density profile. Actually, we must have an antenna capable of changing the elevation of the antenna pattern over a wide /92
range in order to cover measurements over a considerable range of heights and this means spending a great deal of time on covering the whole range of heights because it is necessary to collect the signal scattered from each interval. Moreover, height resolution deteriorates with increase in the height under investigation because of increase in the scattering volume. Practically speaking, the bistatic radar is more efficient for ionospheric measurements in the E and F1 regions.

### 1.3.2. Equipment and procedures

Equipment for investigating the ionosphere by the incoherent scattering of radio waves is expensive and is a complicated engineering complex, so today there are no more than 10 such installations in the world conducting regular scientific research work by this method. The United States, the Soviet Union, France, and England are actively engaged in such research. Table 4 lists the parameters of some of the powerful foreign radar installations. They were designed at different times and when many of the theoretical conclusions still had not been reached. All these installations began operations in the 1960s. The radars in Jicamarca, Arecibo, and Saint-Santin are outstanding in their design features and capabilities, so there is reason to describe them in some detail. The others, including these in planning today, are modifications, or combinations, of these three.

TABLE 4. PARAMETERS OF INCOHERENT SCATTERING OPERATING INSTALLATIONS

| Installation | Geographic latitude | Geographic longitude | Geomagnetic latitude | Working frequency MHz | Type | Antenna characteristics | Effective antenna area, db/m$^2$ | Effective system temperature, T, °K | Maximum radiation, kW |
|---|---|---|---|---|---|---|---|---|---|
| Environmental Science Services Administration (ESSA), USA, radar observatory, Jicamarca, Peru | 11.95°S | 76.87°W | 2° | 49.92 | Vertical beam, pulse | Dipole array, 290x290 m | 45.0 | 6000 | 4000 |
| Cornell University, USA, Ionosphere Observatory, Arecibo, Puerto Rico | 18.3°N | 66.75°W | 30° | 40.12<br>430.0 | Vertical beam, pulse | Spherical mirror, ø 300 m | 43.7<br>41.7 | 10000<br>300 | 2500<br>2500 |
| Stanford Scientific Research Institute, Stanford, California, USA | 37.4°N | 122.17°W | 43° | 1300 | Oblique beam, pulse | Paraboloid, ø 27 m | 23.8 | 300 | 5000 |
| Lincoln Laboratory, Massachusetts Institute of Technology, Millstone Hill, Bedford, Mass., USA | 42.6°N | 71.5°W | 53° | 440.0<br>1295.0 | Vertical beam, pulse<br>Oblique beam, pulse | Paraboloid, ø 68 m<br>Paraboloid, ø 25 m | 32.2<br>22.8 | 200<br>150 | 3000<br>4000 |
| Radar Scientific Research Institute, Great Malvern, England | 52.1°N | 2.14°W | 56° | 400.0 | Vertical beam, pulse | Paraboloid, ø 42.5 m | 28.5 | 200 | 10000 |
| National Center for Long-Range Communication Research (CNET), Saint-Santin, France (transmitter); Nancy, France (receiver) | 44.65°N<br>48.37°N | 2.19°E<br>2.10°E | 47° | 935.0 | Two-position, continuous radiation<br>Transmitter vertical beam<br>Receiver-oblique beam | Mirror 20x100 m<br>Mirror 20x100 m | 30.0 | 130 | 75 |

The Jicamarca radar [175, 176, 162]. The installation was built near the magnetic equator, the idea being to use a radar radiating energy perpendicular to the geomagnetic field as an ion mass-spectrometer [177, 215].

The antenna is an array of half-wave dipoles 0.3 $\lambda$ above the underlying screen on the ground. 96 dipoles are positioned along the side of the square occupied by the array (290 meters). A second array of dipoles orthogonal to the first array occupies the same physical space and is at the same height. Independent power supplies are used for the two orthogonal polarizations. The arrary is broken down into 64 "modules" of 144 dipoles for each polarization. The pattern is scanned electrically near the zenith in small limits. Each dipole is a segment of a coaxial line 6$\lambda$ long, in which the internal and external conductors are shifted at $\lambda/2$ intervals.

The transmitter is assembled from four triodes installed in coaxial cavity resonators, each of which produces a maximum of 1 MW. The tubes are phased in pairs, and each pair works on its part of the antenna array when the radar is in operation. It therefore is possible to radiate pulses with right circular polarization and with left circular polarization in turn. Grid modulation is used in the transmitter and the pulse width can be changed over a wide range.

The receivers are conventional tube-types. Digital voltmeters are used to record data. A special electronic computer that is part of the complex is used to control the radar and to process data operationally. Figure 1.31 is a general view of the installation [182]. The installation is most effective in the heights above 200 km.

The ionosphere observatory in Arecibo. Figure 1.32 is an overall view of /94
the installation. The antenna consists of a grid of reflecting surfaces and feeders. It is built in a karst depression in the mountains in Puerto Rico. The surface of the mirror is part of a sphere with a radius of curvature of 245 meters and a diameter of 300 meters. Use of a spherical mirror makes it possible to rock the pattern by moving the exciter. The exciter can be moved along the arc of a circle with a radius of the mirror, so beam symmetry is maintained. The exciting system is suspended on cables at a height of 144 meters above the surface of the mirror. The beam can scan in limits 20° from the zenith.

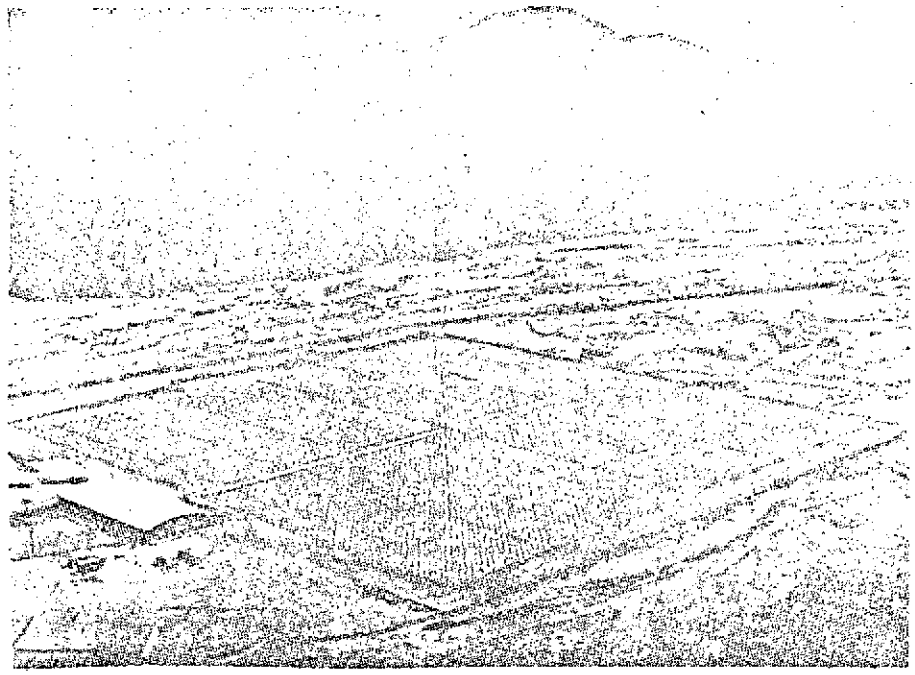

Figure 1.31. The radar installation in Jicamarca, Peru (general view). The antenna array and the building housing the transmitter, receivers, and recorder-computer complex.

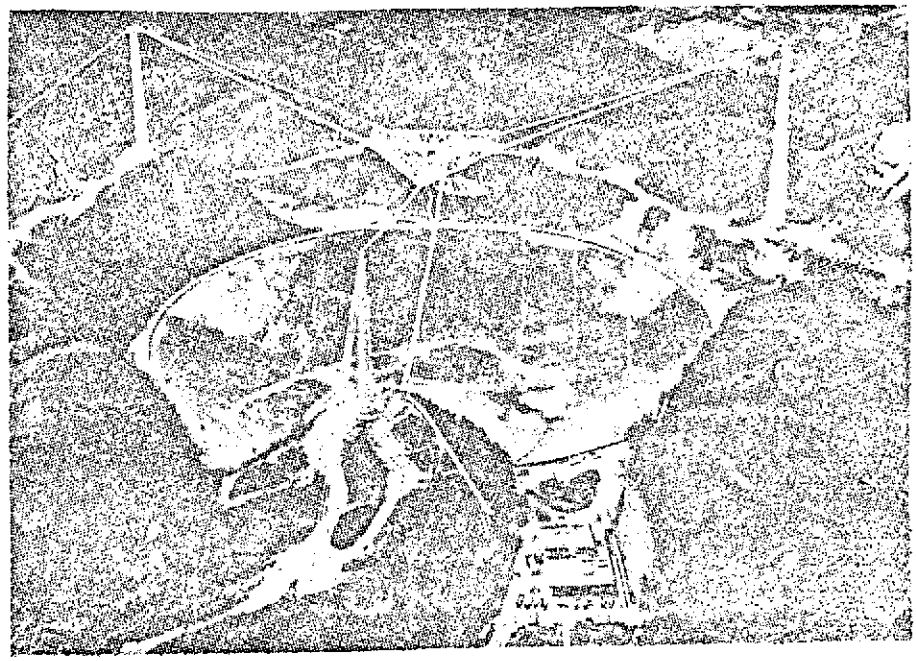

Figure 1.32. Ionosphere observatory in Arecibo, Puerto Rico. The electronic equipment is concentrated in the building at the bottom of the photograph.

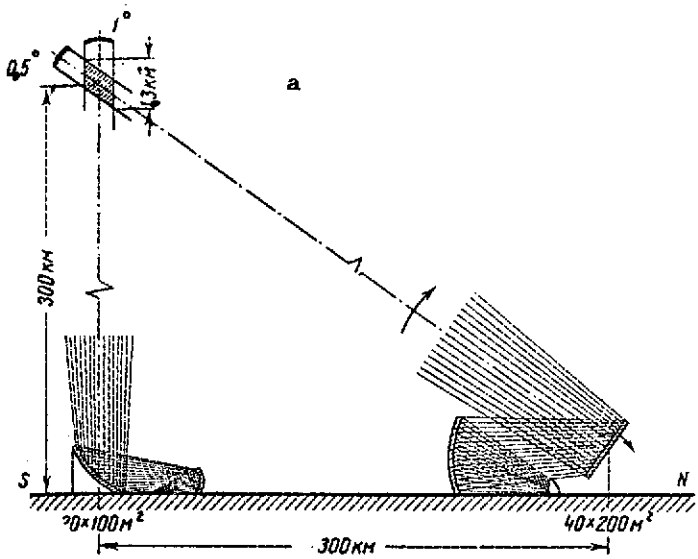


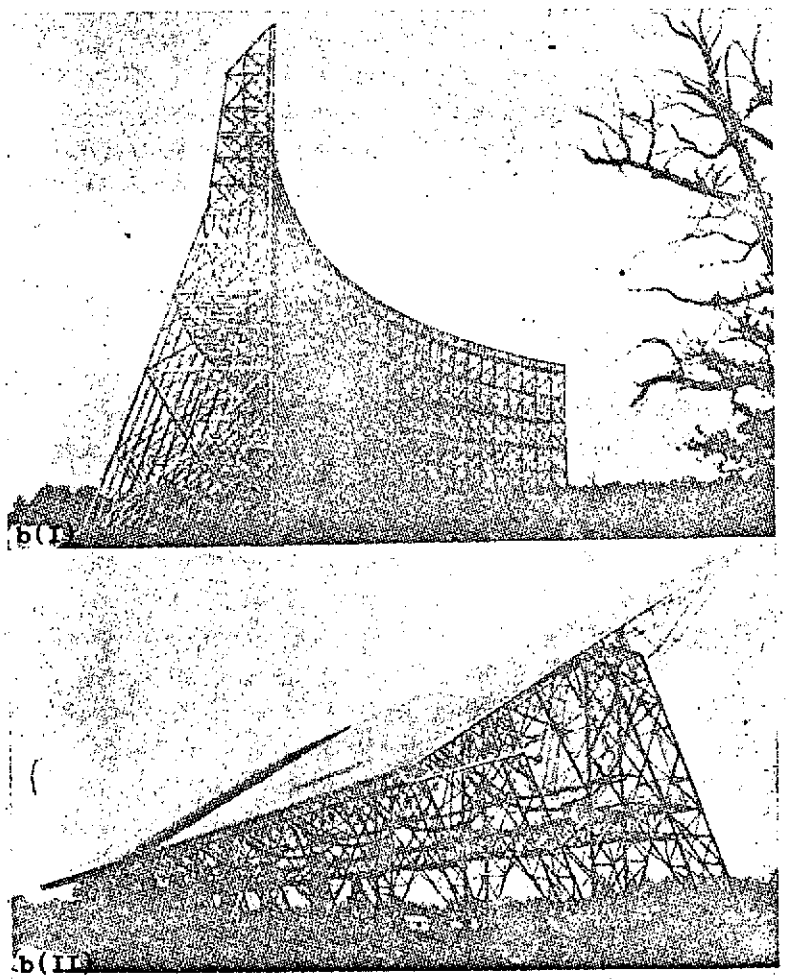


Figure 1.33. Two-position radar in Saint-Santin - Nancy, (France). a - diagram; b - receiving antenna in Nancy. I - vertical spherical mirror; II - flat mirror, tilt is controlled.

The transmitters are in the control center on the edge of the mirror. Used in the transmitter at a frequency of 430 MHz are two klystrons operating as the terminal stages (amplifiers) in the transmitter for coherent radiation. This transmitter can radiate pulses with widths from 10 μsec to 10 msec, and can radiate continuously with the corresponding mean power. Four tubes, operating in parallel push-pull circuits in a circuit with lumped parameters, operate at a frequency of 40.12 MHz in the transmitter's final stage.

The receiver uses a parametric amplifier at 430 MHz as the first amplifier stage. High-speed analog-digital converters (digital voltmeters) are used to obtain the data, and the data thus obtained are processed by an electronic digital computer.

The installation in Arecibo is extremely efficient, multi-purpose, and promising. Observations can be made within a wide range of heights, including the lower exosphere (> 2000 km). An additional outlying antenna evidently is to be built in the future, so the radar will be able to operate in the bistatic mode. This will increase height resolution when investigating the lower ionosphere and will expand the capability for measuring drift motions in the ionosphere.

The French continuously radiating radar. The system uses two beams, the intersection of which determines localization and magnitude of the scattering volume (Figure 1.33a). The radar transmitter, the final stage of which is assembled from klystrons, radiates continuously at a frequency of 935 MHz, switching for calibrated measurements at equal time intervals at a frequency of 935.1 MHz. The transmitting antenna in Saint-Santin is a section of a paraboloid 100 meters long in the east-west direction, making an angle of 45° with the ground. Its projection in the north-south direction is 20 meters. This mirror gathers radiation from an auxiliary mirror, which is a section of an elliptical cylinder 11 meters long in the east-west direction and illuminated by a horn feed.

This design provides the best illumination of the main mirror, and reduces to a minimum the level of the side lobes, which can cause the appearance of scattered signals from undesired heights. The vertical beam of the transmitting

antennas is 2.1° wide in the meridional plane, and 12' wide in the east-west direction, providing a match with the beam from the receiving antenna in the east-west plane at heights of the order of 200 km.

The big radioastronomy antenna in Nancy is used to receive signals scattered by the ionosphere (Figure 1.33b). The main part of the antenna is the main vertical mirror illuminated from the focus. The flat mirror, located some distance away, reflects the beam at the necessary angle. The main mirror is 300 meters in the east-west direction and 35 meters high. The flat mirror is 200 x 40 meters. The antenna forms a fan beam 6' wide in the east-west direction and 36' wide in the meridional direction. The receiver uses a parametric amplifier, and spectral analysis of signals is by quartz filters and a digital integrating and recording system. Operations of the transmitting and receiving /96 sections of the installation are synchronized by a special cable line. The two-position system described is most effective for studying the lower ionosphere, the D and E regions, and particularly for measuring the vertical component of the drift. Height resolution for the lower ionosphere is very great in this installation as compared to all the other operating radars.

The United States currently is engaged in developing a project for a new installation for studying the ionosphere using the incoherent scattering method, and taking into account the principal achievements, and shortcomings, of the systems described above. This installation should have one receiving-transmitting antenna, tilt controlled, with a diameter of some 100 meters, and two smaller diameter receiving antennas some 300 km from the main antenna. The radar will be able to operate in the pulsed mode, as well as in the continuous radiation mode. The scattering geometry will be such that it will be possible to measure a complete vector of drift rate and to make all the other conventional types of measurements in a wide range of heights. 150 cm will be used to investigate the 200-2000 km region, and 25 cm to investigate the 90-125 km region. Maximum power output will be 10,000 kW, mean power 300 kW. The installation will cost about $30 million.

Let us now give further consideration to the features of the procedure for measuring the individual parameters of ionospheric plasma. We have discussed these questions, in part, in section 1.3.1.

Height profile of the electron concentration

The most direct method of determining the height profile, N(h), is to measure scattered signal power, $P_s$, in terms of delay time during vertical radiation from the radar. This simple relationship can be used

$$P_s = \text{const} \frac{N(h)\sigma(h)}{h^2}. \qquad (1.96)$$

The proportionality factor can be found by measuring the parameters of the radar contained in Eq. (1.86), or by calibrating the results of the N measurements at some point by independent measurements (conventional pulse radio sounding, let us say).

The Millstone Hill installation, for example, establishes the shape of the N(h) profile only by measuring $P_s$, with absolute values established by measuring $f_0F2$ with ionospheric sounders located near the incoherent scattering station.

The scattered power decreases in proportion to the square of the distance. Moreover, N decreases rapidly above the F2 layer maximum. Both effects cause a rapid reduction in the magnitude of $P_s/P_N$. The video signal must be integrated with respect to the time sweep in order to increase measurement accuracy. The voltage at the output of the receiver frequency filter is rectified by a square-law detector, and the detected voltage (proportional to the incoming power) is read off a digital voltmeter at several time intervals ($\sim$ 250 μsec) during each pass of the radar time sweep. The readings are synchronized with the transmitter pulse repetition frequency to occur at the same points on the sweep. The levels then are summed in the computer and the mean power of the scattered signal is found for each height. The inaccuracy in the determination of the power, ΔP, for any height is reduced as /98

$$\Delta P = \pm \frac{P_s + P_N}{\sqrt{n}}. \qquad (1.97)$$

when integrating with respect to n passes of the time sweep.

$P_N$, the noise power, is estimated from the mean power for m points corresponding to heights without useful signal. We obtain $P_s$ by subtracting this magnitude from

the power values at all the other points. The error in finding $\Delta P_N$ from the magnitude of the mean noise power will be $P_N/\sqrt{nm}$, and the magnitude for the reflected signal will be

$$\Delta P_s = \pm \sqrt{(\Delta P^2) + (\Delta P_V^2)}. \quad (1.98)$$

The relative error, $\Delta P_s/P_s$ increases rapidly when $P_s/P_N \ll 1$. Practically, we can make the determination to within ±1% for moderate heights by using an integration time of 5 minutes (PRF 50 Hz) [175]. Accuracy is no better than 10% when $P_s/P_N < 0.1$, even with a 10-minute integration. The pulse width must be increased in order to increase $P_s/P_N$ when measurements are at great heights. The concentration changes monotonically above the F2 layer maximum, where this measure becomes necessary (pulses with $\tau \approx 1000$ μsec can be used), and radar resolution is but slightly reduced. Figure 1.34a is a photograph of an A scope when an integrator was used. Figure 1.34b compares data from the N(h) calculation obtained from the image in Figure 1.34a, with the results of the N(h) calculations from measurements by a conventional sounder. The interesting schematic of the accumulator used for measurements by the incoherent scattering method in the USSR is described in references [110, 111].

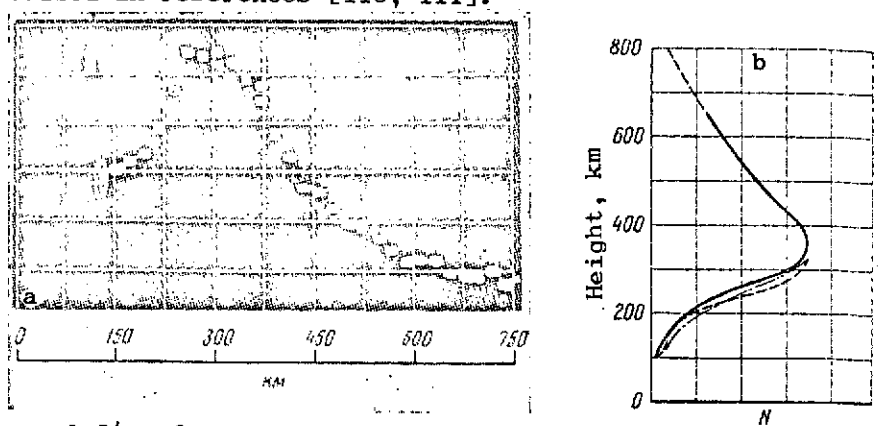


Figure 1.34. Calculation of electron concentration profile. a - photograph of A scope when integrator is used; b - distribution of electron concentration obtained from the A scope picture. The dashed curves are N(h) distributions calculated from ionograms from nearby ionospheric sounders.

Additional difficulties in N(h) measurements arise in connection with the fact that $\sigma$ (h) depends on $\alpha = 4\pi D/\lambda$ and on $T_e/T_i$, which themselves are functions of the height. Only when $\lambda > 1$ m ($\alpha \to 0$) can the dependence on $\alpha$ be ignored, and $T_e/T_i$ must be measured in order to calculate $\sigma$ ($T_e/T_i$) in accordance with

Eq. (1.71), studying the spectra of signals scattered from different heights. This complication can be avoided by using observations of the Faraday rotation of the plane of polarization of incoherently scattered signals in order to determine N(h). The number of rotations of the plane of polarization with respect to the original plane containing the wave's electric field vector will be

/99

$$\Omega = \frac{1}{4\pi} \frac{e^3 \mu_0}{m_e^2 f^2 c \varepsilon_0} \int_0^R N_r H_r \cos\theta_r dr, \tag{1.99}$$

where

$\mu = 1.26 \cdot 10^{-6}$ h/m is the free-space permeability;

$\varepsilon_0 = 8.85 \cdot 10^{-12}$ f/m is the free-space permittivity;

$f \gg f_N$ is frequency of the radio wave exceeding the plasma frequency;

$H_r$ is magnetic field strength;

$\theta_r$ is the angle between the field and the radio beam at any distance along the path, r.

If the rotation of the plane of polarization occurs along a vertical path from the earth to some height $h_1$

$$\Omega \approx \frac{0{,}94 \cdot 10^{-2}}{f^2} \overline{H \cos\theta} \int_0^{h_1} N dh. \tag{1.100}$$

$N_h$ can be found if the magnitude $\overline{H \cos \theta}$ is known, and $\Omega(h)$ has been found and $d\Omega/dh$ has been calculated. This method can be used in practice in coherent scattering installations for heights $h < 500$ km. Above 500 km $d\Omega/dh$ becomes very small and since $T_e/T_i \approx 1$ in this region, N(h) can be found directly from the scattered signal power profile.

N(h) can be determined in many cases by the position of the plasma lines in the spectrum for the electron component when $\alpha$ values are small (see section 1.3.1). The range of height is extremely limited when this method is used. Figure 1.35 illustrates this method of finding N(h).

The use of a two-position radar to measure N(h) has very specific associated difficulties. First of all, the $P_s/P_N$ ratio for the two-position radar with continuous radiation is worse than it is for the pulsed radar with the same mean

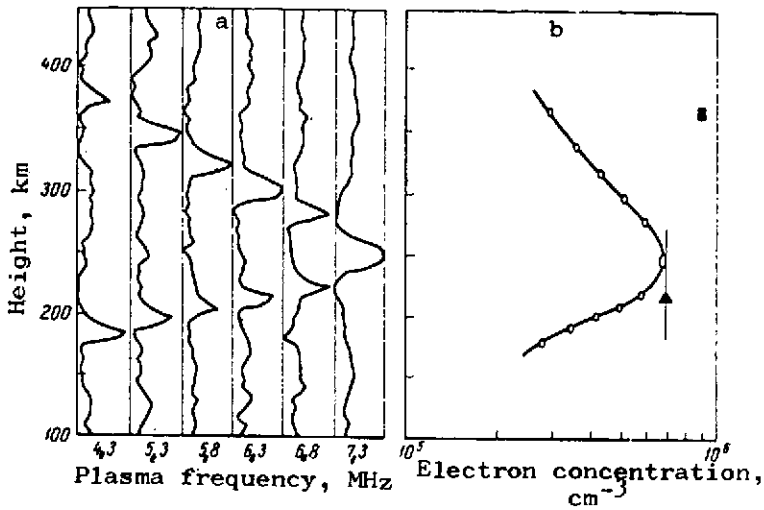


Figure 1.35. Determination of N(h) from the position of the plasma line (Arecibo). a - results of integration with respect to the time sweep with frequency of receivers shifted relative to the transmitter frequency; b - electron concentration profile obtained. The arrow indicates the value of the concentration found for the F2 layer maximum by conventional ionospheric sounder.

power. Second, we only obtain the local concentration value with a given position of transmitting and receiving antennas, and it takes a long time to make the measurements in a range of heights because change in the height under investigation requires mechanical movement of the antennas. Consequently, temporary /100 variations in radar or ionosphere parameters can be superposed on measurement results, at least in principle. Moreover, change in the total scattering volume formed by the intersection of the receiving and transmitting antenna patterns with height always must be taken into consideration when measurements such as these are made.

Temperature profiles

Electron and ion temperatures are determined by carefully measuring the signal spectrum shape. A group of filters is used as a spectrum analyzer and makes direct measurements when used with the two-position radar with continuous radiation. Difficulties in interpretation result from an ion mixture, as well as from thermal nonuniformity when $T_e \neq T_i$ (see section 1.3.1).

Some of the echoes on the radar's time sweep can be selected for spectral analysis when the pulse radar is used. One method [158] involves the use in the receiver circuit of many quartz filters overlapping the 200-212 kHz band

at intervals of some 50 Hz, thus making it possible to investigate the side band of echoes in the 0 to 12 kH band of Doppler frequencies. These filters are connected to the IF gate amplifier which separates the segment of the sweep corresponding to the height interval of interest to us. The output voltage from each filter, which has its own additional amplifier, is fed into a line detector. The currents flowing in the detectors are summed by integrators which are direct current amplififers with a natural time constant of several hours. The voltages reach a value of from 50 to 100 volts within 5 minutes of integration, and this is greatly in excess of the possible zero drift of the direct current amplifiers. The sync circuits are so designed that after each measurement of useful scattered signal energy the segment of the sweep separated by gating coincides with the band in which no signal should have been present, and measurements are repeated only in the presence of noise. The signal/noise thus can be measured at each frequency. An experimental spectrum containing 24 points can be obtained in from 5 to 10 minutes. This method measures the spectrum at just one height. It takes about 1 hour to study the range of ionospheric heights in the daytime, and more than 2 hours to do so at night when signals are so very much weaker.

Another method feeds ungated IF signals into a group of matched filters (that is, filters the transfer functions of which are selected according to the pulse power distribution function). This method provides spectra for a series of delays during one measurement. Equipment effects, particularly the non-monochromatic nature of the radiated pulse, are important in all pulse radar systems [109].

The pulse spectrum width ought not exceed 1/5, or 1/6, the scatter spectrum width if one is to obtain the maximum information contained in the spectrum $W(\Delta f_i)$. The pulse width then is

$$\tau \geqslant 1{,}5/\Delta f_i, \tag{1.101}$$

and the following limitation is applied to the possible height resolution for vertical sounding

$$\frac{c\tau}{2} = \Delta h \geqslant \frac{9 \cdot 10^8}{4\Delta f_i}. \tag{1.102}$$

This means that an acceptable $\tau$ can be selected for heights in excess of 250 to 300 km for pulse radars working on wavelengths $\lambda > 1$ m. This limit can be increased to 1000 km for radars with $\lambda > 1$ m (the one in Jicamarca, for example). /101

One way to increase height resolution is to transmit two successive pulses spaced $\Delta t$ apart and then calculate $\rho(\Delta t)$ between echoes from the heights of interest to us. By varying the time interval, $\Delta t$, in the limits $0 \leq \Delta t \leq 1/\Delta f_i$ we can determine the complete autocorrelation function, that is, the complex Fourier transform of the function $W(\Delta f_i)$. This autocorrelation function contains the same data as does the scattered signal spectrum. But the receiver time constant must be small compared to minimum $\Delta t$ values and this limits the receiver passband to

$$b \geq 10\Delta f_i. \tag{1.103}$$

We can, in order to avoid the statistical ambiguity associated with the mutual interference of echoes because of the simultaneous entry into the ionosphere of both pulses when $\Delta t \ll 10$ msec, transmit pulses that change polarization in turn, and receive the echoes in two corresponding receiving systems. The limitation imposed on receiver passband becomes unacceptable with increase in height, so the paired pulse method is used primarily to investigate the lower part of the ionosphere, up to 300 km, when comparatively long-wave radars are used.

Eq. (1.71) can be used to arrive at an immediate determination of $T_e/T_i$ when $\alpha \to 0$ and if $\sigma$ has been determined, without recourse to analysis of the scattered signal spectrum

$$\sigma = \frac{\sigma_e}{(1+\alpha^2)(1+T_e/T_i+\alpha^2)}. \tag{1.104}$$

Calculation of $\sigma$ requires measurement of the total echo power in the incoherent scattering case, and, in addition, some sort of independent method for finding N at the same height (Faraday rotation, plasma line method, conventional ionospheric sounder). Experiments have shown that $T_e/T_i$ found in this manner concord well with those obtained from spectral measurements [191].

Section 1.3.1, which reviewed the influence of the phenomena discussed on the scattered signal spectrum discusses the procedure for obtaining data on ion composition, charged particle drift, collisions, streams of high-speed

electrons, and magnetic field direction.

The particular efficacy of the incoherent scattering method stems from the fact that many of the observations described here can be made simultaneously, and applies with equal force to the launching of a well-equipped rocket. It is possible to repeat measurements by launching a series of similar rockets, but rockets cannot, in general, duplicate long-term observations. Maximum value of course will be derived from complex matched measurements by rockets, artificial earth satellites, and the incoherent scattering method.

### 1.4. Spaced Reception Methods

Radio waves radiated by natural, or artificial sources outside the earth, or by ground-based radio transmitters, evidence properties attributable to diffraction in the ionosphere after refraction and reflection. Study of the diffraction pattern on the terrestrial surface is the basis of the radiophysical methods used to investigate the speeds and directions of movements of irregularities in the ionosphere, their dimensions, and shapes. The irregular diffraction /102 pattern undergoes constant change. These changes are, in the general case, associated with the drift of the diffraction pattern as a whole, as well as with changes in the structure of this pattern during the movement process. The influence of each of these mechanisms can be separated only if there is simultaneous observation of a reflected, or refracted, radio signal at two or more points on the terrestrial surface. Let us see how we can use these observations to establish the drift rate, and the rate of change in the diffraction pattern as it moves.

Let an irregular amplitude diffraction pattern be moving at constant speed, V, along direction x. Temporal variations, R(t), are recorded simultaneously at points A and B, located in the direction of movement. If no changes occur in the structure as the pattern moves, the records of R(t) at points A and B will be identical, but changes in amplitude at one point will lag, or lead, somewhat those at the other point. In this case the rate of movement of the pattern can be found quite readily from

$$V = \frac{\xi}{\tau} \qquad (1.105)$$

where

$\xi$ is the distance between points A and B.

If the structure of the diffraction pattern experiences chaotic changes as the pattern moves, the degree of similarity of the R(t) records considered will decrease. The task of determining the true rate of motion of this pattern can be carried out only if one assumes the variations in amplitude, R(x, y, t) to be a steady-state ergodic process (x and y are the coordinates of the point here). The task was reviewed in reference [167], and analysis of the solution, and the procedure, are discussed in references [58, 108].

The generalized correlation function

$$K(\xi,\eta,\tau)=\frac{[R(x,y,t)-R(x-\xi,y-\eta,t-\tau)]_m-[R^2(x,y,t)]_m}{R^2(x,y,t)_m-[R(x,y,t)]_m^2}, \qquad (1.106)$$

where

$\xi$ and $\eta$ are the displacements along the respective axes;

$\tau$ is the temporal shift,

must be known if we are to determine the mean shape, dimensions, orientation, and characteristics of the motion of the irregularities in the structure of the diffraction pattern.

What follows from the solution of Eq. (1.106) is that the correlation function is bounded and even. Accordingly, $K(\xi, \eta, \tau)$ describes some central surface with its center in points $\xi = 0$, $\eta = 0$, and $\tau = 0$, and can be presented in the form

$$K(\xi, \eta, \tau) = K(U), \qquad (1.107)$$

where

U is a polynomial of even degree with respect to $\xi$, $\eta$, $\tau$.

Specifically, if $\xi$, $\eta$, $\tau$ are sufficiently small in the vicinity of the center, we can limit ourselves to second order terms

$$K(U) = K(a_{11}\xi^2 + 2a_{12}\xi\eta + a_{22}\eta^2 + 2a_{13}\xi\tau + 2a_{23}\eta\tau + a_{33}\tau^2). \qquad (1.108)$$

The further problem reduces to transformation of the polynomial U, and to finding the values of the $a_{ik}$ coefficients. It should be noted that the surface described by the function U is an ellipsoid. The sections of this surface by planes $\xi$ = constant, $\eta$ = constant, or $\tau$ = constant naturally will be ellipses.

Transformation of the function U is done by converting to a new system of coordinates moving at constant speed, $\bar{V}$, and coinciding with the major axes of the ellipsoid. The argument of the function K(U) then will take the simple form

$$U_0 = a'_{11}\xi_0^2 + a'_{22}\eta_0^2 + a'_{33}\tau^2, \tag{1.109}$$

and

$$\begin{aligned} \xi &= \xi_0 \cos\alpha + \eta_0 \sin\alpha; & V_x &= V_{x0}\cos\alpha + V_{y0}\sin\alpha; \\ \eta &= -\xi_0 \sin\alpha + \eta_0 \cos\alpha; & V_y &= -V_{x0}\sin\alpha + V_{y0}\cos\alpha. \end{aligned} \tag{1.110}$$

/103

In Eqs. (1.109 and 1.110), $a_{11}$, $a_{22}$, $a_{33}$ are new coefficients; $V_{xO}$, $V_{yO}$ are the components of the speed in a new, primary, system of coordinates ($\xi_O$, $\eta_O$), and it is convenient to analyze the function $K(U_O)$ by considering the levels of equal correlation K = constant. If

$$K(U_0) = \text{const} = \gamma, \tag{1.111}$$

then

$$a'_{11}\xi_0^2 + a'_{22}\eta_0^2 + a'_{33}\tau^2 = \text{const} = A$$

and

$$\frac{a'_{11}}{A}\xi_0^2 + \frac{a'_{22}}{A}\eta_0^2 + \frac{a'_{33}}{A}\tau^2 = 1$$

are ellipsoids

$$\frac{\xi_0^2}{a^2} + \frac{\eta_0^2}{b^2} + \frac{\tau^2}{\tau_c^2} = 1, \tag{1.112}$$

where

$$a^2 = \frac{A}{a'_{11}}, \qquad b^2 = \frac{A}{a'_{22}}, \qquad \tau_c^2 = \frac{A}{a'_{33}}.$$

The coefficients a, b, and $\tau_c$ are clearly physical concepts; a and b are the dimensions of the irregularities in the structure at a specified level $\gamma$, the orientation of major axis a determines the direction of prolateness (angle $\alpha$), and the parameter $\tau_c$ characterizes the chaotic changeability in the function R(x, y, t).

So, finding the sections of the function K(U) by experiment, we can find the $a_{ik}$ coefficients and calculate the characteristics of the irregular structure, a, b, $\alpha$, $\tau_c$, and V. The calculations can be made by juxtaposing the space $K(\xi, \eta, 0)$ and time $K(0, 0, t)$ correlations functions [108]

$$K(\xi, \eta, 0) = K(a_{11}\xi^2 + 2a_{12}\xi\eta + a_{22}\eta^2) \tag{1.113}$$

and

$$K(0, 0, t) = K(a_{33}\tau^2). \tag{1.114}$$

Let us consider the section

$$K(0, 0, \tau) = K(\xi, \eta, 0), \tag{1.115}$$

that is,

$$a_{11}\xi^2 + 2a_{12}\xi\eta + a_{22}\eta^2 = a_{33}\tau^2, \tag{1.116}$$

designating

$$V'_{cx} = \frac{\xi}{\tau}, \qquad V'_{cy} = \frac{\eta}{\tau} \tag{1.117}$$

and replacing the variables

$$\xi = V'_{cx}\tau, \qquad \eta = V'_{cy}\tau,$$

we obtain

$$V'^2_{cx}\frac{a_{11}}{a_{33}} + V'^2_{cy}\frac{a_{22}}{a_{33}} + 2V'_{cx}V'_{cy}\frac{a_{12}}{a_{33}} = 1, \tag{1.118}$$

where

$V_c'$ is the so-called characteristic velocity [108, 167].

Eq. (1.118) describes the ellipse of characteristic velocities used to find a, b, $\alpha$. All that need be known in order to construct the Eq. (1.118) ellipse is the values of $V'_c$ in three noncolinear directions. The corresponding values of $V'_c$ can be found by solving

$$V_{C(OA)} = \frac{\xi_1}{\tau_1}; \qquad V_{C(OB)} = \frac{\eta_1}{\tau_2}; \qquad V_{C(AB)}\frac{\sqrt{\xi_1^2 + \eta_1^2}}{\tau_3}, \tag{1.119}$$

where

$\tau_1$, $\tau_2$ and $\tau_3$ are found from Eq. (1.115).

These magnitudes can be found graphically from curves for the cross-correlation and autocorrelation functions of K, calculated for variations in R(t), recorded at three A, B, O) points on the terrestrial surface (Figure 1.36a).

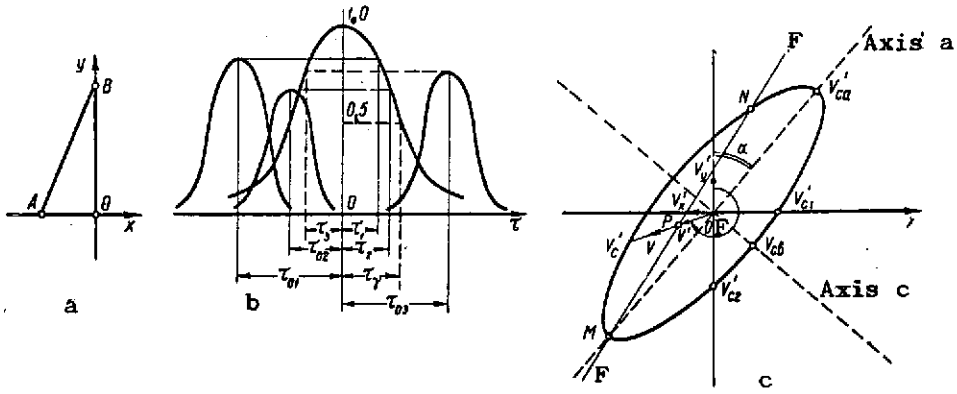


Figure 1.36. How the characteristic ellipse is calculated. a - location of antennas; b - autocorrelation and cross-correlation functions; c - the characteristic ellipse.

Along the coordinate axes, as follows from Eq. (1.118)

$$V'_{cx} = \frac{a_{33}}{a_{11}}; \qquad V'_{cy} = \frac{a_{33}}{a_{22}}. \tag{1.120}$$

The constant coefficient is calculated by finding the radius of correlation at the specified level, $\gamma$, from

$$a_{33}\tau_\gamma^2 = 1.$$

It is customary to take $\gamma = 0.5$. $\tau_\gamma$ is found graphically (Figure 1.36b).

Measuring the $V'_c$ values along the major axis of the characteristic ellipe, we find

$$a = V'_{ca} \cdot \tau_\gamma; \qquad b = V'_{cb} \cdot \tau_\gamma \tag{1.121}$$

and the eccentricity

$$e = \frac{a}{b} = \frac{V'_{ca}}{V'_{cb}}. \tag{1.122}$$

The concept of a front of apparent velocities, V' [108, 167], is introduced to determine the true drift velocity V. Determination of V' requires analysis /105

of the section of function K in the x or y direction. In the x direction, for example, we have

$$K(U) = K(a_{11}\xi^2 + 2a_{13}\xi\tau + a_{33}\tau^2). \tag{1.123}$$

The maximum for this function occurs at the point where the derivative

$$\begin{aligned} K'_\xi(U) &= 0, \\ K'_\tau(U) &= 2a_{13}\xi + 2a_{33}\tau = 0, \end{aligned} \tag{1.124}$$

that is,

$$\tau_{01} = -\frac{a_{13}}{a_{33}}. \tag{1.125}$$

An analogous extremal point exists for the y direction, $\tau_{02}$. The components of the apparent velocity in these directions are equal respectively to

$$V'_x = -\frac{a_{33}}{a_{13}} = \frac{\xi}{\tau_{01}}, \qquad V'_y = -\frac{a_{33}}{a_{23}} = \frac{\eta}{\tau_{02}}. \tag{1.126}$$

A straight line passed through the ends of the components of the apparent velocities $V'_x$ and $V'_y$ is called the front of apparent velocities. The values of $\tau_{01}$ and $\tau_{02}$ can be taken from the curve (Figure 1.36b). References [108, 167] prove that the direction of the true velocity V (the angle F) can be found to be the direction OP (Figure 1.36c) from the coordinate origin to the midpoint of the chord MN, and the magnitude V can be calculated as

$$V = V'^2_c \cdot \frac{1}{V'}. \tag{1.127}$$

It is more convenient to consider the magnitude

$$V_c = \frac{1}{\sqrt{a_{11}}\tau_c}, \tag{1.128}$$

called the chaotic changeability rate, rather than the parameter $\tau_c$, characterizing the chaotic changeability of the function R(x, y, t). This magnitude is associated with the magnitudes $V'_c$ and V by the following relationship

$$V_c^2 = V_c'^2 - V^2 \tag{1.129}$$

or, considering Eq. (1.127)

$$V_c^2 = V(V' - V). \qquad (1.\text{[illegible}])$$

The obvious conclusion derived from this latter equation is that if the chaotic changes are small ($V_c \to 0$), $V' \to V$.

So, in order to determine the dimensions and the orientation of the nonuniform structure of the diffraction pattern and the characteristics of its changeability, we must record the temporal variations in some parameters of the diffracted field, say the amplitudes, or the phases, at three points not lying on the same straight line. The recordings obtained then are used to calculate the autocorrelation and crosscorrelation functions $K_O(\tau)$, $K_A(\tau)$, $K_B(\tau)$, $K_{OA}(\tau)$, $K_{AB}(\tau)$. The curves plotted for these functions then are used to find the characteristic times $\tau_1$, $\tau_2$ and $\tau_3$, the shift in the maxima for the cross-correlation functions and the correlation radius, $\tau_\gamma$. The characteristic velocities $V_c'$ (1.49) in three directions then are calculated, the characteristic ellipse is constructed, and a, b, and e in Eqs. (1.121) and (1.122) are found. The front of apparent velocities, FF, is plotted on the drawing using the calculated magnitudes $V_x'$ and $V_y'$ using Eq. (1.126) in order to calculate V, the true velocity. The direction of the drift velocity V (the angle F) is determined to be the direction OP from the coordinate origin to the midpoint of the chord MN. Measuring V' and $V_c'$ on the drawing, we calculate V by using Eq. (1.127). $V_c$ can be calculated by using Eqs. (1.123)-(1.130). /106

The literature refers to this method as the "complete correlation analysis method." We shall use the correlation analysis method only when the following conditions are satisfied: (a) the unknown statistical process - the temporal variations in the diffraction pattern on the terrestrial surface - is a steady-state ergodic process; (b) approximation of the contours of equal correlation by a linear, positively determined, square shape is valid.

But it is well known from the experimental data [108, 115] that the R(x, y, t) process is not steady-state. So later on what were developed were methods of neutralizing the nonsteady-state condition and criteria for the applicability of the correlation method were developed [58, 108].

The so-called similarity method [108, 115] is the simplified method widely used in practice to calculate the velocities and direction of motion of the diffraction pattern. It is based on measurement of temporal shifts at characteristic points (sharp minima or maxima) on the fading traces. This method yields a precise result when the following conditions are satisfied: (a) the diffraction pattern at the level of the earth should be isotropic; that is, its statistical properties should not depend on direction; (b) the shape of the diffraction pattern does not change during drift. Drift takes place at constant velocity.

Data are processed as follows. Selected from the available traces are those with sufficiently high similarity of $R(\tau)$ on all tracks and with a feeding period such that times of amplitude maxima, or minima, can be fixed with respect to each other. Figure 1.37b is a schematic presentation of an analyzed trace. By projecting a motion picture film of the trace on a screen with a scale grid we can measure temporal shifts $\tau_1$ and $\tau_2$ for each maximum on traces A and B (the north and west antennas, respectively) with respect to the O (the central antenna) trace. The sign of the shift characterizing the direction of the corresponding velocity component is determined using motion to the north and to the east as positive, and to the south and west as negative. Figure 1.37a is the arrangement of the positions of antennas O, A, and B.

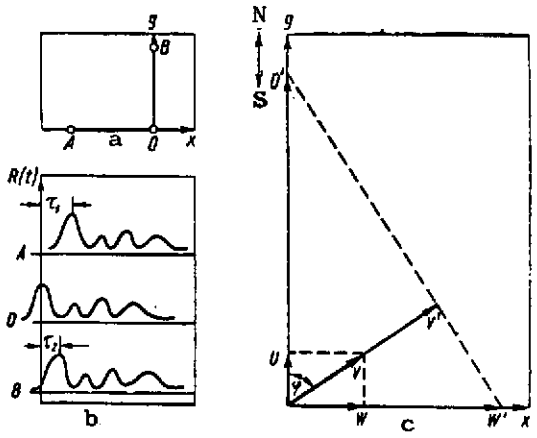


Figure 1.37. The velocity and direction of the drift calculation. a - antenna positions; b - the R(t) traces; c - the calculation diagram.

Let us designate the rate of drift of the diffraction pattern by V', and the direction of drift, reading clockwise from the direction to north, by $\Phi$. Then

$$\frac{1}{V'^2} = \frac{1}{W'^2} + \frac{1}{U'^2} \qquad (1.131)$$ ∠107

$$\operatorname{ctg}\Phi = \frac{W'}{U'}, \qquad (1.132)$$

where

W' and U' are the observed components of the drift rate in the OA and OB directions, that is

$$W' = \frac{d}{\tau_1}, \tag{1.133}$$

$$U' = \frac{d}{\tau_2}, \tag{1.134}$$

where

d is the distance between the antennas.

Figure 1.37c is a diagram of the graphic determination of V' in terms of computed W' and U'. The velocity at which the irregularities drift at the level of the ionosphere has the same direction as does the velocity of the displacement of the diffraction pattern at the level of the earth, but the magnitude is less by a factor of 2.

Thus, we can determine the magnitude of the drift velocity, V', in m/sec, and the azimuth of the motion, $\Phi$, in degrees.

In real cases, sections of maximum extent are selected on the traces, and all possible temporal shifts between minima or maxima on the R(t) curves are determined, while the components W' and U' are determined with respect to the mean values $[\tau_1]_m$ and $[\tau_2]_m$

$$[\tau_1]_m = \frac{\sum \tau_{1,i}}{n}, \qquad [\tau_2]_m = \frac{\sum \tau_{2,i}}{n},$$

where

n is the number of readings.

As many as 100 individual readings can be obtained from good traces of one session of observations lasting 5 minutes.

Numerous observations have established that the R(t) curves in many cases actually are highly similar and can be used to determine temporal shifts $\tau_1$ and $\tau_2$ with good accuracy. However, there often are tracings, such as slow fading, that cannot be processed by the method just described. It is impossible to find well defined maxima or minima on the fading curves. Sometimes the R(t) tracings obtained for different antennas are completely dissimilar, the reasons for which are varied, and include, for example, superposition of wave bundles scattered by several irregularities displaced differently with respect to each

other. The diffraction field also can be complicated by signal fractionation if the ionosphere is in a disturbed state, or in the event of anisotrophy of the diffraction pattern. There are many tracings on which the temporal shifts will change signs repeatedly in a 4 to 5 minute period. Tracings such as these cannot be processed by the similarity method either, and they indicate the presence of complex motions in the ionosphere. In sum, 30 to 40% of available tracings can be processed by the similarity method.

Temporal shifts $\tau_1$ and $\tau_2$ also can be determined by the position of the cross-correlation function maxima (see Figure 1.36b). The number of R(t) tracings processed is increased substantially when this method of finding $\tau_1$ and $\tau_2$ is used.

Measuring Installation for Determining the Directions and Velocities of the Horizontal Drift of Small-Scale Irregularities

Pointed out above was the fact that the R(t) process must be recorded at at least three points on the terrestrial surface in order to establish V (or V') and $\Phi$ of the horizontal drift. The measuring installation (Figure 1.38) described in section 1.1.3, can be used for this purpose.

/108

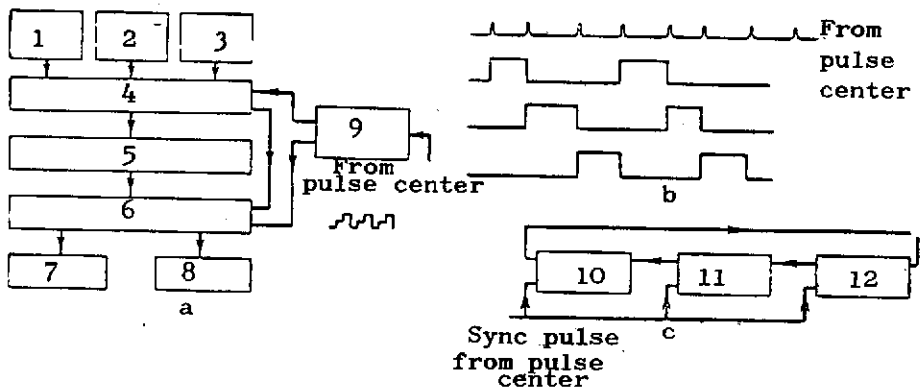


Figure 1.38. Drift measuring installation. a - functional diagram of installation receiving channel; b - antenna switch operating diagram; c - functional diagram of ring generator.

LEGEND FOR FIGURE 1.38

1 - receiving antenna 1; 2 - receiving antenna 2; 3 - receiving antenna 3; 4 - antenna switch; 5 - receiver; 6 - secondary switching unit; 7 - indicator; 8 - recorder; 9 - ring generator; 10 - generator 1; 11 - generator 2; 12 - generator 3.

Three antennas, 1, 2, and 3, are used for signal reception. The antennas are located at the apexes of the measuring triangle. The high-frequency voltage from each antenna is fed into the receiver by a feeder (Figure 1.38a).

It is rational to use one receiver with an antenna switch (Figure 1.38b) to separate and amplify the signals because this approach ensures sequential connecting of the receiving antennas to the receiver with adequate frequency and synchronous recording of the amplitude of the signal reflected from the ionosphere and picked up at three points. An electronic switch is used to connect the antennas to the receiver during primary switching. The switch is a complex of tubes, or semiconductors, blocked in its ordinary state and unblocked in a strictly specified sequence by switching pulses generated by the switching voltage ring generator (Figure 1.38c).

Secondary switching, that is, the separation of the reflected signal after the receiving channel in accordance with receiving antenna, is done directly in the indicator-recorder unit. Height sweep voltage from the pulse center is supplied to the input of the horizontal beam deflection amplifier in the type A indicator. The vertical beam deflection amplifier in this indicator has two inputs, to which the signal from the receiver output and the switching pulses respectively are fed. The amplitude of each of these supplies can be smoothly regulated. The corresponding switching pulse thus connects the particular receiving antenna to the receiver and ensures setting the sweep line, which is tightly coupled to the antenna, at the desired level on the indicator screen.

The receiving channel system described leads to inevitable loss of some information because antenna switch operations result in the recording only of the amplitude of each $k^{th}$ pulse (where k is the number of receiving antennas). Loss of information is insignificant, however, because the highest frequency of fadings of received signals is well below the switching frequency.

The device for obtaining switching pulses consists of three relaxation generators with two stable states. These generators (Figure 1.38c) are connected in a ring and are triggered by a pulse from the pulse center [40, 108]. This arrangement can be used to cut in four and more stages. Vaccum tubes, or semiconductors, can be used as the relaxation generators.

The devices for separating the required signal (for gating), and for observing and recording R(t), are completely similar to those described in section 1.1.3. It should be emphasized that the time involved in correlation function calculations makes it particularly desirable to record the R(t) process in a form convenient for direct computer input [16, 228]. /109

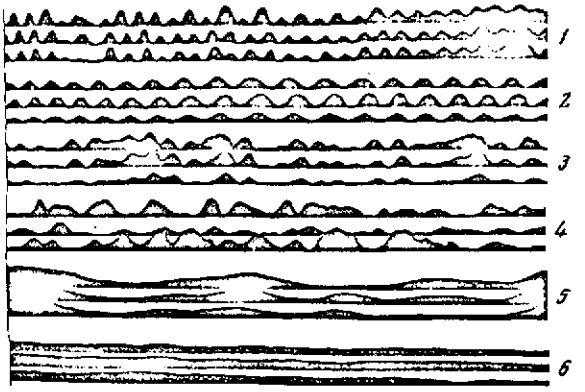


Figure 1.39. Examples of different types of fading. 1, 2, 3 - rapid quasi-periodic fading; 4 - chaotic fading; 5, 6 - slow fading.

All types of antennas described in section 1.1.3 can be used as receiving antennas. Polarizing antennas must be used for working different frequencies. It is convenient to locate the receiving antennas at the apexes of an equilateral right triangle, the legs of which are oriented along the points of the compass. This arrangement of the measuring triangle simplifies somewhat the V and $\Phi$ calculations. The length of the sides of the triangle ought not exceed the radius of the space correlation of the diffraction pattern [108]. This magnitude can be taken as 100-200 meters for small-scale irregularities, and 20-40 km for large-scale irregularities.

Figure 1.39 shows sample R(t) tracings obtained by the Irkutsk radar for different ionospheric conditions [94].

Space-frequency-diversity reception

As has been pointed out above, recording the parameters of a reflected signal at several points on the terrestrial surface makes it possible to determine the motion and structure of ionization irregularities at the corresponding height; that is, at some horizontal section. Quite naturally, an irregular structure is characteristic of the ionosphere as a whole, so measurement of the principal parameters of ionospheric irregularities at different heights is of great interest. There are no limitations, in principle, on the conduct of such observations at the measuring installation described above. All that is necessary in order to do so is to make a sequential series

of observations at several frequencies. However, the extremely rapid change in the principal ionospheric characteristics makes it very desirable to study the properties of ionospheric irregularities simultaneously at several height levels. This can be done with a special measuring installation capable of working on two, or more, frequencies simultaneously.

Moreover, if fluctuations in a parameter at four points not in the same plane are recorded for a medium that is irregular with respect to all three coordinates, the procedure described in reference [108] permits determination of the vector, the average shape of the orientation, and the parameters of the changeability of volume irregularities. The combination of space-diversity and frequency-diversity reception provides a way to investigate the volumetric properties of ionospheric irregularities. References [108, 68, 152] describe measuring installations that operate on several frequencies. It is customary to use a broadband amplifier in the transmitter and two, or more, master oscillators similar to those described in section 1.1.3 for this purpose.

The master oscillators operate in the pulse mode and are connected to the /110
amplifier in sequence at a frequency half that of the usual sounding PRF.

For example, oscillator 1 in a dual-frequency radar can be connected to the amplifier by even command pulses, while generator 2 can be connected by odd pulses. The variant in which frequencies are connected by semiconductor diodes connected in parallel with the continuously-functioning local oscillator circuit is more convenient (see 1.1.1). The capacity of its junction can also be changed in accordance with the sounder's working frequency, depending on the voltage applied to the diode. The controlling voltage, in the form of pulses corresponding to the repetition frequency, can be obtained from the pulse center. Adjustment of the amplitude of the controlling pulses in the range from 0 to 100 volts provides working frequencies with a difference from 2 to 800 kHz [68]. These installations, in order to receive reflected signals, usually use separate receivers for each frequency. The indicator-recorders do not differ significantly from those described.

The radio astronomy method

The radio astronomy method of investigating the irregular structure of the ionosphere is based on study of signals from "radio stars" [43, 189]. The

diffraction pattern from extra-terrestrial sources is investigated on the terrestrial surface. Since in this case what is being studied is the field of refracted ionospheric waves, the observed velocity of the migration of the diffraction pattern will correspond to the velocity at which the irregular screen is moving.

Radio astronomy observations usually are made in the 30-100 MHz band. The lower limit of this band is fixed by the critical frequency of the F region in the ionosphere. The influence of ionospheric irregularities evidently is slight at frequencies higher than 100 MHz. Observations such as these are convenient because they require no radio transmitting equipment.

What has to be considered is that the migration in the diffraction pattern with respect to the earth is the result of the drift of the ionosphere and the earth's diurnal rotation. The summed velocity of this migration can be measured by observing the motion of the diffraction "spots" with three receivers, the antennas of which are located at the apexes of a triangle on the terrestrial surface. Now the velocity can be determined from the time it takes the spot to move between each pair of antennas, and the size of the spot from the time it takes the spot to pass over each of the antennas.

The most convenient sources of radiation, in terms of power, as well as coordinates (for observations in the middle latitudes), for studying the ionospheric irregularities and winds by the radio astronomy method are the "radio stars" in the constellations Cygnus ($\alpha$ = 19°57', $\delta$ = +40°) and Cassiopeia ($\alpha$ = 23°21', $\delta$ = +58°). Their declinations ($\delta$) differ by 18°, so the radio radiation from the common sources can be received by the same fixed antenna, the pattern width of which is greater than 20° in the north-south direction if its axis is directed in the plane of the meridian with a declination $\delta = \frac{1}{2}(\delta_1 + \delta_2)$.

A brief description of a radio astronomy measuring installation follows [43].

Three identical fixed antennas with a wavelength of $\lambda$ = 6 m are used for the investigations. The antennas are oriented in the plane of the meridian with declination $\delta$ = 49.5°. Each antenna is a paraboloidal grating reflector with a square aperture with an area of 170 $m^2$. The antenna pattern is 21° in

width (at the half-power level). The focal length of the paraboloid is 6.7 m. A half-wave dipole is located in the reflector focus, and a parasitic half-wave reflector is located at a distance of $0.2\lambda$ from it.

The installation uses three receivers, all located at the same point. This simplifies control of the installation and all three recordings can be made on one tape. Each receiver contains a two-stage high-frequency amplifier, a local oscillator, a mixer, a four-stage intermediate-frequency amplifier, a detector, a two-stage direct-current balanced amplifier, and a recorder. The receiver intermediate frequency is 10 MHz, the passband is 0.4 MHz, the output device time constant is 0.5 sec. The supply for plate and filament circuits in each receiver is stabilized (stabilization factors are $\sim 10^{-3}$ for the plate and $\sim 5 \cdot 10^{-2}$ for the filament circuit). /111

The time shifts $\tau$ are determined from the R(t) recordings. The magnitude $\tau$ can be found by the similarity method, or by calculating the mutual correlation functions.

A correction that takes the earth's rotation into consideration must be introduced in the velocity component corresponding to the west-east direction. This correction is equal to (m/sec)

$$\Delta V_{W-E} = \frac{2\pi h \cos \delta}{86 \cdot 10^3 \cos(\varphi - \delta)}, \qquad (1.135)$$

for "radio stars" near culmination. Here h is the height of the diffracting layer, $\varphi$ is the latitude of the observation site, and $\delta$ is the declination of the "radio star."

If h = 400 km, $\Delta V_{W-E}$ = 16 m/sec for the "radio star" in the constellation Cygnus, and $\Delta V_{W-E}$ = 23 m/sec for that in the constellation Cassiopeia. Because the correction itself is small, it can be taken that $\Delta V_{W-E}$ = 20 m/sec for both "radio stars." It is convenient to find the velocity and to introduce the above-indicated correction graphically. This results in the immediate obtaining of the absolute magnitude, as well as the direction, of the velocity relative to the point of the compass.

Multiantenna Reception

The methods used to find V and $\Phi$, described above, do not yield true

instantaneous drift velocity. This could be done if the researcher had available to him a model of the diffraction pattern, the movement of which with respect to the terrestrial surface was associated with the horizontal drift of the irregular ionization in the ionosphere. This sort of model can be obtained by using an array consisting of a great many receiving antennas.

The antennas can be positioned in a circle with radius A [58] for example, spaced, let us say, 30° apart, with a reference antenna set up in the center of the circle. It can be anticipated that when there is a great similarity in the R(t) recordings at each receiving antenna the mutual correlation between recordings at the reference antenna, and at antennas located closest to the direction in which the pattern is moving, for some $\tau_0$ values will differ little from unity. It is obvious that the maximum mutual correlation between R(t) recordings at the reference antenna and at any other antenna will be less. We therefore can establish the direction in which the pattern is moving from the location of the antennas (with respect to the reference) for which the maximum mutual correlation is greatest. Knowing $\tau_0$ corresponding to the greatest maximum correlation, we can calculate the velocity at which the pattern is moving from

$$V = \frac{A}{\tau_0}.$$

An experiment such as this also makes it possible to make a direct estimate of the influence of irregular changes in the structure of the diffraction pattern on change in the magnitude of the velocity at which it is moving.

Another series of experiments designed to make a detailed verification of the temporal dependence of the velocity of the ionospheric drift and using a 4 x 4 antenna matrix is described in reference [200]. Sixteen untuned loop antennas with preamplifiers were positioned in the form of a 4 x 4 square with a base of 100 meters. The incoming signals were fed into a special device over /112 separate cables. The device connected the antenna to the receiver in turn, and the output signal from the receiver was fed into a cathode ray tube. The amplitude of the particular reflection separated by this device brightened the corresponding spot, the position of which on the tube face corresponded to the position of the particlar receiving antenna. The result was a set of spots, 4 x 4, the brilliance of which simulated the diffraction field on earth. The distribution of the brilliance of the spots could be recorded along with the

simultaneous evaluation and recording of direction $\Phi$, velocity V, and the characteristic features of the pattern. A motion picture film also could be made.

Reference [168] describes a system of antennas consisting of 89 crossed dipoles. This system is an approximately circular array and can be used for 2.0 or 6.0 MHz. This antenna system is a very flexible instrument, one that can be used in different experiments concerned with the physics of the upper atmosphere. The electrical length of each feeder line is made to be a multiple of half the wavelength at both frequencies in order to maintain the phase. Each pair of crossed dipoles can be used to provide circular polarization, if necessary. The experimenter can connect the antennas he needs through a manually operated antenna switch.

Ionospheric drift is observed by connecting each of the 89 antennas to its own receiver. Signal amplitude at the receiver output is determined by the brilliance of the corresponding individual indicator on some screen. The individual indicators are oriented in the system in a manner such that a plausible model of the ground pattern can be observed after the pattern has been smoothed by a ground glass screen.

The installation provides a recording of the signal from the output of the receivers in digital form. The scanner connects the 89 channels in sequence with the frequency 5 Hz per channel. The drift rate is found by calculating the two-dimensional correlation function of the R(t) amplitude for fixed temporal intervals. This function will be a minimum at some point corresponding to the vector for pattern velocity during the time between two scans. Measurement results are not related to change in the shape of the pattern as it moves [168].

A matrix of antennas similar to that described in references [168, 186, 200] naturally can be used as a single system for phase measurements.

### Measurement of Velocities and Directions of the Horizontal Drift of Large-Scale Irregularities

The amplitude method cannot be used to observe irregularities with horizontal dimensions tens and hundreds of kilometers in size because there is a rapid decorrelation of the R(t) processes with increase in distance between reception points of several working wavelengths. References [60-62] have pointed out that the method that records temporal variations in the phases of signals reflected

from the ionosphere is free of this shortcoming. They point out that the influence of small and large irregularities in the phase of the radio signal differ in that the former change phase by a magnitude of the order of $2\pi$, the latter by several tens of $\pi$.

The measuring system for observations by this method consists of three identical installations positioned at the apexes of a triangle 28-62 km on a side [60-62, 108]. Communication lines for transmitting sync signals connect the installations. Each has a system of transmitting and receiving antennas, a transmitter, receiver, phase meter, indicator, and recorder (Figure 1.40a). The operating band is 1.5-20.0 MHz [108].

/113

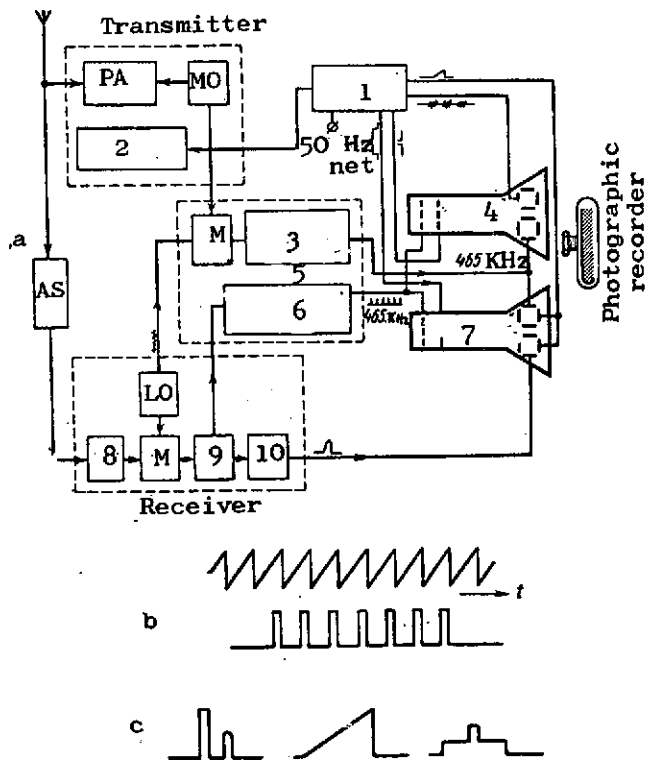


Figure 1.40. Functional diagram of the receiver channel in the installation for measuring drift by the phase method. See text for explanation.

LEGEND FOR FIGURE 1.40.

1 - synchronizer; 2 - modulator; 3 - reference voltage channel; 4 - photo indicator; 5 - phasemeter; 6 - intensifier pulse channel; 7 - visual indicator; 8 - HFA; 9 - IFA; 10 - LFA.

The continuous high-frequency oscillations from a master oscillator (MO) are supplied to the input of a pulse power amplifier (PA) in the transmitter where the oscillations are amplified and then are radiated by an antenna. An antenna switch (AS) blocks the input to the receiver for the time the antenna is being fed the powerful main pulses from the transmitter.

The signal reflected from the ionosphere is supplied to the input of the phasemeter in the channel for forming the "phase pulses" for intensification from the output of the receiver's intermediate-frequency amplifier (IFA). This channel converts sinusoidal oscillations at 465 kHz into a train of short (approximately 0.2 μsec) negative polarity pulses with a repetition rate of 465 kHz. These pulses are supplied to the cathodes of the photoindicator and visual indicator as the intensifier voltage. The 465 kHz coherent reference voltage to which the phase of the received signal is compared is formed in another channel in the phasemeter (in the sawtooth reference voltage channel, or in the "sawtooth" channel for short). Oscillations from the master oscillator are mixed with the oscillations generated by the receiver's local oscillator (LO) tuned to the transmission frequency. Difference frequency oscillations, that is the 465 kHz oscillations, then are converted into a sawtooth voltage with the same repetition frequency of 465 kHz. This reference voltage is supplied to the vertical deflection plates of the cathode ray tube indicators.

Figure 1.40b shows the shapes of the voltages at the outputs of the phasemeter's two channels. Note that the sawtooth voltage is continuous, but that the phase pulses are in the form of a wave train, the width of which corresponds to that of the reflected signal (approximately 100 μsec). The result is to cause the phase pulses to intensify on the scope the phase point on the /114
coherent sawtooth voltage. This brilliance (the phase point) moves up, or down depending on the sign of the change in the phase difference when the difference in phase between the received signal and the coherent voltage is measured. Movement of the motion picture film mechanically in the horizontal direction while photographing produces a recording in the shape of a "sawtooth" with a different slope. One such sawtooth corresponds to a $2\pi$ change in phase.

A mechanical film movement rate of approximately 3 cm/min is sufficient when investigating large irregularities. Gating pulses of regulated width (0-350 μsec),

amplitude, and delay are supplied from a timer to the control electrode of the cathode ray tube indicator so that what is seen on the photoindicator is just the phase point without the coherent voltage sawtooth. Required brilliance and focusing of the phase points is achieved by regulating the static blanking of the tubes, amplitudes, and gate widths, as well as the amplitudes of the phase pulses. Gating pulses are provided by adjusting the temporal delay with respect to the main signal.

The visual indicator provides for selection and monitoring of the object to be recorded. The amplitude and phase patterns, as well as the position of the gating pulse, may be seen on the scope (type A). A mixed intensifying signal consisting of a positive rectangular pulse corresponding to the forward movement of the horizontal sweep, and a gating signal, is supplied to the control grid of the visual indicator from the timer. The voltage diagram is shown as Figure 1.40c.

Phase changes are recorded simultaneously at three points. The length of a round of observations should be such as to provide an adequate sample, and usually takes 4 hours. Processing the recordings reduces to counting the number of $2\pi$ phase changes per minute; that is, to determining the magnitude $\Delta\varphi/\Delta t$. The data obtained are the original data required to obtain the correlation functions and to determine the parameters of the irregular structure of the ionosphere by the correlation analysis method.

Steps must be taken during the recording processing procedure to eliminate slow diurnal variations in phase.

### Measurement of Direction and Velocity of Ionospheric Drift Using an Ionospheric Sounder Installed in an Aircraft

The method that measures drift using a sounder moving in space is as follows [126, 181]. Let it be possible for us to move the sounder in space at known speed. This movement is most conveniently accomplished over a circular trajectory. The sounder should operate at a fixed frequency. The amplitude of the reflected signal is recorded.

The rate at which the signal fades, g, can be calculated from the results of the measurements in terms of the course, $\varphi$, over which the sounder is moving

$$g(\varphi)=\frac{\Delta R}{\Delta t},$$

where

$\Delta R$ is change in signal amplitude in time $\Delta t$.

$g(\varphi)$ will be a minimum when the sounder course and drift direction coincide and their speeds are commensurate, and a maximum when the reverse is true.

If g changes linearly with respect to the difference between sounder velocity, $V_s$, and irregularity velocity, V, then

$$\frac{V_s+V}{V_s-V}=\frac{a}{b}=r, \tag{1.36}$$

/115

where

$a = g(\varphi)_{max}$, $b = g(\varphi)_{min}$.

Calculating r from experimental data, we can find the magnitude

$$V=V_s\frac{r-1}{r+1}.$$

This method can be put to practical use by installing the sounder in an aircraft and recording R(t) while flying in a circle. The method is highly important in research on drifts in the ionosphere over regions access to which is difficult (the Arctic, Antarctic, and the like). Moreover, if a straight line is flown and conventional ionograms of the ionospheric layers are recorded, we can arrive at a judgement as to the dimensions of the irregularities. A brief description of an ionospheric measuring installation installed in an aircraft follows [126].

The ionospheric sounder provides height-frequency characteristics from the aircraft, or we can record the amplitude of the reflected signal at a fixed frequency. The equipment is designed for installation in an IL-14 type aircraft. The sounder's functional schematic is conventional.

Two antennas, one for the receiver and one for the transmitter, are used with the airborne sounder. The aircraft's electrical net is the power supply. Net voltage is 28 volts, but is converted into 115 volts 400 Hz by two MA-1500 converters.

The device for measuring drift from the aircraft is an adapter to the sounder that can record the amplitude of any of the magnetoionic components of the reflected signal at one of the fixed frequencies in the 2-10 MHz band. The adapter consists of a gating pulse generator, an output device, and a recorder.

The signal needed to record is separated by the gating pulses, which control the operation of a peak detector in a manner such that the reflected signal is fed to the recorder only during the time the pulses appear, with the result that the output voltage across the peak detector contains only the voltage of the selected component. The peak detector time constant is 0.5 sec. At the same time, the output voltage will follow slow, as well as fast, changes in signals. The signal voltage at the peak detector output is fed to the current amplifier, the cathode circuit of which is connected to the dipole of a type MPO-2 (N-102) loop oscillograph. Time markers are supplied to the second dipole. Film transport rate is 12 cm/min.

### 1.5. Radar Tracking of Meteor Trails

Meteors observed visually, or by radar, are produced by meteoric bodies of mass less than 1 g. Meteoric bodies are accelerated by the earth's gravity, and vaporize in the dense layers of the upper atmosphere. Meteoric bodies vaporize at between 80 and 115 km, that is, in the E region, and in part in the D region, of the ionosphere. The region of the atmosphere in which meteor trails can be observed is called the meteor zone. A trail with a linear electron density of $10^{11}$-$10^{13}$ e/cm forms when a meteoric body vaporized. The entire ionization process takes $10^{-4}$-$10^{-5}$ sec [87], and practically all the ions are at a distance of several neutral particle free path lengths at the time the trail is formed. The meteor trail therefore is a formation, the longitudinal dimensions of which are much greater than the transverse. The trail begins to drift with the surrounding masses of gas immediately after its formation and expands. The cause of trail expansion is ambipolar diffusion.

Observations of meteor trails provide information on regular and irregular /116
movements of air masses, enable us to find the coefficient of ambipolar diffusion, and to calculate the height of the homogeneous atmosphere, atmospheric density, and pressure. The chief method for observing meteor trails involves the use of radar. The working frequency most often is between 30 and 50 MHz. An increase in frequency causes a drop in the number of meteors observed, and shortens time of observations, whereas decrease in frequency brings with it strong interference attributable to the reflection of radio waves from the different irregularities in the ionization in the ionosphere [89]. Conditions for the reflection of radio waves from meteor trails are discussed in detail in the survey contained

in reference [87].

Radar observations provide the distance to the trail (the range), the height of the trail, direction and speed at which it is moving, and change in the amplitude of the reflected signal as the trail dissipates.

The distance, d, to the meteor trail is determined directly from radar data. The height of the reflecting region in which the trail is located, h, can be calculated from the formula

$$h = d \sin \psi, \tag{1.137}$$

where

$\psi$ is the angle of elevation.

The direction and speed at which the trail is moving can be found from the change in distance d in a predetermined time interval, or by the shift in the frequency of the reflected signal. A frequency shift

$$\Delta f = \frac{1}{c} 2 V_d f, \tag{1.138}$$

in which f is the radar's working frequency, will occur because of the Doppler effect when the meteor trail is moving at speed $V_d$ (with respect to the radar beam). Finding $\Delta f$ from the experimental data, we can calculate the radial component of the drift speed, $V_d$.

The amplitude of the reflected signal will decrease exponentially as the trail expands as a result of diffusion. Reflection duration, $\tau$, defined as the time it takes to reduce the amplitude by a factor of e, is equal to [87]

$$\tau = \frac{c^2}{16\pi^2 f^2 D}, \tag{1.139}$$

where

D is the coefficient of ambipolar diffusion.

The height of the homogeneous atmosphere, H, can be determined from the following formula using the values of the coefficient of ambipolar diffusion obtained from the experimental data [89]

$$H = \frac{dh}{d \ln D}. \tag{1.140}$$

Reference [86] contains a detailed discussion of the limits of applicability of Eqs. (1.139) and (1.140).

Radar observations of meteor trails can be made in the mode of continuous generation of oscillations, as well as in the pulse mode. Operation in the continuous mode [216] is a comparatively simple method for measuring the Doppler shift in the frequency, $\Delta f$. But much of the data on the meteor trail, and on the processes in the upper atmosphere, is lost in the process. Moreover, there are technical difficulties involved, such as the need for a spatial separation of transmitter and receiver, and others.

Recording amplitude and time characteristics of a reflected signal using the pulse mode provides more complete data on the processes taking place in the upper atmosphere. Still the mean wing velocities in the meteor zone are several tens of meters per second, and reflections of radio waves from meteor trails can /117 be observed only for tenths of a second, and these factors must be taken into consideration. So the distance from the radar to the meteor trail can change by several meters during the time the reflection exists. It is difficult to record changes such as these when the observation range is between 200 and 300 km. No significant results are obtained by complicating the recorder with a precise range sweep and the corresponding range marker generator. In one of the first installations the fine sweep duration was selected as equal to 5 km, and range markers were at 1 km intervals. The resolution was approximately 50 meters. Despite the simplicity and the possibility of using a standard transmitter, the method of determining wind speed and direction by measuring the distance to the trail over a known time span is not widely used. Therefore, what is used in order to obtain the maximum data is the pulse-coherent method of sounding and recording the amplitude-time and phase-time characteristics of the reflected signal [88, 182]. Pulse-coherent sounding in essence involves having the radar transmitter power amplifier working in the pulse mode, and separating the Doppler frequency by comparing the reflected signal frequency with that of the master oscillator. The USSR conducted a big program of investigating the processes in the meteor zone from Khar'kov [86-89]. A brief description of the main units in this installation follows.

Transmitter

The radar in Khar'kov operated at a frequency of 36.9 MHz. The master

oscillator operated in the continuous mode at 6.15 MHz. Frequency was quartz-crystal controlled. Frequency multiplication, pulse modulation, and power amplification took place in succeeding stages. Pulse width was 10 μsec, pulse repetition frequency 500 Hz, code (dual) 100 Hz, and pulse power at the transmitter output 75 kW. Coded radiation provided unambiguous range to the trail.

Antennas

Antennas of the "wavechannel" type are most often used for transmitting and receiving in this frequency band. Three to five elements are needed for each antenna, and it is desirable to use antennas with a narrow beam pattern in the horizontal plane, such as the cophasal antenna consisting of several "wavechannel" type antennas, in order to increase the accuracy with which the components of the drift velocity can be measured. Two antennas oriented north-south and east-west must be planned to measure the different components of the drift velocity, or else a rotatable antenna must be used.

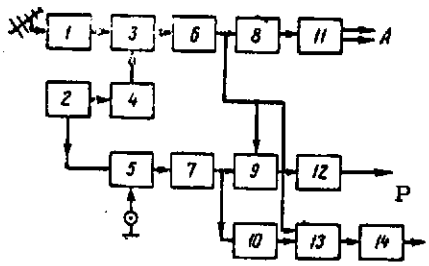


Figure 1.41. Functional diagram of the receiver channel in an installation for radar observations of meteor trails [87]. 1 - high-frequency amplifier; 2 - local oscillator; 3 - mixer; 4, 7 - frequency multipliers; 5 - reference signal mixer; 6 - intermediate-frequency amplifier; 8 - amplitude detector; 9 - phase detector; 10 - phase shifter; 11, 12, 14 - video amplifiers; 13 - phase detector; A - amplitude output; P - phase outputs.

Receiver-Recorder

The receiver consists of two main receivers: the first is designed to obtain phase-time and amplitude-time characteristics; the second to determine elevation (for calculating the heights of passage of the trace for known distance and elevation. Let us call the first receiver the phase receiver, conditionally, and the second the height receiver. Moreover, there is a noise receiver for protection against pulse noise.

The phase receiver (Figure 1.41) is a superheterodyne with a quartz oscillator. The receiver has two channels; the amplitude (the upper part of the diagram), and the phase (the lower part of the diagram). The amplitude channel /118

is necessary to obtain the amplitude-time characteristics (to calculate the speed of the meteoric body and to find the individual radiant) and to determine the distance to the trail.

The Doppler frequency is separated in the phase channel. This channel is the main channel when wind measurements are made. The Doppler frequencies are separated as follows. Two signals, the reference signal, and the echo from the trail, are fed into the receiver's phase detector. The reference signal results from the conversion and multiplication of the signal from the receiver's quartz-crystal local oscillator and the 6.15 MHz signal supplied from the radar transmitter's driver stage. The signal reflected from the trail and fed into the detector is obtained from the same receiver local oscillator and the 36.9 MHz signal after conversion and amplification. The signal frequencies, reference and echo, differ only by the frequency of the Doppler shift. This frequency is in hertz and tens of hertz when the operating wavelength is $\lambda$ = 8 m. A second phase detector, supplied with a reference signal after a preliminary 90° shift, is used to determine the direction in which the meteor trail is moving ("toward" or "away" from us). Thus, reference signal voltage

$$U_0 = U_{m0} \cos \omega_0 t \tag{1.141}$$

is supplied to the first detector and the following echo voltage is obtained from the receiver

$$U_n = U_{mn} \cos \omega_n \left[ t - \frac{2(d + V_d t)}{c} \right], \tag{1.142}$$

where

d is the distance to the trail;

$V_d$ is the radial velocity of the trail.

The voltage obtained at the detector output is

$$U_{b1} = U_{mb} \cos (\Omega t + \varphi_d), \tag{1.143}$$

where

$\Omega$ is the Doppler frequency.

The voltage at the output of the second detector, supplied with signal $U_n$ but shifted by $\pi/2$, is

$$U_{b2} = U_{mb} \cos \left( \Omega t + \varphi_d + \frac{\pi}{2} \right). \tag{1.144}$$

The signals at the detector outputs will be described by the following equations if the direction in which the trail is moving is reversed

$$\left.\begin{aligned} U_{b1} &= U_{mb}\cos(\Omega t - \varphi_d), \\ U_{b2} &= U_{mb}\cos\left(\Omega t - \varphi_d - \frac{\pi}{2}\right). \end{aligned}\right\} \qquad (1.145)$$

The voltage at the outputs of the phase detectors is amplified and supplied to the vertical deflection plates for the individual beams in the dual-beam oscillograph tubes. The sawtooth voltage generated by the driven sweep unit is supplied to the horizontal plates. /119

Elevation, as well as the radial value, must be known to find the horizontal velocity component. This angle establishes the height of the reflecting region of the meteor trail for known distance. There are different ways to find the angle, or the position, of the trail. Reference [87] describes a method in which two receiving antennas with different vertical plane patterns were used. Simple antennas, horizontal dipoles, or dipoles with reflectors positioned above ground level one-quarter, or one-half wavelenth, usually can be used to obtain an unambiguous result and to simplify the calibration and checking. It is recommended that the antennas be set up over a metal grid. The size of the grid should exceed that of the first Fresnel zone for the elevation, which can be measured.

The use of a code increases accuracy in fixing the signal relationship as received at the altimeter's receiving dipoles. The two dipoles are connected to an antenna switch. The switch connects the dipoles to the input to the height receiver (one dipole is connected at 500 Hz, the other at 100 Hz) in a definite sequence, but only for the time the second coding sequence of pulses is flowing. Feeding the voltage from the output of the height receiver to the vertical deflection plates, and the sawtooth voltage to the horizontal deflection plates, we obtain two superposed amplitude-time curves on the scope, one with a 500 Hz pulse train, the other with a 100 Hz train.

Identity of the channels in both dipoles of the altimeter is checked systematically, and both dipoles are set to the same height for this purpose. The check can be made under working conditions (while receiving signals reflected from a meteor trail), or by using a special remote radiator. If the

amplitudes differ, the signal gain in one of the channels is equalized. Some supplementary method usually is used to check the results and thus increase the accuracy in determining the height.

The height receiver is of the superheterodyne type. Particular attention should be given to attaining linearity of the characteristic curve and to expanding the dynamic range.

Experience has shown that it is quite possible to bring the error in finding the height to ±(2-3) km in the working section of elevation angles. The height can be determined in terms of the time constant by reducing the amplitudes of signals reflected from unsaturated meteor trails, if accuracy of this degree is not required. Here the height relationship of the coefficient of ambipolar diffusion must be known in addition to the amplitude-time characteristics.

The range sweep is triggered by 100 Hz pulses generated by the synchro-oscillator. The sweep for the amplitude and phase channels is triggered by pulses formed from the signals reflected from the trail and passing through the noise protection system. Their level is higher than that of discrimination.

The cathode ray tube screen remains dark if useful signals are not received. The lens of the recording camera is open. Pulses intensifying signals supplied to the tube plates are formed in the sweep trigger channel and last for 0.2-0.4 sec (depending on the sweep width selected). Frame change takes place when the sweep is concluded. Frame-by-frame recording is the most appropriate. The trigger channel is blocked during frame change so the film cannot be exposed at this time.

The error in finding the height depends on just how accurately the distance /120
to the trail was measured. Two sets of range markers, every 100 and 25 km, or every 100 and 10 km, can be introduced for each range sweep to increase accuracy in determining the distance. These types of markers differ in amplitude.

### 1.6. F-Scatter as a Method of Studying Ionospheric Irregularities

A signal reflected from the ionosphere carries a great deal of data on the structure of the reflecting region. Specifically, the data are contained in the form of an incoming signal. Sounding usually is by pulses very nearly rectangular in shape. The shape of the pulse changes when it is reflected in the ionosphere.

What is found in addition to a purely dispersion [53] expansion of the signal is distortion in shape as a result of reflection by irregularities. These changes are quite considerable, even under quiet ionosphere conditions (Figure 1.42a). A signal reflected from the F region of the ionosphere when ionospheric disturbances are taking place is much longer than the main pulse (Figure 1.42b). This phenomenon can be interpreted as in part due to scattering of signals from the F region - diffuse reflection, multiplets, scattered reflections. It is accepted [3, 115, 166] that when scattered reflections exist the reflecting region of the ionosphere consists of many groups of clouds (irregularities) encompassing a vast space, in height, as well as in the horizontal direction. It is during periods such as these that the ionosphere has its most marked irregular structure. The appearance of scattered reflections is associated with increase in irregularities in the F region, and with their movement. "The scattered reflections phenomenon" is established in the following manner [206].

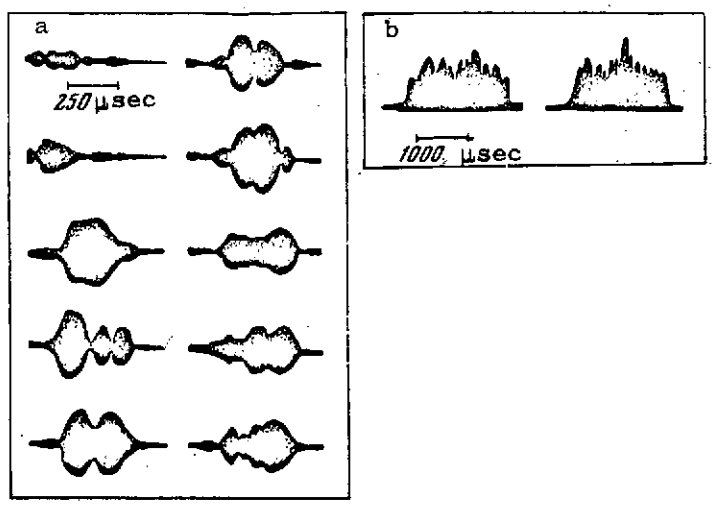


Figure 1.42. Distortion in the shape of a pulse because of scattering in the ionosphere. a - sequence of frames (2 seconds apart) showing distortion of the main pulse; b - shape of reflected signal when diffusibility is present.

We apply the term "scattered reflections phenomenon" to that observed in the middle and low latitudes, and most often to the polar regions, when a signal reflected by the ionosphere becomes diffuse, loses its well-defined structure and extends into the band of frequencies above the critical. This is not an adequately correct mathematical definition and is quite subjective.

Scattered reflections appear on ionograms in quite different forms. They sometimes cover almost the entire band of frequencies, sometimes will be found only near the critical frequency, or, contrariwise, at the low-frequency end of the trail. The degree (intensity) of scatter can change greatly. Several classification schemes have been suggested in order to describe and assess scattering. /121

The general classification scheme breaks scattered reflections down into three large groups by geomagnetic latitude of the observation station [115] as follows: (1) low latitude (below 20° geomagnetic latitude); (2) middle latitude (20°-60° geomagnetic latitude); and (3) high latitudes (above 60° geomagnetic latitude).

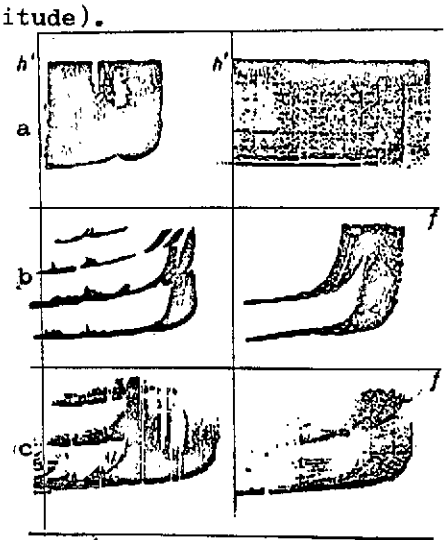


Figure 1.43. Examples of F-scatter in the ionosphere. a - high latitudes; b - middle latitudes; c - low latitudes.

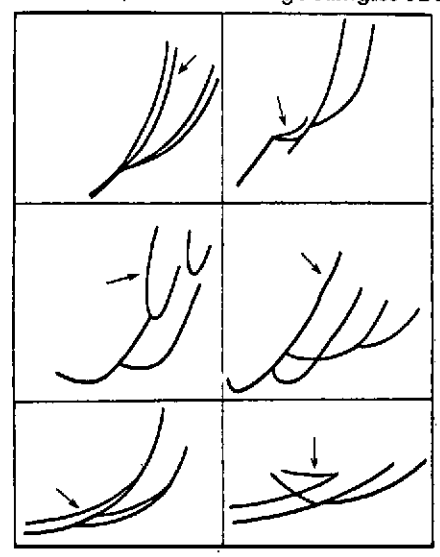

Figure 1.44. Diagrams of multiplets.

Ionograms from low latitude radars (Figure 1.43c) show the phenomenon of scattered reflections to extend along the frequency axis and does not depend on the frequency in a broad band. On the other hand, in the case of the high and middle latitude radars the scattered reflections are concentrated along the vertical on the ionogram (Figures 1.43a and b) covering the region of critical frequencies. It should be noted that the classification of scattered reflections is not unique in terms of the latitude criterion because sometimes the ionograms obtained in the equatorial regions greatly resemble those obtained in the polar regions [115, 210].

So the system proposed by McNicol, Webster, and Bowman [201] may be preferred to this classification. They proposed breaking down the phenomenon of scattered reflections into two types. (1) "Height scattering," when the low-frequency end of the ionogram has a diffuse pattern because of additional reflections, making it difficult to determine the apparent height. Critical frequencies are readily determinable in this type of scattering. (2) "Frequency scattering" when the ionogram has a diffuse pattern near the critical frequencies (the critical frequency of the additional reflections is higher than it is for the main trail) making it difficult to determine the critical frequencies. Both types sometimes can be observed simultaneously.

Frequency scattering usually is identified with the middle latitude type of scattering, height scattering with equatorial.

A great many multiplets (satellite or twin reflections near the main reflection from the F region) may be found on many ionograms containing scattered reflections. The well developed phenomenon of scattered reflections often /122
precedes the doublet reflection from the R region (in this case one satellite reflection is clearly separated from the main trail). Figure 1.44 shows diagrams of double reflections.

The presence of scattered reflections is readily determinable from ionograms, or from ionosphere tables of hourly values of F2 parameters in which the presence of scattered reflections is indicated by the symbol F. But the fact of a symbol provides no data on the intensity of scattered reflections. The intensity can change from slight scattering with virtually no effect on critical frequency determination to total masking of the critical frequencies. Several schemes have been suggested for assessing quantitatively the intensity of scattered reflections appearing on ionograms.

The most widely used classification of scattered reflections is that suggested in references [166, 266, 277]. The degree of scattering is determined from tabulated F2 data, or directly from the ionograms [182], with the scatter index determined on a 0-3 scale for each case according to the following rule: 0 - no scattering; 1 - very slight scattering; critical frequency for the F2 layer readily determinable; 2 - scattering quite extensive and determination of critical frequency in doubt; symbol placed in front of F2 values in the tables; 3 - scattering so great that the magnetoionic components merge and the critical

frequency for the F2 layer cannot be determined. Figure 1.45 shows this classification scheme composed using ionograms obtained by the Irkutsk radar.

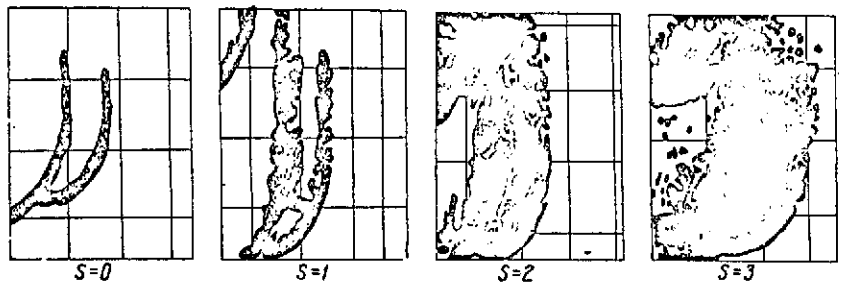


Figure 1.45. Classification of scattered reflections [115].

Comparing the diurnal curve indices for scattered reflections obtained from the tables with those obtained directly from the ionograms, one notes that the actual value of the indices obtained from the ionograms are higher than those obtained from the tables. This makes use of the ionograms desirable when investigating the intensity of scattered reflections. This system is very convenient for studying the middle latitude type of scattered reflections because the intensity of scattering in the critical frequency area is determined.

Other systems of indices are used to study the equatorial and high latitude types of scattered reflections.

Thus, we can observe a scattered reflection, classify it, and assess its intensity by looking at standard ionograms of vertical sounding by ground-based, or space ionospheric sounders. However, special observations methods are used to make a detailed study of some of the special features of the phenomenon discussed. We can investigate the dynamics of the process involved in the occurrence and development of the scattered reflection phenomenon by making a continuous recording of virtual heights and critical frequencies (see section 1.1.1).

Observation of the shape of a reflected signal on a type A scope (at fixed frequency). A reflected signal, when scattered, usually is a group of pulses /123 consisting of a great many discrete, constantly changing signals. A group such as this will cover a distance on the height scale from a score to several hundred

kilometers. Observation of these reflections on a type A sweep, and subsequent recording (on motion picture film), enables us to study their basic temporal variations [2]. This method is suited mainly for investigating "height scattering." These observations are extremely time consuming and expensive to make.

Study of angles of arrival of a reflected signal. Measurement of angles of arrival (azimuth and zenith angle) of individual signals in a group of pulses from a scattered reflection in combination with precise measurements of the range of a signal such as this is the most important task in investigating scattered reflections. Measurements such as these would enable us to respond to the question of localization of ionization irregularities causing the unknown phenomena. Unfortunately, the data thus far known of in the literature on this type of observation were compiled at but a few points in accordance with a very incomplete program. The explanation evidently is found in the very great technical difficulties involved in building pencil-beam antennas for the shortwave band. Radio signal reception for this purpose usually is by parallel spaced loop antennas that limit measurement to azimuths only.

Measurements of fluctuations in the intensity of radio signals from extra-territorial sources. Discrete sources of cosmic radio-frequency radiation and artificial earth satellites have expanded the height in the ionosphere accessible for observations and, in particular, have made it possible to obtain information on irregularities in electron density above the F region ionization maximum [160]. Investigations of irregularities in the electron density in the ionosphere using radio-frequency radiation from extra-territorial sources are based on an analysis of the diffraction pattern on the terrestrial surface occurring when radio waves pass through an irregular ionosphere. Investigations of scattered reflections usually are limited to study of temporal variations in the intensity of a radio signal at a fixed frequency using a Ryle interferometer.

Observation of scattered reflections during sounding of the outer side of the ionosphere. First investigations of reflected signals from the outer side of the ionosphere (see sections 1.1.1, 1.1.2) already have shown the presence of irregular scattering analogous to that in the lower part of the F region. Active sounding methods are used to investigate scattered reflections from the

outermost ionosphere. These measurements provide valuable information on the F region above the ionization maximum. The high speeds at which artificial earth satellites move, and the repeated flights around planets made by them, have added substantially to our concepts of the spatial distribution of F-scatter.

PART TWO

MEASUREMENTS DURING IONOSPHERIC PROPAGATION OF RADIO WAVES

## 2.1 Measurement of Absorption Coefficients During Vertical Sounding of the Ionosphere

### Absorption of Radio Waves in an Isotropic Ionosphere [53]

/124

The absorption of radio waves in the ionosphere can be estimated by taking into consideration conditions under which a wave is propagated in an ionized gas, including collisions between charged particles and molecules of a neutral atmosphere. According to elementary theory, collisions of an electron with neutral particles results in conductivity other than zero and, as a result, to the absorption of energy. Collisions between electrons do not lead directly to absorption because of pulse conservation.

Let us suppose we have the electric field of a plane wave being propagated in an ionized gas which then will be characterized only by the law of change in time

$$E = E_0 e^{i\omega t}. \tag{2.1}$$

The equation of motion for a charged particle with charge e and acted on by this field can be written

$$m\frac{d^2L}{dt^2} + m\nu\frac{dL}{dt} = eE, \tag{2.2}$$

in which the second term on the left-hand side of the equality includes the friction force. m is the electron mass, $\nu$ is the number of electron collisions per second, and L is the electron path. In solving the problem we shall consider only the electron motion. We shall evaluate the specific weight of the participation of the other charged particles later on.

A pulse of the order m(dL/dt), in which dL/dt is the ordered velocity communicated to the electron by field E, is transmitted as a mean by each electron impact. If we assume that the velocity at which the field causes the electron to move changes in accordance with the same temporal law as does the field, that is, if $V = V_0 e^{i\omega t}$ we can write $L = L_0 e^{i\omega t}$ and $d^2L/dt^2 = i\omega(dL/dt)$. Then Eq. (2.2) can be reduced to

$$\frac{dL}{dt} = \frac{eE}{m(\nu + i\omega)} = \frac{eE(\nu - i\omega)}{m(\nu^2 + \omega^2)}. \tag{2.3}$$

Taking the derivative with respect to time from Eq. (2.1) and substituting into Eq. (2.3), we will have $\frac{dL}{dt} = -i\frac{e(\nu - i\omega)}{m\omega(\nu^2+\omega^2)} \cdot \frac{dE}{dt}$.

Taking the total current in the ionized gas as the sum of the conduction current, $j_c = eN(dL/dt)$ (where N is the number of electrons per unit volume) and the displacement current, $j_d = (\varepsilon_0/4\pi)\cdot(dE/dt)$ (where $\varepsilon_0$ is the dielectric constant for the gas), we can write the expression for total current in the form

$$j_t = \frac{1}{4\pi}\left[\varepsilon_0 - \frac{4\pi e^2 N}{m(\nu^2+\omega^2)} - i\frac{4\pi e^2 N\nu}{m\omega(\nu^2+\omega^2)}\right]\frac{dE}{dt}.$$

And we can consider it as the displacement current flowing in an ionized gas characterized by the complex dielectric coefficient /125

$$\varepsilon' = \varepsilon_0 - \frac{4\pi e^2 N}{m(\nu^2+\omega^2)} - i\frac{4\pi e^2 N\nu}{m\omega(\nu^2+\omega^2)} = \varepsilon - i\frac{4\pi\sigma}{\omega}, \qquad (2.4)$$

but because $\varepsilon_0$ is 1 for a gas for all practical purposes, the formula can be simplified and

$$\varepsilon = 1 - \frac{4\pi e^2 N}{m(\nu_2+\omega^2)}, \qquad \sigma = \frac{e^2 N\nu}{m(\nu^2+\omega^2)}$$

($\sigma$ is the electrical conductivity for the gas).

Recognizing that an electron can collide with neutral atoms and molecules, as well as with charged particles, and with ions, some effective collision frequency equal to $\nu_e = \nu_{en} + \nu_{ei}$ must be taken as the collision frequency $\nu$. Here $\nu_{en} = 4/3\pi\alpha^2 nV_e \simeq 3.6\cdot10^{-10}n\sqrt{T}$, which is the frequency of collision between electron and neutral particles with concentration n and temperature T, and $\nu_{ei} = (5.5n_i/T^{3/2}) \times \ln(220T/\sqrt[3]{n_i})$ is the frequency of collision between electron and ions of concentration $n_i$. It should be pointed out that the effective section ($\pi\alpha^2$) of the collision between an electron and an ion is much greater than the effective section of the collision between an electron and a neutral particle, so collisions between electrons and ions begin to play a significant role in the ionosphere at a certain height, then predominate.

There are collisions between ions and neutrals and ions, as well as collisions between electrons and neutrals and ions, but their specific role in determining the magnitudes $\varepsilon$ and $\sigma$ is negligible because the mass of the ion, $m_i$, is greater than the mass of the electron by a factor of several tens of thousands.

Now the expression for the field intensity of a plane wave can be written in complete form as

$$E = E_0 e^{i(\omega t - kL)},$$

where

L is the wave propagation path;

$k = \frac{\omega}{c}\sqrt{\varepsilon'\mu}$ is the wave number.

In our case k is a complex magnitude presentable in the form

$$k = \frac{\omega}{c}(n - i\varkappa) \quad \text{or} \quad (n - i\varkappa)^2 = \varepsilon - i\frac{4\pi\sigma}{\omega},$$

After separation of the real and imaginary magnitudes in the left-hand side of the equality we obtain $n^2 - \varkappa^2 = \varepsilon$ and $2n\varkappa = 4\pi\sigma/\omega$, or $\varkappa = (2\pi\sigma/n\omega)$, and as a result of their simultaneous solution, assuming $\mu = 1$, we have

$$\left.\begin{aligned} n &= \sqrt{\frac{\varepsilon}{2}\left[\sqrt{1+\left(\frac{4\pi\sigma}{\omega\varepsilon}\right)^2}+1\right]}, \\ \varkappa &= \sqrt{\frac{\varepsilon}{2}\left[\sqrt{1+\left(\frac{4\pi\sigma}{\omega\varepsilon}\right)^2}-1\right]}. \end{aligned}\right\} \qquad (2.5)$$

Here the expression $\Gamma = -2(\omega/c)\varkappa$ is the wave absorption coefficient.

Eqs. (2.4) and (2.5) show that the magnitude of the absorption depends on the frequency of the propagating electromagnetic wave, $\omega$, as well as on the collision frequency, $\nu_e$.

Two extreme cases can be analyzed: (1) when $\omega > \nu_e$, or $\varepsilon = 1 - \frac{4\pi e^2 N}{m\omega^2}$, $\sigma = \frac{e^2 N \nu_e}{m\omega^2}$, that is, the absorption depends on collision frequency as well as wave frequency; and (2) when $\omega \gg \nu_e$ $\varepsilon = 1 - \frac{4\pi e^2 N}{m\nu_e^2}$, $\sigma = \frac{e^2 N}{m\nu_e}$, that is, the absorption is determined only by the collision frequency, $\nu_e$. /126

## Absorption of Radio Waves in an Anisotropic Ionosphere [112]

Consideration of the presence of a magnetic field in the ionosphere in solving the motion equation for a charged particle during the propagation of an electromagnetic wave results in a more complicated expression for the complex dielectric coefficient, one that can be written

$$\varepsilon = 1 + \frac{1}{(\alpha + i\beta) - \frac{\gamma_T^2}{2(1+\alpha+i\beta)} \pm \sqrt{\frac{\gamma^4 T}{4(1+\alpha+i\beta)^2} + \gamma_L^2}}, \qquad (2.6)$$

where

$$\alpha = -\frac{m\omega^2}{4\pi e^2 N} = -\frac{\omega^2}{\omega_0^2}; \qquad \beta = \frac{m\omega\nu}{4\pi e^2 N} = \frac{\omega}{\omega_0^2}\nu;$$

$$\gamma_T = \frac{\omega\omega_{HT}}{\omega_0^2}; \qquad \gamma_L = \frac{\omega\omega_{HL}}{\omega_0^2}; \qquad \omega_H = \frac{eH}{mc}; \qquad \omega_0^2 = \frac{4\pi e^2 N}{m};$$

H is the earth's magnetic field in the ionosphere;

$\omega_H$ is the electron's gyroscopic frequency;

$\omega_{HT}$ and $H_T$ are the transverse components;

$\omega_{HL}$ and $H_L$ are the longitudinal components of the electron's gyroscopic frequency and of the magnetic field in the ionosphere with respect to the direction of propagation of the radio wave.

A plus sign in front of the square root defines the ordinary, a minus sign the extraordinary, wave component.

It is very cumbersome to find the coefficient of absorption, $\Gamma = -2(\omega/c)\kappa$, in the general form shown as Eq. (2.6), so a practically simplified solution considers the special cases of quasilongitudinal and quasitransverse propagation of radio waves.

Quasilongitudinal propagation of a wave will be the case when the magnitude $\gamma T$ can be disregarded because of its smallness compared to $\gamma L$. Quasitransverse propagation is the case when the reverse is true. But consideration must be given to the fact that the solution can be simplified even further if we give individual consideration to the cases when $\omega \gg \omega_H$, which corresponds to the shortwave band, and $\omega \ll \omega_H$, which corresponds to the longwave band of radio waves.

## Absorption in Deviating and Nondeviating Regions

The estimate of absorption of radio waves in the ionosphere can be made conveniently by considering two cases; absorption in deviating, and nondeviating, regions of the ionosphere. This dicotomy is based on such considerations as a radio wave experiencing only absorption before the reflecting layer, the base of which is located at height $h_0$, begins and when the index of refraction of the lower-lying medium, n, is close to unity. The absorption then is called

nondeviating. The index of refraction of the medium tends to zero as the wave penetrates the layer and will equal the medium's plasma frequency, $\omega_0^2 = 4\pi e^2 N/m$; that is, when n = 0 the wave is completely reflected from the layer. Since $\varkappa = (2\pi\sigma)/(n\omega)$, when $n \to 0$ we have specific absorption associated with the penetration of the wave into the layer, and this is called absorption in the deviating region.

Let us say that we have $k' = (\omega/c)$, and $n' = (\omega/c)(n - i\varkappa)$. The expression /127 for the wave's electric field will be

$$E = E_0 \exp\left(-2\frac{\omega}{c}\int_0^{h(\varepsilon=0)} \varkappa dh\right) e^{i(\omega t - \frac{\omega}{c} nh)}.$$

Let us take the integral of this expression instead of $\varkappa$ because $\varkappa$ depends on the height. Then the coefficient of reflection of the wave from the ionosphere can be written

$$\rho = \frac{E}{E_0} = \exp\left(-2\frac{\omega}{c}\int_0^{h(\varepsilon=0)} \varkappa dh\right), \tag{2.7}$$

and total, or integral, absorption will be

$$-\ln\rho = 2\frac{\omega}{c}\int_0^{h(\varepsilon=0)} \varkappa dh. \tag{2.8}$$

The dependencies

$$n^2 - \varkappa^2 = \varepsilon = 1 - \frac{\omega_0^2}{\omega^2 + \nu_e^2} \quad \text{and} \quad \varkappa = \frac{2\pi\sigma}{n\omega} = \frac{2\pi e^2 N \nu_e}{n\omega m(\omega^2 + \nu_e^2)},$$

can be used for the component of an ordinary wave, so

$$\varkappa = \frac{\nu_e}{2\omega}\left(\frac{\varkappa^2}{n} + \frac{1}{n} - n\right).$$

Eq. (2.8) absorption then will be

$$-\ln\rho = \frac{1}{c}\int_0^{h(\varepsilon=0)} \nu_e \left(\frac{\varkappa^2}{n} + \frac{1}{n} - n\right) dh.$$

Eq. (2.8) can be reduced to the form

$$-\ln\rho_{(h_0)} = \frac{1}{c}\int_0^{h_0} \varkappa dh = \frac{4\pi e^2}{mc}\nu_e \int_0^{h_0} \frac{N dh}{(\omega^2 + \nu_e^2)},$$

in the nondeviating region from 0 to $h_0$ where n is close to 1, and we will, for

the deviating region where $\varepsilon = 0$ and $n \to 0$, so that $1/n - n \gg \varkappa^2/n$, have $h_{\varepsilon=0}$

$$-\ln \rho_{00} = \frac{1}{c} \int_{h_0}^{h(\varepsilon=0)} \nu_e \left(\frac{1}{n} - n\right) dh.$$

Thus, absorption delimited to absorption in the nondeviating and deviating regions and expressed by the optical and group paths will be written

$$-\ln \rho \cong \frac{4\pi e^2}{mc} \int_0^{h_0} \frac{\nu_e N}{\omega^2 + \nu_e^2} dh + \frac{\nu_e}{c} (L_g - L_0), \tag{2.9}$$

where

$L_g$ and $L_o$ are the group and optical paths of the wave in the ionosphere.

Absorption will be determined by the following expression in the deviating region, where we can set $L_g = L_o$, and where $\omega \pm \omega_H \gg \nu_e$ for the short-wavelength band, with the earth's magnetic field taken into consideration and the case of longitudinal propagation pertinent /128

$$-\ln \rho = \frac{1}{c} \frac{4\pi e^2}{m} \int_0^{h_0} \frac{N \nu_e \, dh}{(\omega \pm \omega_H) + \nu_e^2}.$$

This leads to the absorption ratio for ordinary and extraordinary wave components

$$\frac{\ln \rho^{(o)}}{\ln \rho^{(x)}} = \frac{(\omega - \omega_H)^2}{(\omega + \omega_H)^2}.$$

The following expressions will yield absorptions for ordinary and extraordinary wave components for the deviating region

$$-\ln \rho^{(o)} = \frac{\nu_e}{c} (L_g - L_0),$$

$$-\ln \rho^{(x)} = \frac{\nu_e}{c} \left(\frac{L_g - L_o}{\omega - \omega_L}\right) \omega.$$

If the ionosphere layer is considered as a simple layer

$$N = N_{om} \exp \frac{1}{2} (1 - h + \sec \varkappa e^{-h}),$$

where

$h = (h_m - h)/H$;

$\nu = \nu_0 e^{-h}$;

and we can take the recombination coefficient as a constant, $\alpha = \alpha_0$, or as

depending on the height in the form of an exponential function, we obtain two expressions for the absorption magnitude

$$-\ln\rho = \frac{4\pi Ne^2 H\nu_0}{mc}\cdot\sqrt{2\pi l}\cdot\frac{\cos\chi^{1/2}}{(\omega\pm\omega_L)^2}, \quad \text{if } \alpha=\alpha_0,$$

and

$$-\ln\rho = \frac{4\pi Ne^2 H\nu_0}{mc}\cdot\sqrt{4l}\cdot\frac{\cos\chi}{(\omega\pm\omega_L)^2}, \quad \text{if } \alpha=\alpha_0 e^{-h},$$

in which the recombination coefficient to height difference relationship leads to coefficient of absorption to cosine of the sun's zenith angle, cos X, difference relationships.

Determination of Effective Collision Frequency $\nu_e$ [3]

It must be pointed out that Eq. (2.9) provides a numerical determination of the magnitude of collision frequency for a definite region of the ionosphere. The wave's optical path changes much less than the group path for small change in frequency (Figure 2.1), so change in the optical path can be disregarded and Eq. (2.9) yields

$$-\delta(\ln\rho) = \frac{\bar{\nu}_e}{2c}\delta h_{\text{гр}},$$

from which, knowing the change in the group path for two frequencies, and the change in the absorption, we can find the mean effective collision frequency, $\nu_e$.

A stricter solution will yield

$$-d(\omega\ln\rho) = \omega\frac{\bar{\nu}_e}{c}dh_{\text{гр}},$$

which provides a means for finding $\bar{\nu}_e$ graphically /129

$$\omega_1\ln\rho_1 - \omega_2\ln\rho_2 = S\frac{\bar{\nu}_e}{c},$$

where

S is the hatched area in Figure 2.1.

Methodology for Finding Coefficient of Absorption [192]

What follows from Eqs. (2.7) and (2.8) is that once the field intensity of two reflected signals has been found, we can calculate the magnitude of the integral absorption of radio waves in the ionosphere from the difference multiplicity. This method of recording absorption has come to be called the Al

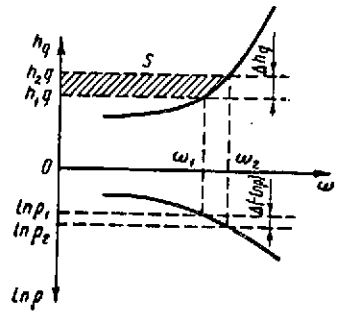


Figure 2.1. Graphical determination of magnitude of mean effective collision frequency from height-frequency curve and absorption data measured at frequencies $\omega_1$ and $\omega_2$ [3].

method in the literature.

If we consider a transmitter on the terrestrial surface to be a point radiator, we can operate with an equation for the propagation of a spherical wave which yields the following expression for the coefficient of reflection of first and second multiplicity

$$\rho_{1,2}\rho_e = \frac{2E_2}{E_1} \text{ or } \rho_{1,2} = \frac{2E_2}{\rho_e E_1},$$

where

$E_1$ and $E_2$ are the signal field strengths for single and double reflections;

$\rho_e$ is the coefficient of reflection of radio waves from the earth.

If the amplitudes of the $n^{th}$ and $k^{th}$ reflections are used the coefficient of reflection will have the following form when $n > k$

$$\rho_{kn} = \sqrt[n-k]{\frac{nE_n}{kE_k\rho_e^{n-k}}}.$$

Finding the natural logarithm of the coefficient of reflection, we obtain the absorption in nepers, which, in order to convert to the decibel scale more widely used, must be multiplied by 8.686, or the common logarithm of the coefficient of reflection can be taken at once and this then can be multiplied by 20, that is

$$-\Gamma = 20 \lg \rho_{kn}.$$

All too often we cannot record a double signal reflection in daylight hours because absorption is substantial. But here the absorption can be calculated by using the equipment constant, determined during nighttime hours when the double reflection minimum occurs.

A correction factor for difference in gain must be introduced because the receiver channel operates at different gains during the day and during the night. This will reduce the gain to one value, that is, the signal field strength is represented by the magnitude of the amplitude and the corresponding gain factor /130

$$E_g = A_g k_g, \qquad E_n = A_n k_n.$$

We can write

$$\rho_{0,1n} = \frac{2h_n E_{1n}}{E_0} = \frac{2E_{2n}}{\rho_e E_{1n}} = \rho_{1,2n},$$

where

$h_n$ is the height of the reflecting layer,

for nighttime observations.

Now the equipment constant can be written

$$G = 20 \lg \frac{1}{E_0} = 20 \lg \frac{A_{2n}}{\rho_e h_n A_{2n}^2 k_n}.$$

Then we can find the absorption in the daytime when there is but one reflection by using the equipment constant and the following formula

$$-\Gamma = 20 \lg 2h_g A_{1g} k_g + G,$$

If we have a double reflection in the daytime the absorption can be calculated by using the multiple reflection ratio

$$-\Gamma = 20 \lg \frac{2A_2}{\rho_e A_1},$$

as well as the equipment constant in terms of the amplitude of the double reflection and the formula

$$-\Gamma = 20 \lg \frac{4h_g A_{2g} k_g}{\rho_e} + G.$$

It should be noted that absorption calculations usually take the coefficient of reflection from the earth as equal to unity, something that is not fact [77].

Observations have revealed that the magnitude of the amplitudes of signals of all multiplicities can change in wide limits and at different speeds, sometimes within very short periods of time. So individual samplings of amplitudes will yield distorted absorption values when substituted into the formula.

Signal fading can occur for two reasons; interference of the wave's two magnetoionic components, and movement of the diffraction pattern of signal field strength over the terrestrial surface as a result of the drift of small-scale irregularities in the electron density in the ionosphere in the reflection region.

Interference fading can be eliminated by using polarized receiving antennas so as to receive only one of the signal's magnetoionic components [104] (see section 1.1.3).

All measures designed to eliminate errors in the absorption calculations

attributable to diffraction fading can be limited to a set of a great many measurements and their subsequent averaging. This is why the magnitude of the amplitude in all of the formulas previously cited must be understood to be referring to its mean value.

The Influence of an Irregular Structure of the Ionosphere on ρ

The ionosphere has irregularities in electron concentration on a most diverse scale, ranging from small ones of several tens of meters to large ones of several tens of kilometers leading to the scattering of reflected signal energy, as well as to the focusing of that energy at the terrestrial surface, /131 so it is necessary to calculate their influence on the coefficient of reflection of a wave from the ionosphere.

Calculation of the influence of small-scale irregularities on the coefficient of reflection of a wave from the ionosphere when it is found in terms of the amplitudes of double and single reflected signals yields the expression [3]

$$\frac{A_2^2}{A_1^2} = \frac{\rho\rho_e}{2}\left(\frac{\beta^4 + 4\beta^2 + 2}{\beta^4 + 2\beta^2 + 1}\right)^{1/2},$$

where

$A_1$ and $A_2$ are the amplitudes of the single and double reflected signals;

$\rho$ and $\rho_e$ are the coefficients of reflection of a signal from the ionosphere and from the earth's surface;

$\beta$ is the ionosphere's turbidity factor, defining the ratio of the specular component to the energy scatter component in the reflected signal.

Formulas are available for finding the coefficient of reflection to include small-scale irregularities in terms of the amplitudes of single and triple reflections, of double and triple reflections, but they contribute nothing new, in principle, and we shall not include them here because they are too cumbersome [13].

The influence of large-scale irregularities on the coefficient of reflection reduces to cases of recording $\rho$ for magnitudes greater than unity, something that contradicts the law of conservation of energy. Consideration of their influence on $\rho$ has not yet been resolved analytically [70, 212].

It should be pointed out that inclusion of the influence of small-scale irregularities through $\beta$ makes sense if the installation receiver channel has a good linear amplitude curve. Otherwise the effort to obtain a high degree of accuracy in the evaluation of absorption will be useless because the error in the absorption attributable to poor linearity of the receiver channel exceeds the correction for small-scale irregularities.

Thus, the simplest method to use when measuring the absorption of radio waves in the ionosphere by the A1 method and eliminate errors attributable to the influence of irregularities, and to the interference of the signal's ordinary and extraordinary components, is a set of a great many statistics on amplitudes, which then is averaged.

## Equipment and Observation Procedure

The task of achieving a high degree of accuracy in the recording of the amplitudes of signals of different multiplicity, that is a set of sufficient statistics on magnitudes of amplitudes over a limit period of observations, poses specifications for equipment designed to measure the absorption of radio waves. The general operating principle for such equipment duplicates that for the ionospheric sounder used for vertical sounding of the ionosphere, but the transmitter operates on fixed frequencies, and a cathode-ray tube oscillograph with a type A sweep is used as the indicator [116].

More stringent requirements are imposed on equipment for measuring the absorption of radio waves as opposed to the conventional panoramic type sounder, and this applies to the transmitter as well as to the receiver.

The transmitter should be able to radiate power that will be temporarily constant at all working frequencies and, at the same time, be quite frequency stable.

The receiver should meet the following specifications: (a) have a broad IF passband, at least 16 kHz, for a radiated pulse of width 100 $\mu$sec; (b) good linear amplitude curve for all gains in the working amplitude band. The best type of gain adjustment is step-type using an IF attenuator with 10 db steps in the 70-80 db range; (c) time to restore receiver sensitivity to 90 percent after the /132
transmitter has radiated a pulse should be within 200 $\mu$sec; (d) good constancy of the temporal gain factor at working frequencies. There are two ways to prevent pulses radiated from the transmitter from causing receiver sensitivity to

deteriorate and thus cause signals with different frequency of reflection to be amplified differently in the receiver channel, and the two usually are used simultaneously. A pulse from the transmitter modulator detunes the local oscillation in the receiver and the IF stages thus are not overloaded by the incoming pulse. Moreover, all decoupling HF and IF tube circuits in the receiver channel should have a time constant equal to the leading edge of the main pulse, that is a time of the order of 10 μsec.

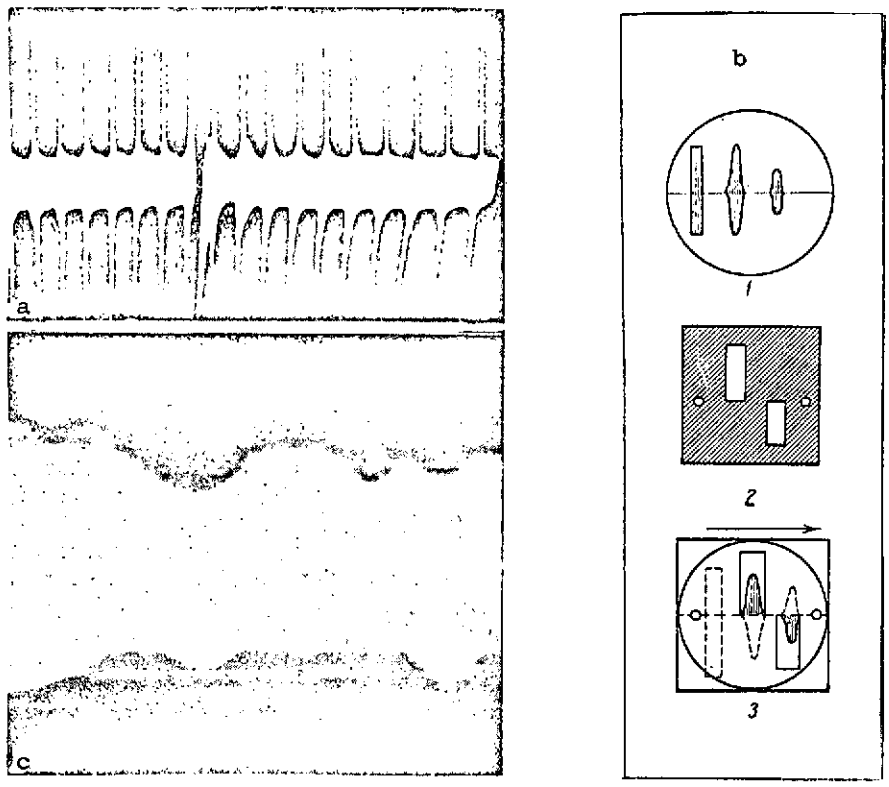


Figure 2.2. Recordings of signal amplitude on oscillograph scope. a - for evaluating desensitization of receiver by transmitter main pulse and temporal restoration of receiver sensitivity. The example is at 2 MHz. The standard signal generator signal is in the form of pulses, the distance between which corresponds to a height of 100 km; b - example of the use of a "mask" when recording a signal to determine absorption of radio waves; 1 - image on oscillograph scope; 2 - view of "mask"; 3 - position of reflected signal sweep relative to the "mask" [36]; c - example of a recording during continuous recording of amplitudes of first and second multiplicity.

When these measures can be used in part only, and blocking of the receiving

channel is sufficiently important, the standard signal generator must be used to calibrate the amplification according to the position of the reflected signal on the time axis of the cathode ray tube oscillograph sweep. This is done by supplying the input to the receiving channel with the voltage from the standard signal generator and keying the transmitter. The correction factors by which the /133 amplitudes of the corresponding signal multiplicity are multiplied depend on the degree of change in the envelope of the electromotive force from the standard signal generator (Figure 2.2a) near the main pulse.

A logarithmic signal amplification scale is used to expand the receiver's dynamic range, but if there is no such scale those sections of amplitude recording with off-scale amplitudes are not included in the processing to avoid errors in the measurement.

It now remains to consider methods of recording amplitudes of several reflected signals received and separated on the time sweep of a cathode ray oscillograph. The visual procedure for recording amplitudes has been used right from the very beginning of experiments to measure absorption. Recordings were logged at equal, possibly short, time intervals throughout the observation period. Accuracy was poor, of course, and depended on the experience and accuracy of the observer. An experimental check of several observations has yielded a 15 percent scatter in values.

A subsequent refinement in the recording method was photography of the patterns on the scope using a type A sweep and picture taking at the rate of one frame per second for between 4 and 5 minutes, so that a set of between 240 and 300 amplitude values was assembled in that time. This method, despite the time required for processing the materials from observations, is in use even today when data on amplitudes of signals of all multiplicities are needed.

All that is needed to calculate absorption is the amplitudes of two reflected signals, so the method that moves film continuously after a "mask" has been placed over recorded signals has been suggested (Figure 2.2b) [36]. A photograph of this recording method is shown in Figure 2.2c. The accuracy in amplitude recording has been increased to between 5 and 7 percent.

The double reflection of the signal usually is missing in daytime hours because of absorption so only a single reflection is recorded, and the magnitude

of the absorption is calculated using the amplitude of one reflection and the equipment constant determined during the nighttime hours.

It must be pointed out that the use of this method to determine absorption requires strict constancy in transmitter power radiation time and good constancy of receiver gain. Atttempts to obtain a double reflection by increasing transmitter power have resulted in an increase in the amplitude of a single reflection such that it goes off scale and measurements lose all meaning. Receivers with an expanded dynamic range resulting from the use of a logarithmic amplification scale are not widely used, evidently because of their complexity and the instability in their parameters.

Development of the photography of amplitude recordings is time consuming, and for this reason there have been a number of attempts to automate not only the development, but the observations as well.

Equipment has been proposed that would make a continuous recording of the absorption, the magnitude of which would be self-recorded in the form of a curve throughout the observation period [119]. The principle of operation of the equipment is based on the use of an amplifier with a logarithmic amplification scale in the receiving channel. Two identical amplification channels which record each signal separately, have output voltages corresponding to the logarithm of each of the amplitudes. The voltage difference therefore is the magnitude characterizing the absorption. The calculation of the numerical coefficients for the amplitude, for which there is required the corresponding formula for calculating the magnitude of the absorption, is made by a simple schematic solution.

The proposal that signal amplitudes be recorded in numerical values, and /134
thus simplify subsequent processing of the observation data, can be considered a second variant in the automation of absorption recording [72]. The scaler for one of the channels, that for recording a single reflection, for example, works as follows. The signal flows from the receiver output to the scaler input where it first is fed into a time selector which always is closed when in the normal position, and is opened only at the time of arrival of the reflected signal by a special selector pulse formed on signal from the observer. Figure 2.3 shows the shape of the signal at individual elements in the scaler.

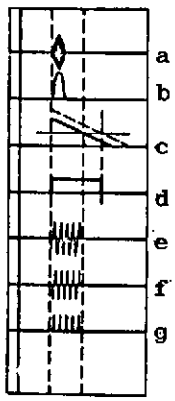


Figure 2.3. Sequence in which signal amplitude is converted in individual elements in the scaler for recording absorption [72].

A signal separated in this manner (Figure 2.3a) is detected (Figure 2.3b) and fed into a phantastron which converts the pulse supplied into a pulse with a trailing edge that falls linearly (Figure 2.3c). The parameters of this signal are proportional to the amplitude of the received signal and deviate from the true by no more than 1 percent. This signal then is fed into the amplitude discriminator which generates a rectangular pulse, the width of which is proportional to the amplitude of the received signal (Figure 2.3d). This "wide" pulse is amplified and fed into a pulse generator which operates on low frequency and generates a pulse "package" during the time the "wide" signal lasts (Figure 2.3e). Thus, there will be a "package" containing a number of pulses proportional to the amplitude of the received signal for each received amplitude. The pulses then are fed into an amplifier-limiter where they are shaped (Figures 2.3f and g) and can be fed into a summer, a special recorder (magnetic tape, punched tape, or punched cards).

The scaler for recording absorption consists of two identical channels and a monitor oscillograph with a type A sweep which is used to make a visual setting on the signal of the first and second reflections of the selector pulses opening the scaler channels for operation.

Further development of the A1 method involves recording the amplitude of a reflected signal during vertical sounding of the ionosphere on alternating frequency. This recording method is abbreviated A5 [19]. Technically, it can be realized with a conventional ionospheric sounder, the main pulse from which covers the entire band in a short period of time [76]. The procedure for determining the equipment constant and for processing observation data is similar to that for the A1 method.

## 2.2. Measurement of Absorption by the Method That Records Extraterrestrial Sources

The A1 method for recording absorption of radio waves in the ionosphere

has one significant drawback. There may be no signal reflected from the ionosphere anywhere in the frequency band in the event of the appearance of abnormally increased absorption at the receiver. This method cannot provide a numerical estimate of the absorption, therefore, so all we can do is assert that at a given moment in time the absorption exceeds, for example, 70 db, which has been determined as the upper limit of the equipment for vertical sounding. /135

Cases of abnormally high absorption such as these are very rarely observed in the middle latitudes, no more than a few times a year, the result of very powerful chromospheric flares on the sun, so the A1 method is widely used in the middle latitudes.

Cases of abnormal absorption become so frequent in the polar regions, beginning at the southern boundary of the aurorae zone and higher to the pole, that it is necessary to use another method to find the absorption, one capable of recording absorption and doing so at a very high level. One such method is that which records the intensity of the radiation from extraterrestrial radio-frequency sources (A2), or records the intensity of cosmic noise.

A quite detailed survey of the A2 method, together with an extensive bibliography, was published in 1969 [25].

By recording the strength of a signal from an extraterrestrial radio-frequency source using ground-based receivers we can write as the basic expression for its strength

$$E = E_0 e^{-\frac{2\omega}{c}\int \varkappa dL} = E_0 e^{-\Gamma},$$

where

$E_0$ is the "primary" field strength of the signal from the radio-frequency source beyond the limits of the ionosphere;

$\Gamma$ is the magnitude of the integral absorption of the radio waves in the ionosphere, and can be established in decibels from

$$-\Gamma = 20 \lg \frac{E}{E_0}.$$

It should be noted that the concept of power usually is operative in the calculations of absorption when the A2 method is used, and in this case the expression for absorption in decibels will be

$$-\Gamma = 10 \lg \frac{E}{E_0}.$$

So if we are to find the absorption $\Gamma$ we must know strength $E_0$, as well as the recorded signal strength E. E will vary during the 24-hour period because of the diurnal change in the absorption of radio waves in the ionosphere, as well as because of change in $E_0$ attributable to the nonuniform distribution of the strength of the radio-frequency sources throughout the firmament.

Considering the curve for the temporal change in E for a quiet ionosphere, that is, when anomalous absorption is lacking, we note the presence of a maximum ($E_{max}$) which occurs at night in the premorning hours and which corresponds to the minimum absorption in the ionosphere. Ignoring this absorption, and, consequently, equating the obtained maximum strength to the "primary" strength of the source, $E_{max} = E_0$, we can determine the absorption contributed by the ionosphere for any other hours of the day. This determination will be precise when the condition is one of constancy of $E_0$. In this case, of course, we do not determine the absolute magnitude of the absorption, but the increment with respect to night absorption which, because of its smallness, we equate to zero.

Practically speaking, the distribution of the intensity of the radio sources throughout the firmament is uneven and the "primary" strength $E_0$ will experience temporal changes with a periodicity equal to the sidereal day. In turn, the magnitude of the absorption of radio waves in the ionosphere will change with the periodicity of mean solar days.

Because sidereal days are shorter than solar days by approximately 4 minutes (3 minutes 56 seconds, to be precise), and in order to eliminate the influence of nonuniform distribution of intensity of radio sources throughout the firmament, that is, in order to take into consideration diurnal changes in the "primary" strength $E_0$ when calculating absorption, it is necessary to have a long, at least one year, continuous series of observations of the intensity of cosmic radio radiation. This condition imposes additional technical requirements on the recording equipment which should maintain its parameters constant over the entire period of observations. /136

The influence of the nonuniformity in the distribution of radio-frequency sources throughout the firmament can be eliminated by using the recording of cosmic radio-frequency radiation from the Polaris region, or from the celestial poles, areas that are fixed in the firmament. In this case the absorption

determined equates to the oblique propagation of radio waves in the ionosphere and can be roughly converted to the vertical by

$$\Gamma_v = \Gamma_o \cos \alpha,$$

where

$\alpha$ is the latitude of the point of observation, degrees.

The principal difficulty in successful realization of this variant of the observation is building a receiving antenna with a narrow cone-shaped lobe in its pattern. Modern antennas do not have this good a pattern so strength $E_0$, as before, undergoes diurnal variations, although they are weaker. Therefore, if we do not take into consideration the magnitude of the diurnal variation in $E_0$, we obtain a rough estimate of the magnitude of the absorption. There are certain scientific tasks, the investigation of anomolously increased absorption in the high latitudes, for example, when this recording variant is completely acceptable, so today it is widely used.

Selection of the working frequency for recording the intensity of cosmic radio-frequency radiation depends on a great many conditions which in turn depend on the scientific task posed, as well as on the engineering of the receiving antennas. The basic condition will be the requirement for a considerable increase in the working frequency over the critical frequency of the maximum for ionization of the ionosphere, $f_0F2$.

We can, for this condition, write

$$\omega_w^2 \gg (f_0F2)^2,$$

and since this is the same as

$$\omega_w^2 \gg \omega_H^2,$$

we will have, for an undeflecting region, when the index of refraction is $n \sim 1$, the expression defining absorption in the form

$$\varkappa = \frac{1}{2} \frac{\omega_0^2 \nu_e}{\omega (\omega^2 + \nu_e^2)}.$$

Inclusion of the earth's magnetic field leads to the expression

$$\varkappa_{1,2} = \frac{1}{2} \frac{\omega_0^2 \nu_e^2}{\omega [(\omega \pm \omega_L)^2 + \nu_e^2]},$$

where the indices 1, 2 and the signs ± equate to different magnetic components of the wave and $\omega_L = \omega_H \cos\alpha$ and $\alpha$ is the angle between the direction of the wave and the direction of the earth's magnetic field. In this case the integral absorption will be

$$\Gamma = \frac{1}{c}\int \frac{\omega_0^2 \nu_e}{(\omega \pm \omega_L)^2 + \nu_e^2} ds.$$

We can write the inequality $\omega^2 \gg \nu_e^2$ for the entire ionosphere, with the exception of the D region. The D region, where we will have $\omega^2 \simeq \nu_e^2$ makes but a slight contribution to the integral absorption when anomalous absorption is lacking. The last formula then can be written as follows for a quiet ionosphere

/137

$$\Gamma = \frac{1}{\omega^2 c}\int \omega_0^2 \nu_e \, dL$$

What follows from this expression is the fact that a reduction in the working frequency will provide us with more favorable conditions for recording variations in absorption, but the critical frequency for the ionosphere's F region sets the limit for the reduction in the working frequency.

Another recording method, that which records cosmic radio-frequency radiation simultaneously on two spaced frequencies [18], has been recommended to eliminate the diurnal variations in $E_0$ from the absorption calculations. In this case, with measurements on two frequencies, we will have

$$-\Gamma_1 = 10 \lg \frac{E(\omega_1)}{E_0(\omega_1)}; \quad \Gamma_1 = \frac{1}{c\omega_1^2}\int \omega_2^0 \nu_e \, dL$$

and

$$-\Gamma_2 = 10 \lg \frac{E(\omega_2)}{E_0(\omega_2)}; \quad \Gamma_2 = \frac{1}{c\omega_2^2}\int \omega_0^2 \nu_e \, dL,$$

from whence, after simultaneous solution

$$\Gamma_2 = \Gamma_1 \left(\frac{\omega_1}{\omega_2}\right)^2 \text{and} \Gamma_1 = \frac{10\left[\lg \frac{E_0(\omega_1)}{E_0(\omega_2)} - \lg \frac{E(\omega_1)}{E(\omega_2)}\right]}{1 - \left(\frac{\omega_1}{\omega_2}\right)^2}. \qquad (2.10)$$

The last two expressions can be used to calculate absorption for the condition of constancy of the magnitude $E_0(\omega_1)/E_0(\omega_2)$. This ratio can be determined from night observations in accordance with the earlier accepted assumption that absorption at night is very small and we can, therefore, ignore it.

But the ratio $E_0(\omega_1)/E_0(\omega_2)$ will not remain constant throughout the 24-hour period because it is practically impossible to manufacture two antennas for different frequencies with identical patterns.

Eq. (2.10) can be used to make the calculations for those time intervals in which this ratio is not subject to significant changes.

The polarization method [21] can be used as one of the modifications of the two-frequency method, and so can the dual polarization method wherein the intensity of the signal for the ordinary and extraordinary components of the wave can be measured.

The intensities of the ordinary and extraordinary components of the wave differ after passage through the ionosphere and their relationship can be represented in the form

$$\frac{E^+}{E^-} = e^{\Gamma^- - \Gamma^+};$$

the ratio of their difference to the sum after use of the $e^x = shx + chx$ transform will be

$$\frac{E^+ - E^-}{E^+ + E^-} = th\frac{\Gamma^- - \Gamma^+}{2},$$

which does not depend on the "primary" intensity $E_0$.

The expression

/138

$$\Gamma = \Gamma^- - \Gamma^+ = \frac{\Delta\Gamma}{\bar{\Gamma}},$$

where

$\Delta\Gamma = \Gamma^+ - \Gamma^-$ and $2\bar{\Gamma} = \Gamma^+ + \Gamma^-$,

can be written in place of the last expression for the case of the quiet ionosphere when anomalous absorption is lacking.

At the same time, by using Eq. (2.8), it can be shown that the difference in absorption is

$$\Delta\Gamma = \frac{2\omega}{c}\int(\varkappa^- - \varkappa^+)\,dL \simeq \frac{2}{c}\int\frac{\omega_0^2\omega_L\nu_e}{\omega^3}\,dL = 4\,\frac{\bar{\omega}_L}{\omega}\,\bar{\Gamma},$$

where

$\omega_L$ is the mean magnitude of the gyrofrequency,

and $\bar{\Gamma} = \dfrac{\Gamma^+ + \Gamma^-}{2}$ can be assumed for the mean absorption.

These formulas can be used to calculate the absorption.

It should be pointed out that this method is most effective only at low frequencies because the $\omega_L/\omega$ ratio should be adequate in magnitude, and not less than 0.1 in any case. Today, despite definite technical difficulties, this method is considered to be the one with the best prospects [69] because sufficiently precise data on absorption can be obtained after several weeks of observations.

Equipment for Recording Cosmic Radio-Frequency Radiation (Riometers)

The equipment used to record the intensity of cosmic radio-frequency sources has been named the riometer (an acronynm for Relative Ionospheric Opacity Meter). It consists of an antenna, a receiver, and a calibration source, a noise generator.

The basic requirement imposed on the riometer is constancy of parameters during continuous observations over a long period of time.

Riometers, in most cases, contain modern communication receivers with quite good operating stability. Given this use, the major recommendation is to pay particular attention to the stabilization of the receiver power supply.

The receiving antenna is the most critical component of the riometer. Its design is determined by the scientific task posed, as well as by the band of operating frequencies selected. The feeder connecting the antenna to the receiver is a high-frequency coaxial cable, the length of which is fixed by the inserted attenuation, as well as by the magnitude of the thermal noise that arises in the installation with change in the ambient temperature. Based on these considerations, it is desirable to make the length of the cable as short as possible.

The antenna should be well matched to the feeder line, but at the same time the whole of the receiver channel should have some bandwith (of the order of 0.2 MHz) within the limits of which it would be possible to change the working frequency so as to tune out possible interfering radio stations. Recommended for a more certain selection of the working frequency is a preliminary round of observations of sufficient length to load the bands of the other stations working on frequencies interferring with our own so we can find the "window" free of the interfering radio stations.

The antenna usually used with the riometer is of the limited type, the simplest version of which is an antenna consisting of a single dipole located at a height of one-quarter wavelength above a metallized ground, made in the form of a wire grid. This antenna has quite a wide lobe in the pattern, one that is directed upward. Several dipoles in the form of a cophased array can be set up to form a narrow lobe in the pattern. /139

The most widely used is the "wave channel" type of multielement antenna, which can be directed toward the zenith, as well as to other points in the celestial dome, and in particular at the celestial pole.

Quite complicated antennas are used for separate reception of the ordinary and extraordinary signal components. They are spiral in shape, or are mutually perpendicular dipoles with the corresponding phasing [104, 207], as already described in section 1.1.3.

One of the basic requirements imposed on antennas is the presence of one pencil lobe. If side lobes do exist they should have little effect.

Existing riometers can be broken down into two classes by the principle involved in recording the intensity of cosmic noise.

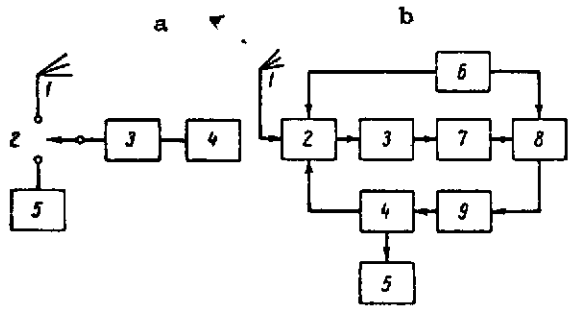


Figure 2.4. Block diagram of most often used riometers. a - riometer using the method that provides a standard source; b - riometer using the modulation-zero method [146]. See text for explanation.

In the first case the signal is received by antenna 1, amplified in receiver 3 and fed into the recorder (Figure 2.4a). The installation is calibrated by noise generator 5, connected to the input of the receiver instead of the antenna periodically by switch 2, in order to determine field strength. Here we have the example of the simplest possible method of comparing signal field strength by substituting a standard source. We can familiarize ourselves with the description of this equipment [29], but it does not yet enjoy widespread use because measurements are not very accurate, and it is hard to service.

The drawback in these riometers is their poor stability in operation, primarily the instability of the receiver gain factor, which reflects on measurement accuracy.

The so-called modulation-zero recording method is used in the second variant. Here equipment instability is not as significant.

Figure 2.4b is the block diagram of this riometer. The antenna (1), then the noise generator (4) with frequency $f_0$, is connected in turn through the switch (2) to the input of the receiver (3). The frequency is set by the switching generator (6). The signal that appears at the receiver output will have frequency $f_0$ and will be proportional to the difference in the strengths of the signals at the antenna and that supplied by the noise generator. The signal is amplified by the tuned amplifier of frequency $f_0$ (7) and supplied to the phase-sensitive detector (8), which is a type of ring converter. The detector produces a rectified voltage, the magnitude of which will be proportional to the difference in the strengths of antenna and noise generator signals, and the polarity of the rectified signal will be determined by the greater strength.

The signal produced by the detector is fed to the noise generator through /140
the direct current amplifier (9), controlling its filament current (and, as a result, the plate current) in such a way that its power corresponds to the signal power at the antenna at all times. The recorder (5) records the current from the noise generator, which in this case corresponds to the intensity of the cosmic radiation at the antenna.

Reference [146] describes a similar type of apparatus for recording the intensity of cosmic radiation on two frequencies.

The operation of riometric installations involves the engineering problem of increasing their resistance to interference from transmitting radio stations and from the most diverse of pulse type interference. The only way to cope with interference from transmitting radio stations operating on the riometer frequency is to detune, that is, to change the riometer working frequency. Protection against pulse interference requires the use of special pulse limiter circuits, called minimal detectors, a description of which, with some updating, is contained in reference [24]. But positive results are obtained only in the case of short duration pulse interference.

Procedure for Processing Observation Data

The procedure used to process recorded data on cosmic radio-frequency radiation depends to a large extent on the nature of the experiment in accordance with

the scientific task. Today there already is available a great deal of experience in the operation of riometers, definite indications concerning the potentials of the method have been compiled, and a standard procedure for processing observation data has been formulated [69].

Method A2 permits us to determine the integral absorption of radio waves in the ionosphere, and at the same time provides us with knowledge of the height of the absorbing region when working on several frequencies [18], to construct the profile of the electron density in the lower ionosphere [23], to assess the electron temperature and the effective frequency of collision in the F region of the ionosphere [20], and to solve some of the problems of the helio-geophysical profile associated with the development of anomalous absorption in the ionosphere [22].

The standard processing method gives the rule for the construction of the diurnal curve of change in the "primary strength of the $E_0$ signal," which, in the literature has come to be called the sidereal curve. But depending on which of the absorptions we must analyze, regular or anomalous, we have different requirements for the accuracy with which the sidereal curve must be constructed.

The calculation of regular absorption requires the annual cycle of continuous riometric observations so we can determine E and $E_0$ for any sidereal time whatsoever, and then construct the diurnal absorption curve for local standard time.

Practically speaking, the sidereal curve is constructed as follows [69]. The magnitudes of E signal strength are taken from the riometer tape and plotted in the form of points on a graph to the scale of sidereal days. The graph is divided into 24 hours in 4 minute intervals on the x-axis, and the E signal strength scale is laid off on the y-axis, or the scale can be the magnitude 10 lg $(E/E_n)$, where $E_n$ is the level of the signal provided by the calibration generator [18]. The recording on the tape is on a local time scale, so when the graph is constructed on the sidereal time scale it must be remembered that sidereal days differ from solar by approximately 4 minutes.

In order to convert the observation data from one time to the other we begin to read both time scales from the beginning of the observations; for example, from the first of the month at midnight, that is at 00 hours. On the first day all 24 hours coincide on both time scales, and hourly E values are taken off the tape and

plotted on the graph for the first minute of each hour. The E values for the second day are taken from the tape and plotted on the graph with a time shift of 4 minutes for each hour, so that, for example, for 02 hours sidereal time what is taken from the tape is the E value at 01 hour 56 minutes standard time. The third day has an additional time shift of 4 minutes and now the E value for 01 hours 52 minutes standard time is taken off the tape for the 02 hour sidereal time plot. On the X$^{th}$ day the shift is (X - 1)·4 minutes, and thus we have a shift of 24 hours for the whole year, for the 12 months. With this graph for the year available, we can plot the sidereal curve in the form of an upper envelope of maximum values of E signal strength, assuming that it corresponds to no absorption. /141

Care must be exercised when constructing the sidereal curve to consider the individual scattering that can occur in the points used for the plot as a result of interference. This calls for particularly close attention when constructing the graph and for the elimination of such interference, even to the point of smoothing the recorded curve where necessary and extrapolating E values. The work can be reduced by limiting the plots made on the graph to E values for the night hours recorded by the riometer only.

Tabulated E data for the first minute of each hour, but in local time, can be used to obtain absorption from the riometer tape recording, but this is secondary. The time we are interested in requires our taking the E value from the table, and the $E_0$ value from the sidereal curve, but now if we are to find the corresponding $E_0$ we must consider the time correction, which now will be added, rather than subtracted. For example, for the third of the month at 03 hours 00 minutes standard time we find the value for E on the sidereal curve to be 03 hours 08 minutes sidereal time, and the correction taken for the X$^{th}$ day will be (X - 1)·4 min.

The regular absorption thus can be calculated for the entire observation period. When the sidereal curve is constructed on the 10 $\lg(E/E_n)$ scale, the table is compiled on the same scale, and finding the absorption reduces to subtraction.

The sidereal curve can be constructed free of large errors only for night (winter) when the regular absorption must be calculated in the high latitudes,

and practically, the sidereal curve for the year provides winter values in these latitudes.

Receiving antennas usually are pointed at the celestial pole when the anomalous absorption is to be studied, and small sidereal variations are disregarded. The sidereal curve is constructed as described above, but the monthly intervals are taken in days for all hours of observations. Monthly sidereal curves such as these are good indicators of normal equipment performance. When the equipment is performing normally the monthly sidereal curves retain their magnitude, as well as the nature of the change, but shift with respect to each other for neighboring months by 2 hours.

The most promising is the polarization method, for its use results in the construction of a sidereal curve after a short period of observations [69]. It can be taken that the intensity of both of the magnetoionic components used will be the same, that is, that $E^+ = E^-$, if absorption of cosmic radio-frequency radiation in the ionosphere is lacking. The inequality $E^+ > E^-$ always will prevail if absorption is present. If we were to construct a graph on which $E^+$ were plotted on the x-axis, and the ratio $E^-/E^+$ were plotted on the y-axis, we would, for the absence of absorption case, have a striaght line passing through the origin at an angle of 45° (Figure 2.5). Now, if we take all $E^-/E^+$ ratios for some sidereal hour and plot them on the graph, we would get another straight line passing below the first and intersecting it at a point determined by the sidereal magnitude $E_0^+$ and $E_0^-$ for the particular sidereal hour. Constructing graphs such as these for all hours of sidereal days, we obtain sidereal curves for $E^+$ and $E^-$. /142

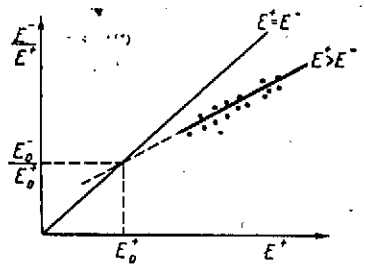

Figure 2.5. Graphical method of determining the sidereal variation in the reception of ordinary and extraordinary signal components [69].

It must be pointed out that evaluation of the error in the method requires a detailed consideration of extraneous noise created by the channel and amplified by the receiver. The presence of intense extraneous noise can reduce substantially the accuracy with which absorption is measured. In practice, every possible step is taken to reduce this noise and to ensure that it will reamin temporally constant. It is particularly important

to maintain receiver gain constant.

Experience gained in the operation of riometers shows that we can, with correctly designed equipment and normal maintenance, expect a root-mean-square error in absorption measurement no larger than 0.1 db. Reference [69] cites the following magnitudes for maximum errors in measuring absorption in the ionosphere using the riometer method.

| Source of error | Error, db | |
|---|---|---|
| | limit | probable |
| Errors in the method: | | |
| temperature variations | ±0.13 | ±0.13 |
| imprecise knowledge of the intensity of cosmic noise in the absence of the ionosphere | ±0.1 | ±0.1 |
| Equipment errors: | | |
| fluctuation in noise | ±0.08 | ±0.06 |
| fluctuation in amplification | ±0.03 | ±0.02 |
| inaccuracy in the recorder | ±0.22 | ±0.15 |
| Processing errors: | | |
| inaccuracy in construction of the sidereal curve | ±0.1 | ±0.1 |
| Maximum error attributable to all causes | ±0.66 | ±0.25 |
| Root-mean-square error | ±0.22 | ±0.09 |

### 2.3. Measurement of Absorption from Data on the Field Strength of Signals from Sending Stations

One of the methods in use to determine the absorption of radio waves in the ionosphere is the A3 method. This method records the field strength of a signal from an outlying, continuously operating, radio station. This method has come to be called the "comparison" method (from the Latin comparare - to compare) because it is based on the principle of comparing the voltage of the incoming signal with the voltage of a signal from a standard source.

As distinguished from the A1 and A2 methods, this method records at the point of reception the field strength of a radio-frequency source located on the terrestrial surface at quite a long distance from the recording site. Here the electromagnetic wave radiated by the transmitter is propagated at an oblique to the terrestrial surface, undergoing one, or several, reflections from the ionosphere and from the terrestrial surface in the distance between the receiver

and transmitter (Figure 2.6a).



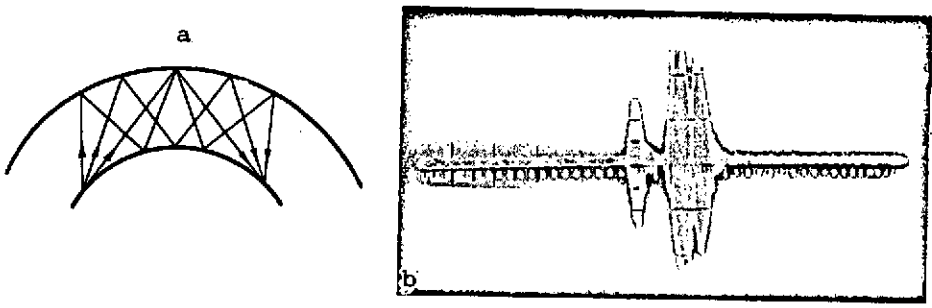


Figure 2.6. Multiplicity of paths of radio waves in the short wave band. a - schematic of possible trajectories of the propagation of a signal from transmitter to receiver; b - photogram of the multiplicity of paths of a signal between Moscow and Irkutsk at a frequency of 21 MHz at 1320 hours on 22 February 1969. The time markers are shown on the sweep axis.

The number of reflections, or skips, of the propagating wave is determined by the ratio between the working frequency and the maximum usable frequency (MUF) for the path, the latter of which depends on the critical frequency for the reflecting region of the ionosphere and on path geometry.

The magnitude of signal field strength created at the reception site by the distant radio station can be determined from [81]

$$E = \frac{222\sqrt{0{,}2\,P_a\varepsilon(\Delta)}(1+|F|)}{2D}|F|^{n-1}e^{-n\Gamma_m}, \qquad (2.11)$$

where

$P_a$ is the power input to the transmitter antenna;

$|F|$ is the modulus of the coefficient of reflection of the wave from the terrestrial surface;

$\Gamma_m$ is the mean absorption of the radio wave in the ionosphere;

D is the length of the path over which the wave is propagated, measured along the arc of a great circle on the globe;

$\varepsilon(\Delta)$ is the gain factor for the transmitting antenna;

$\Delta$ is the angle of inclination of the beam above the horizon;

n is the number of skips.

So, if we are to determine $\Gamma_m$, the mean magnitude of the absorption of radio waves along the path of one skip, we must know many of the above magnitudes, in addition to the magnitude of the incoming signal field strength. Of these, the most complicated to determine is the number of incoming signals, that is, the signal propagation path, or the signal propagation mode.

Often recorded in practice are cases of the signal from the transmitter arriving at the point of reception with several modes of propagation at the same time. All signals arriving by the different skips must, in this case, be taken into consideration to calculate the absorption. This can be done, at least in principle, but it usually is difficult to determine the number of skips, and their quantitative relationship to the received signal during continuous radiation [67, 85]. Consequently, if it is suspected that multiplicity of paths is present in the recorded signal we cannot use Eq. (2.11) to calculate absorption. Disregard for this rule will result in distorted absorption values [143].

Method A4, a method that records the signal from a transmitter operating in the pulse mode with short pulses, can be used to determine the multiplicity of paths and to evaluate the number of skips. Figure 2.6b is an example of photography taken of the oscillograph scope for the case of multiplicity of paths for a signal between Moscow and Irkutsk.

The number of skips per pulse can be found with sufficient reliability by measuring the magnitudes of the time of relative delays between pulses, and by considering the condition of the ionsophere along the path. The procedure has been explained in [131, 145]. We will know the mode of propagation with complete certainty when it is possible to measure the angle of arrival (the elevation) of each pulse and the absolute time of its propagation. /144

The resultant signal field strength at the reception site will be determined from the following expression, if multiplicity of path occurs,

$$E = \sqrt{\sum_{n=1}^{m} E_n^2}, \qquad (2.12)$$

where

$E_n$ is the pulse field strength;

n is the number of reflections from the ionosphere;

m is the number of received pulses.

The technical difficulties involved in measuring angles of arrival in the vertical plane are great, particularly when an installation has special antenna systems. The antenna described in [130] is an example of such an antenna system. Determination of the absolute time of propagation is less costly and is based on the responder beacon method with precise determination of signal propagation time in both directions.

However, all that need be known to determine the mean absorption of the radio waves along the path is the number of skips for the received signals, and this can be obtained quite reliably by processing the data obtained using the A4 observation method.

Comparator Point Equipment

The principle on which the comparator point operates is similar to that for the A2 method receiver, but the receiving antenna is of different design, not only because of other signal propagation conditions, but also because of another method for processing observation data.

Let us erect a receiving antenna with effective height $H_e$ parallel to the electric field vector E for a plane wave at the observation point. The electromotive force at the antenna terminals will be

$$E_{emf} = H_e E. \tag{2.13}$$

Because $\sqrt{\mu}H = \sqrt{\epsilon}E$ for a plane wave, we can with equal justification measure the magnetic field of the wave, H, rather than the electric field. It is practice to determine the electromagnetic field by measuring the electric field, which is expressed as a potential gradient in V/m.

So, in order to measure signal strength we should use a receiving antenna of a type such that its effective height, $H_e$, can be calculated, or measured. Moreover, the antenna pattern and the antenna gain factor must be determined if the strength of the measured signal is low. Now the angle of arrival of the signal must be evaluated. Good antennas for shortwave use have large geometric dimensions, so the field strengths measured by different types of such antennas are different [145], creating additional difficulties in measuring field strength.

So what follows from what has been said is that the principal element in the comparator installation is the receiving antenna, the parameters of which must be known precisely.

The second element is a receiver with good stability and an output indicator in the form of a recorder, or other registering device. The receiver should be well calibrated with respect to output in terms of the input voltage, or a standard oscillator should be used to do the calibrating while the voltage comparison measurement process proper is going on. /145

The antennas most widely used in comparator installations are loop antennas, the effective height (m) of which can be found from

$$H_e = \frac{2\pi nS}{\lambda}, \qquad (2.14)$$

where

n is the number of turns in the loop;

S is the area of a loop turn, $m^2$;

$\lambda$ is the wavelength, m.

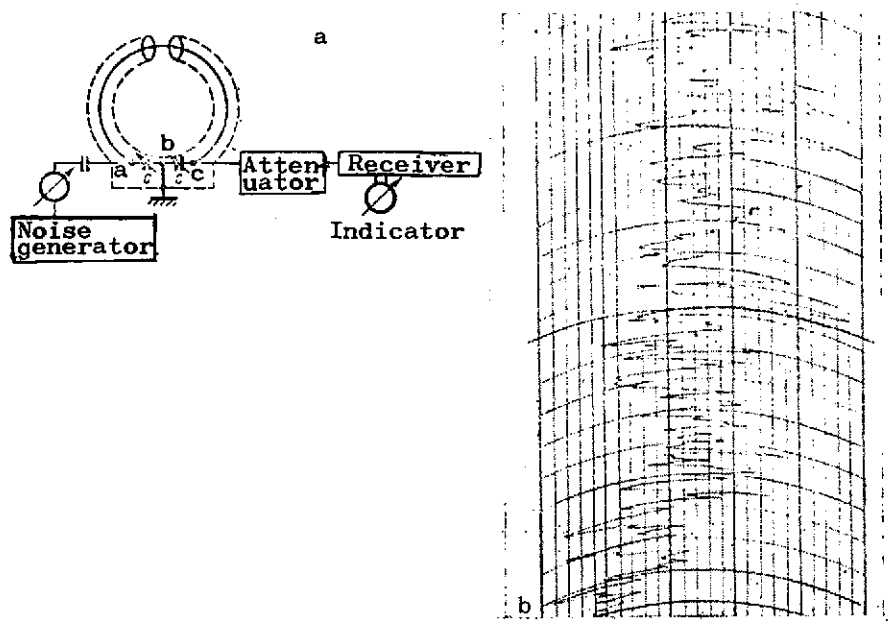


Figure 2.7. Block diagram of a loop comparator [118] operating on the principle of substituting a standard source (a) and specimen of a recording of the field strength of an incoming signal (b).

Figure 2.7a is the block diagram of a comparator with a loop antenna with

high frequency gain adjustment and noise generator calibration. This comparator measures field strength as follows. The loop and the receiver are tuned to the carrier frequency of the received station and the loop is oriented for maximum reception strength. The receiver AGC should be off. The fact of optimum loop position for maximum reception can be judged by the loudness of the reception, but the best approach is to read the meter on the indicator at the receiver output. The received signal is amplified, or attenuated, to that magnitude convenient to read on the indicator. Then, leaving the gain as is, the loop is rotated 90° relative to the position of maximum reception so as to cause the signal to disappear. The noise generator is cut in. The signal from the noise generator now is increased until the indicator reads the same as it did when the signal was being received.

The measured field, E, induces an emf in the loop when tuned to the station corresponding to the expression $E_e = E \cdot H_e$. The voltage supplied from the loop to the right condenser, c (to points b-c) at the receiver input will be

$$\frac{EH_e}{R} \cdot \frac{1}{2\omega c} = v_r,$$

where

/146

2c is the capacitance of each of the condensers for tuning the loop;

R is the ohmic resistance of the loop at the received frequency.

A noise voltage equal to $U_m = I_m[L/(ncR)]$ appears at the receiver input when the noise generator, the active load for which will be the total resistance of the loop at points a-b, equal to L(4cR) (L is loop inductance), is cut in. Here $I_m^2 = 2eI_s\Delta f$, where e is the electron charge, $I_s$ is the saturation current, a, and $\Delta f$ is the receiver passband.

The noise generator diode filament is adjusted so the reading of the receiver's output indicator is the same as that when reception is from the radio station, so that $U_r = U_m$, and

$$\frac{EH_g}{R} \cdot \frac{1}{2\omega c} = I_m \frac{L}{4cR},$$

from whence

$$E = I_m \frac{\omega L}{2H_g}$$

or

$$E = \frac{8{,}46 \cdot 10^{-2} L}{Sn} \sqrt{I_s \Delta f}\ \mu v/m,$$

where L is the μh, $I_s$ in a, Δf in Hz, and S in $m^2$.

Often used in addition to the loop antenna is a short vertical whip of length h(m), the effective height of which is equal, approximately, to half its length. Here the receiving channel is calibrated through the antenna switch (AS) by a standard signal generator (SSG) connected to the antenna switch through a dummy antenna (Figure 2.8).

The antenna switch must meet the following specifications: (a) the decoupling between antenna channels and the dummy antenna should be at least 60 db; (b) the main characteristics of the channels should be identical; (c) the switch should cause no significant mismatch with the feeder.

The effective height of a directional antenna, when such antenna is used, is either calculated, or measured. The necessary calculations can be found in the appropriate literature on shortwave antennas [2]. A standard field generator can be used for the measurement [118]. The effective height is defined as the coefficient of proportionality between the antenna emf and the field strength, given the condition that the direction of arrival of the wave coincides with the direction of maximum antenna reception.

The correct selection of the dummy antenna for the above antennas is a very difficult problem, so it is recommended that the comparator installation be built with the idea in mind that the dummy antenna selected will be calibrated by a standard comparator.

The receiver ordinarily used is any one of the major shortwave receivers with good local oscillator frequency stability, high response, stability of all parameters, and a variable reception channel passband. This latter is desirable so the installation can be used to record the fields of stations operating continuously (band set to minimum) as well as when operating in the pulse mode (when the passband is expanded), and thus avoid distorting the shape of the signal.

A number of receiver parameters are checked systematically when the installation is in operation. The frequency scale calibration is checked and adjusted if

necessary, amplitude curves are plotted, and the range of linearity, which should be at least 40 db, is determined. Gain stability is checked, as is the traveling-wave coefficient at the receiver input, which should be at least 0.9. /147

This comparator measures field strength as follows. The antenna is connected and the receiver is carefully tuned to the frequency of the station to be recorded. The tuning is for maximum reception if the frequency is unknown. Receiver gain is set so changes in the output voltage attributable to fading of the incoming signal will be recorded on the linear section of the amplitude curve for the receiver channel. It is desirable to make changes in gain at fixed levels.

The receiver channel is calibrated at definite time intervals during signal level recording. This calibration should be made mandatory every time receiver gain is changed.

The antenna is calibrated by opening the antenna switch and connecting the SSG, which should be carefully tuned to the frequency of the station being received, and for which the signal level in microvolts, is known precisely, through the dummy antenna. The value of the recorder scale division, in microvolts, is first determined by calibration using the SSG.

Determination of the magnitude of the received station field strength now reduces to processing the recordings on the recorder tape. A specimen tape is shown in Figure 2.7b.

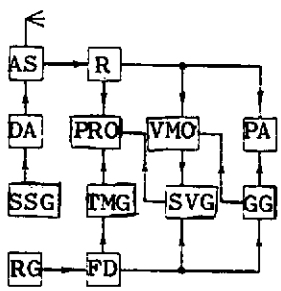


Figure 2.8. Functional diagram of a comparator for recording pulse signals from a radio station (method A5).

Recording the field strength of stations operating in the pulse mode requires additional equipment for the comparator described, and should provide for synchronization between reception and the pulse signal radiated by the transmitter. Figure 2.8 is an example of a block diagram of such a comparator.

The most critical element in the synchronization units is the reference generator (RG), which should provide a frequency stable within $10^{-8}$ over a 24-hour period. Ordinarily used for this purpose are highly stable quartz

crystal oscillators normalized to the same stability for transmitting and receiving points prior to the commencement of measurements.

A frequency divider (FD) reduces the reference generator frequency to that needed for the radiated pulse sampling frequency. This low frequency triggers the time marker generator (TMG), the sawtooth voltage generator (SVG) for the sweeps of the photorecording oscillograph (PRO) and the visual monitoring oscillograph (VMO), as well as the gate generator (GG), the pulse width of which should be capable of being changed. This gate pulse is supplied to the VMO to separate a pulse for additional recording, by a pulse analyzer (PA), for example, if this is part of the assignment.

The specifications for the antenna switch, receiver (R), and the dummy antenna (DA), are the same as those for the comparator used to record continuously radiated signals. Pulse signals on the PRO are recorded by a movie camera for the frequency required by the assigned task, using a pulse analyzer to obtain the amplitude distribution law. The receiver channel is calibrated as /148 described above, but it must be remembered that the SSG output is calibrated in the effective values of a sine voltage, so the readings on the SSG output meter must be multiplied by 1.41 in order to determine the amplitude of pulse signals.

It should be noted that the comparator block diagram we have considered for recording pulse signals is a model, and can be made more complicated by adding additional units, depending on the requirement of the assigned task.

The selection of the territory upon which to set up the receiving antenna is one of the major requirements for the comparator point. Bear in mind that the antenna pattern in the vertical plane is very much determined by the relief of the underlying surface, the area of which is determined by the dimensions of the first Fresnel zone. This area (which can be 2 km in diameter for the shortwave band when large antennas are used) should be quite flat, devoid of heavy vegetation, structures of different types, and, in particular, of metal surfaces and conductors. The cutoff horizon in the directions of interest to us should not exceed 3-5°. It is mandatory that a plot be made of the antenna pattern if these conditions cannot be met.

In conclusion, it should be noted that the measurement of radio station field strength is one of the more complicated radio engineering measurements and that the equipment described has a 30-40% measurement error.

## 2.4. The Oblique and Return-Oblique Sounding Method

A detailed investigation of the conditions under which radio waves are propagated within the limits of one, or of several skips in a broad band of frequencies will provide a wealth of information on the condition of the ionosphere over the length of the path and its reaction to the different helio- and geophysical processes, as well as data needed to maintain radio communications.

There are two ways to obtain information on the conditions under which radio waves are propagated. One involves recording signal parameters by locating the transmitting and receiving stations at opposite ends of the radio path. The other combines both at one of the ends. The former is called the oblique sounding (OS) of the ionosphere method, the latter the return-oblique sounding (ROS) of the ionosphere method.

The equipment used will differ according to the research tasks and the possibilities of reaching an engineering solution.

The condition for the reception of a signal reflected from the ionosphere is determined by the relationship between the transmitter's working frequency, the critical frequency for the ionosphere, absorption in the ionosphere, and the geometry of the path over which the signal is propagated when transmitter and receiver are quite a distance apart, thus precluding the possibility of arrival of a wave propagating along the terrestrial surface. At the same time, communication between the transmitting station and the receiving station is possible, at least in principle, in some band of frequencies, the upper and lower limits of which are fixed by the following conditions. The upper limit of the communication band, called the maximum usable frequency (MUF), is established for the case of a flat earth and ionosphere by the expression

$$f_{MUF} = f_c \sec\theta,$$

where /149

$f_c$ is the critical frequency for the ionosphere's reflecting layer;

$\theta$ is the beam angle of incidence at the ionosphere (see Figure 0.3), equal to

$$\theta = \operatorname{arc\,tg} \frac{D}{2h_e}.$$

The lower limit of the communication band, called the lowest useful frequency

(LUF), depends on the level of absorption of radio waves along the path, on the level of noise at the receiver, as well as on the level of field strength needed to maintain stable radio communications and, consequently, definitely depends on the power of the signal radiated by the transmitter.

The analysis of the conditions under which radio waves are propagated over a path with multiple hops is made by individual hop calculations, determining the MUF and the LUF for each. If equality conditions can be satisfied, radio communications are possible over the entire path in a band of frequencies contained between the MUF and the LUF.

Our presentation has given a broad overview of the principle involved in solving this particular problem, that of explaining the conditions under which a signal is propagated between transmitter and receiver. A strict theoretical review of questions concerned with the oblique propagation of radio waves in the shortwave band will be found in the corresponding literature [3, 53], and from the standpoint of a practical solution in [31, 54, 67, 82, 157].

Thus, the decisive condition on which the passage of radio waves in a definite part of the band of frequencies for a particular path will depend, will be the condition of the individual ionosphere parameters at the signal reflection site. In the example considered, the slope of a surface of equal electron concentration can have a strong effect on signal propagation conditions, as well as on signal trajectory after reflection, because this will change angle $\theta$, and, as a result, will change the MUF and the trajectory, which already will be asymmetrical. This is in addition to the effect created by critical frequency and by the effective height of the reflecting layer. Slopes such as these in the ionosphere can appear regularly, the result of diurnal change in the height of the reflecting layer, or randomly, the result of the appearance of large-scale irregularities of increased, or decreased, electron concentration.

The accumulation of a great deal of experimental data from vertical sounding of the ionosphere has resulted in the establishment of a behavior pattern for the appearance of regular slopes in the ionosphere, and the proposal of a method for including them in radio path calculations [90]. But it also was found that inclusion of the slope in the form of a horizontal irregularity in the electron concentration for the reflecting layer will result in an increase in the MUF in the majority of cases, and to a major change in path geometry.

The influence of large irregularities, the appearance of which is random in nature, and which cannot be taken into consideration mathematically, is to cause extensive focusing of the signal at the receiving point [96].

Quite a few publications, foreign and domestic [71, 84, 230], have calculated the trajectories over which a shortwave signal is propagated, as well as the characteristics of such signal for different laws of electron concentration distribution in terms of height in the reflecting region of the ionosphere. Of the foreign sources, mention should be made of the subject collection in Radio Science, 1968 [230].

More precise answers to the question posed can be given only after strict solution of the wave equation for a three-dimensional problem for a specified anisotropic medium and specified characteristics of its irregular structure. The problem reduces to that of solving second-order differential equations with variable coefficients, the precise solution of which can be obtained only for certain cases, and this does not provide answers to all the questions faced in practice.

Calculations using the approximate methods of wave theory, as well as numer- /150
ical calculations methods, are widely used because of the great difficulties involved in arriving at a strict solution of the wave equation.

The geometric optics methods is one of the approximate methods of wave theory worthy of note. It differs from the other methods in that it is simple, yet provides somewhat greater possibilities for obtaining an analytical solution of a number of problems. But even this method encounters great difficulties if the parameters of the medium depend on more than one coordinate.

A detailed consideration of these questions is of great independent scientific and practical interest, so we invite the reader's attention to the corresponding literature [1, 230].

So far as the conduct of the experiment is concerned, modern equipment, in the form of an oblique variable frequency pulse sounder, can, within a short time interval, cover a broad band of frequencies and thus provide us with data on many questions of interest to us immediately after the measurements have been made. This equipment is used to change reception frequency at the receiver in synchronism with the transmitter and to record incoming signals in the form of a

distance-frequency curve for oblique sounding of the ionosphere (Figure 2.9). We can, at once, establish the MUF and LUF for a particular path, calculate the temporal distribution of the signal, make an estimate of the wave multiplicity for the frequencies of interest to us, and construct the height-frequency curve for the ionosphere at the signal reflection point [92].

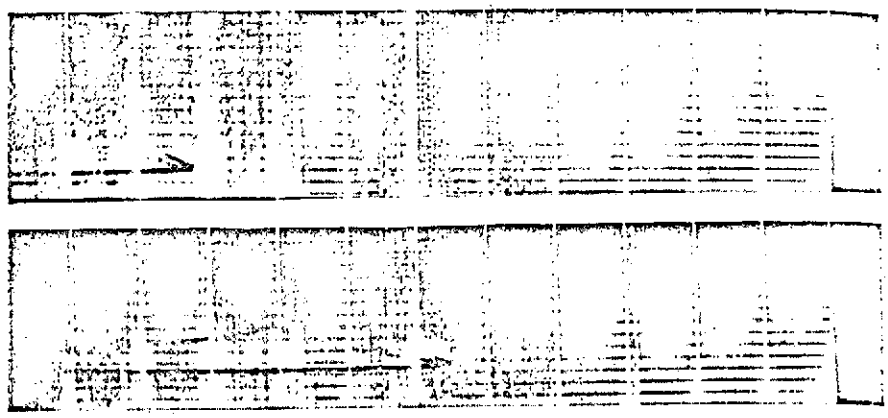

Figure 2.9. Sample signal distance-frequency curve for oblique variable frequency sounding of the ionosphere [125].

The advantage of this method is that systematic observations with OS equipment gives the operator great potential, because he can observe at once the nature of the change in conditions for the propagation of radio waves over the path when there is any sort of ionospheric disturbance, and take steps to ensure uninterrupted radio communications. The OS method also has great potential for conducting scientific investigations of the ionosphere.

Data from investigation of individual parameters of an incoming signal can be used to study the behavior pattern of change in phase, amplitude, and polarization of a signal. The results of study of the amplitude-phase characteristics of a signal [51], as well as of its polarization [142], can be used to develop methods for increasing the dependability of shortwave radio communications.

A second variant for investigating the conditions under which radio waves /151
are propagated during oblique sounding of the ionosphere is the ROS method. This variant includes, in addition, consideration of the mechanism involved in the reradiation of a signal from the terrestrial surface in the return direction to the transmitter, and does so from the point of view of the theory of radio wave propagation. That part of the energy returning over the reciprocal path to the transmitter is received by a receiver at the transmitter station and recorded on

an oscillograph scope in the form of a broad pulse packet with time delay relative to the radiated pulse equal to the time of its propagation to the reradiating surface and back.

The MUF, and the skip distance, can be found at once if the effective height of the reflecting layer of the atmosphere in terms of ROS signal delay time has been estimated correctly. ROS signals can arrive from the first hop, as well as from the second, and succeeding hops reflecting from quite different heights in the ionosphere. The ROS method provides nothing in the way of direct information on the height of the reflecting region in the ionosphere, so ambiguity in estimating this height is the chief source of possible errors when interpreting data from ROS observations. This problem can be solved by improving the equipment, primarily by building pencil-beam transmitting and receiving antennas [130], and by improving the procedures used to process ROS data [97, 140, 141, 149, 150, 151].

Precise determination of the reradiating properties of the terrestrial surface in the opposite direction is a second complicated problem in interpreting ROS data. Experiments [220, 221] led one to conclude that the backscatter factor for dry land was 10 db lower than for the ocean surface, and decreased sharply beginning at an angle of 15° for dry land, and 8° for the ocean surface. This conclusion was confirmed by experiments conducted in Irkutsk using ROS at 17 MHz, during which longer range reception of ROS signals from the ocean surface, and a broader signal packet, were recorded than for ROS recordings from the earth [12].

The ROS method is currently used to solve the following problems: (1) rapid determination of the MUF; (2) communicate regardless of signal scatter (3) study the condition of the ionosphere at long distances from the sounding station; (4) detect irregularities with an increased electron concentration and observe their movements.

The ROS method is realized in two ways in practice. One sounds the ionosphere at constant frequency, using circular scan (Figure 2.10a, b). The other uses a variable frequency on some azimuth (Figure 2.10c). The latter can be accomplished by overlapping the band by a series of fixed frequencies, or by a smooth change in frequency over the entire band.

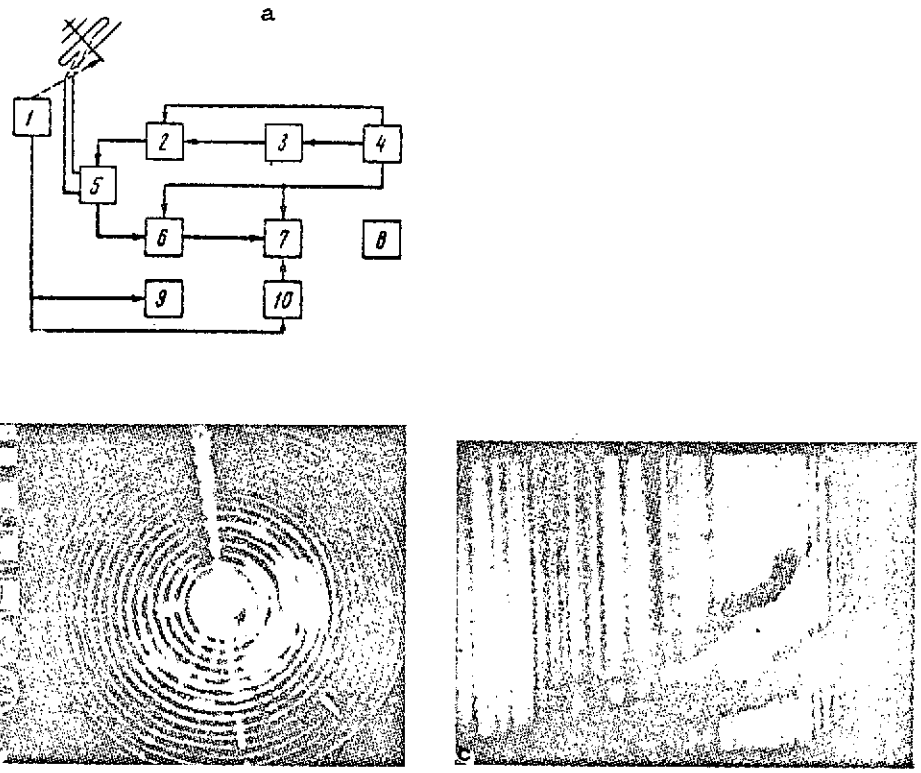


Figure 2.10. Return-oblique sounding of the ionosphere. a - functional schematic of a constant frequency ROS installation with circular scan [10]: 1 - antenna rotator; 2 - transmitter; 3 - master oscillator; 4 - synchrogenerator; 5 - antenna switch; 6 - receiver; 7 - scope with circular sweep; 8 - motion picture camera; 9 - angle of rotation indicator; 10 - servoamplifier; b - photograph of scope of a constant frequency, 17 MHz, circular scan ROS installation [11] with signals reflected from the E layer in the east and southeast sectors; c - sample recording of the distance-frequency curve for a variable frequency ROS signal, in which the lower curve corresponds to one-hop signal propagation, and the upper indicates the presence of two-hop propagation.

The ROS method is more convenient for determining the MUF, or the optimum working frequency (FOT) using ROS of the ionosphere with variable frequency, but this determination also can be made using a single fixed frequency. In this latter case we must know the height of the reflecting layer, or the angle of incidence of the wave at the reflecting layer. We then can use the formula

$$f_1 = f_1 \frac{\cos\theta_1}{\cos\theta_2} = f_1 \cdot m$$

to find the FOT we need for the distance. Here $f_i$ is the sounding frequency, $\theta_1$ is the angle of incidence of the beam at the layer for the distance at which the frequency used is optimum, and $\theta_2$ is the angle of incidence for the distance at which it is required to determine the FOT. The first distance is determined

experimentally, but the second is given.

Reference [219] contains the results of the MUF determination and an evaluation of the errors. Analysis of a comparison made of MUF obtained from VS, OS, and ROS data showed that ROS gave the best results. It was found that there is a small difference (of the order of +0.5%) between the MUF determined using /152
ROS and OS methods. At the same time, a large difference was noted in the MUF obtained from VS and OS data (of the order of 1 to 2%). This led to the conclusion that the ROS method with smooth changes in frequency can be used for a regular determination of the MUF for large areas, particularly if the antenna is pointed in different directions. Here one must point out the feasibility of using the method to evaluate the role of the sporadic, the $E_s$, layer, in shortwave communications. The $E_s$ layer will be the determinant for radio communications when the MUF reflected from it at a given time is higher than the MUF for the regular layers. Calculations made for the line at 2000 km [147] for the middle latitudes, that is, equal to the maximum distance of the hop through the $E_s$ layer, showed that the probability of communication through the $E_s$ layer in the daytime is a maximum in July (44%). The $PE_s$ (percentage of appearance of the $E_s$ layer) in the period from October to March is less than 10. The $PE_s$ has two maxima at night: in May-July (10-13%), and December (80%). These calculations were made for years in which solar activity was at a maximum.

Communications can be maintained by the scattered signal in some cases because direct reflection from the layer is interrupted after transmission. The signal can be a maximum if the transmitting and receiving antennas are pointed in the direction from which the reflection from the earth is coming. An ROS installation can be used to establish this direction. The best azimuth for communications for stations located along a north-south line in the USA [229], for example, will be south-east in the morning, and south-west in the evening. Two stations using this method can easily maintain radio communications at a frequency which is too high for direct communications by reflection from the ionosphere. Reference [187] contains the results of several experiments on communicating by using an ROS signal. /153

This method of communication can be used in individual cases when the ionospheric situation along a direct path between correspondents is unfavorable, such

as would be the case if a polar absorption zone were present, or the time were that of the transition from day to night, and the like [203].

A comparison made between the results of RS and ROS of the ionosphere turned attention to the fact that the ROS method is advantageous for studying disturbances in the ionosphere characterized by opposite changes in critical frequency and height of the reflecting layer of the ionosphere, and this leads to significant changes in skip distance.

Reference [208] includes the results of an analysis of observations of ROS of the ionosphere during heavy disturbances. Sounding was on two frequencies (18.6 and 22.3 MHz) using circular scan. The following relationships, from a morphological point of view, were established: (1) the zone in which the maximum increase in skip distance occurs during an ionospheric storm lies in the direction of the magnetic north, approximately; this zone will move to the west, or east, during the initial phase of the development of the disturbance; (2) the size of the region from which the ROS signals arrive has a tendency to increase along the direction, after which the reflections resume their original form.

Reference [171] contains the results of observations of ROS during disturbances of the sudden burst of absorption (SBA) type. Observations were made on three fixed frequencies (12, 18, and 30 MHz). Two relationships evolved as a result: (1) equatorial stations experienced the greatest effect on the ROS signal by this type of disturbance, and polar stations the least; (2) a reduction in the region of reflections in terms of ROS signal width, and an increase in skip distance, occurs during disturbances.

The ROS method of sounding the ionosphere was used to make a great many observations of the movement of the sporadic formations of increased electron concentration in the E layer. Reference [171] contains data on ROS observations at two frequencies (17.3 and 30.66 MHz) using circular scan, from which evolved a predominant movement to the west at an optimum speed of 250 kmh, for a mean life of recorded clouds in the $E_s$ layer of 3 hours. This same order of magnitude of the speed was obtained in experiments, the results of which have been pulbished in [11, 184, 214, 218].

The dimensions of these clouds in the direction of propagation are

approximately 250 km [174, 184], whereas the clouds are from 500-1000 km long, and 200 km wide, from research on radio communication conditions through the $E_s$ layer [173].

The procedure for determining the speed at which irregularities move by using the ROS method with circular scan contains no assurance that true values will be obtained because it has been shown that the magnitude of the speed depends on the averaging time interval [10], and if the time interval is short, very high values sometimes result. A more detailed analysis of the nature of the change in the sporadic E layer and of the change in the magnitude and direction of the speed of movement of an irregularity in the direction of the sounding for ROS showed that these movements can, in the majority of cases, be explained by changes in the limit frequency and height of the $E_s$ layer.

Equipment for OS and ROS Stations

The basic engineering design for equipment for an oblique sounding station using a sliding frequency is no different from that for a vertical sounding station.

The transmitter for an OS station should have high power and a broad band of frequencies. Transmitter power and the working band for the OS station are determined by data on the path for which this equipment will have to be used. /154
The basic unit, determining the operating effectiveness of the particular equipment, is the synchronizer with automatic matching of phases of transmitter and receiver reference generators and synchronous frequency retuning. Reference [125] contains a brief description of the operation of the OS equipment, and of synchronizer principles. Reference [17] contains some synchronization considerations. The reference generators must maintain a constant frequency if the synchronizers are to perform satisfactorily, and this can be done by receiving exact time signals. One can become familiar with the equipment and the procedure for receiving exact time signals by reading references [17, 132].

The problem of how to maintain reference generator frequency precisely is of paramount importance to signal phase measurements as well [33, 51]. Reference [52] describes a phasemeter that will measure phase difference within 3° to 4°.

One cam become familiar with the procedure and equipment for investigating the polarization characteristics of shortwave signals from the brief description

contained in references [33, 129]. It is more desirable to set the phaser to one frequency of the intermediate amplifier of a two-channel receiver with a common local oscillator, than to put a phase-shifter in the antenna and strive for its good operation over a broad band of high frequencies when recording the polarization of a shortwave signal. Here complete identity over the whole of the curves for both receiver channels is necessary.

One of the technically difficult, but very important measurements for calculating the trajectory over which radio waves are propagated is the angle of arrival. Reference [106], which contains quite a complete bibliography, will acquaint the reader with this problem.

The constant frequency circular scan ROS equipment operates on the principle shown in the functional block diagram in Figure 2.10a [10]. These installations usually have one antenna, which is used to transmit and receive. This antenna is small in size at high frequencies and can be made in the form of a rotating wave channel. The receiver input is protected against overload by an antenna switch, which is a quarter-wave loop of a long line with a spark discharger, when the transmitter is operating. Figure 2.10b is an example of a signal trace.

The sliding frequency ROS equipment operates on the same principle as the oblique sounding installation (in approximately the same frequency band), but the reception and transmission of radio-frequency pulses is by different antennas which are highly directional but oriented in the same direction. The transmission and reception frequencies are changed in synchronism, and the panoramic method is used as the indicator, for VS as well as for OS. A high transmitter power is desirable. A sample trace is shown in Figure 2.10c.

## 2.5. Round-the-World Propagation of Radio Signals

The recording of cases of round-the-world propagation of shortwave signals attracted the attention of researchers, and many papers were published on the subject between the 30's and the 50's. Equipment that could accurately measure echo signal delay time was developed for experimental purposes. Observations in the 10-20 MHz band were made in Denmark. The most favorable time of day for the propagation of a signal around the world is when the propagation path (the arc of a great circle) is in the region near the eclipse belt.

Systematic radio communications between Moscow and the Antarctic (Mirnyy) made it possible to analyze the conditions for round-the-world propagation of a shortwave signal. It was established that optimum conditions correspond to that period of time when the path makes the smallest angle with the day and night boundary. However, optimum conditions for back forward echoes differ. Back echoes pass better when the forward path is illuminated, but the back echo is in the eclipse region for the most part, and vice versa [55]. /155

Forward echoes are attenuated an average 20-30 db as they go around the world, and by 15 db during the second passage, which is not part of the calculation for the conventional skip mechanism of propagation.

The time it takes an echo signal to travel around the world has turned out to be very constant, 0.13760-0.13805 second [188], with the mean 0.13788 second, and does not depend on sounding frequency, time of day, or season of year.

The distance between receiver and transmitter can be calculated from the difference in delay times for the forward and back signals when signals going around the earth in the opposite directions were observed. Stability in propagation time made it possible to determine this distance with an error of 30 km per 1000 km, with the error sometimes merely 3 to 5 km.

The main signal often arrived over several paths when distances to the transmitter were less than 1000 km.

There were cases when the amplitude of the received signal was modulated, as it were, by a frequency the limits of which were from 01 to 0.5 Hz, but if the path traversed the polar regions the frequency of the oscillations changed to limits of from 5 to 30 Hz.

## 2.6. Measurement of the Parameters of the Ionosphere in Terms of the Characteristics of ULF Radiation

Lightning is the most regularly acting source of ultra-low frequency radiation near the terrestrial surface. A lightning discharge is accompanied by the radiation of a packet of electromagnetic waves in the band from hertz 30-50 kHz. Packets such as these are called atmospheric packets. It is very difficult to create a sufficiently powerful artifical radiator in this band of frequencies. At the same time, lightning discharges are quite frequently observed and occur over many regions of the terrestrial surface, so analysis of the properties of

the radiation accompanying such discharges can give us a great deal of valuable information on the condition of the ionosphere.

Numerous experiments tell us that recordings have their own characteristic shapes, depending on the distance these electromagnetic oscillations are successful in covering from site of occurrence to point of recording, as well as depending on where their propagation trajectories are located.

Direct propagation of radiation generated by lightning discharge over the terrestrial surface is the result of reflection of this radiation from the lower boundary of the ionosphere and thus takes place in the "earth-ionosphere" waveguide. The recorded signal has the shape shown in Figure 2.11a in direct proximity to the source, at distances from a few tens of kilometers to 100-200 km. Figure 2.11b shows the shape of a signal recorded at distances in excess of 200 km from the radiation sites. As we see, the signal consists of two parts. The high-frequency part, formed by 1-30 kHz waves, is in the form of quasiperiodic amplitude attenuated oscillations with increasing period, the width of which is of the order of 500-1000 μsec. Following this part, the last period of which has very small amplitude, comes the low-frequency part, formed by waves with frequency less than 1 kHz. The maximum energy of this part of the signal is in the 60-200 Hz region /156 of the band. The tail of the atmospherics usually consists of one or two half-cycles, and its width is a few tens of milliseconds.

Questions of the propagation of ultra-low frequency oscillations in the lower ionosphere still are under serious theoretical consideration (see [8], for example). Caculated theoretical spectra of atmospherics coincide closely with those obtained experimentally. Comparison of these results allows a judgement to be made as to the properties of the lower ionosphere, such as estimating the resonance properties of the waveguide in which atmospherics are propagated, determining the influence of interface boundaries, (of the irregular structure of the ionosphere in particular), of the outer terrestrial magnetic field, and the /157 like. Reference [8] discusses in detail the whole gamut of questions associated with the theoretical consideration of ultra-low frequency radiation in the lower ionosphere, as well as with the experimental results of investigation of this phenomenon.

Signals generated by lightning discharges are reflected from the lower boundary of the ionosphere, but they also can penetrate deep into the ionosphere along

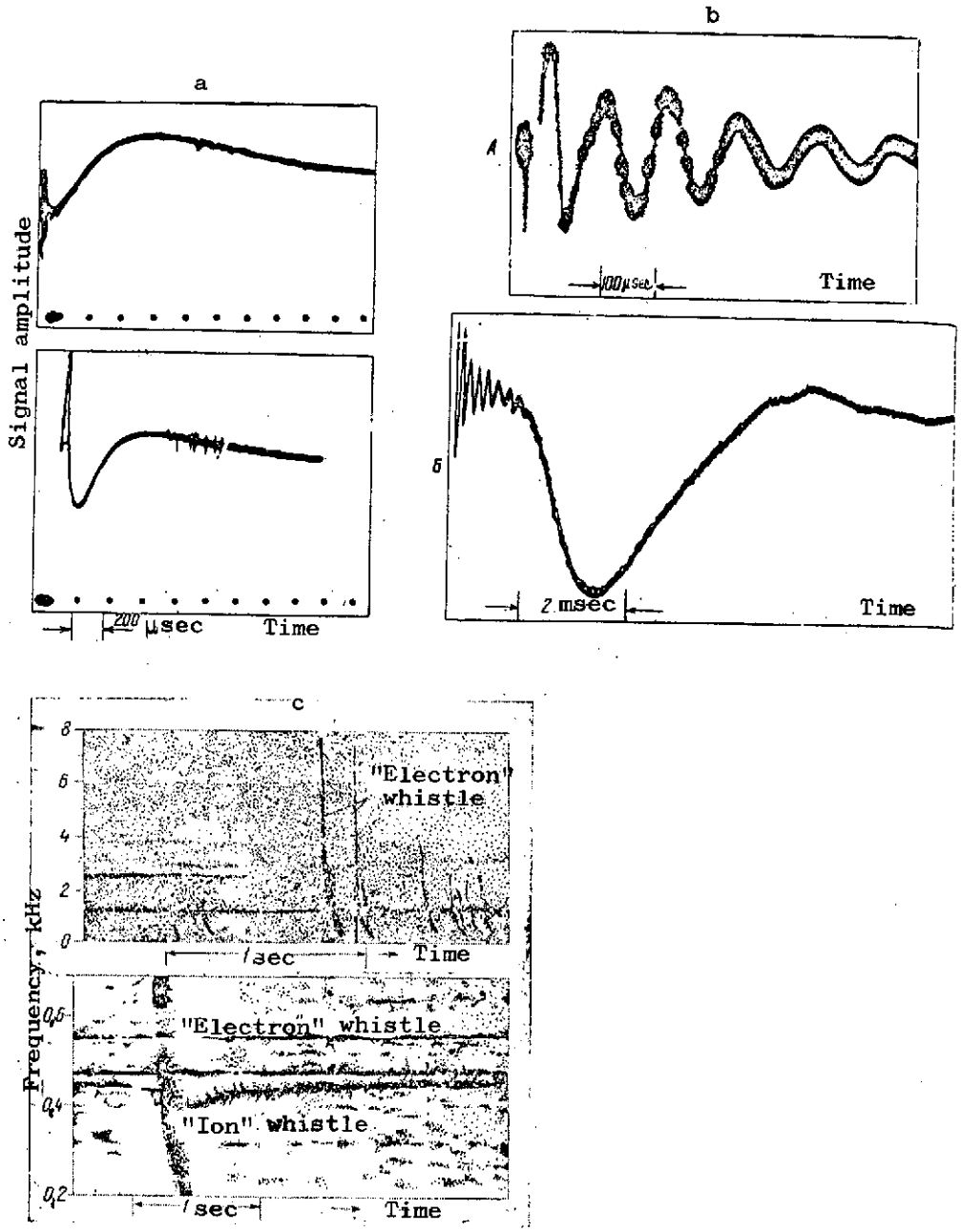


Figure 2.11. Results of the recording of atmospherics propagating in the "earth-ionosphere" waveguide at different distances from the source [8, 9]. a - classical shapes of atmospherics recorded by ground-based equipment; b - the high-frequency part of the ionospherics (A) and its tail (B); c - electron and ion whistles recorded in direct proximity to the satellite [9].

the lines of force of the magnetic field. Channeled by these lines, a wave packet, forming atmospherics, can move a considerable distance and reach the

opposite end of the force tube. The packet will be recorded at a point magnetically associated with that at which the radiation originated. It is possible that atmospherics such as these will complete multiple passages from one end of the tube to the other along the lines of force. Free electrons (as well as ions) tend to disperse the propagating signal, so the shape of the signal, as recorded, will differ significantly from the shape of signals recorded as a result of propagation in the atmospheric waveguide (the spectrum of the recorded signal is greatly extended on the time line, and delay increases with decrease in frequency). A wave packet such as this is heard at the receiver output as a signal with a temporally diminishing tone. This is why signals of this type have been dubbed whistling atmospherics.

The low-frequency waves in the whistling atmospherics cover a broad band of frequencies from $f \ll \Omega_L$, where $\Omega_L$ is the gyroscopic frequency of the ions, to $f \approx \Omega_L$. We can distinguish between "electron" and "ion" (proton) whistles according to which movement, electrons or ions, causes their propagation. Ion whistles are propagated and recorded only at frequencies less than $\Omega_L$. They are cut off when $f \approx \Omega_L$ because of cyclotron resonance. Figure 2.11c is an example of an ion whistle.

Ion whistles, as well as the low-frequency part of electron whistles (with $\omega$ of the order of tens of hertz), have been successfully, and clearly, recorded by equipment installed in artifical earth satellites. The illustration cited shows that the structure of signals recorded by artificial earth satellites differs from the conventional type of whistling atmospherics as recorded by ground-based equipment. This can be explained by the fact that in this case the signal had to cover a very small part of the trajectory (from the site of the occurrence of the atmospherics to the point at which the satellite was located), so its spectrum was but slightly deformed.

The picture that evolves when we are successful in recording electron and ion whistles simultaneously yields quite a bit of valuable information. Questions concerned with the interpretation of the results still are in the formative stages of resolution (see [6, 100], for example). We shall, here, limit ourselves to the statement that, as is known, so long as the whistle cutoff takes place at the cyclotron frequency, trace cutoff (trace frequency coordinate, which can be taken as equal, approximately, to $\Omega_L = (eH)f/(M_i c)$, where H is the magnetic field, and

$M_i$ is ion mass) can be used to determine the ion composition of the ionosphere along the path over which the atmospherics are propagated. Reference [6] states that we can attempt to estimate the ion concentration in terms of the point of intersection of the electron and ion whistles (see Figure 2.11c).

There is little attentuation of electron whistles over the band of frequencies from $f \ll \Omega_L$ to $f \approx \Omega_L$. Figure 2.12 shows examples of their recordings. Conventional whistling atmospherics, in which the delay time for the spectral components, $\tau(f)$, changes monotonically with the frequency (Figure 2.12a, b), differ, as do so-called nose whistles (Figure 2.12c), characteristic of which is a point of inflection where $d\tau(f)/df = 0$. The so-called noise frequency, $f_N$, determined at the point, corresponds to the apogee of the wave trajectory in the region of the magnetic equator.

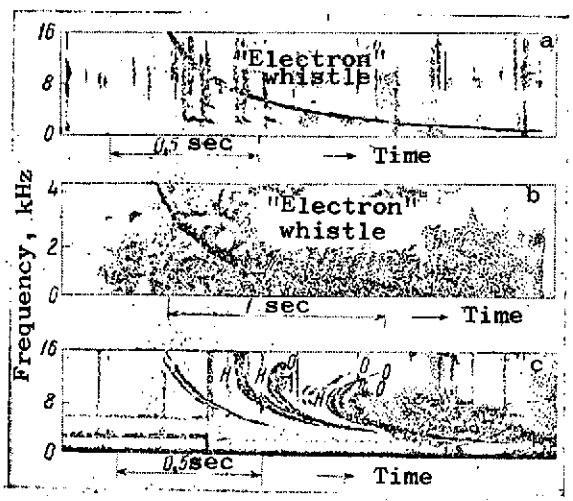


Figure 2.12. Electron whistles of different configurations [9]. a, b - atmospherics with a linear change in the delay to frequency relationship; c - a group of nose whistling atmospherics.

The maximum delay time, $\tau_N$, corresponding to $f_N$ is taken from the oscillogram at the same time as the $f_N$ value. The $f_N$ and $\tau_N$ values, determined experimentally, then are compared with the family of $\tau(f)$ curves calculated theoretically. The distribution of the electron concentration in terms of height is given in analytical form in the calculations. The most frequently used functions are

$$N(h) \sim c_0 \left(\frac{R_0}{R_0 + h}\right)^3$$

and

$$N(h) \sim c_0 \left(\frac{R_0}{R_0 + h}\right)^3 \exp\left(\frac{R_0}{R_0 + h}\right),$$

/158

where

$R_0$ is the radius of the earth;

h is the height of the apogee of the trajectory over which the atmospherics are propagating.

The value of the electron concentration in the region of the apogee results from the comparison. The task of determining the behavior of the electron

concentration with height in the outer ionosphere is reviewed in detail in reference [114].

Whistle characteristics depend on electron distribution, the magnitude of the magnetic field, and its configuration. The magnetic field usually is assumed to be a dipole field when interpreting whistles. But the deviation from dipole distibution can be quite substantial in the presence of magnetic perturbability. The conventional interpretation of whistles in such situation can be incorrect [102]. The effectiveness of the whistle sounding method can be increased markedly by taking into consideration the real configuration of the magnetic field in the magnetosphere.

Reference [101] advances the suggestion that a solution to the reverse is possible; use the whistle configuration to determine the perturbability of the magnetic field. Also indicated is the existence of the principal possibility of estimating changes in the field strength vector, and modulus.

Recording Methods

Two methods are known for obtaining the spectra of atmospherics; the tuned receivers method, and the method that makes a complete harmonic analysis of individual atmospherics. The first of these uses several tuned, narrow-band, receivers to record atmospherics simultaneously, so the amplitude spectrum is obtained directly [225]. The second method assumes the recording of the summed field of an atmopsheric using some broadband device, and then making a harmonic analysis so as to separate the components. References [103, 127] describe a /159
variant of such equipment. The recorder proper comprises a vertical antenna, an antenna amplifier with a pass band of 400 Hz to 18 kHz, and an MEZ-15 recorder. The sensitivity of the recording device for the full pass band is 10 $\mu$V/m. The recording is made on a magnetic tape in the frequency band up to 18 kHz at a speed of 770 mm/sec.

The signal, after being recorded, is fed into a spectrum analyzer, the block diagram of which is shown in Figure 2.13. The ASNChKh-1, the video portion of which was changed somewhat, is the basic unit in the device.

The analyzed signal is rerecorded on a spool of magnetic tape, so it can be reproduced repeatedly. A frequency modulated beat-frequency oscillator is used to obtain successive conversion of the different spectral components to 3 kHz,

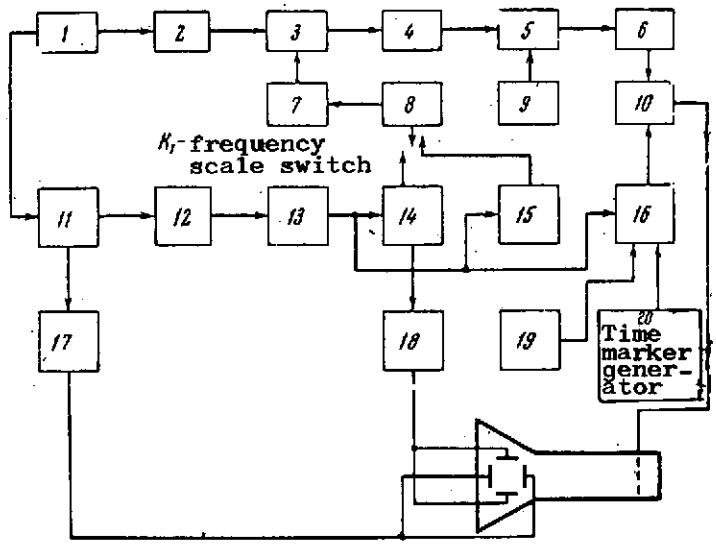


Figure 2.13. Functional diagram of a spectrum analyzer [127]. 1 - MEZ-15 recorder; 2 - input stage; 3 - balance mixer; 4 - resonance amplifier, f = 50 kHz; 5 - second mixer; 6 - resonance amplifier, f = 3 kHz; 7 - frequency modulated generator; 8 - band switch; 9 - voltage generator, f = 47 kHz; 10 - final amplifer; 11 - horizontal sweep voltage generator; 12 - amplifier of pulses switching the ShI-50/4; 13 - ShI-50/4 switching device; 14 - first row of ShI-50/4 contacts with linear voltage divider; 15 - second row of ShI-50/4 contacts with nonlinear voltage divider; 16 - third row of contacts - beam marker key; 17 - horizontal beam deflection amplifier; 18 - vertical beam deflection amplifier; 19 - source of f = 50 Hz voltage for frequency marker lines intensification; 20 - generator.

which is isolated by a special resonance amplifier. The isolated component is supplied to the modulating electrode of the tube.

The horizontal beam deflection generator is synchronized with the movement of the magnetic spool and is triggered at every revolution. A step voltage is supplied to the vertical plates of the cathode ray tube, and to the frequency modulated beat-frequency oscillator. A 50-line raster is obtained on the tube screen. A definite frequency from the beat-frequency oscillator, and a new turn of the spool, correspond to each line of the raster. The complete spectral analysis is made after the fiftieth turn of the tape on which the original signal has been recorded with a discreteness determined by the law in accordance with which the frequency of the beat-frequency oscillator is changed.

This instrument has some shortcomings, including the high ratio of analysis time to width of analyzed signal (>50) and the difficulty involved in analyzing a signal lasting for longer than 2 seconds. There is a multichannel spectrum /160

analyzer [93] free of these shortcomings that analyzes the spectrum using a single movement of the magnetic tape on which the original signal was recorded.

The input amplifier for this analyzer terminates in a complicated cathode follower, the load for which is a bank of 31 filters. The resonant frequencies of the filters are distributed uniformly in a band from 0.5 to 8.0 kHz in 250 Hz steps. Each filter consists of two coupled circuits. The first of the circuits, connected in series, provides low input resistance for the whole filter in the pass band, and high resistance outside it. The filters are the detector load, the pass band is 200 Hz. A diode matrix, controlled by a pulse generator, is used to periodically connect selective channels in the analyzer to the output device. The matrix switching period can be 2, or 5 msec, and the time each of the channels of the matrix is connected to the indicator is 62.5, or 157 μsec. A series of pulses of width $\tau$ and amplitude equal to the output voltage across the corresponding filter occurs at the matrix output when the device is in operation. A sequence of these pulses is fed into the oscillograph amplifier.

The pulses are supplied to the tube's modulating electrode to obtain the dynamic spectrum of the atmospherics. The sweep is the result of a sawtooth voltage, the duration of which coincides with the matrix switching period. One of the pulses controlled by the matrix is used to synchronize the sweep. The pattern that appears on the scope is photographed on film moving at a uniform rate, and this creates a temporal spectrum sweep.

This analyzer also provides a conventional spectrum, amplitude averaged in terms of time.

Analysis of the properties of whistling atmospherics today is acknowledged to be one of the most promising methods to use to determine the parameters of the outer ionosphere.

## 2.7. The Use of Ionosphere Data in Radio Communications Practice

In conclusion, we should, even if briefly, touch on the question of the applied aspect of using those parameters of ionospheric plasma that can be obtained, using the ionosphere measurement methods described above. The most important of the applied aspects is shortwave radio communications. Communication on short waves is, up to this point, the basic type of main radio communications over long (several thousand kilometers) distances. Radio broadcasting,

radio navigation, over-the-horizon radar, and communications with ships and aircraft also use the ionospheric propagation of short radio waves. Finally, short radio waves are used successfully to communicate with low-flying artificial earth satellites and spacecraft.

The propagation of short waves over long distances usually occurs in hops, by means of successive reflections from the "walls" of the "earth-ionosphere" waveguide. Skip distance, angles of departure and arrival, and the band of frequencies in which radio communications can be carried on over the particular path, all these magnitudes are a complex function of the parameters of the equipment used and the condition of the ionosphere along the path.

Skip distance, an important characteristic of radio communications, for example, depends on the antenna pattern in the vertical plane, and on the working frequency, which determine the depth to which waves penetrate into the ionosphere, and that electron density at which reflections from the ionosphere are possible, as well as on the height of the reflecting layer. The maximum /161
usable frequency (MUF), that is the highest frequency that can be reflected from the ionosphere for a given distance, is one of the basic characteristics of radio communications, controls the upper boundary of the band of working frequency, and is linked with the critical frequency for the reflecting layer in the ionosphere, that is, with the electron concentration at the layer maximum. The MUF can be calculated in terms of the high-frequency curve for the ionosphere at the point of reflection, obtained using the vertical pulse radio sounding method.

The frequency of radio communications limiting the band of working frequencies on the down side, that is, the lowest useful frequency (LUF), depends on the degree of absorption of radio waves in the ionosphere, measurement of which was discussed in detail in preceding sections.

The horizontal irregularity of the ionosphere, the presence in the ionosphere of scattering centers, the slopes of the surfaces of equal concentrations, the presence of the ionosphere of large irregularities oriented along the geomagnetic field, the sporadic, the $E_s$, layer, and sporadic formations in the F region, all have a significant effect on radio communications because they are the causes of "nonstandard" propagation of radio waves. The influence of these factors may improve, or worsen, radio communications, depending on concrete conditions.

This is why detailed and systematic measurements of the parameters of ionospheric irregularities, of the dynamic regime in the ionosphere on a global scale, must be made.

There are methods for calculating the characteristics of radio communications in terms of ionosphere characteristics, as well as methods for predicting conditions for radio communications for average quiet conditions in the ionosphere (long-range radio prediction [73]) and for disturbed conditions (short-range radio prediction [75]). The long-range radio prediction reduces to calculating the band of working frequencies for the particular path and for a particular time in advance. The compilation requires study of the space-time variations in ionosphere parameters as measured by the worldwide network of ground-based installations for vertical radio sounding of the ionosphere, by flying and floating ionosphere stations, by incoherent scattering installations, and the like. The locations of the stations that were engaged in ionosphere measurements as part of the unified agreed program during the period of the International Year of the Quiet Sun (1964-1965) are listed in reference [73]. The obtaining of height-frequency curves for the ionosphere was basic to the measurements. Analysis of these data made it possible to establish the nature of diurnal, seasonal, heliocyclical, latitudinal, and longitudinal variations in the N(h)-profile of the ionosphere.

There are worldwide MUF maps for the regular layers of the ionosphere for use in determining the MUF for shortwave radio lines in any direction, and of any length, based on predictions for the individual stations, and subsequent interpolation for the coordinates between these stations.

The empirical relationship between critical frequencies and the level of solar activity, or the phase of the solar cycle, can be used to predict the critical frequencies for the ionosphere's regular layers, the F2, F1, and E, at individual stations. The empirical curves are constructed using long series of observations and continuously refining them by inputting new data. The result is that we can construct a worldwide map of predicted critical frequencies for each hour, local time, from the MUF for the particular layer and distance. Figures 2.14 and 2.15 [73] are examples of such maps. The MUF for the regular layers is determined as the median of daily values over the month, that is, the frequency that will provide a reflection 50% of the time. The selection of

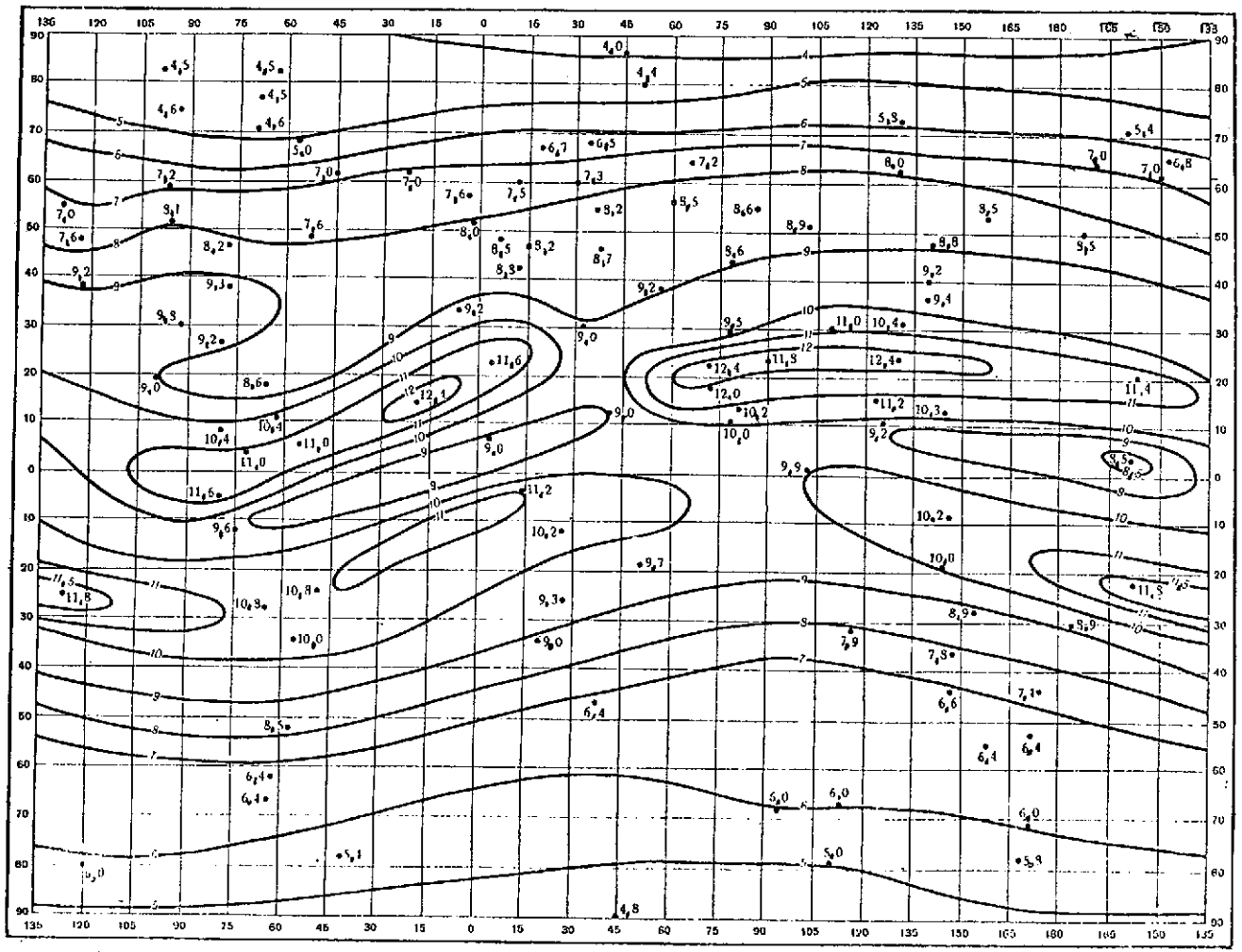

Figure 2.14. Map of the $f_0F2$ prediction for 12 hours local time. January, 1967 [73].

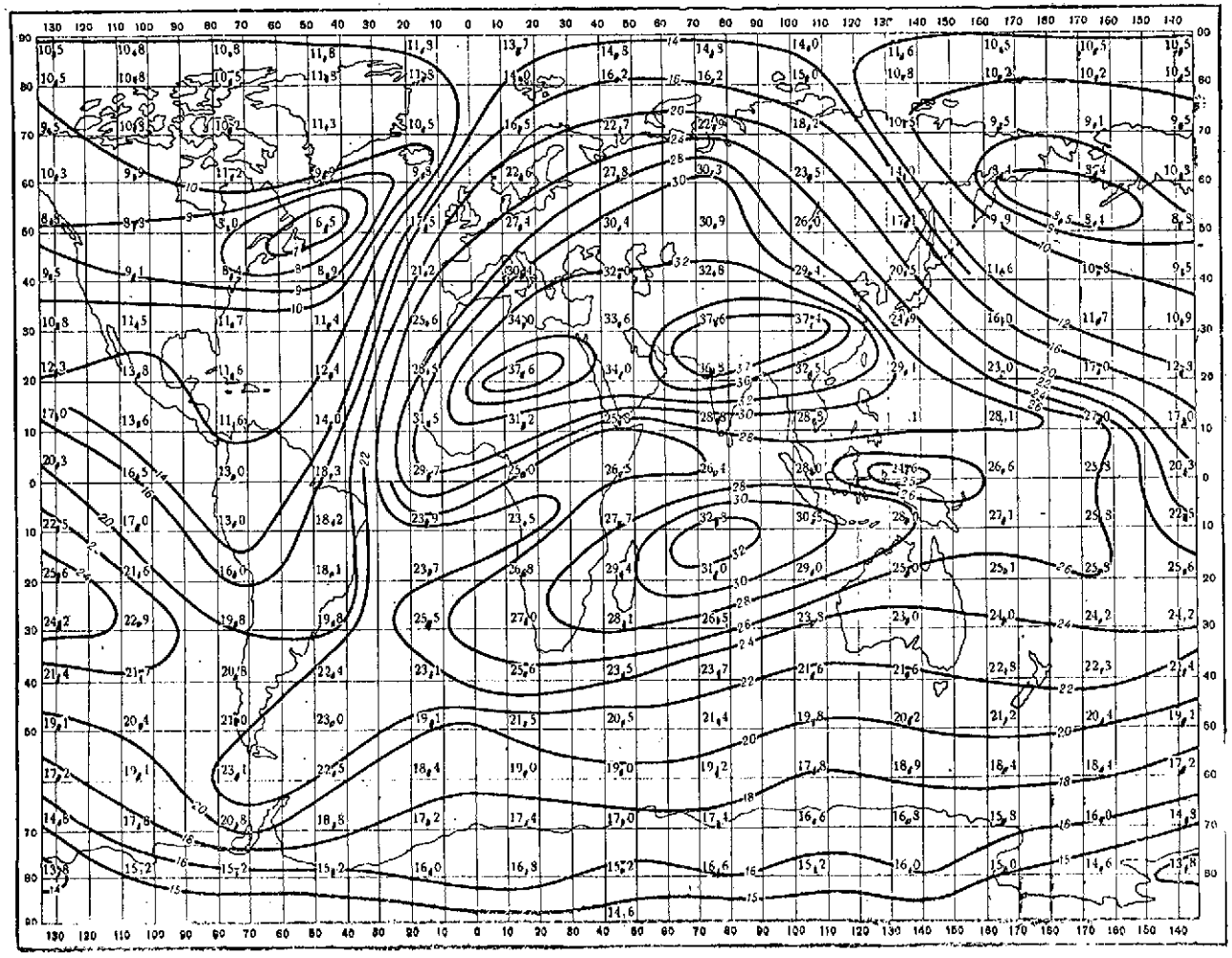

Figure 2.15. Map of the MUF prediction for the F2 layer. Skip distance 4000 km. January, 1967 [73].

working frequencies that are 5 to 10% below the MUF for the regular E layer, or 15-25% below the MUF for the F2 layer, provides stable radio communications using the reflections from these layers with a probability of ~ 90%. By using maps such as these, as well as certain additional data (maps of the global distribution of the probability of the appearance of the sporadic, the $E_s$, layer with different electron densities, the height of ionosphere layers in terms of time of day, and the like), we can obtain the diurnal behavior of the MUF for radio lines of any length and orientation. Figure 2.16 is an example of such curves. Electron computers are used for mass calculations for concrete radio lines [95]. /164

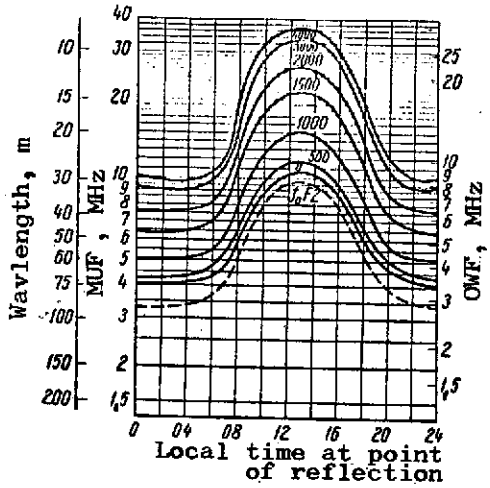


Figure 2.16. Diurnal behavior of the F2 MUF. January 1968. Latitude 55-65°N.

Radio communication conditions, in the final analysis, are determined by the field strength at the receiving point. Strictly speaking, we must know the propagation trajectory, and the degree to which radio waves are absorbed by the medium, if we are to determine this magnitude. Moreover, we also must include in the fading calculation that fading caused by the interference at the receiving station created by beams which have experienced different numbers of reflections from the ionosphere (multiple wave propagation), as well as that caused by the irregular structure of the ionosphere. Practically speaking, what is calculated is the mean effective values of the field strength.

The procedure for calculating the field strength at the receiving point is semiempirical; that is, it is based on the use of numerical coefficients in the calculating formulas, determined experimentally by comparing theoretical behavior patterns with the results of systematic ionosphere measurements, by comparison and study of the relationship between the absorption of radio waves and the season of the year, latitude, time of day, solar activity, working frequency, and other factors. The method devised by A. N. Kazantsev [82] is widely used in radio communication practice. This method calculates absorption in all layers of the

ionosphere through which radio waves pass, and from which they are reflected. The absorption-frequency relationship is calculated separately for each layer. Absorption is proportional to 1/f when reflection is from the E and F1 layers, and to $1/f^2$ when reflection is from the F2 layer. The absorption coefficient in the general case, that of reflection from the F2 layer when the lower-lying D, E, and F1 layers are present, is

$$\Gamma = \frac{3f_E^2 \sec \varphi_D}{(f + f_L)^2} + \frac{2{,}5f_E^2 \sec \varphi_E}{(f + f_L)^2} + \frac{0{,}4f_E^2 \sec \varphi_{F1}}{(f + f_L)^2} + 0{,}02 \cos^3 f_{F2} f^2,$$

where

f is the working frequency;

$f_L$ is the longitudinal component of the gyrofrequency for the electrons;

$F_D$ is the E layer critical frequency;

$\varphi$ is the angle of incidence of the radio wave at the corresponding layer.

The lowest useful frequency, which it is particularly important to know for lengthy multiship radio paths, depends on the field strength at the receiving point and on the noise level (and, naturally, on the parameters of the receiving and transmitting equipment and type of communications). Predicting the MUF-LUF for a radio path that will pass through the high latitudes is particularly complicated. The ionosphere of the high latitudes can be characterized by anomalous-high absorption of radio waves, observed simultaneously over a wide area at the polar cap and in the aurora zone. The behavior patterns of these phenomena have been under recent study, thanks primarily to systematic riometric measurements. This absorption measurement method has proven to be most effective in the high latitudes.

Making a radio prediction for communication with moving objects means giving /165 consideration to changes in all of the path characteristics as the object moves. Conditions for shortwave radio communications with artificial earth satellites at distances exceeding the line of sight zone depend on the height of the orbit, the degree to which the path is illuminated, and the condition of the ionosphere. If an artificial earth satellite has an orbit passing below the F2 layer maximum in the coverage by ground-based sounders, radio wave passage conditions will be determined by the multi-hop mechanism, although this is not the only such

mechanism. Radio waves often are propagated by multiple reflections from the ionosphere without reflection from the earth when effective ionosphere slopes are present. This leads to the possibility of radio communications on frequencies outside the "standard" working band. Ionospheric irregularities, and the E layer, play a big part when communicating with artificial earth satellites. There is severe deterioration in shortwave communication conditions when artificial earth satellites are in an orbit that passes above the F2 layer maximum.

Besides, the radio prediction, its accuracy, and its effectiveness, can be checked against data obtained from sounder observations. The best method to use to check the prediction and select the optimum working frequencies for stable radio communications is oblique sounding of the ionosphere, described in section 2.4.

Ionospheric disturbances are one of the basic causes of disruption of radio communications. Their effects manifest themselves in a reduction in the effect of field strength, in an intensification of fading, and in a rise in the noise level. These phenomena can be explained by the changes that take place in the characteristics of the ionosphere layers during disturbances. The physical mechanism of ionosphere disturbances is not fully understood as yet, but research of the observation data obtained by the worldwide network of ionosphere, magnetic, and solar observatories already has established their basic behavior patterns; dependence on geomagnetic latitude, time of day, and level of solar activity.

These behavior patterns serve as the basis for making a prediction of ionospheric disturbability and of the short-range radio prediction associated with it.

REFERENCES


1. Avtoreferaty Dokladov, IX Vsesoyuznaya Konferentsiya Po Rasprostraneniyu Radiovoln [Author's Summary of Reports, IX All-Union Conference on Radio Wave Propagation], Khar'kov AN UkSSR Press, 1969. /166

2. Ayzenberg, G. Z., Korotkovolnovyye Antenny [Short-Wave Antennas], Svyaz'izdat, Moscow, 1962.

3. Al'pert, Ya. L., Rasprostraneniye Radiovoln I Ionosfera [Radio Wave Propagation and the Ionosphere], "Nauka" Press, Moscow, 1960.

4. Al'pert, Ya. L., "The Procedure for Investigating the Ionosphere Using an Artificial Earth Satellite," Uspekhi fiz. nauk, Vol. 64, Nos. 1, 3, 1958.

5. Al'pert, Ya. L., Belyanskiy, V. B., Kutyakov, A. F., "A Coherent Radio Receiver for Recording the Difference in the Doppler Shift in the Frequencies of Radio Waves Radiated from an Artificial Earth Satellite," Geomagnetizm i aeronomiya, Vol. 3, No. 1, 1963.

6. Al'pert, Ya. L., "Low-frequency Waves Near the Earth and in the Cosmos," Zemlya i Vselennaya, No. 6, 1967.

7. Al'pert, Ya. L., "Some Investigations of the Ionosphere Using Radio Waves Radiated from an Artificial Earth Satellite," V kn. Uspekhi SSSR V Issledovanii Kosmicheskogo Prostranstva [In book: Successes of the USSR in Investigating Space], "Nauka" Press, 1968.

8. Al'pert, Ya. L., Guseva, E. G., Fligel', D. S., Rasprostraneniye Nizkochastotnykh Elektromagnitnykh Voln V Volnovode "Zemlya-Ionosfera" [The Propagation of Low-Frequency Electromagnetic Waves in the "Earth-Ionosphere" Waveguide], "Nauka" Press, 1967.

9. Al'pert, Ya. L., "The Outer Ionosphere and Its Transition to an Interplanetary Medium," Uspekhi Fiz. Nauk, Vol. 90, No. 3, 1966.

10. Akeksandrova, L. V., Yerofeyev, N. M., Nosov, V. Ye., et al., "Observation of Large-Scale Formations of the Sporadic Layer $E_s$ by the VNZ Circular Scan Method in Irkutsk," V sb. Resul'taty Nablyudeniy I Issledovaniy V Period MGSS, No. 2 [In collection: Results of Observations and Investigations During the Period of the IQSY, No. 2], "Nauka" Press, Moscow, 1966.

11. Aleksandrova, L. V., "Determination of the Velocity and Direction of Movements of Large $E_s$ Formations by the VNZ Method," V sb. Ionosfernyye Issledovaniya, No. 17 [In collection: Ionospheric Investigations, No. 17], "Nauka" Press, Moscow, 1969.

12. Aleksandrova, L. V., "Evaluation of MPCh from VNZ Data and Correctness of a Long-Range Forecast," Geomagnetizm i aeronomiya, Vol. 8, No. 3, 1968.

13. Amayev, O. M., "The Influence of an Irregular Ionosphere Structure on the Absorption of Radio Waves," Radiotekhnika i elektronika, Vol. II, No. 5, 1957.

14. Aseyev, V. P., Kolebatel'nyye Tsepi [Oscillating Circuits], Gosradioizdat, Moscow, 1955.

15. Afraymovich, E. L., Yegorov, Yu. A., "Installation for Mass Input Into a Computer of the Coordinates of Curves Appearing on an Image With High Noise Levels," Geomagnetizm i aeronomiya, Vol. 5, No. 4, 1965.

16. Afraymovich, E. L., "Device for Automatic Multichannel Recording and Input Into a Computer of Experimental Information During Investigation of the Ionosphere," V sb. Issledovaniya Po Geomagnetizmu I Aeronomii [In collection: Geomagnetism and Aeronomy Research], "Nauka" Press, Moscow, 1966.

17. Barabashev, B. G., Gurniy, V. V., Kalyadin, B. G., "Device for Synchronizing Sweep for an Oblique Sounder," Geomagnetizm i aeronomiya, Vol. 9, No. 5, 1969.

18. Benediktov, Ye. A., Korobkov, Yu. S., Mityakov, N. A., et al., "Results of Measuring Absorption of Radio Waves in the Ionosphere," Izv. vysshikh uchebnykh zaved. Radiofizika., Vol. 3, No. 6, 1960.

19. Ben'kova, N. P., "Conference on the Ionosphere (NITSTSA, 11-17 December 1961), Geomagnetizm i aeronomiya, Vol. 2, No. 4, 1962.

20. Benediktov, Ye. A., Mityakov, N. A., "Absorption of Cosmic Radio Radiation in the Ionosphere," Izv. vysshikh uchebnykh zaved. Radiofizika., Vol. IV, No. 1, 1961.

21. Benediktov, Ye. A., "One Radio Astronomy Method for Determining Absorption of Radio Waves in the Ionosphere," Radiotekhnika i elektronika, Vol. IV, No. 7, 1959.

22. Besprozvannaya, A. S., Gorbushina, G. I., Morfologiya Vozmushchennoy Ionosfery Vysokikh Shirot (Po Dannym MGG) [Morphology of the High Latitude Perturbed Ionosphere (IGY Data)], Gidrometizdat, 1965.

23. Belikovich, V. V., Itkina, M. A., Rodygin, L. V., "Finding the Profile of the Electron Concentration in the Lower Ionosphere from the Frequency Behavior of Absorption," Geomagnetizm i aeronomiya, Vol. 4, No. 4, 1964.

24. Belikovich, V. V., "Equipment for Recording the Level of Cosmic Radio Radiation in the Decameter Band," Izv. vysshikh uchebnykh zaved. Radiotekhnika., Vol. XI, No. 8, 1968.

25. Belikovich, V. V., Benediktov, Ye. A., "The Radio Astronomy Method of Measuring the Magnitude of the Absorption of Radio Waves in the Ionosphere," Izv. vysshikh uchebnykh zaved. Radiofizika., Vol. XII, No. 10, 1969. /167

26. Belrouz, J. S., "Measurements of Electron Concentration in the D Region by the Frequency Reflection Method," V kn: Elektronnaya kontsentratsiya v ionosfere i ekzosfere [In book: The Electron Concentration in the Ionosphere and Exosphere], "Mir" Press, Moscow, 1966.

27. Uspekhi SSSR V Issledovanii Kosmicheskogo Prostranstva, 1957-1967 [Successes of the USSR in Space Research, 1957-1967], Editor A. A. Blagonravov, "Nauka" Press, Moscow, 1968.

28. Bonch-Bruyevich, A. M., Radioelektronika v eksperimental'noy fizike [Radioelectronics in Experimental Physics], "Nauka" Press, Moscow, 1966.

29. Bonchkovskaya, Yu. S., Vasil'yev, G. V., "An Installation for Measuring Absorption by the A2 Method," Dokl. nauchnogo simpoziuma no ionosfere [Reports of the Scientific Symposium on the Ionosphere], Izd. Rostovsk. gos. un-ta, 1961.

30. Brillouin, L., Nauchnaya neopredelennost' i informatsiya [Scientific Ambiguity and Information], "Mir" Press, Moscow, 1966.

31. Bulatov, N. D., Ulanova, R. A., Kpayushkina, V. F., "Selection of Working Frequencies for High-Speed Short-Wave Radio Communication Via the Ionosphere," Trudy TsNIIS, No. 11, 1964.

32. Bulatov, N. D., Kulakov, V. T., Ulanova, R. A., Preobrazhenskiy, Yu. I., "On Investigations of the Thin Structure of Short-Wave Signals Reflected from the Ionosphere," Trudy TsNIIS, No. 5, 1964.

33. Bykov, Yu. V., Mirkotan, S. F., "Verification of the Relationship for Estimating the Error in Phase Measurements," Geomagnetizm i aeronomiya, Vol. 7, No. 4, 1967.

34. Vaynshteyn, L. A., Zubakov, V. D., Vydeleniye signalov na fone sluchaynykh pomekh [Separating Signals from Random Noise], Sov. radio" Press, Moscow, 1960.

35. Vasil'yev, G. V., "A Small-Sized Ionospheric Sounder Operating on Fixed Frequencies," Geomagnetizm i aeronomiya, Vol. 7, No. 4, 1967.

36. Vasil'yev, G. V., "The Question of Measuring Absorption in the Ionosphere," Trudy SFTI pri TGU, No. 37, 1959.

37. Vasil'yev, K. N., Agafonnikov, Yu. M., "A Positive System for Recording Ionospheric Characteristics With a Type AIS Ionospheric Sounder," Geomagnetizm i aeronomiya, Vol. 5, No. 5, 1965.

38. Vasil'yev, G. V., Vasil'yev, K. N., Goncharov, L. P., "The Type AIS Automatic Panoramic Ionospheric Sounder," Geomagnetizm i aeronomiya, Vol. 1, No. 1, 1961.

39. Vasil'yev, K. N., "Continuous Recording of Minimal Effective Heights of the Ionosphere," Geomagnetizm i aeronomiya, Vol. 6, No. 4, 1966.

40. Vasil'yev, G. V., Kushnerevskiy, Yu. V., "A Manually Controlled Ionospheric Sounder with Mechanical Gang Tuning of Receiver and Transmitter," Dokl. nauchnogo simpoziuma po ionosfere [Reports of the Scientific Symposium of the Ionosphere], Izd. Rostovsk. gos. un-ta, 1961.

41. Vartanesyan, V. A., Goykhman, E. Sh., Rogatkin, M. I., Radiopelengatsiya [Radio Direction Finding], Voyenizdat, Moscow, 1966.

42. Veter v ionosfere [Wind in the Ionosphere], Gidrometeoizdat, Leningrad, 1969, (Translated from English, Editor E. S. Kazimirovskiy).

43. Vitkevich, V. V., Kokurin, Yu. L., "Investigation of Irregularities in the Ionosphere by Radio Astronomy Methods," Radiotekhnika i elektronika, Vol. IV, 1959.

44. Voprosy interpretatsii i obrabotki vysokoshirotnykh ionogramm [Questions of the Interpretation and Processing of High-Latitude Ionograms], Izd-vo AANII, Leningrad, 1967.

45. Galkin, A. I., Kasimanov, A. S., Matyushonok, S. M., et al., "An Electronic Device for Automatically Obtaining Data from Panoramic Vertical Sounding in Digital Form," V sb: Issledovaniye ionosfery [In collection: Investigation of the Ionosphere] "Nauka" Press, Novosibirsk, 1970.

46. Galkin, A. I., Yerofeyev, N. M., "Short Periodic Changes in the Heights of Ionospheric Reflections," Geomagnetizm i aeronomiya, Vol. 9, No. 3, 1969.

47. Galkin, A. I., Issledovaniye informatsionnykh vozmozhnostey metoda panoramnogo vertikal'nogo zondirovaniya ionosfery i dal'neyshiye puti ikh passhireniya (Kand. dissertatsiya) [Investigation of the Information Potential in the Panoramic Vertical Sounding of the Ionosphere Method and Future Ways to Expand that Potential (Candidate Dissertation)], Irkutsk, 1968.

48. Galkin, A. I., Dvinskikh, N. I., "Computer Processing of Data from Panoramic Vertical Sounding," Geomagnetizm i aeronomiya, Vol. 5, No. 5, 1965.

49. Galkin, A. I., "Some Questions of Automatic Processing of Panoramic Vertical Sounding Data," Geomagnetizm i aeronomiya, Vol. 2, No. 4, 1962.

50. Galkin, A. I., "On the Accuracy of Recording Ionospheric Parameters During Vertical Sounding," V sb. Ionosfernyye issledovaniya [In collection: Ionospheric Investigations], No. 17, "Nauka" Press, Moscow, 1968.

51. Gaylit, T. A., Gusev, V. D., Romashkina, A. S., "Measurements of Fluctuations in the Phase of a Signal Reflected from the Ionosphere in the Oblique Incidence Case," Geomagnetizm i aeronomiya, Vol. 9, No. 1, 1969.

52. Gaylit, T. A., "Measurement of Rapid Fluctuations in the Phase of a Signal Reflected from the Ionosphere," Geomagnetizm i aeronomiya, Vol. 6, No. 2, 1966.

53. Ginzburg, V. L., Rasprostraneniye elektromagnitnykh voln v plazme [Propagation of Electromagnetic Waves in Plasma], "Nauka" Press, Moscow, 1967.

54. Ginzburg, V. L., Teoriya rasprostraneniye radiovoln v ionosfere [Theory of the Propagation of Radio Waves in the Ionosphere], Gostekhizdat, Moscow, 1949.

55. Golyan, O. F., Shlionskiy, Sh. G., "Propagation of Back and Direct Around the World Echo Signals," Avtoreferaty dokl. IX Vses. konfer. po rasprostraneniyu radiovoln [Author's Summary of Reports, IX All-Union Conference on Radio Wave Propagation], Izd-vo AN UkSSR, Khar'kov, 1969.

56. Gringauz, K. I., Rudakov, V. A., Kaporskiy, A. V., "Equipment for Rocket Measurements of the Concentration of Free Electrons in the Ionosphere," V sb. Iskusstvennyye sputniki Zemli [In collection: Artifical Earth Satellites], No. 6, Moscow, Izd-vo AN SSSR, 1961. /168

57. Gringauz, K. I., Rudakov, V. A., "Measurements of Electron Concentration in the Ionosphere up to 420-470 km Made During the IGY Using Radio Waves Radiated from AN SSSR Geophysical Rockets," V sb. Iskusstvennyye sputniki Zemli [In collection: Artificial Earth Satellites], No. 6, Moscow, Izd-vo AN SSSR, 1961.

58. Grishkevich, L. V., "The Applicability of Correlation Analysis When Investigating Ionosphere Drifts," Dokl. nauchnogo simpoziuma po ionosfere [Report of the Scientific Symposium on the Ionosphere], Izd. Rostovsk. gos. un-ta., 1961.

59. Grudinskaya, G. P., Rasprostraneniye radiovoln [The Propagation of Radio Waves], Moscow, "Vysshaya shkola," 1967.

60. Gusev, V. D., Drachev, L. A., Mirkotan, S. F., et al., "Structure and Movement of Large Irregularities in the F2 Layer in the Ionosphere," Dokl. AN SSSR, Vol. 123, No. 5, 1958.

61. Gusev, V. D., Mirkotan, S. F., Drachev, L. A., et al., "The Results of an Investigation of the Parameters of Large-Scale Irregularities in the Ionosphere by the Phase Method," V sb. Dreyfy neodnorodnostey v ionosfere [In collection: Drifts of Irregularities in the Ionosphere], Moscow, Izd-vo AN SSSR, 1959.

62. Gusev, V. D., Drachev, L. A., "The Phase Method of Recording Large Irregularities in the Ionosphere," Radiotekhnika i elektronika, Vol. 1, 1956.

63. Danilov, A. D., Khimiya ionosfery [Chemistry of the Ionosphere], Gidrometeoizdat, Leningrad, 1967.

64. Dzhelli, D. Kh., "The Influence of Absorption at the Polar Cap on the Passage of High-Frequency Radio Waves Over High Latitude Paths," V sb. Pogloshcheniye radiovoln v polyarnoy shapke [In collection: Absorption of Radio Waves at the Polar Cap], "Mir" Press, Moscow, 1965.

65. Okolozemnoye kosmicheskoye prostranstvo (spravochnyye dannyye) [Circumterrestrial Space (Handbook Data)], Editor F. S. Johnson, "Mir" Press, Moscow, 1966.

66. Dokuchayev, V. P., "On the Movement of Ionospheric Irregularities," Izv. vysshikh uchzaved. Radiofizika, Vol. 1, No. 1, 1958.

67. Dolukhanov, M. P., Rasprostraneniye radiovoln [The Propagation of Radio Waves], Svyaz'izdat, Moscow, 1965.

68. Drobzhev, V. I., "Investigation of the Irregular Structure of the Ionosphere by the Frequency-Space-Spaced Reception Method," V sb. Ionosfernyye issledovaniya [In collection: Ionospheric Research], No. 15, "Nauka" Press, Moscow, 1968.

69. Driatskiy, V. M., Smirnov, V. B., Khodzha-Akhmedov, Ch. L., Instruktsiya po obrabotke zapisey intensivnosti kosmicheskogo radioizlucheniya [Instructions for Processing Recordings of Cosmic Radio-Frequency Radiation Intensity], AANII Press, Leningrad, 1965.

70. Drachev, L. A., Berezin, Yu. V., "The Influence of Large F2 Layer Irregularities on the Coefficient of Reflection of Radio Waves," Radiotekhnika i elektronika, Vol. II, No. 10, 1957.

71. Yegorov, I. B., Kiyanovskiy, M. P., "One Way to Solve the Problem of the Propagation of Electromagnetic Waves in a Three-Dimensional Irregular Isotropic Ionosphere," Geomagnetizm i aeronomiya, Vol. 10, No. 1, 1970.

72. Yerofeyev, N. M., Petinov, V. G., Shirmamedov, M., "A Converter for Measuring the Absorption of Radio Waves in the Ionosphere," Izv. AN SSSR, Seriya Fiz-tekhn., khim., i geol. nauk, No. 3, 1963.

73. Zhulina, Ye. M., Kerblay, T. S., Kovalevskaya, Ye. M., et al., Osnovy dolgosrochnogo radioprognozirovaniya [Fundamentals of Long-Range Radio Forecasting], "Nauka" Press, 1969.

74. Zasenko, V. Ye., "Some Questions of Increasing the Noise Resistance of Systems Used for Radio Sounding the Ionosphere," V sb. Issledovaniye ionosfery [In collection: Investigation of the Ionosphere], "Nauka" Press, Novosibirsk, 1970.

75. Zevakina, R. A., Lavrova, Ye. V., Lyakhova, L. N., Osnovy prognozirovaniya ionosferno-magnitnykh vozmushcheniy i sluzhba kratkosrochnykh radioprognozov [Fundamentals of Forecasting Ionospheric-Magnetic Disturbances and of Short-Range Radio Forecasting Service], "Nauka" Press, Moscow, 1967.

76. Zelenkova, I. A., Zelenkov, V. Ye., Zaytsev, V. P., "The Measurement of Absorption in the Ionosphere by the A5 Method. Equipment. First Results," Geomagnetizm i aeronomiya, Vol. 6, No. 1, 1966.

77. Zelenkova, I. A., Zelenkov, V. Ye., "A Procedure for Investigating the Absorption of Radio Waves in the Ionosphere Under Rugged Terrain Conditions," Geomagnetizm i aeronomiya, Vol. 8, No. 5, 1968.

78. Ivanov-Kholodnyy, G. S., Nikol'skiy, G. M., Solntse i ionosfera [Sun and Ionosphere], "Nauka" Press, Moscow, 1969.

79. Kazimirovskiy, E. S., Kokourov, V. D., "Drift of Small Scale Irregularities in the Ionosphere," Dokl. nauchnogo simpoziuma po ionosfere [Report of the Scientific Symposium on the Ionosphere], Izd. Rostovsk. gos. un-ta., 1961.

80. Kabanov, N. I., Osetrov, B. N., Vozvratno-naklonnoye zondirovaniye ionosfery [Return-Oblique Sounding of the Ionosphere], "Sov. Radio" Press, 1965.

81. Kazantsev, A. I., "Absorption of Radio Waves in the Ionized Layers of the Atmosphere," Trudy IRE AN SSSR. Radiotekhnika, No. 2, 1956.

82. Kazantsev, A. N., "Refining the Procedure for Calculating the Maximum Usable Frequencies for Shortwave Radio Communication Lines," Trudy IRE AN SSSR. Radiotekhnika, No. 2, 1956.

83. Kazimirovskiy, E. S., "Wind Systems in the Lower Ionosphere," Geomagnetizm i aeronomiya, Vol. 3, No. 3, 1963.

84. Kalinin, Yu. D., Vsekhsvyatskaya, I. S., "A Method for Calculating Signal Strength Along a Shortwave Path," Geomagnetizm i aeronomiya, Vol. 7, No. 1, 1967.

85. Kashprovskiy, V. Ye., Lyannoy, B. Ye., "The Field Calculation for Long Length /169 SW paths," Geomagnetizm i aeronomiya, Vol. 9, No. 3, 1969.

86. Kashcheyev, B. L., "Investigation of the Properties of the Upper Ionosphere from Radio Observations of Meteors," V sb. Meteory [In collection: Meteors], No. 2-3, Izd. Khar'kovsk. gos. un-ta, 1960.

87. Kashcheyev, B. L., Lebedinets, V. I., Radiolokatsionnyye issledovaniya meteornykh yavleniy [Radar Investigations of Meteor Phenomena], Izd-vo AN SSSR, Moscow, 1961.

88. Kashcheyev, B. L., "Radar Observations of Meteors in the IGY Program," V sb. Issledovaniye ionosfery i meteorov [In collection: Investigation of the Ionosphere and Meteors], No. 2, Izd-vo AN SSSR, Moscow, 1960.

89. Kashcheyev, B. L., Tsesevich, V. P., Issledovaniye tsirkulyatsii atmosfery v meteornoy zone. (Instruktsiya) [Investigation of the Circulation of the Atmosphere in the Meteor Zone (Instructions)], "Nauka" Press, Moscow, 1965.

90. Kerblay, T. S., Kovalevskaya, Ye. M., "The MUF Calculation for Horizontal Irregularities in the Ionosphere," Geomagnetizm i aeronomiya, Vol. 7, No. 1, 1967.

91. Kessenikh, V. N., Rasprostraneniye radiovoln [The Propagation of Radio Waves], GITTL, Moscow, 1952.

92. Kiyanovskiy, M. P., Novikova, L. N., Mitrofanova, T. A., "The Conversion of Typical Vertical Sounding Characteristics into an Oblique Sounding Ionogram by the Smith Method," Avtoreferaty dokl., IX Vses. konfer. po rasprostraneniyu radiovoln [Author's Summary of Report, IX All-Union Conference on the Propagation of Radio Waves], Izd-vo AN UkSSR, Khar'kov, 1969.

93. Kiselev, Yu. V., Likhter, Ya. I., Sobolev, Ya. P., "A Multichannel Spectrum Analyzer for Whistling Atmospherics and ULF Radiation," Geomagnetizm i aeronomiya, Vol. 7, No. 6, 1967.

94. Kokourov, V. D., Kazimirovskiy, E. S., "Drifts of Small-Scale Irregularities in the Ionosphere," V sb. Issledovaniye neodnorodnostey v ionosfere [In Collection: Investigation of Irregularities in the Ionosphere], No. 4, Izd-vo AN SSSR, Moscow, 1960.

95. Kovalevskaya, Ye. M., Shlionskiy, Sh. G., Algoritmy rascheta maksimal'nykh primenimykh chastot, naimen'skikh primenimykh chastot i napryazhennosti polya korotkovolnovoy radiosvyazi [Algorithms for Calculating Maximum Usable Frequencies, Lowest Useful Frequencies, and Field Strength for Shortwave Radio Communications], Moscow, 1963.

96. Kovalevskaya, Ye. M., Kerblay, T. S., Raschet rasstoyaniya skachka, minimal'-noy primenimoy chastoty, uglov prikhoda radiovoln s uchetom gorizontal'noy neodnorodnosti ionosfery. (Instruktsiya) [Calculation of Skip Distance, Lowest Useful Frequency, and Angles of Arrival of Radio Waves Considering Horizontal Irregularity of the Ionosphere. (Instructions)], Moscow, 1969.

97. Kol'tsov, V. V., "Finding Effective Reflection Heights from ROS Data," Geomagnetizm i aeronomiya, Vol. 9, No. 5, 1969.

98. Levin, Yu. S., Optimal'nyye fil'try i nakopiteli impul'snykh signalov [Optimum Filters and Accumulators of Pulse Signals], "Sov. radio" Press, Moscow, 1963.

99. Levin, B. R., Teoriya sluchaynykh protsessov i yeyo primeneniye v radio-tekhnike [The Theory of Random Processes and its Application in Radio Engineering], "Sov. radio" Press, Moscow, 1960.

100. Likhter, Ya. I., "Whistling Atmospherics and the Earth's Outer Ionosphere," V sb. Ionosfernyye issledovaniya [In collection: Ionospheric Research], No. 19, "Nauka" Press, Moscow, 1970.

101. Likhter, Ya. I., Molchanov, O. A., "Detection of Disturbances of the Geomagnetic Field in the Magnetosphere from the Dynamic Spectra of Whistling Atmospherics," Kosmicheskiye issledovaniya, Vol. 7, No. 1, 1969.

102. Likhter, Ya. I., Molchanov, O. A., "Analysis of Whistling Atmospherics During a Period of Magnetic Disturbance," V sb. Solnechno-zemnaya fizika [In collection: Solar-Terrestrial Physics], No. 1, Moscow, 1969.

103. Likhter, Ya. I., Prozumentshchikov, S. M., Sobolev, Ya. P., "A Spectrum Analyzer For Variable Frequency Signals," Pribory i tekhnika eksperimenta, No. 1, 1961.

104. Maysuradze, P. A., Yanovskiy, G. N., "An Antenna System Preventing Polarization Fading," Dokl. nauchnogo simpoziuma po ionosfere [Report of the Scientific Symposium on the Ionosphere], Izd. Rostovsk. gos. un-ta, 1961.

105. Mal'tseva, O. A., Korrektiruyushchiy metod rascheta N(h)-profiley ionosfery (Kand. dissertatsiya) [The Correcting Method for Calculating the N(h)-profile of the Ionosphere (Candidate Dissertation)], Rostov-na-Donu, 1970.

106. Mezin, V. K., Avtomaticheskiye pelengatory [Automatic Direction Finders], "Sov. radio" Press, Moscow, 1969.

107. Metodicheskiye ukazaniya po interpretatsii nekotorykh slozhnykh ionogram [Procedural Instructions for Interpreting Certain Complex Ionograms], Izd-vo AANII, Leningrad, 1965.

108. Mirkotan, S. F., Kushnerevskiy, Yu. V., "Irregular Structure and Movement in the Ionosphere," V sb. Ionosfernyye issledovaniya [In collection: Ionospheric Research], No. 12, "Nauka" Press, Moscow, 1964.

109. Misyura, V. A., Tkachev, G. N., Yerokhin, Yu. G., et al., "Toward Ionosphere Measurements by the Incoherent Scattering of Radio Waves Method," Geomagnetizm i aeronomiya, Vol. 9, No. 1, 1969.

110. Misyura, V. A., Tkachev, G. N, Yerokhin, Yu. G., et al., "Toward a Procedure for Ionosphere Measurements by the Incoherent Scattering of Radio Signals," Geomagnetizm i aeronomiya, Vol. 7, No. 3, 1967.

111. Misyura, V. A., Tkachev, G. N., Bluzkov, V. Ya., Yerokhin, Yu. G., "Ionosphere Measurements by the Incoherent Scattering of Radio Waves by the Ionosphere Method," V sb. Ionosfernyye issledovaniya [In collection: Ionospheric Research], No. 18, "Nauka" Press, Moscow, 1969.

112. Mitra, S. N., Verkhnyaya atmosfera [The Upper Atmosphere], IL, 1955.

113. Mozerov, N. S., Vasil'yev, G. V., Zasenko, V. Ye., et al., "A Small 20-Frequency Ionospheric Sounder," V sb. Issledovaniya po geomagnetizmu, aeronomii, fizike solntsa [Investigations of Geomagnetism, Aeronomy, and Physics of the Sun], No. 10, "Nauka" Press, Moscow, 1970.

114. Molchanov, O. A., "The Height Distribution of the Electron Concentration in the Magnetosphere from Whistling Atmospherics Data," Geomagnetizm i aeronomiya, Vol. 7, No. 4, 1967.

115. Polyakov, V. M., Shchepkin, L. A., Kazimirovskiy, E. S., Kokourov, V. D., Ionosfernyye protsessy [Ionosphere Processes], "Nauka" Press, Novosibirsk, 1968.

116. Prokopchuk, S. I., Karnaukhov, V. P., "An Installation for Measuring Absorption of Radio Waves and Drifts in the Ionosphere," V sb. Issledovaniya po geomatnetizmu i aeronomii [In collection: Investigations of Geomagnetism and Aeronomy], "Nauka" Press, Moscow, 1966. /170

117. Ratcliffe, G. A., Fizika verkhney atmosfery [Physics of the Upper Atmosphere], Fizmatgiz, Moscow, 1963.

118. Remez, G. A., Kurs osnovnykh radiotekhnicheskikh izmereniy [Course in the Fundamentals of Radio Engineering Measurements], Svyaz'izdat, Moscow, 1962.

119. Rapoport, Z. Ts., Izmereniye pogloshcheniya radiovoln v ionosfere i issledovaniye svyazi pogloshcheniya s vysotoy Solntsa i solnechnoy aktivnost'yu [Measurement of the Absorption of Radio Waves in the Ionosphere and Investigation of the Connection Between Absorption and the Altitude of the Sun and Solar Activity], Trudy NIIZM, Moscow, 1952.

120. Razmakhin, M. K., "Broadband Communications Systems," Zarubezhnaya radioelektronika, No. 8, 1965.

121. Rukovodstvo po vertikal'nomu zondirovaniyu ionosfery [Handbook for Vertical Sounding of the Ionosphere], Izd-vo AN SSSR, Moscow, 1957.

122. Rukovodstvo po interpretatsii i obrabotka ionogramm [Handbook for the Interpretation and Processing of Ionograms], Translated from English, Editor N. V. Mednikova, "Nauka" Press, Moscow, 1969.

123. Savich, N. A., Avramenko, A. N., "The Panoramic Ionospheric Sounder at the Crimea Astrophysical Observatory of the Academy of Sciences of the USSR," Izv. KRAO, Vol. 17, 1957.

124. Siforov, V. I., Radiopriyemnyye ustroystva [Radio Receivers], Voyenizdat, Moscow, 1954.

125. Smirnov, V. B., Balakin, R. A., Kosterin, I. N., "Experiment Using Oblique Sounding of the Ionosphere in the Shortwave Band," Avtoreferaty dokl., IX Vses, konfer. po rasprostraneniyu radiovoln [Author's Summary of Report, IX All-Union Conference on the Propagation of Radio Waves], Izd-vo AN UkSSR, Khar'kov, 1969.

126. Smirnov, V. B., "Aircraft Measurements of Drift and the Dimensions of the Irregularities in the E layer in the Central Arctic," V sb. Ionosfernyye issledovaniya [In collection: Ionospheric Research], No. 9, Izd-vo AN SSSR, Moscow, 1961.

127. Sobolev, Ya. P., "Equipment for Recording and Analyzing Whistling Atmospherics," V sb. Ionosfernyye issledovaniya [In collection: Ionospheric Research], No. 10, Izd-vo AN SSSR, Moscow, 1962.

128. Solodovnikov, V. V., Statisticheskaya dinamika lineynykh sistem avtomaticheskogo upravleniya [Statistical Dynamics of Linear Systems for Automatic Control], Gos. izd. fiz.-mat. lit., Moscow, 1960.

129. Taran, V. M., "Measurement of Drift in the Ionosphere and the Simultaneous Investigation of the State of Polarization," V sb. Issledovaniya neodnorodnostey v ionosfere [In collection: Investigation of Irregularities in the Ionosphere], No. 4, Izd-vo AN SSSR, Moscow, 1960.

130. Tvetin, L. T., Khansaker, R. D., "Remote Investigation of the Circumterrestrial Medium Using a High-Frequency Radio System with High Resolution and Scan in Azimuth and Elevation," Trudy In-ta inzhenerov po elektronike i radiotekhnike, "Mir" Press, Moscow, Vol. 57, No. 4, 1969.

131. Tel'pukhovskiy, N. A., "Determination of Transit Time for a Signal from Shortwave Stations from the Nature of the Distortions at the Receiving Point," Trudy 15-y Astron. konfer. SSSR [Proceedings of the 15th Conference on Astronomy in the USSR], Izd-vo AN SSSR Moscow-Leningrad, 1963.

132. Tel'pukhovskiy, N. A., "New Equipment for the Reception of Time Signals and the Procedure for Using It," Trudy 14-y Astron. konfer. SSSR [Proceedings of the 14th Conference on Astronomy in the USSR], Izd-vo AN SSSR, Moscow, 1960.

133. Radiopriyemnik R-250, tekhnicheskoye opisaniye [The R-250 Radio Receiver, Technical Description], Moscow.

134. Radiopriyemnoye ustroystvo "Volna-K", tekhnicheskoye opisaniye i instruktsiya po obsluzhivaniyu [The "Volna-K" Radio Receiver, Technical Description, and Maintenance Instructions].

135. Kratkoye opisaniye i instruktsiya k radiopriyemniku US-9 [A Brief Description of the US-9 Radio Receiver and Instructions].

136. Tekhnicheskoye opisaniye ustroystva "Siluet" [Technical Description of the "Siluet" Device].

137. Tekynicheskoye opisaniye avtomaticheskoy ionosfernoy stantsii AIS [Technical Description of the AIS automatic ionospheric sounder].

138. Thomas, G. O., Long, A. R., Westover, D., "The Calculation of Electron Concentration Profiles from Ionospheric Sounder Ionograms," V kn. Electronnaya kontsentratsiya v ionosfere i ekzosfere [In book: The Electron Concentration in the Ionosphere and the Exosphere], "Mir" Press, Moscow, 1966.

139. Thomas, G. O., Ricroft, M. G., Kochesh, L., Chai, K. L., "The Outer Ionosphere. 1. Analysis of Ionograms of the Outer Ionosphere Obtained by the Satellite 'Alouette-1'." V kn. Raspredeleniye elektronov v verkhney atmosfere [In book" Distribution of Electrons in the Upper Atmosphere], "Mir" Press, Moscow, 1969.

140. Tushentsova, I. A., "The Possibility of Determining Ionosphere Slopes by the Return-Oblique Sounding Method," Geomagnetizm i aeronomiya, Vol. 9, No. 1, 1969.

141. Tushentsova, I. A., "The Influence of Sphericity on the Determination of the Horizontal Gradients of the Parameters of the Ionosphere from Data Obtained by the ROS method of Equivalent Slopes," Geomagnetizm i aeronomiya, Vol. 10, No. 1, 1970.

142. Ulanova, R. A., Savin, Yu. K., "Some Results of the Use of Polarization-Spaced Reception to Increase the Dependability of Radio Communications Over Short Shortwave Paths," Trudy TsNIIS, No. 1, 1966.

143. Fligel', M. D., "A Method for Calculating the Absorption and Field Strength of Radio Waves for Oblique Incidence at the Ionosphere," Geomagnetizm i aeronomiya, Vol. 9, No. 6, 1969.

144. Kharkevich, A. A., Spektry i analiz [Spectra and Analysis], Gostekhteorizdat, 1953.

145. Khmel'nitskiy, Ye. A., "Special Features of Determining Field Strength in the Shortwave Band," Elektrosvyaz', No. 10, 1969.

146. Khodzha-Akhmedov, Ch. L., "A Dual Frequency Riometer for Measuring Ionospheric Absorption," Izv. vysshikh uchebnykh zavedeniy. Radiotekhnika, Vol. VII, No. 3, 1964.

147. Chasovitin, Yu. K., Fesenko, S. G., "The Probability of Radio Communications Via the $E_s$ layer, Elektrosvyaz', No. 8, 1964.

148. Chapman, J. H., Warren, E. S., "The Airborne Ionospheric Sounder 'Alouette'." V kn. Elektronnaya kontsentratsiya v ionosfere i ekzosfere [In book: The Electron Concentration in the Ionosphere and Exosphere], "Mir" Press, Moscow, 1966.

149. Chernov, Yu. A., "Number of Echoes With Reflection from the F2 Layer During /171
Return-Oblique Sounding (ROS)," Geomagnetizm i aeronomiya, Vol. 6, No. 6, 1966.

150. Chernov, Yu. A., "The Influence of the Earth's Magnetic Field on a Return-Oblique Sounding Signal," Geomagnetizm i aeronomiya, Vol. 6, No. 5, 1966.

151. Chernov, Yu. A., "Experimental Verification of the Validity of a Parabolic Model of the Ionosphere for Return-Oblique Sounding (ROS)," Geomagnetizm i aeronomiya, Vol. 6, No. 6, 1966.

152. Checha, V. A., "An Ionospheric Sounder for Space-Frequency-Spaced Receiver," V sb. Ionosfernyye issledovaniya [In collection: Ionospheric Research], No. 17, "Nauka" Press, Moscow, 1969.

153. Shapiro, B. S., "Distribution of Ionization with Height and Variations in its Parameters from Ground-Based Vertical Sounding Data." V sb. Ionosfernyye issledovaniya [In collection: Ionospheric Research], No. 19, "Nauka" Press, Moscow, 1970.

154. Shapiro, B. S., "Calculation of the Distribution of Ionization with Height Using Computers," V sb. Issledovaniye ionosfery [In collection: Investigation of the Ionosphere], No. 5, Izd-vo AN SSSR, Moscow, 1960.

155. Shapiro, B. S., Kim, K. V., "Computer Programs for Calculating N(h)-profiles," V sb. Ionosfernyye issledovaniya [In collection: Ionospheric Research], No. 10, Izd-vo AN SSSR, Moscow, 1962.

156. Shkurin, G. P., Spravochnik po elektroizmeritel'nym i radioizmeritel'nym priboram [Electrical and Radio Measurement Instrument Handbook], Voyenizdat, Moscow, 1960.

157. Shlionskiy, Sh. G., Instruktsiya po raschetu korotkovolnovykh liniy radiosvyazi [Instructions for Calculating Shortwave Radio Communications Lines], Moscow, 1961.

158. Evans, J. V., "Observations of Incoherent Back-Scatter from the Ionosphere at Millstone Hill," V. sb. Elektronnaya kontsentratsiya v ionosfere i ekzosfere [In collection: The Electron Concentration in the Ionosfere and Exosphere], "Mir" Press, Moscow, 1966.

159. Atlas of Ionograms. Central Radio Propagation Laboratory National Bureau of Standards, 1957.

160. Booker, H. G., "Turbulence in the Ionosphere with Applications to Meteor Trails, Radio Star Scintillations, Auroral Radar Echoes and Other Phenomena," J. Geophys. Res., Vol. 61, No. 4, 1956.

161. Booker, H. G., Ratcliffe, G. A., Shinn, D. N., "Diffraction from an Irregular Screen with Applications to Ionospheric Problems," Philos. Trans. Roy. Soc., Vol. 242, 1960.

162. Bowles, K. L., "Measuring Plasma Density in the Magnetosphere," Science, Vol. 139, 1963.

163. Booker, H. G., "A Theory of Scattering by Non-Isotopic Irregularities with Application to Radar Reflection," J. Atmos. and Terr. Phys., Vol. 8, 1956, p. 204.

164. Booker, H. G., Seaton, S. L., "Relation Between Actual and Virtual-ionospheric Height," Phys. Rev., Vol. 57, No. 2, 1940.

165. Bowles, K. L., "Observations of Vertical Incidence Scatter from the Ionosphere at 41 Mcs," Phys. Rev. Letters, Vol. 1, 1958.

166. Briggs, B. H., "A Study of the Ionospheric Irregularities Which Cause Spread-F Echoes and Scintillations of Radio Stars," J. Atmos. and Terr. Phys., Vol. 12, 1958, p. 1.

167. Briggs, B. N., Phillips, G. J., Shinn, D. N., "The Analysis of Observation of Spaced Receivers of the Fading of Radio Signals," Proc. Phys. Soc., Vol. 63B, 1950, p. 106.

168. Briggs, B. N., Elford, W. C., "The Buckland Park Antenna Array," Austral. J. Phys., Vol. 5, No. 7, 1968.

169. Budden, K. G., "A Method for Determining the Variation of Electron Density with Height (N (h) Curves) from Curves of Equivalent Height Versus Frequency h'(f)," Rept. Cambridge Conf. Ionospher. Phys. (Phys. Soc. London), 1954, pp. 332-339.

170. Buneman, O., "Scattering of Radiation by the Fluctuations in a Non-Equilibrium Plasma," J. Geophys. Res., Vol. 67, 1 62, p. 2050.

171. Clarc, C., Peterson, A., "Motion High-Frequency Back-Scatter Records," Nature, Vol. 178, 1956.

172. Coll, D. C., Storey, J. K., "Ionospheric Sounding Using Coded Pulse Signal," J. Res. Nat. Bur. Standards, D68, No. 10, 1964.

173. DeGrigorio, J. F., Finney, J. W., Kildahl, K., Smith, E. K., Recent Sporadic E Experimental Works in the United States, "Ionospheric Sporadic E," Oxford, London, N. Y., Paris, 1963.

174. Dominici, P., "Sporadic E Ionization Observed by the Backscatter Technique," Ann. Geophys., Vol. 16, No. 1, 1963.

175. Evans, J. V., "Theory and Practice of Ionosphere Study by Thomson Scatter Radar," Proc. JEEE, Vol. 57, No. 4, 1969.

176. Evans, J. V., "Design Considerations for a Thomson Scatter Radar," Aeron. Rept., Univ. Illinois, No. 17, 1967.

177. Farley, D. T., Dougherty, J. P., Barron, D. W., "A Theory of Incoherent Scattering of Radio Waves By a Plasma. II. Scattering in a Magnetic Field," Proc. Roy. Soc., A 263, 1961,(Russian translation in collection Nekogerentnoye rasseyaniye radiovoln [Incoherent Scattering of Radio Waves], "Mir" Press, Moscow, 1965).

178. Fejer, J. A., "Scattering of Radiowaves by an Ionized Gas in Thermal Equilibrium," Canad. J. Phys., Vol. 38, 1960, p. 1114.

179. Franklin, C. A., Maclean, M. A., "The Design of Swept-Frequency Topside-Sounders," Proc. IEEE, Vol. 57, No. 6, 1969.

180. Franklin, C. A., Bibby, R. J., Hitchcock, N. S., "A Data Acquisition and Processing System for Mass Producing Topside Ionograms," Proc. IEEE, Vol. 57, No. 6, 1969. /172

181. Gassmann, G. I., "Airborne Ionospheric Measurements in the North Pole Area;" J. Geophys. Res., Vol. 61, No. 1, 1956.

182. Greenhow, J. S., "Systematic Wind Measurements at Altitudes of 80-100 km Using Radio Echoes from Meteor Trails," Philos. Mag., Vol. 45, No. 364, 1954.

183. Hagg, E. L., Hewens, E. J., Nelms, G. L., "The Interpretation of Topside Sounder Ionograms," Proc. IEEE, Vol. 57, No. 6, 1969.

184. Harwood, I., "Some Observations of the Occurrence and Movement of Sporadic E Ionization," J. Atmos. and Terr. Phys., Vol. 20, No. 4, 1961.

185. Harnischmacher, E., Porsche, H., "Active High-Frequency Spectrometer for Ionospheric Sounding. IV. Numerical Recording of Travel Time Values," Arch. elektr. Übertragung, Vol. 14, No. 11, 1960.

186. Haubert, A., Dogen, G., "Improvement of Devices for Measuring Winds and Diffraction of Radio and Electrical Waves in the Ionosphere," Ann. Géophys., Vol. 22, No. 3, 1966.

187. Hedlund, D. A., et al., "Some Ionospheric Scatter Techniques," Trans. IRE, Vol. 4, No. 1, 1956.

188. Hess, H. A., "Investigations of Shortwave Echoes," Z. Naturforsch., Vol. 1, 1946, p. 499; Vol. 2a, 1947, p. 528.

189. Hewish, A., "The Diffraction of Galactic Radiowaves as a Method of Investigating the Irregular Structure of Ionosphere," Proc. Roy. Soc. A, Vol. 214, 1952.

190. Hugill, J., Field, M. J., "Resonance Relaxation Sounder for the Multiple Ionospheric Probe," Rev. Scient. Instrum., Vol. 38, No. 12, 1967.

191. Ingvesson, K. O., Perkins, F. W., "Radar Thomson Scatter Studies of Photoelectrons in the Ionosphere and Landau Damping," J. Geophys. Res., Vol. 73, 1968.

192. Instruction Manual, No. 5. The Ionosphere, Vol. II. The Measurements of Ionospheric Absorption, London, 1956.

193. Jackson, J. E., "The Reduction of Topside Ionograms to Electron-Density Profiles," Proc. IEEE, Vol. 57, No. 6, 1969.

194. Jackson, J. E., "Comparisons Between Topside and Ground-Based Soundings," Proc. IEEE, Vol. 57, No. 6, 1969.

195. Kenneth, D., "The Use of Topside Sounders in Ionospheric Research," Telecommuns J., Vol. 32, No. 3, 1965.

196. Kelso, J. M., "A Procedure for Determination of the Vertical Distribution of the Electron Density in the Ionosphere," J. Geophys. Res., Vol. 57, 1952, p. 357.

197. Lundquist, R. B., "The Recording of Ionospheric Sounding Data in a Digital Format," Radiolocat. Res. Lab., Univ. Illinois, 1965.

198. Lockwood, G. E. K., "A Computer - Aided System for Scaling Topside Ionograms," Proc. IEEE, Vol. 57, No. 6, 1969.

199. Mar, J., Garrett, T., "Mechanical Design and Dynamics of the Alouette Spacecraft," Proc. IEEE, Vol. 57, No. 6, 1969.

200. MacDougall, I. W., "The Interpretation of Ionospheric Drift Measurements," J. Atmos. and Terr. Phys., Vol. 28, 1966, p. 1053.

201. McNicol, R. W. E., Webster, H. C., Bowmann, G. G., "A Study of Spread - F Ionospheric Echoes at Night at Brisbane," Austral. J. Phys., Vol. 9, 1956.

202. Michio, O., Fumio, O., Nobuo, O., Koichi, A., "Automatic Ionogram Scaler," J. Radio Res. Labs., Vol. 8, No. 35, 1961.

203. Mitra, S. N., Ivengar, V. C., "Observations of Scatter Echoes on High Power Pulsed Transmissions," Indian J. Phys., No. 4, 1954, p. 147.

204. Moorcroft D. R., "On the Determination of Temperature and Ionic Composition by Electron Backscattering from the Ionosphere and Magnetosphere," J. Geophys. Res., Vol. 69, 1964, p. 955, (Russian translation in collection Nekogerentnoye rasseyaniye radiovoln [Incoherent Scattering Of Radio Waves], "Mir" Press, Moscow, 1965).

205. Nakata, Y., Kan, M., Uyeda, H., "Simultaneous Measurement of Sweep Frequency h(t) and $f_c$(t) of the Ionosphere," Rept Ionosphere Res. Japan, Vol. 7, 1953.

206. Penndorf, R. A., "A Spread-F Index," J. Atmos. and Terr. Phys., Vol. 24, 1962, p. 543.

207. Phillips, G. I., "A Wide-Band Aerial System for Circularey Polarized Waves Suitable for Ionospheric Research," Proc. IRR, Part III, 1951, p. 237.

208. Ranzi, I., Dominici, P., "Back Scatter Sounding During Ionospheric Storms, Effect Disturbances Solar Origin Commens," Oxford, London, N. Y., Paris, Pergamon Press, 1963, p. 143.

209. Rassel, S. II., Zimmer, F. C., "Development of the Fixed-Frequency Topside-Sounder Satellite," Proc. IEEE, Vol. 57, No. 6, 1969.

210. Rastogi, R. G., Deshpande, M. R., Harishandra, H., "Elongation of Irregularities in Ionospheric F-Region Over the Magnetic Equator in India," J. Atmos. and Terr. Phys., Vol. 30, No. 8, 1968.

211. Ratcliffe, G. A., "Some Aspects of Diffraction Theory and Their Application to the Ionosphere," Repts. Progr. Phys., Vol. 19, 1956, p. 188.

212. Rawer, K., "Focusing on a 'Rippled' Ionosphere," J. Atmos. and Terr. Phys., Vol. 8, No. 4, 1956.

213. Rawer, K., Suchy, K., "Radio-Observations of the Ionosphere. - In: Encylopedia of Physics, Vol. XLIX/2 Geophysics III, part II, Berlin, Heidelberg, N. Y., 1967. /173

214. "Long-Range Reception of Foreign Television Transmission in Czechoslovakia," Bull. docum. et inform. organis. internat. radio. diff., Vol. 49, 1954, p. 216.

215. Renau, J., Camnitz, M., Flood, W., "The Spectrum and the Total Intensity of Electromagnetic Waves Scattered from an Ionized Gas in Thermal Equilibrium in the Presence of Static Quasi-Uniform Magnetic Field," J. Geophys. Res., Vol. 66, 1961, p. 2703, (Russian translation in collection Nekogerentnoye rasseyaniye radiovoln [Incoherent Scattering of Radio Waves], "Mir" Press, Moscow, 1965).

216. Revah, J., "Study of Small-Scale Winds Observed in the Middle of Meteor Trails," Ann. geophys., Vol. 25, No. 1, 1969.

217. Schmerling, E. R., "An Easily Applied Method for the Reduction of h'(f) Records to N(h) Profiles Including the Effects of the Earth's Magnetic Fields," J. Atmos. and Terr. Phys., Vol. 12, 1958, p. 8.

218. Shearman, E. D. R., Harwood, I., "Spoaradic E as Observed by Back-Scatter Techniques in United Kingdom," J. Atmos. and Terr. Phys., Vol. 18, 1960, p. 29.

219. Silberstein, I., "The Use of Sweep-Frequency Back-Scatter Data for Determinating Oblique-Incidence Ionospheric Characteristics," J. Geophys. Res., Vol. 63, No. 2, 1958.

220. Steele, T. G., "The Effect of the Ground Back-Scatter Coefficient on Observations of Sporadic E Over Sea, Land and Mountains," J. Atmos. and Terr. Phys., Vol. 26, 1964, p. 2.

221. Steele, I. G., "Backscatter of 16 mc/s Radio Waves From Land and Sea," Austral. J. Phys., Vol. 18, No. 4, 1965.

222. Thomson, J. J., Conduction of Electricity Through Gases, London, Cambridge Univ. Press, 1906, p. 321.

223. Titheridge, J. E., "A New Method for the Analysis of Ionospheric h'(f) Records," J. Atmos. and Terr. Phys., Vol. 2, No. 1, 1961, p. 1.

224. Titheridge, J. E., "The Calculation of Real and Virtual Heights of Reflection in the Ionosphere," J. Atmos. and Terr. Phys., Vol. 17, 1959, p. 96.

225. Wadehra, N. S., Tantry, B. A. R., "Audio Frequency Spectrum of a Radio Atmospheric at Large Distances," J. Atmos. and Terr. Phys., Vol. 28, No. 12, 1966.

226. Wright, R. W., Knecht, R. W., Davies, K., Ann. IGY, Vol. 3, Part 1, 1957.

227. Wright, R. W., Koster, Y. R., Skinner, N. Y., "Spread-F Layer Echoes and Radio Star Scintillation," J. Atmos. and Terr. Phys., Vol. 8, 1956, p. 240.

228. Wright, J. W., "Some Current Developments in Radio Systems for Sounding Ionospheric Structure and Motions," Proc. IEEE, Vol. 57, No. 4, 1969.

229. Villard, O. C., Peterson, A. M., "Scatter-Sounding: A New Technique in Ionospheric Research," Science, Vol. 116, No. 300, 1952.

230. Radio Science, Vol. 3, No. 1, 1968.

Translated for National Aeronautics and Space Administration under contract number NASw-2038 by Translation Consultants, Ltd., 944 S. Wakefield Street, Arlington, Virginia 22204.



☆ U.S. GOVERNMENT PRINTING OFFICE: 1974—739-162/149